THE UNIVERSITY
of EDINBURGH

Ph.D. Thesis
Framework for testing the fundamental principles in gravitation and cosmology

重力および宇宙論の基礎原理を検証する枠組み

Science department in Nagoya University
School of Physics and Astronomy in University of Edinburgh

461501013, s1885627

Shun Arai

Abstract

In this thesis, we consider how in practice fundamental principles can be constrained by cosmological surveys, mainly by considering popular modifications of Einstein's general relativity. We specifically investigate (1) breaking the equivalence principle in the generalised scalar-tensor gravity and its observational consequences, (2) the validity of Lorentz invariance in the inflationary universe, and (3) practical observations for testing gravity by CMB lensing data.

In the first part, we investigate the parameter distributions of viable generalised scalar-tensor theories with conventional dust matter. We numerically construct the models consistent with the observed Hubble parameter in the redshift range, $0 < z < 2$. We show the model parameter distributions in the degenerate higher-order scalar-tensor (DHOST) theory, and its popular subclasses (e.g., Horndeski and GLPV theories).etc. We specify the differences and characteristics of the subclasses in the space of observable quantities for forthcoming galaxy surveys and planned gravitational-wave observations, arguing how to differentiate the theories.

In the second part, we consider primordial perturbations with a single inflaton field in the framework of 4d-Hořava-Lifshitz gravity. For the sake of Lorentz violation in gravity, all the components obey Lifshitz scaling and one additional scalar degree of freedom appears, which is called "Khronon". The Khronon gravitationally couples to the inflaton, but it has been less known how the Khronon behaves in the inflationary universe. We show that the curvature perturbation is preserved at super-horizon scales. We demonstrate that the scalar perturbations where Lorentz invariance is explicitly broken are still consistent with cosmological observations whereas the primordial tensor perturbation undergoes a significant modification of the shape of its power spectrum. As a result, we conclude that testing Lorentz symmetry of the gravity sector at the inflationary energy scale is quite possible by a direct measurement of primordial gravitational waves.

In the last part, we develop the methodology of testing gravity at high redshifts. We consider the gravitational lensing of the CMB, so-called CMB lensing, by massive radio galaxies, aiming to measure the growth history of the large scale structure at $z > 1$. We construct all-sky data of radio surveys and develop the method of how we properly assign the redshift distribution and bias of radio sources. We identify redshift information as the main difficulty for the extraction of the growth history of large scale structure from the existing data of galaxy and radio surveys, and CMB lensing, discussing possible improvements in future radio and galaxy surveys.

In conclusion, we discuss the levels of violation of fundamental principles in gravitation and cosmology that might be detectable in future observations.

Lay summary

The ultimate significance of physics is to provide an overview of the elements of all things in the world based on universal principles. As a result of scientific developments throughout history, the principles that make up the laws of nature have been narrowed down through numerous experiments and observations. The principles and laws obtained so far are now considered to govern the birth and evolution of the Universe through the operation of Big Bang cosmology and the Standard Model of particle physics. Between these, "cosmological physics" was established.

Cosmological physics is founded on general relativity, locality, Lorentz invariance, equivalence principle, all of which are cornerstones of modern physics. Cosmological physics can explore the details of physical phenomena at extremely high energy (10^{16}GeV) from data at extremely low energy (10^{4}eV) such as the current Hubble scale, even though the high-energy processes cannot be reached experimentally. The physics that can be explored in this way is unique, and cosmology is therefore a great research area to gain new knowledge about the basic principles of physics.

The discovery of the accelerating expansion of the Universe in 1999 presented one of the greatest challenges of modern physics, the cosmological constant problem. In addition, as a result of precise astronomical observations such as the measurement of cosmic microwave background radiation temperature and polarisation fluctuations, it was reported that there was a discrepancy between independent measurements of the space expansion coefficient predicted by the standard cosmological model. Under such circumstances, the fundamental principles that form the basis of cosmological physics are beginning to be reviewed. While the accuracy of observations is expected to improve, theories describing physics beyond basic principles are very rich and can predict various phenomena. These predictions should eventually be verified through experiments and observations.

In this doctoral thesis, conclusions have been reached through a series of researches on both theory and observation in gravitational and cosmological physics. Most importantly, we conclude that the fundamental principles in the gravitation and cosmology are able to be tested by forthcoming cosmological surveys, perhaps bringing us to a new paradigm of cosmological physics.

Acknowledgements

I would like appreciate all who have come along with my Ph.D. research. The work for this thesis is publicly supported by Research Fellow of the Japan Society for the Promotion of Science. No. 17J04978 and the aid from the budget of the Nagoya University - University of Edinburgh Joint Degree Program. To begin with, I would like to thank Prof. Naoshi Sugiyama, who has patiently taught me, giving fruitful comments and opportunities to develop my Ph.D. work. As different from an ordinal style of supervision, Prof. N. Sugiyama have prescribed a broader opportunities to allow me to join the cutting-edge studies with young researchers and international collaborations. In particular, the postgraduate program between Nagoya University and the University of Edinburgh, I have a precious chance to be supervised by Prof. John. A. Peacock, who gave me a new field of research. I would like to thank John to spend time on my startup of data analysis and many insightful discussions.

I would like to thank to Dr.Yuko Urakawa and Dr. Hiroyuki Tashiro who enlightened me to get involved in the study of gravity in the first two years for the master course. Thanks to the early experiences of research, I could find my own interests to look into further both in theoretical and observational ways of studies. I would like to thank Dr. Atsushi Nishizawa and Dr. Purnendu Karmakar to have unveil a new domain of research to probe the large class of the modified gravity theories by upcoming observations. I would like to those who have discussed and commented on my works in various conferences.

I would like many of friends and staffs to share joyful time with me in sports, games, short travels, drinking, chatting, and any other than research duties. Those have made me refreshed and more insightful for my life.

In the end, I would give special thanks for my parents to be patient for my way of achievement of Ph.D. study. As our family has been going through the difficult time that my father has caught dementia, being required long-term care. Nevertheless in such a hard circumstance, my mother have whenever I am not with her. Moreover, colleagues of my mother and caregivers have helped my father while I was working on Ph.D. studies. I would like to thank you for all people who have patiently helped my father during my Ph.D. study. I would devote this thesis to my father, who have inspired me to be a scientist in my youth.

List of Publications

1. **S. Arai** , S. Sibiryakov, and Y. Urakawa, "Inflationary perturbations with Lifshitz scaling universe", JCAP 1903. no.**03**,-034 (2019)

2. **S. Arai** , H. Tashiro, and D. Nitta, "Test of the Einstein equivalence principle with spectral distortion of the cosmic microwave background", Phys. Rev. D **85**, 124048 (2016)

3. **S. Arai** and A. Nishizawa, "Generalized framework for testing gravity with gravitational waves propagation II: Constraints on Horndeski theory", Phys. Rev. D **97**, 104038 (2018)

4. A. Nishizawa and **S. Arai**, "Generalized framework for testing gravity with gravitational waves propagation III: Future prospect", Phys. Rev. D **99**, 104038 (2019)

5. **S. Arai**, P. Karmakar, and A. Nishizawa, "Cosmological evolution of viable models in the generalized scalar-tensor theory", arXiv: 1912.01768 (submitted in Physical Review D on Dec.7th)

Contents

Chapter 1

Introduction

"I am just a child who has never grown up. I still keep asking these 'how' and 'why' questions. Occasionally, I find an answer."
The Brief History of Time, Stephen Hawking

Curiosity of human-kind has been the main engine to discover a new item to look through the world. Throughout the human history, curiosity has played an essential role to develop the civilisations, changing the ways of living. When it comes to think of the world itself, the history shows the human curiosity on the recognition of the world has been deepened and detailed, resulting in abundant knowledge. On one hand, the knowledge of the world has been developed in religions all over the world. Ancient mythologies in different parts of the world synchronously describes the "origin" or "fate" of the world. A famous example is told in The Bible as such the holy light emerges from the vacant space, which is created by the God. One the other hand, science has been established to pursue the ultimate description of the world. Since G. Galilei claimed that the geo-centrism supported by Christian authorities was less fitting with real observations of the moons of Jupiter than herio-centric explanation of circular motion, experimental and observational results have been regarded as powerful tools to understand the world. Science is thus a peculiar form of the curiosity such that it is verified by producing experiments and observations, transforming our knowledge in more conclusive ways. In modern perspective, science is the arena for human curiosity, which is open for us.

Prof. Stephen Hawking (CH, CBE, FRS, and FRSA) is one of the established

scientists with his extraordinary curiosity. Prof. Stephen Hawing may be the first person how obtained some concrete grasp of the origin of the Universe without the help of Gods/Goddesses, in the mean time other philosophers may have tried to answer the same questions. On the basis of mathematics and physics, Prof. Hawking can describe why the Universe exists and how it begins. What Prof. Hawking uses to describe the origin of the Universe is Einstein's general relativity and thermo-dynamical features of matters. The laws of physics have been established by a number of experiments on Earth. However, it is still hypothetical that the matters distributed in the Universe really obeys the standard laws of physics. Therefore, it is essential to verify the laws of physics throughout the history of the Universe. This is what we have to answer beyond what Prof. Hawking has done.

Cosmological physics

Cosmological physics is a part of physics such that at a "cosmological timescale", being constructed via fundamental mathematics and physics. The cosmological timescale may be infinite amount of time, or some finite timescale. This may depend on some conceptual questions; what is the Universe exactly? It was not clear until Albert Einstein invented the general relativity in 1915. Interestingly, the general relativity gives us a universe with finite lifetime e.g. the big crunch. By contrast, the universe never stops expanding, reaching the state called "big rip" where every elementary particle is believed to be striped away with each other. Some intermediate phase of the universe is called big bounce. The fate of the Universe highly depends on the composition of matters. In the microscopic level, the lifetime of the vacua is not infinite, i.e., the spontaneous symmetry-breaking. In fact, phase transitions of the vacuum states occurs in the early universe, such as QCD and Electro-Weak scales. In modern perspective, cosmological physics well describes the co-evolution of matters and the Universe, summarising in Big Bang Theory.
Another aspect of cosmological physics is the falsifiability that hypothetical arguments by astronomical observations. Starting from the successful measurement of the cosmic expansion by E. Hubble in 1929 (Recently, it has been pointed out that G. Lemaître theoretically discovered the cosmic expansion earlier than Hubble based on Einstein's general relativity.) The cosmic microwave background (CMB) was firstly discovered by A. Penzias and R. Wilson in 1964, which is one of the direct evidence of Big Bang theory. Observations of CMB anisotropy by using the well-resolved space satellites (e.g., WMAP, Planck) explicitly. The measurement of Baryon Acoustic Oscillation (BAO) by CMB or the distribution of galaxies evidently show that the elemental particles

and atoms are well described by electro-magnetic plasma with gravitational constraint force. Mechanically speaking, the acoustic waves are generated by vibration of gravity and relativistic pressure of baryons. This implies that standard physics of gravity and electro-magnetism are in the early Universe. The ratios of the light elements such as hydrogen and helium is well coincident with the theoretical prediction of Big Bang Nucleosynthesis (BBN). The sky surveys have shown that galaxies are clustering as they gather by gravitational interactions at density peaks. The peaks of density corresponds to the slight inhomogeneous fluctuations at the beginning of the Universe, so-called the primordial fluctuations. The origin of the primordial fluctuation is understood the Heisenberg's uncertainty relation of space-time itself. After all, Big Bang theory is established in theory and observation.

Riddles in cosmology

The cosmological physics confronts against new findings as observations reach at more precision. One of the biggest findings is that the discovery of late-time acceleration of the Universe, the cosmic acceleration, by the observations of Type-Ia supernovae in 1998. According to the measurements. The domination of matter should end at present Universe, somehow making the cosmic expansion accelerated "against" attractive nature of gravity. Although the smallness of vacuum energy, the cosmological constant, has been believed to be accountable for the cosmic acceleration, the smallness of the cosmological constant would make the hierarchy problem in particle physics much worse.

As commonly noted in cosmology, the initial conditions of the Universe looks extremely homogeneous and isotropic. We shall hypothesise as the cosmological principle. The cosmological principle is satisfied with an inflationary initial condition of the Universe, i.e., the exponentially fast expansion of the Universe. Interestingly, the energy scale of the inflationary Universe that is consistent with observational data is close to the symmetry breaking scales of the standard model of particle physics. Moreover, an additional scalar degree of freedom induced by symmetry breaking, i.e., Nambu-Goldstone mode can be a good candidate of the dynamical degree of freedom that dominates the inflationary Universe, i.e., inflaton. However, it is uncertain to determine the specific mechanism of symmetry breaking by experimental or observational ways.

The question of the initial condition of the inflationary Universe is also not fully understood. To deal with phenomenological arguments above the inflationary energy scales, we should construct concrete description of quantum gravity since the quantum

correction at Planck scale, 10^{19}GeV, is no longer negligible. Except the string theory, it has been little known how we compute the quantum gravity of gravity. More conceptual issues related to the origin of space and time, e.g., cyclic, ekypilotic, initial conditions are also possible way out from the difficulty of quantum gravity, the falsifiability of such scenarios has not been established.

Cosmological playground

One might be suspicious whether or not the riddles can be solved at the end of the day. In physics, the falsifiability of the physical principles we have believed in is an essential key, or the only path, to get an answer of the true description of the Universe.

There is a playground in which one breaks the fundamental principles without conflicting with the existing experiments and observations. A popular way to do this is to introduce an Effective Field Theory with a certain cutoff scales. The mathematical extension of a theory is another possible way to find a new framework to describe. Note that the string theory is one of the possible realisation that has been actively investigated in physics and mathematics. In the past decades, the modification of gravity has been intensively researched as a new way of explaining the cosmic acceleration and inflation. In wider perspective, it is able to construct a more general framework of physics.

On top of theoretical frameworks to discuss new venue of physics, data and computational resources give chances to go beyond the existing theories. Thanks to the national and public funding, astronomical observation has been rapidly developed, being considered as the precision science. In fact, the precise measurement of CMB anisotropy by Planck satellite has cosmology has been matured as the science in high precision. In the next decades cosmology sees the most speculating and challenging moment in human history. The computational resources are more enlarged in memory storage and CPU operations. Hence, we have a variety of opportunities to start to probe physics with unprecedented realisations of tests.

What this thesis answers

In this doctoral thesis, we develop the framework for testing the fundamental principles lied behind the gravitational and cosmological physics. More specifically, we address the following questions;

- Phenomenological behaviour of additional scalar degree of freedom that couples with gravity and observational consequences

- The local Lorentz invariance is really preserved at the early Universe? If it is not, how can we test that?
- Whether or not structure formation really follows Einstein gravity? Can we conclude that statement is true by existing observational data?

Each of these questions is discussed in Chapter 4, 5, and 6, respectively. At last, we summarise our results with new answers and questions. In Chapter 4, we consider the generalised scalar-tensor theories, arguing how the additional light scalar degree of freedom behaves at late-time Universe. In Chapter 5, we consider the local Lorentz invariance of the Universe in the initial state, i.e., inflationary Universe. Then we argue how the primordial fluctuations carries the information of Lorentz invariance. In Chapter 6, we try the data analysis to measure the gravitational lensing of CMB. We use the data of galaxies measured in radio wavelength. We discuss how it is possible to test Einstein gravity at high redshifts. Throughout this thesis, we take the conventional cold dark matter. The chapters 4, 5, and 6 are based on the publication of the authour shown in [1, 2, 3, 4] (my publication), or alternatively in the beginning of the thesis. Note that the figures, tables, derivations, and analyses shown in 4, 5, and 6 are the original works developed by the authour.

Chapter 2

Standard gravitation and cosmology

The double pillars of gravitation and cosmology describe the physics for of the largest distances. Since firstly Sir. I. Newton discovery the universal law of gravity for planet motions as an augmentation of free falling law of gravity on the Earth, gravity has become the fundamental force that organises phenomena out of the Earth. Cosmology had been in in mythology and religion for dozens of centuries, until it became what was scientifically treated after Einstein's extension of gravity in space and time, that is a virtual foundation of our recognition of the Universe. No sooner developments for science for cosmology did happen if Einstein's gravity theory was not constructed. After the discovery of Einstein gravity theory, one one hand, Einstein's general relativity has been mathematically deepened. On the other hand the bunch of astronomical observations has caught the signals from outer space and mapped millions of galaxies in the sky. By focusing on the latest two decades, scientific cosmology has seen the swiftest developments as the technologies for astronomical surveys are upgraded and computational sources of simulations achieved, where we are living a golden age for cosmological science. Besides, the very recent discovery of gravitational waves and the visualisations of black holes have opened up the new phase on gravitational science. In this chapter, we review the established understanding of gravitation and cosmology throughout history, finding scientifically robust and conclusive scenarios how the observed Universe looks like in prior to jump into the frontier of gravitation and cosmology in the forthcoming Chapter 3.

2.1 Standard gravity

The theory of gravity stared with an analysis of hyperbolic trajectory of falling matters in acient Greek,for which was available for developing weapons in wars. In the mean time, Aristotle made a theory of elements so-called classical elements,i.e., earth, water, air, fire. Classical elements tells that gravity differently works on each elements in accordance with the closeness of its origin to the Earth. After the long domination of the classical element, Galileo Galilei pointed out the law of inertia by falling-matter experiments, showing indistinguishability of matters in gravity force. I.Newton invented the law of dynamics, as well as finding the universal law of gravity for the orbital motions of celestial bodies. At this time, the mass or inertia of gravitational interactions was tacitly assumed to be exactly the same as the inertial mass. In other words, the oldest law of gravity already contains the assumption of the equivalence between the true mass of a matter and the strength of gravity, which is later introduced by Einstein in the form of the equivalence principle.

2.1.1 Newtonian gravity

In a homogeneous gravitational field, such as on the Earth surface, the equation of motion of free falling is written as

$$m_I \frac{d^2x}{dt^2} = 0\,, \tag{2.1.1}$$

$$m_I \frac{d^2y}{dt^2} = -m_G g\,, \tag{2.1.2}$$

where g denotes the gravitational acceleration $g = 9.80665\ \mathrm{m}^2 \cdot \mathrm{s}^{-1}$. We assume that

$$m_G = m_I\,, \tag{2.1.3}$$

which is the primitive form of the equivalence principle. Newton extended the gravity theory for the explanation of Kepler's law;

1.

The Kepler's law of planet motions are mathematically described by the Newton's equation of motion and the gravity force with inverse squared law,

$$F_G = \frac{G_{\mathrm{N}} m_G M}{r^2}\,, \tag{2.1.4}$$

We show that gravity makes system bounded. Provided that an object whose mass and velocity is m and v respectively falls by gravity. The total energy E is given by

$$E = \frac{1}{2}mv^2 - \frac{G_{\rm N}M}{r}\,, \tag{2.1.5}$$

The systems are classified as Then the maximum radius where the object can be dragged back by gravity is given as

$$r_{\rm esc} = \sqrt{\frac{2G_{\rm N}M}{v^2}}\,, \tag{2.1.6}$$

Although gravitational force are nothing to do with the property of a matter which feels gravity, the strength of gravity fields around a matter is created by the distribution of matters. Formally, the law of gravity is defined with Poisson equation in a given density field is given as

$$\nabla^2\Phi = 4\pi G_{\rm N}\rho\,, \tag{2.1.7}$$

The equation has the exact solution,

$$\Phi(\mathbf{r}) = -G_{\rm N}\int d^3\mathbf{r}'\frac{\rho(\mathbf{r}')}{|\mathbf{r}-\mathbf{r}'|}\,, \tag{2.1.8}$$

Then the equation of motion in gravitational potential is given as

$$\frac{d^2\mathbf{r}}{dt^2} = -\nabla\Phi\,, \tag{2.1.9}$$

The dynamics of continuous fluid is described by Euler equations

$$\frac{\partial\rho}{\partial t} + \nabla\cdot(\rho\mathbf{u}) = 0\,, \tag{2.1.10}$$

$$\frac{\partial\mathbf{u}}{\partial t} + \mathbf{u}\cdot\nabla\mathbf{u} = -\nabla P - \nabla\Phi\,, \tag{2.1.11}$$

These equations give a number of applications in astrophysics to picture the gravitationally bounded objects, such as planets, stars, and galaxies. Poisson equation is linear in a density field and a gravitational field. Therefore it is reasonable that gravitational fields from multiple sources of density are given by the superposition of the fields that are solutions for each distinct sources.

2.1.2 Theoretical difficulty in Newton gravity

Newtonian gravity has plagued with the theoretical pathology and observational discrepancies in the late 19th century. In theory, it is the fact that Newtonian gravity at the largest scale with non vacuum state has no solution. Provided that the density field is homogeneous in the whole space, i.e., $\rho = \bar{\rho} = \text{const.}$. By inserting $\rho = \bar{\rho}$ into Eq. (2.1.8), then Φ is constantly divergent. This means that the Newton potential with the homogeneous medium does not exist. Another perspective of the illness of Newtonian gravity is shown by applying Poisson equation in Eq. (2.1.8) and considering Euler equation of a fluid in Eq. 2.1.11. In the static and homogeneous medium, the velocity field $\mathbf{v} = \mathbf{0}$ and the pressure P is constant. As a result, the second Euler equation reduces to $\nabla\Phi = 0$, which does not accommodate with the Poisson equation in Eq. (2.1.7) except $\bar{\rho} = 0$. The non-existence of the homogeneous solution with matters eventually lead an inhomogeneous universe. Since the gravity force is attractive, the inhomogeneous matters will collapse within a finite time. Then this lead to the revival of the the thought that the Universe has its centre by means of the centre of the current Universe we lived in. However, the break of Copernican principle seems not fit with a majority of observational evidences, replaced by the cosmological principle.

Gravity at short distances, the self interaction of gravitational field at smaller scale is divergent in distance,i.e., $r \to 0$ since the gravitational field Φ is given as $\Phi \sim -G_{\mathrm{N}}M(r)/r$ where $M(r)$ denotes the mass within radius r, $M(r) = \int^r dr' 4\pi r'^2 \rho(r')$. The similar problem is happening in Coulomb potential, but it is removed in the process of renormalisation of electric charge. In the gravitational field, in contrast, the prescription does not work because of the non renormalisability of gravity.

The difficulty of Newtonian gravity in a strong field limit is also described from another perspective. Since the Poisson approximation is a linear equation, in prior assuming that the gravitational field is small, i.e., gravity is weakly coupled with density fields. The insights how the weak filed approximation would break down come along with considering as follows. In 18th century by P.S.Laplace and (someone), the idea of an object such that the light no longer comes out the object was firstly proposed. The outer boundary of the object is given by the radius $r_s = 2G_{\mathrm{N}}M/c^2$ where M is the mass of the object, namely that the escape velocity reaches at the speed of light. This conceptual object is later identified as "Black Hole" in the context of the Einstein's gravity theory. What is peculiar of this object is that it states the limit of visual recognition. In other words, there are very few way to prove the existence of the objects by experiments and observations. Experimentally, the object is hard to see because it does not emit any light outside. Observationally, the object is extremely massive and

compact, such as 1mm for the Earth mass or 3km for the solar mass. Thus there is no physical evidence to believe that the Newtonian weak field limit of gravity for this object is still available or not. In the current establishment of physics, hundreds of black holes has been found and the Newtonian gravity is actually broken requiring the sophistication of Einstein's gravity. To see that weak field approximation breaks down, the observational phenomena called perihelion motion of the mercury was discovered, which did not fit in the Newtonian gravity at perturbative order, except assuming the unknown planet "Vulcan" as a source of gravity. All the problems of the Newtonian gravity was smartly solved with the Einstein's gravity. The Einstein's gravity successfully explain the perihelion motion of the mercury, whereas the homogeneous solution at the largest scale exists.

2.1.3 Einstein gravity

What makes the Einstein's gravity characterised is the existence of geometrical curvature on top of the normal Newtonian gravity and the principle of general relativity. Although the equivalence principle holds in the Einstein's gravity, the curvature plays a novel role to predict the gravitational lensing, the propagation of the gravitational waves, and the causal structure of the universe, i.e., light-cone effect. The gravitational lensing was measured in 1919 for the first time in the solar eclipse, and then we have seen the lensing effect even at cosmological scales nowadays. The gravitational waves, on the contrary, has been unveiled in the next 100 years since its prediction, however the detection of gravitational waves is realised by LIGO observatory in September in 2015. Therefore, there are no more doubt that the approximation what Einstein made is true. What is left as a problem, however, reaches a new realm of physics; the cosmological constant problem, weakness of gravity in the perspective of grand unification of physical theories, and the quantum feature of gravity.

A trajectory of a free fall particle is replaced by the geodesic equation

$$\frac{d^2x^\mu}{d\tau^2} + \Gamma^\mu_{\nu\lambda}\frac{dx^\mu}{d\tau}\frac{dx^\nu}{d\tau} = 0\,, \tag{2.1.12}$$

where $\Gamma^\mu_{\nu\lambda}$ is the Christoffel symbols defined as

$$\Gamma^\mu_{\nu\lambda} \equiv \frac{1}{2}g^{\mu\rho}(\partial_\nu g_{\rho\lambda} + \partial_\lambda g_{\nu\rho} - \partial_\rho g_{\nu\lambda})\,, \tag{2.1.13}$$

The Riemann curvature tensor is given with the Chrisotoffel symbols

$$R^\mu_{\nu\rho\sigma} = \partial_\rho\Gamma^\mu_{\nu\sigma} - \partial_\sigma\Gamma^\mu_{\rho\nu} + \Gamma^\mu_{\rho\lambda}\Gamma^\lambda_{\nu\sigma} - \Gamma^\mu_{\sigma\lambda}\Gamma^\lambda_{\rho\nu}\,, \tag{2.1.14}$$

In 4d space-time, it is useful to think the decomposition of Riemann tensor which is given as

$$R_{\mu\nu\rho\sigma} = \frac{R}{12}(g_{\mu\rho}g_{\nu\sigma} - g_{\mu\sigma}g_{\nu\rho}) + \frac{1}{2}(g_{\mu\rho}S_{\nu\sigma} - g_{\mu\sigma}S_{\nu\rho} - g_{\nu\rho}S_{\mu\sigma} + g_{\nu\sigma}S_{\mu\rho}) + W_{\mu\nu\rho\sigma}\,, \tag{2.1.15}$$

where $S_{\mu\nu}$ is the trace-less part of Ricci tensor given

$$S_{\mu\nu} = R_{\mu\nu} - \frac{R}{4}g_{\mu\nu}\,, \tag{2.1.16}$$

$$R_{\mu\nu} \equiv R^{\rho}_{\mu\rho\nu}\,, R \equiv g^{\mu\nu}R_{\mu\nu}\,, \tag{2.1.17}$$

$$W^{\rho}_{\mu\rho\nu} = 0\,, \tag{2.1.18}$$

The tidal gravitational interactions is given via the geodesic deviation equation

$$\frac{d^2V^{\mu}}{d\tau^2} = -R^{\mu}_{\nu\rho\sigma}u^{\nu}u^{\rho}V^{\sigma}\,, \tag{2.1.19}$$

where u^{μ} is the tangent vector for geodesic equation and V^{μ} is the displacement vector of geodesic equation.

The condition of matter is given by the conservation law of matters,i.e. Euler equations,

$$\nabla_{\mu}T^{\mu}_{\nu} = 0\,, \tag{2.1.20}$$

meaning the energy and momentum conservation of matters. After specifying the geometrical quantity that satisfies the Bianchi identity as the Einstein tensor, $\nabla_{\mu}G^{\mu}_{\nu} = 0$, then we obtain the Einstein equation,

$$G_{\mu\nu} = \frac{8\pi G_{\rm N}}{c^4}T_{\mu\nu}\,, \tag{2.1.21}$$

In terms of the action principle, the Einstein equation is obtained from

$$S_G = \frac{1}{16\pi G_{\rm N}}\int d^4x\sqrt{-g}R\,, \tag{2.1.22}$$

where R is the Ricci scalar.

2.2 Principles and symmetries in Einstein's gravity

The establishment of the Einstein gravity has impacted on the description of space and time, replacing the old Newtonian gravity. Observationally, Einstein gravity has confronted a number of tests and experiments, leaving as the well-supported theory of gravity ever made. Theoretically, on the contrary, it has been revealed that Einstein gravity is the simplest and unique realisation of geometrical gravity under the following principles; the equivalence principle, the general covariance, Lorentz invariance, and locality in the dimension four.

The question arises as how the fundamental principles of the Einstein gravity play their roles in theory and phenomenology. For instance, how crucial is the dimension of spacetime set to four?. Another one can be asked as what is expected when the equivalence principle does not work? These questions make an interesting direction to probe gravity. Theoretically, the UV incompleteness of the Einstein gravity is a thorny issue, but there can be a way out to change some of the principles of the Einstein gravity, being healthy in UV. Or, the change of the principles may create unwanted plagues of theory in physics. Phenomenologically, the change of the principles may differ the gravitational interactions from that of Einstein gravity, bringing an opportunity for testing the fundamental principles of gravity. By these motivations, one can get interested in the field of studies of what the gravitational physics can be more profound than Einstein gravity.

2.2.1 Equivalence principle

The equivalence principle simply states the equivalence of the inertial mass and the gravitational mass. Let us consider test particles that flow along a gradient of a gravitational potential.As a result, all the test particles feel the exactly the same gravitational force in space-time. The equivalence principle is satisfied in Newtonian gravity, meaning that the principle is not the necessity condition for the Einstein gravity. Therefore, it is necessary to test the equivalence principles by experiments and observations. In accommodation with the general relativity, the equivalence principle is more extended into the strong equivalence principle, meaning the gravitational energy is always equivalent to the inertial mass energy that makes gravitational fields in any spacetime, such as black holes and expanding universe. In this sense, a cosmological model in Einstein gravity gives a significant test of the equivalence principle. Once the equivalence principle is broken, it is not necessary that all the degree of freedoms follows the minimal coupling of gravity.

2.2.2 Lorentz invariance

Lorentz invariance was firstly suggested in the argument of electro-magnetism and its extension to the dynamics; the special relativity. Lorentz invariance simply determines that the speed of any massless particles universally the same to that of speed of light. In the quantum field theory, Lorentz invariance, or Poincare invariance gives fundamental representations of fields, and it is known that Lorentz invariance is stable at quantum level without causing any pathology such as acausal interactions or anomalies. The observational and experimental tests of Lorentz invariance have been made especially in the particles of standard model of particle physics.

$$x^\mu \to x'^\mu = \Lambda^\mu_\nu x^\nu \,, \tag{2.2.1}$$

Lorentz coordinate transformation unchanges the metric $\eta_{\mu\nu} = \mathrm{diag}(-,+,+,+)$,

$$\eta_{\mu\nu} = \Lambda^\rho_\mu \Lambda^\sigma_\nu \eta_{\rho\sigma} \,, \tag{2.2.2}$$

In four dimensional space, the spacetime metric with Lorentz invariance is uniquely given as the Minkowski space. Lorentz invariance determines the causal structure of a theory,

$$ds^2 = \eta_{\mu\nu} dx^\mu dx^\nu \,, \tag{2.2.3}$$

- timelike : $ds^2 < 0$,
- null : $ds^2 = 0$,
- spacelike : $ds^2 > 0$,

Except the non infinitesimal transformation such as the parity transformation or time reversal transformation, Lorentz transformation does not mix the timelike/null/spacetime structures with each other. Under the general covariance, Lorentz invariance is locally satisfied irrespective to a local coordinate transformation. The Lorentz invariance with the general covariance determines the causal structure of spacetime.

2.2.3 General covariance

General covariance fundamentally determines the geometrical structure of Einstein gravity. General relativity is considered as the general extension of the Galilean invariance in the Newton mechanics. The mathematical expression of general relativity

is given by the invariance under the coordinate transformation $x^\mu \to x'^\mu(x)$. The metric tensor $g_{\mu\nu}$ transforms in the coordinate transformation,

$$g_{\mu\nu} \to \frac{\partial x^\rho}{\partial x'^\mu}\frac{\partial x^\sigma}{\partial x'^\nu} g_{\rho\sigma}\,, \tag{2.2.4}$$

All the physical quantities are required to be invariant under the coordinate transformations. In the mathematical language, the general relativity is nothing but the diffeomorphism invariance on a Riemannian manifold. All the symmetries in the general covariance are divided into global or local symmetry. The global symmetries in the general covariance is

- time translation
- global spatial homogeneity
- global spatial isotropy

all of which are the sub-transformation of the global Lorentz symmetry. The specific configurations of space-time are Minkowski space or de Sitter space. The FRW spacetime does not have the time translation symmetry. The local symmetries, on the contrary, are given by any infinitesimal transformation between the space-time coordinates. In other words, the local symmetries are described with a group of a local gauge transformation. In a specific case, one enables to confirm that the local Lorentz symmetry is actually conserved in general covariant theory. We specifically see the subgroup of the general covariance.

Translation invariance

Translation invariance denotes the system does not change the time translation by any constant, i.e.,

$$x^\mu \to x^\mu + \text{const.}\,, \tag{2.2.5}$$

In theories without gravity, since the space-time is given as the Minkowski space-time, the translation invariance always realises. When including gravity, however, the time translation invariance is no longer respected, except the de Sitter space. Note that is the generalisation of the Galilean translation invariance in the Newton's classical theory of motion.

Parity invariance

The parity invariance is the symmetry such that physical quantities does not change by a coordinate transformation in spatial coordinates, i.e., $\mathbf{x} \to -\mathbf{x}$. Under the general covariance, it is possible to make operators in a Lagrangian that breaks the parity invariance. For instance, we consider the term like $R_{\mu\nu\rho\sigma}\tilde{R}^{\mu\nu\rho\sigma} \equiv \epsilon^{\rho\sigma\rho'\sigma'}R_{\mu\nu\rho\sigma}R^{\mu\nu}{}_{\rho'\sigma'}$. Here $\epsilon^{\rho\sigma\rho'\sigma'}$ is the totally anti-symmetric epsilon tensor. The Einstein gravity is given only by the Ricci scalar R in the Lagrangian formulation, automatically parity invariant.

Diffeomorphism invarinace

The rest part of the general covariance is the diffeomorphism invariance, stating that all the physical quantities are invariant under any infinitesimal coordinate transformation. In Riemaniann geometry, the diffeomorphism invariance is realised any qunatity contracted by the metric tensor, $g_{\mu\nu}$ in the line element $ds^2 = g_{\mu\nu}dx^\mu dx^\nu$.

2.2.4 Locality

The locality is fundamental so that the physical phenomena would be well isolated once we assume the interaction would decay as the distance gets large. The locality firstly came out with the conceptual controversy on the instantaneous interaction in the Coulomb's law of electric forces. The issue of instantaneous interactions in the Coulomb's law was theoretically superseded by Maxwell's Equations of electromagnetism, and accomplished for the Newton law of gravity by Einstein in the framework of general relativity. Previously, the homogeneous solution in the Newtonian gravity would violate to the locality or homogeneity (see Jean's swindle), but this reconciles when we assume the general relativity and the equivalence principle (see Birkov's theorem). In the context of quantum theory, the locality is not satisfied by observing the violation of Bell's inequality. In quantum mechanics, the entanglement will carry the non-local information, or global symmetry will take place as non-local effects.

2.2.5 Observational tests of gravity

The experiments and observations for testing gravity has been presented for many years. The discovery of the Hulse-Taylor pulsar measured the decrease rate of the orbital period, proving it precisely matches what the Einstein's gravity predicts. The Cassini space craft firstly achieved the Shapiro time-delay made by the Sun's gravity field. The lunar laser ranging measures how the mutual orbit at the centre of the mass

of the Moon and the Earth fit with the Newton's gravity law. Recently, the detection of gravitational waves has open up a test of Einstein gravity in strong field regime, showing no significant evidence of a violation of Einstein gravity. In conclusion, we recognise that there is no evidence of any deviation from the Einstein's gravity.

2.3 Standard cosmology

More than 70 years have passed since G. Gamow proposed Big Bang Theory, and as a collection of research in astronomy, Big Bang Theory has become a monument in human history. Based on Big Bang theory, the universe begins with a high temperature and density, and then becomes a dynamic universe that expands. Cosmic expansion was firstly discovered in 1929 by observations of nearby galaxies by E. Hubble. Furthermore, as a remnant of the universe being in thermal equilibrium, the current universe is filled with Cosmic Microwave Background (CMB). After the discovery of CMB by A.Penzias and R.Wilson in 1964 by measuring $3K$ black-body radiation from the sky, the number of probes has been done. The first satellite mission to catch CMB light is COBE [5], finding $2.725 \pm 0.0001\ K$ with the temperature fluctuations at μK level.

WMAP [6] and Planck satellites [7]. WMAP and Planck satellites precisely measured the anisotropy of CMB temperature and polarisation. Since the angular correlations of CMB anisotropy is precisely measured, the parameters of the Big Bang Universe model are precisely determined by the observation data of CMB. Meanwhile, observations of distant type Ia supernovae [8, 9] revealed that the current universe is acceleratingly expanding. In the end, the standard model of the Universe, i.e,, the ΛCDM model has been established. The matter content of the Universe is well approximated by the pressure-less matter. This is called the Cold Dark Matter. The insufficiency of the atomic or baryonic matter by the explanation of galaxies rotation curves, it is commonly accepted that the majority of the matters that gravitates the galaxies is believed to be a dark matter.

2.3.1 Cosmic expansion

Cosmological principle

The cosmological principle has been argued one of the fundamental property of the Universe we observed. In the mid 1920, the majority of astronomer blindly believed that the universe has a centre, i.e, the break of Copernican perspective or Copernican principle. However, Edwin Hubble observationally prove that the measurement of the recession velocity of galaxies is almost isotropic from us Inhomogeneity of the

Universe falsified by 6dF galaxy surveys, which achieved the Large Scale Structure of the Universe for the first time, revealing that the distribution of the galaxies looks fluctuated on the homogeneous mean density field. The measurement of the CMB conclusively suggests that the microwave radiation follows isotorpy at the 10^{-5} accuracy. In a practical application, the statistical analysis of observable. The cosmological principle is a strong working principle to compare the observable quantities and theoretical predictions.

Friedmann-Lemaître-Robertson-Walker spacetime

The homogeneity and the isotropy of the spacetime is uniquely given by the FLRW metric at four dimension. Under the cosmological principle and a simple topology, the geometry of the universe is uniquely determined in FLRW metric. The solution described as a solution when the space-time is considered to be uniformly isotropic. A homogeneous and isotropic spacetime metric is Friedmann Robertson Waker (Lametre) metric is given by

$$ds^2 = -dt^2 + a^2(t)\gamma_{ij}dx^i dx^j \,, \tag{2.3.1}$$

Here, a is the scale factor, γ_{ij} is the spatial metric. The temporal component of Ricci tensor is given by

$$R_{00} = -\frac{3\ddot{a}}{a} \,, \tag{2.3.2}$$

$$R_{0i} = 0 \,, \tag{2.3.3}$$

$$R_{ij} = \left[\frac{\ddot{a}}{a} + 2\left(\frac{\dot{a}}{a}\right)^2 + \frac{2K}{a^2}\right]\delta_{ij} \,, \tag{2.3.4}$$

In general, the curvature of the Universe is non-zero value, K. The 3d Riemann curvature tensor is given by

$${}^{(3)}R_{ijkl} = K(\gamma_{ik}\gamma_{jl} - \gamma_{il}\gamma_{jk}) \,, \tag{2.3.5}$$

and 3d-Ricci tensor is given as

$$\begin{aligned} {}^{(3)}R_{ij} &\equiv \gamma^{kl\,(3)}R_{ijkl} \\ &= 2K\gamma_{ij} \,, \end{aligned} \tag{2.3.6}$$

Hubble - Lametre's Law

The cosmic expansion given in the Friedmann equations gives the time evolution of the expansion history. The Hubble - Lametre's Law states how the expansion looks like from a local observer in a fixed cosmological time. The Hubble - Lametre's Law is briefly derive from the metric in Eq. (2.3.1). Let's consider a local observer located at $(x, y, z) = (0, 0, 0)$. To the observer, the velocity at the physical distance at $\mathbf{x} = a(t)\mathbf{x}_{\rm com}$ with is

$$\frac{d\mathbf{x}}{dt} = a\dot{\mathbf{x}}_{\rm com} + H\mathbf{x}\,, \tag{2.3.7}$$

where $H = \dot{a}/a$ is the Hubble rate. The first term is called the peculiar velocity, while the second term is called recession velocity. When the peculiar velocity is smaller that the recession, the Hubble - Lemaître's Law

$$\frac{d\mathbf{x}}{dt} \simeq H\mathbf{x}\,, \tag{2.3.8}$$

is obtained. This is what E. Hubble found.

Redshifting

Since an object in a distance from an observer always has a recession velocity in an expanding universe. As a result, the Doppler effect is induced in frequency of observables. This is redshifting.

$$\frac{\lambda_{\rm obs}}{\lambda_{\rm em}} \equiv 1 + z\,, \tag{2.3.9}$$

The light propagation in the expanding universe follows null world line $ds^2 = 0$.

$$\int_{t_{\rm em}}^{t_{\rm obs}} \frac{dt}{a(t)} = \chi_{\rm obs} - \chi_{\rm em}\,, \tag{2.3.10}$$

where $\chi_i (i = {\rm em}, {\rm obs})$ is the co-moving coordinate of an emitter and and observer, respectively Since the co-moving distance unchanges, then we obtain for an infinitesimal time interval for the emitter and the observer as,

$$\int_{t_{\rm em}}^{t_{\rm obs}} \frac{dt}{a(t)} = \int_{t_{\rm em}+\delta t_{\rm em}}^{t_{\rm obs}+\delta t_{\rm obs}} \frac{dt}{a(t)} \tag{2.3.11}$$

and equivalently obtain

$$\frac{\delta t_{\rm em}}{a(t_{\rm em})} = \frac{\delta t_{\rm obs}}{a(t_{\rm obs})}\,, \tag{2.3.12}$$

Then we apply that $\delta t_i = \lambda_i$ for $|\delta t_i| \ll 1/H$. In comparison to Eq. (2.3.9) we obtain

$$\frac{a_{\rm obs}}{a_{\rm em}} = \frac{1+z_{\rm em}}{1+z_{\rm obs}}\,, \tag{2.3.13}$$

This is well known the redshifting by cosmic expansion. Hereafter, the observer frame is fixed to the present universe, i.e., $z_{\rm obs} = 0$. Correspondingly, we set $a_{\rm obs} = 1$ as a reference scale factor. Then, the scale factor is given via the redshift $z_{\rm em}$,

$$a_{\rm em} = \frac{1}{1+z_{\rm em}}\,, \tag{2.3.14}$$

Cosmic distance

A way to measure distance to an object in cosmology is different from the static space-time such as Minkowski space. The distance will change as universe expands, resulting departures from the Euclidean measures in 3d space. Let us introduce two distance indicators. Luminosity distance and angular diameter distance should be shown. The luminosity distance is defined via the energy flux,

$$\mathcal{F} = \frac{\mathcal{L}_{\rm em}}{4\pi d_L^2}\,, \tag{2.3.15}$$

Here $\mathcal{L}_{\rm em}$ denotes the absolute luminosity of the emitter at a static frame. Provided that a photon in a single wavelength $\lambda_{\rm em}$, since the luminosity is in a unit in energy per time $\mathcal{L}_{\rm em} \propto 1/\lambda_{\rm em}\delta t_{\rm em}$. Recall that $\lambda_{\rm em} = a_{\rm em}\lambda$ and $\delta t_{\rm em} = a_{\rm em}\delta t$ by redshifting. The distance without cosmic expansion is nothing but the co-moving scale, χ. By replacing $\lambda_{\rm em}$ and $\delta t_{\rm em}$ by λ and δt, we eventually obtain

$$d_L = {a_{\rm em}}^{-1}\chi\,, \tag{2.3.16}$$

The angular diameter distance is a distance measured by an object whose real size is l and observed angular size is θ. As similar to the Euclidean geometry, it is possible to relate the angular to the distance from l/θ. In an expanding universe, $l = a_{\rm em}\chi\theta$ and thus

$$d_A = a_{\rm em}\chi\,, \tag{2.3.17}$$

is the distance measured by the angular scale. This is called angular diameter distance. Here, χ is co-moving distance.

2.3.2 Cosmic expansion with Einstein's gravity

The FLRW metric successfully explains the Hubble - Lemetre's Law and redshifting. The entire time evolution of the universe, however, yet given. The Einstein equation play a role to determine the cosmic expansion history at a given initial conditions. The Einstein equation is given as

$$G_{\mu\nu} + \Lambda g_{\mu\nu} = 8\pi G_{\rm N} T_{\mu\nu}\,, \tag{2.3.18}$$

The right hand side of the Einstein equation Eq. (2.3.18) is determined when we pick the matter component of the Universe. Conventionally, the covariant energy momentum tensor of the perfect fluid is considered.

$$T_{\mu\nu} = \rho u_\mu u_\nu + P(g_{\mu\nu} + u_\mu u_\nu)\,, \tag{2.3.19}$$

where $u^\mu = (-1, \mathbf{0})$. From Eqs. (2.3.1) - (2.3.19), the Einstein equation Eq. (2.3.18) is obtained as

$$H^2 = \frac{8\pi G_{\rm N}\rho}{3} - \frac{K}{a^2} + \frac{\Lambda}{3}\,, \tag{2.3.20}$$

$$\frac{\ddot{a}}{a} = \dot{H} + H^2 = -\frac{4\pi G_{\rm N}}{3}(\rho + 3P) + \frac{\Lambda}{3}\,, \tag{2.3.21}$$

2.3.3 Composition of Universe

The matter composition of the universe should be observationally given. The universe was made of the relativistic and non-relativistic matters at certain fractions of them, although the current state of the universe is exceptionally dominated. The number of the relativistic species is given by the black body radiation of the cosmic microwave background, unless before CMB was emitted in the bulk. The number of baryonic matter in the total matter density is nicely determined by the amplitude of the baryon acoustic oscillation. The curvature components that could be generated at the birth of the universe is consistent with zero by observing the peak position of the first peak of the CMB anisotropy that is determined by the time when the recombination is achieved.

$$\sum_i \Omega_i(a) = 1\,, \tag{2.3.22}$$

$$\Omega_i \equiv \frac{8\pi G_{\rm N}\rho_i}{3H^2}\,, \tag{2.3.23}$$

where $i = (\text{radiation}, \text{dust}, \text{cosmological constant}, \text{curvature})$.

For clarifying the property of matters in cosmic expansion, it is useful to introduce the equation of state parameter,

$$w_i \equiv \frac{P_i}{\rho_i}\,, \tag{2.3.24}$$

From the Friedmann equations in Eqs. (2.3.20) and (2.3.21), we obtain the following differential equation

$$\rho_i + 3H\rho_i(1+w_i) = 0\,, \tag{2.3.25}$$

This is nothing but the continuity equation of the matter i. In the case of the dust, $w_{\rm dust} = 0$, and relativistic matters. $w_{\rm rad} = 1/3$. Most of the case we consider as a matter, it is justified to set w_i is constant. In this case, the solution of the Friedmann equations in Eqs. (2.3.20) and (2.3.21) is exactly given. Provided that i-th component dominates the universe, i.e, $\Omega_i \sim 1$. Then the solution of Eqs. (2.3.20) and (2.3.21) are obtained as

$$a \propto t^{\frac{2}{3(1+w_i)}}\,, \tag{2.3.26}$$

$$H = \frac{2}{3(1+w_i)t}\,, \tag{2.3.27}$$

here we remove the cases $1 + w_i \leq 0$. In terms of the acceleration is given by

$$\frac{\ddot{a}}{a} = \frac{1+3w_i}{3(1+w_i)}H^2\,, \tag{2.3.28}$$

The condition for the acceleration under $1 + w_i > 0$ is thus

$$\frac{\ddot{a}}{a} > 0 \Leftrightarrow w_i < -\frac{1}{3}\,, \tag{2.3.29}$$

Cosmological constant

Historically the well-known "mistake" of the cosmological constant by Einstein is for evading the cosmic instability with the positive curvature. Based on Lovelock theorem,

the only two parameters, the gravitational constant and the cosmological constant is the free parameter of the Einstein's theory. In the weak field limit of a static spacetime, the gravitational constant uniquely determined, regardless of what value of the cosmological constant. This is because, the cosmological constant is the homogeneous part of the Einstein's field equations completely eliminated from the spacetime via background subtraction. The only way to determine the cosmological constant is thus to measure the expansion rate of the universe. Interestingly the domination of the cosmological constant leads a universe to an accelerating phase; de Sitter universe. The de Sitter models is given with the Friedmann equations

$$H^2 = \frac{\Lambda}{3}\,, \tag{2.3.30}$$

$$\dot{H} = 0\,, \tag{2.3.31}$$

The exact solution is $a \propto \exp(\sqrt{\Lambda/3}t)$, leading the well known exponential expansion of the universe. In summary, the evolution of the universe with different value of the curvature and the cosmological constant are shown.

Relativistic components

The Hot Big Bang Theory presume that in the very early universe, the matter components are relativistic. The peculiar features on the relativistic components is that the density is given in particle physics. The effective degree of freedom g_* will change in time as the detailed nucleic interactions changed. When the relativistic species are in thermal equilibrium, the temperature is uniformly determined. By summing up all the bosonic or Fermionic species

$$\rho_r = \frac{\pi^4}{30} g_* T^4\,, \tag{2.3.32}$$

where

$$g_* = \sum_{\text{boson}} g_{\text{boson}} + \frac{7}{8} \sum_{\text{fermion}} g_{\text{fermion}}\,, \tag{2.3.33}$$

The precise value of g_* is dependent on what type of particle theory you use. In the present universe, the photon (or graviton?) is the only relativistic species. The photon is currently in the state of CMB, and thus the temparature T_0 is measured by COBE $T_0 = 2.725 \pm 0.0001$K. Moreover, the effective degree of freedom $g_* = 2$?. Therefore,

the density parameter for the relativistic components at present, Ω_{r0} is given by

$$\Omega_{r0} = 4.155h^2 \times 10^{-5}\,, \tag{2.3.34}$$

Neutrinos

$$\rho_\nu = \frac{\pi^4}{30} N_{\rm eff} T_\nu^4\,, \tag{2.3.35}$$

Note that $T_\nu = (4/11)^{1/3}T$ because of the entropy transfer at the time when the electron positron annihilation completed. Then the total energy density of the relativistic components are

$$\rho_r = \left(1 + N_{\rm eff}\frac{7}{8}\left(\frac{4}{11}\right)^{4/3}\right) T^4\,, \tag{2.3.36}$$

where the effective degree of freedom $N_{\rm eff}$ is given by $N_{\rm eff} = 3.046$. Recently, the effects of the neutrinos are important to develop the structure in the universe.

Spatial curvature

The value of spatial curvature K is undetermined in theory, and thus it is common that the density parameter for the curvature is in the matter component as well. The density parameter is defined as

$$\Omega_K \equiv -\frac{K}{H^2a^2}\,, \tag{2.3.37}$$

Note that the positive curvature induce the instability of the Universe as a solution of the Friedmann equations in Eqs. (2.3.20) and (2.3.21). The feature of the density parameter of curvature is that it decrease in time when the universe is acceleratingly expanding, i.e., $1/Ha$ decreased in time . This means that any accelerating phase of the Universe may smooth out the information of curvature.

Commenting on that FLRW spacetime itself does not give any instability without the positive curvature case ($K > 0$). The bouncing universe. The summary figure is important to show here.

2.3.4 Structure formation

The structure in the universe evolves by gravity. Current observations show that the current universe has hierarchical structures such as stars, galaxies, galaxy clusters, and

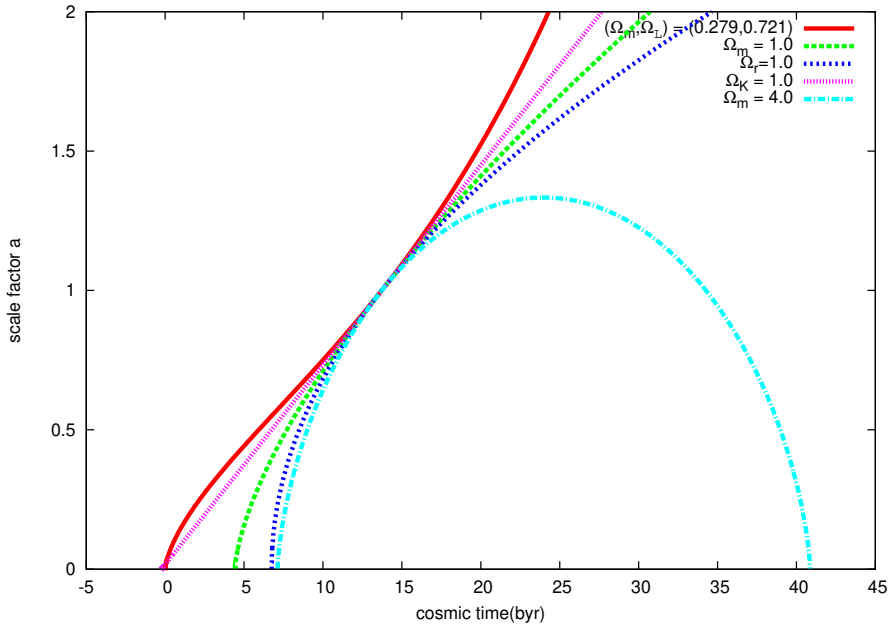

Figure 2.1. The Friedmann equations (2.3.20)[6]

large-scale structures. Cosmological perturbation theory is a powerful technique for calculating the evolution of first order perturbations on a background spacetime. Here we treat only on scalar perturbations.

Evolution of density fields

Time evolution of perturbative quantities, are described through linearised Einstein equation and the energy momentum tensor in Eq. (2.3.19). As a local observer, we take the Conformal Newtonian gauge. In this gauge, the metric is

$$ds^2 = -a^2(1+2\Phi)d\eta^2 + a^2(1-2\Psi)\delta_{ij}dx^i dx^j\,, \tag{2.3.38}$$

Here Φ is Newton potential and Ψ is the scalar curvature perturbation. The density perturbation δ is defined as

$$\delta \equiv \frac{\delta\rho}{\rho}\,, \tag{2.3.39}$$

We consider the evolution of the density field in Fourier space. We define

$$\tilde{\delta}(\mathbf{k},t) = \int d^3x e^{-i\mathbf{k}\cdot\mathbf{x}}\delta(\mathbf{x},t) \tag{2.3.40}$$

Then in the Conformal Newtonian gauge the linearised Einstein equations are decomposed into the two dynamical equations

$$\tilde{\delta}' = -(1+w)(k\tilde{V} - 3\Phi') + 3aHw\left(\tilde{\delta} - \frac{\delta\tilde{P}}{P}\right), \tag{2.3.41}$$

$$\tilde{V}' = -aH(1-3w)\tilde{V} - \frac{w'}{1+w}\tilde{V} + k\frac{\delta\tilde{P}}{P} - \frac{2}{3}k\frac{w}{1+w}\tilde{\Pi} + k\tilde{\Phi}\,, \tag{2.3.42}$$

$$\tag{2.3.43}$$

and the two constraint equations

$$\tilde{\delta} + 3\frac{aH}{k}(1+w)\tilde{V} = -\frac{2}{3}\left(\frac{k}{aH}\right)^2\tilde{\Psi}\,, \tag{2.3.44}$$

$$\tilde{\Pi} = \left(\frac{k}{aH}\right)^2(\tilde{\Phi} - \tilde{\Psi})\,, \tag{2.3.45}$$

V is the divergent term of velocity field. $w \equiv P/\rho$, and Π is the anisotropic stress. Note that the variables with tilde denotes the Fourier mode for corresponding variables. By solving the above four equations, we obtain the time evolution of the density perturbation. When we focus on the matter dominant epoch, $w = 0$ and $\delta P = 0$ are satisfied. If we assume $\Pi = 0$. From Eqs. (2.3.41), (2.3.45), (2.3.68), and (2.3.69), δ follows the second order differential equation,

$$\tilde{\delta}'' + \mathcal{H}\tilde{\delta}' - \left(4\pi G\rho - c_s^2k^2\right)\tilde{\delta} = 0\,, \tag{2.3.46}$$

At larger scales than the Jeans scale, i.e., $k < (4\pi G\rho/c_s^2)^{-1/2}$, we obtain

$$\tilde{\delta}'' + \mathcal{H}\tilde{\delta}' - 4\pi G\rho\delta = 0\,, \tag{2.3.47}$$

This equation has two analytic solutions as

$$\delta = D_+(a)\delta_i\,, \tag{2.3.48}$$

$$D_+(a) = \frac{5}{2}H\Omega_{m0}\int_0^a \frac{dx}{x^2H^2}\,, \tag{2.3.49}$$

where δ_i denotes the initial value of the density perturbation. We define the linear

growth rate f as

$$f \equiv \frac{d \ln D_+}{d \ln a}\,, \tag{2.3.50}$$

If we take the background with Λ-CDM model, f is given as

$$f = -1 - \frac{\Omega_m}{2} + \Omega_\Lambda + \left[\int_0^1 \frac{dx}{(\Omega_m/x + \Omega_\Lambda x^2)^{3/2}}\right]^{-1}\,, \tag{2.3.51}$$

Note that Ω_m and Ω_Λ are time-dependent density parameters,

$$\Omega_m \equiv \frac{\Omega_{m0} a^{-3}}{\Omega_{m0} a^{-3} + \Omega_{\Lambda 0}}\,, \Omega_\Lambda \equiv \frac{\Omega_{\Lambda 0}}{\Omega_{m0} a^{-3} + \Omega_{\Lambda 0}}$$

In the Einstein de Sitter universe ($\Omega_{m0} = 1$), $f = 1$ is satisfied. Moreover, δ grows with the scale factor a, namely reflecting the gravitational evolution of structures as the universe expands. Therefore, the index f is useful to test gravity at cosmological scales.

2.3.5 Initial conditions

The initial condition of the Universe are considered in accommodation with the Big Bang Theory. However, the Big Bang Theory has a pathology to argue the initial state of the universe consistent within the framework of physics.

Flatness problem

The curvature constant could be arbitrary with a nonzero value. The flatness problems appears the subsequent evolution in the universe, the curvature term will exceed the universe than the matter or radiation components. The observations, in contrast, the curvature is should be smaller at present value. Then this puzzles in rationalising how the present curvature is small. This is called Flatness problem.

Horizon problem

The COBE satellite prove that the temperature of CMB is almost isotropic at the level of μK, that is 10^{-5}. Moreover, the successor satellites such as WMAP and Planck virtually found that there are certainly the anisotropic fluctuations of temperature and polarisation exist, revealing that the statistical property of the fluctuations are almost Gaussian. This fact looks strange with second thoughts when the causal interactions in

the very early universe are taken into account. As the universe expands with relativistic or non relativistic matters, the maximum length for physical interactions, the event horizon, shrinks. The present horizon scale, on the contrary, much larger than the past horizons, where the physical interactions in the early universe should have been disorganised in their initial conditions. The CMB measurements are obvious counterexamples for the non-correlations well beyond the limit of any physical contact, by the fact well-correlated physical states as shown in the data. This is called horizon problem.

Relic problem

In the early universe, due to a number of phase transitions including the beyond Standard Model physics, particles generated. The lightest relics or topological defects have yet to be found by observations. This strongly bounds the ways of phase transitions in the early universe, ending up with the normal standard model prediction.

2.3.6 Inflation

Nowadays, inflation is a well-census mechanism to deal with all the problem shown in above. The idea is the provision such that we insert the acceleration of the universe, inflation, before hot Big Bang started. Inflation has been considered as the state in the very early Universe since it was firstly invented [10, 11, 12]. In modern perspective, inflation is defined as the state of the universe that is given by the condition below. The definition of inflation is

$$\ddot{a} = \frac{d}{dt}Ha > 0 \Leftrightarrow \frac{d}{dt}Ha > 0\,, \tag{2.3.52}$$

Slow roll inflation

It has been understood that the acceleration phase of the universe is realised by the slow roll condition. In the literature, the mechanism of the inflation explains with a single scalar field.

$$3M_{\rm pl}^2H^2 = \frac{\dot{\phi}^2}{2} + V(\phi)\,, \tag{2.3.53}$$

$$M_{\rm pl}^2(2\dot{H} + 3H^2) = -\frac{\dot{\phi}^2}{2} + V(\phi)\,, \tag{2.3.54}$$

and the Klein Gordon equation is

$$\ddot{\phi} + 3H\dot{\phi} + V_\phi = 0\,, \tag{2.3.55}$$

The slow roll inflation are given with the following conditions,

$$\epsilon_1 \equiv -\frac{\dot{H}}{H^2} \ll 1\,, \tag{2.3.56}$$

$$\epsilon_2 \equiv \frac{1}{H}\frac{d\epsilon_H}{dt} \ll 1\,, \tag{2.3.57}$$

These conditions are equivalent to

$$|\epsilon_V| \ll 1\,, |\eta_V| \ll 1\,, \tag{2.3.58}$$

for

$$\epsilon_V \equiv \frac{M_{\rm pl}^2}{2}\left(\frac{V_\phi}{V}\right)^2\,, \tag{2.3.59}$$

$$\eta_V \equiv M_{\rm pl}^2\frac{V_{\phi\phi}}{V}\,, \tag{2.3.60}$$

Under the slow roll conditions, Eq. (2.3.55) approximates to

$$\dot{\phi} \simeq -\frac{V_\phi}{3H}\,, \tag{2.3.61}$$

Primordial fluctuations during inflation

In the inflationary universe, quantum fluctuations of the metric and scalar field exists at perturbative level. The canonical quantisation

$$\zeta \sim -\frac{H}{\dot{\phi}}\delta\phi\,, \tag{2.3.62}$$

The novel property of the power spectrum of the fluctuations is the scale independence. The power spectrum of the curvature perturbations is given

$$\mathcal{P}_\zeta = \left(\frac{H}{\dot{\phi}}\right)^2\left(\frac{H}{2\pi}\right)^2\,, \tag{2.3.63}$$

Besides, the quantum fluctuation of tensor filed simultaneously exist and

$$\mathcal{P}_h = \left(\frac{H}{2\pi}\right)^2\,, \tag{2.3.64}$$

The scalar to tensor ratio

$$r \equiv \frac{\mathcal{P}_h}{\mathcal{P}_\zeta}\,, \tag{2.3.65}$$

The consistency condition

$$n_t = -\frac{r}{16}\,, \tag{2.3.66}$$

2.3.7 Observational understandings

Current observations show that the universe is flat. More precisely, the curvature of the universe is determined by the prospective angle of CMB's first peak. In actual observations, the cosmological parameter $\Omega_K = -K/a^2{H_0}^2$ is limited to the accuracy of $\Omega_{K0} = -0.0052(64)$ [13, 6, 14]. Therefore, it is reasonable to assume that $\Omega_{K0} = 0$.Therefore, we assume zero three-dimensional curvature, i.e., $K = 0$. The FRW metric with $K = 0$ is given by

$$ds^2 = -dt^2 + a^2(t)\delta_{ij}dx^i dx^j\,, \tag{2.3.67}$$

Friedmann equations Eqs. (2.3.20) and (2.3.21) are given as

$$H^2 = \frac{8\pi G\rho}{3} = H_0^2\Omega\,, \tag{2.3.68}$$

$$\frac{\ddot{a}}{a} = \dot{H} + H^2 = -\frac{4\pi G}{3}(\rho + 3P) = -\frac{H_0^2}{2}(\Omega_{m0}a^{-3} - 2\Omega_{\Lambda 0})\,, \tag{2.3.69}$$

where H_0 is the Hubble constant and Ω is the total density parameter

$$\Omega = \Omega_{m0}a^{-3} + \Omega_{\Lambda 0}\,, \tag{2.3.70}$$

H_0 and Ω_{m0} are constrained from observations. The Hubble constant can be estimated from the receding velocity of nearby galaxies at redshift $z = 0.01 \sim 0.1$ [15]. Restrictions on $\Omega_{\Lambda 0}$ and Ω_{m0} from the magnitude function of type Ia supernovae, etc. [8, 9]. One the other hand, There is a method to describe the structure evolution in the universe in detail as a theoretical model, and to limit the cosmological parameters by comparing the model with observations, which makes it possible to determine the parameters in more detail. The optical depth τ, density parameter for baryons Ω_b, and the amplitude of the primordial fluctuation A_s and its spectral index of power spectrum n_s, additionally appears, Λ - CDM model is described by six paramters:Ω_{m0}, Ω_b, H_0, τ, A_s, and n_s. The latest constraints on the six parameters by Planck satellite is shown

in [16]. The scalar to tensor ratio is measured by Planck, $r < 0.07$ (95 % C.L.).

Chapter 3

Beyond standards

The standard theories of gravity and cosmology have succeeded in the explanation of astrophysical and cosmological phenomena. One could argue that the model of our Universe has been well established from small to large scales, few problems being left. However, this is not true, proceeding to the bunch of scientific controversy. At present, the majority of discussions in the studies of gravity and cosmology are involved with the physics of the two ends of energy scale; the lowest or highest regime.

In theory, the physics of the two ends of the lowest or highest energy can end up with the failure of perturbative approaches, particularly pathological when including gravity. Phenomenologically, the cosmic accelerations, i.e., the inflation and the late-time acceleration would give a good probe for the two extreme ends of energy scales. The acceleration of the cosmic expansion has been investigated with the de Sitter space, leading the quasi-de Sitter approximations. A prominent example is the slow-roll approximation, which has been developed in the context of inflation [10, 11, 12]. Except some extreme cases such that the kinetic motion of the energy components of the universe drives the acceleration, it has been known that the cosmic acceleration can be well described with the slow-roll approximation. This approximation is simply characterised as called so-called "Dark Energy" in the following papers [17, 18, 19] In a more general point of view, the cosmic acceleration can be approached in terms of the modification of gravity, which has been intensively progressed studied in the last decades. Interestingly, the modification of gravity make an interesting way of thinking about cosmic acceleration beyond the quintessence model.

The modification of gravity is not only motivated by the cosmic acceleration. But also, Einstein's gravity is very naive at high energies mostly above the Planck scale, i.e., 10^{19}GeV. The issues are relatively older than the issues for cosmic acceleration, having been well described into the singularity problem or cosmic censorship. Most

importantly, the UV incompleteness of the Einstein's gravity has lead the disability of quantum gravity. The UV incompleteness of Einstein gravity should be solved in a more profound stage of theoretical physics, such as string theory. Most of the possible deformations of Einstein gravity provide a new dynamical degree of freedom, consequently changing the phenomenology. Some signatures of the additional degree of freedom are able to be measured by observations.

From the observational point of view, the precision of forthcoming cosmological probes have been sophisticated has improved up to the percent level. Particularly, the Planck legacy survey for the CMB accomplished percent-level constraints on the ΛCDM concordance cosmology. Practically speaking, the accuracy that has been achieved for the ΛCDM model is transferable to constrain the modification of gravity at cosmological scales.

In this chapter, we sculpture summarise the upfront issues of Einstein gravity and the concordance ΛCDM cosmology, and argue the observational possibility to probe any phenomenology in modifications of gravity.

3.1 Problems left

3.1.1 Quantum gravity

Apart from the fine-tuning problem in phenomenological parameters, Einstein gravity is doubtful in the framework of quantum theory. The long argued problem is the non-renormalisability of Einstein gravity. As first pointed out by Stelle 1977 [20], and investigated by G. t'Hooft in 1993 [21], pure gravity with simple matter fields such as a scalar or vector field could not be renormalisable as well. What non-renormalisability causes in phenomenology is the failure of prediction of quantum features in gravity. Although many alternative ideas have been considered, the problem is still unsolved, which is one of the hardest problems left in physics. The prominent imperfection of Einstein gravity to describe the quantum nature of gravity is highlighted as follows.

Planck scale

The Planck scale is the limit of the scale at which the quantum coherent length, i.e., the Compton wavelength is equivalent to the Schwartzshild radius. In the equation

$$\frac{h}{mc} = \frac{G_{\rm N} m}{c^2}\,, \tag{3.1.1}$$

where h is the Planck constant. The mass scale is derived from Eq. (3.1.1), which is the Planck mass defined as

$$m_{\rm pl} \equiv \sqrt{\frac{hc}{G_{\rm N}}}\,, \tag{3.1.2}$$

The Planck length $\ell_{\rm pl}$ is then given as $\ell_{\rm pl} = G_{\rm N} m_{\rm pl}/c^2 = \sqrt{hG_{\rm N}/c^3}$. Below the Planck scale $\ell_{\rm pl}$. All the information is inside the black hole, which cannot be probed from the outside. Consequently, the quantum coherence at the Planck scale is not able to be detected in principle. In many papers, people have argued how we physically investigate at the Planck scale. In this thesis, however, we would not deal with scales above the Planck scale.

Non-renormalisability

When it comes to considering low energy physics, it is possible to ignore any physical process at short distance with high energy: it can be integrated out over observing scale or time we are looking at. The process of such integration is generally termed renormalisation. More specifically, renormalisation is a procedure such that we change the strength of a field, or coupling between matters we observe while the mathematical structure of a theory we use remains unchanged. Renormalisation is well formulated for quantum field theory and atomic physics. One could think if renormalisation works in Einstein gravity, but it is not the case.

Essentially, the reason why renormalisation fails is related to the strong coupling nature of Einstein gravity. The gravitational strength at smaller scales becomes stronger as a high energy excitation of matter occurs at short distances, making a back reaction to lower energy scales. Especially when taking into account the quantum corrections from shorter scales, there are no parameters that regularise the divergent contribution of the quantum corrections. As a result, the parameters, namely $G_{\rm N}$ or Λ do not work for the describing quantum corrections. It is one of the cutting edge areas of study to investigate what properly regularises the quantum corrections.

Cosmologically, the non-renormalisability of Einstein gravity matters at the beginning of the Universe which is assumed to be around the Planck scales. At least for phenomenological reasoning of how the initial conditions of the Universe are given, non-renormalisability may not cause any struggles. In fact, many of the scenarios of inflation work below the Planck scale where gravitational back reaction is negligible, and the most of the models succeed in explaining the initial power spectrum of the cosmological perturbations from the CMB. However, possible regularisation for the

quantum correction of gravity may make imprints on the primordial spectra. For example, the non -Gaussian departure of primordial fluctuation can pick up information from higher energy scales. The difficulty for these studies is the separation from systematises non linearity during the evolution of the Universe, i.e., the phase transitions, energy injections, or the gravitational structure formations. Apart from such obstruction, it is interesting to look into what difference the quantum regulators make to the cosmological initial conditions.

After all, we would not wish to increase the theoretical difficulty of Einstein gravity. We once motivate ourselves on the renormalisability of gravity in the context of the test of Lorentz invariance. In that chapter, however, the main argument is how it is possible to test Lorentz invariance from cosmological observations.

3.1.2 Observational shortcomings of the standard cosmology

cosmological constant problem

The problem appears when we interpret the observed value of the cosmological constant with fundamental theories. In comparison of the energy scale of gravitational coupling and the cosmological constant, i.e., the reduced Planck mass scale $M_{\rm pl} = m_{\rm pl}/\sqrt{8\pi}$ and Λ, there is a huge hierarchy in energy scale. Hereafter the explanation is based on L. Amendola and S. Tsujikawa 2010 [22] In the energy density scale,

$$\Lambda \approx H_0^2 = (2.1332h \times 10^{-42}\mathrm{Gev})^2\,, \tag{3.1.3}$$

The corresponding energy density ρ_Λ is given as

$$\rho_\Lambda \simeq M_{\rm pl}^2 H_0^2 \sim 10^{-123} M_{\rm pl}^4\,, \tag{3.1.4}$$

where we have used $h \approx 0.7$ and $m_{\rm pl} \approx 10^{19}$GeV. The enormous difference of the energy scale between the Planck scale and the cosmological constant could be milder, if the history of phase transitions of the vacuum state is treated more carefully. The matter energy momentum tensor in the right hand side of the Einstein equation has a term from the vacuum energy, which is mathematically equivalent to the cosmological constant. Then one can expect that the non-trivial contributions from the vacuum energy can tune the cosmological constant. Suppose that the zero-point energy of a free field with mass m and momentum k, the vacuum energy of the field is $E = \omega/2$. Here ω is the frequency of the field given by the dispersion relation $\omega = \sqrt{k^2 + m^2}$. Summing over all the vacuum energy up to the momentum cut off $k_{\rm max}(\gg m)$, we

obtain

$$\rho_{\rm vac} = \int_0^{k_{\rm max}} \frac{dk\ 4\pi\ k^2}{(2\pi)^3} \frac{1}{2} \sqrt{k^2 + m^2} \approx \frac{k_{\rm max}^4}{16\pi^2}\,, \tag{3.1.5}$$

For the second equality in we use $k_{\rm max} \gg m$ and the dominance of the mode with large k. When we take $k_{\rm max}$ to be $m_{\rm pl}$, we obtain $\rho_{\rm vac} \simeq 10^{74}({\rm GeV})^4$, that is still 10^{121} larger than ρ_Λ. This huge gap of energy scale still exists even we take the QCD scale, i.e., $k_{\rm max} \approx 0.1{\rm GeV}$ we have $\rho_{\rm vac} \approx 10^{-3}({\rm GeV})^4$ and thus $\rho_{\rm vac} \gg \rho_\Lambda$. Hence, it has been recognised that the tuning problem of the cosmological constant from the fundamental theories is left to be the worst hierarchy problems[1].

The coincidence problem

The second problem in observational cosmology is called the coincidence problem. This problem asks why the observed cosmological constant is of the same order as the matter density in the Universe. It is observationally determined that the curvature of the Universe is almost zero, leading the relation between the matter density parameter Ω_m and the density parameter of the cosmological constant Ω_Λ satisfy the relation $\Omega_m + \Omega_\Lambda = 1$. According to the SN Ia surveys and the WMAP CMB measurements, the present values of the density parameters, Ω_{m0} and $\Omega_{\Lambda 0}$ are observationally given as $\Omega_{m0} \sim 0.3$ and $\Omega_{\Lambda 0} \sim 0.7$. In theory, the cosmological constant is nothing to do with the matter density of the universe, and thus we may ask why the two values are close with each other. In the current studies we consider some possible solutions for the coincidence problem, but none of the models are satisfactory to reveal how the coincidence of the two density parameters happen.

Tension of the Hubble constant

The third problems has arisen much more recently than the above two problems after the Planck CMB measurement was released in 2013. The problem is that the measured Hubble constant by Planck is significantly different from the local measurement of it, at more than 3σ confidence level. To make matters worse, the tension in very recent measurement via the strong gravitational lensing of quasars tightened the tension toward 5.3σ confidence level. As a third way to measure the Hubble constant, gravitational waves have constrained the Hubble constant. Currently, the constraint

[1] A more careful relativistic calculation is needed, and then one finds a density not M^4, where M is the cutoff mass, but $m^4 \ln(M/m)$, where m is the particle mass. Note that $m = 0$,i.e., the vacuum energy is zero if the particle is mass-less In more detail, see [23]

on the Hubble constant is with the constant has large variations, hopefully improved by future observations.

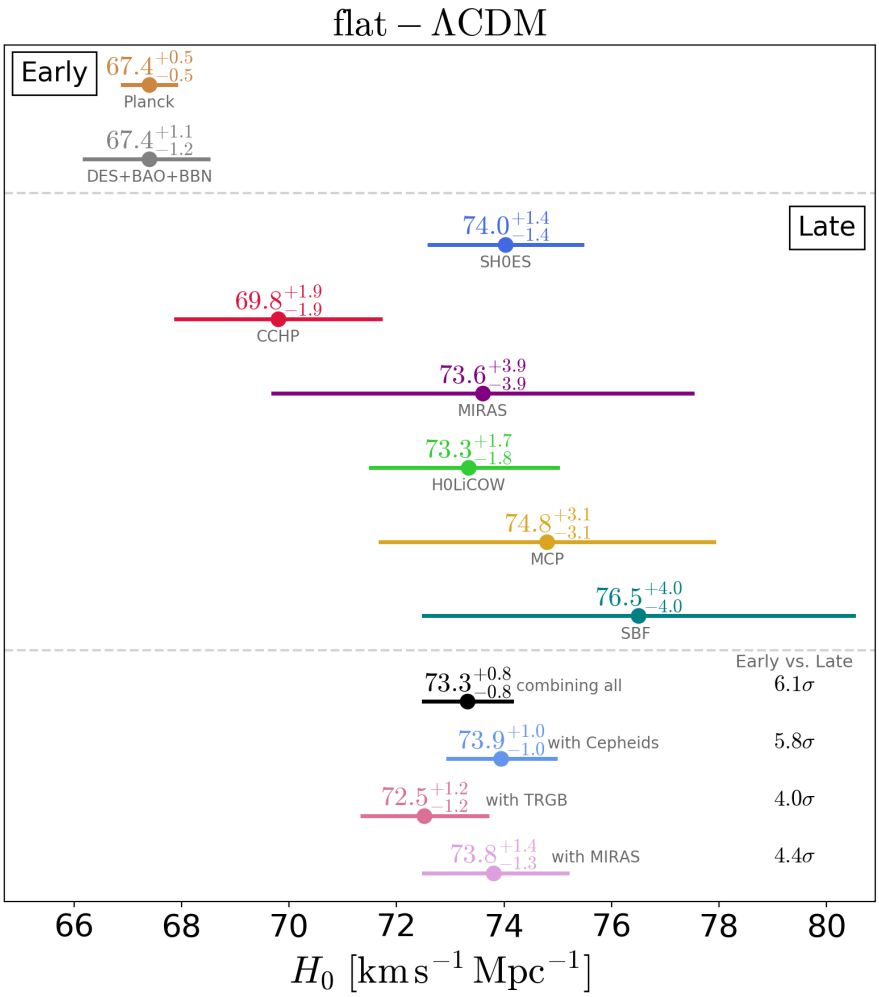

Figure 3.1. The Hubble tension from L. Verde, T. Treu, and A. G. Riess [24]

3.1.3 Other issues

Other problems in cosmology are represented as

- CP violation
- Strong CP problem
- Matter - antimatter asymmetry

In this thesis, we will not consider these issues because these are less involved with the space-time symmetry.

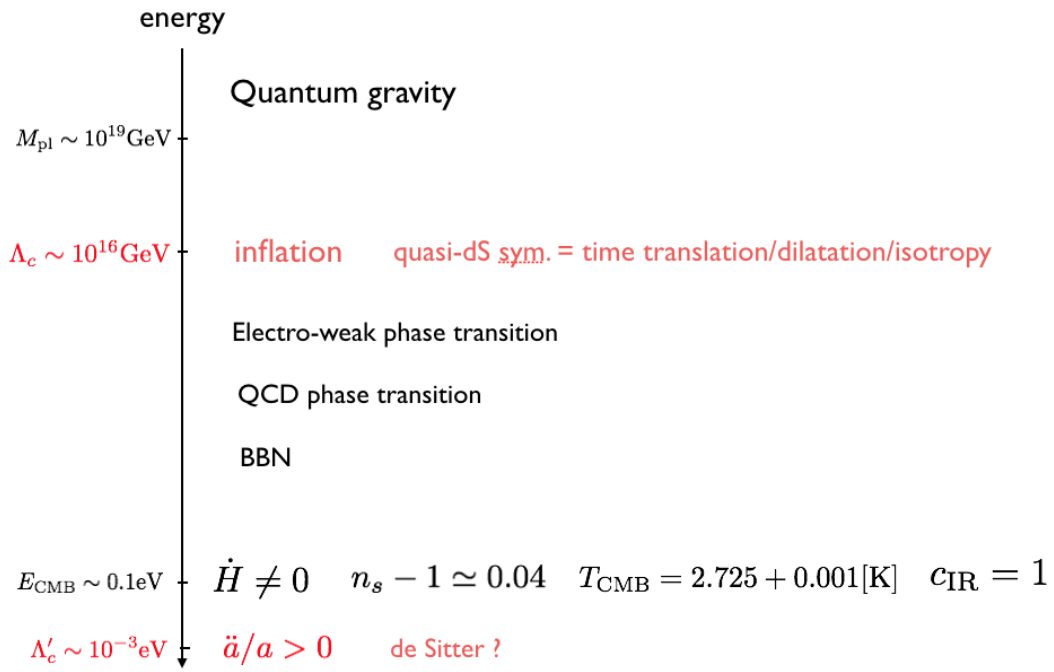

Figure 3.2. Energy hierarchy in cosmology

3.2 Dark Energy paradigm

Let us think about the cosmological constant problem. At present, there are so many models of alternative explanations for the late-time acceleration. One of the common features of the models proposed is that they give the time-evolving energy component, called "Dark Energy" [17, 18]. Another is that the dark energy appears associated with a new scalar field. This essential characteristic of dark energy is firstly proposed in J. Peebles and B. Ratra 2002 [19]. We mainly pick up two representative models for dark energy, i.e., the quintessence and XCDM model. As an alternative way to explain dark energy, the modification of gravity is also taken into account.

3.2.1 Quintessence

Quintessence is a model such that a very light scalar field dominates the present universe. The idea is very similar to the inflaton in an inflationary universe. The action is in quintessence is given as

$$S_Q = \int d^4x\sqrt{-g}\left(-\frac{1}{2}g^{\mu\nu}\nabla_\mu\phi\nabla_\nu\phi - V(\phi)\right), \tag{3.2.1}$$

The scalar field behaves as a perfect fluid, and it possesses the effective energy density and the pressure as

$$\rho_Q = \frac{1}{2}\dot{\phi}^2 + V(\phi)\,, \tag{3.2.2}$$

$$p_Q = \frac{1}{2}\dot{\phi}^2 - V(\phi)\,, \tag{3.2.3}$$

As similar to the case of the inflaton, the accelerating expansion like the cosmological constant realises when $\dot{\phi}^2 \ll 2V(\phi)$, $p_Q \simeq -\rho_Q$. In addition, quintessence is consider as a consequence of spontaneous symmetry breaking. If this quintessential scalar field drives the late-time acceleration, the mass of the scalar field, m_Q, is extremely light, i.e., $m_Q \sim H_0 \sim 10^{-33}$[eV]. Scalar fields are generally predicted in beyond standard model of particle physics or string theory, but such a tiny mass often suffers from the large quantum correction from the vacuum. This may require that the quintessential dark energy should be improved.

3.2.2 XCDM model

Another possible scenario of dark energy is a some kind of perfect fluid, represented as X, whose equation of state, w_X, is constant [18]. The argument is equivalently written

as

$$p_X = w_X \rho_X \,, \tag{3.2.4}$$

In the XCDM model, w_X is a constant fixed by microscopic processes. In other words, the fluid is something unknown. One of the interesting features of the X-fluid is that it may contain a new type of matter in the Universe. Note that when $w_X < -1$, that is called "phantom energy". A novel feature of phantom energy is that it breaks the null energy condition, i.e., $\rho_X + p_X \leq 0$. The breaking of the null energy condition, however, can induce instability of the background space-time. This is well known in the case of the quintessence field. Therefore the X-fluid would be carefully constructed in order not to spoil the expanding evolution of the universe. As we see from the two representative models for the cosmic acceleration at late times, it is known that the simplest thought would not be enough to solve the cosmological constant problem.

3.3 Modified Gravity

The modification of gravity gives one of the possible ways to explain the cosmic acceleration. By contrast to quintessence or the X-fluid, the cosmic acceleration is given by modifying the strength of gravity at cosmological distances. What is interesting in modified gravity is that a theory of modified gravity may succeed in constructing quantum gravity. In other words, the cosmic acceleration may signify certain features of quantum gravity. Currently, in the case of modification with a scalar field, the universal description to treat dark energy and modified gravity together is called scalar-tensor theory. In particular, Horndeski theory [25, 26] is the most general form of these theories with a space-time curvature and a scalar field whose equations of motion contain second-order space-time derivatives. The Horndeski theory includes not only quintessence and nonlinear kinetic theory, but also many specific theories: $f(R)$ theories [27], covariant Galileons [28], and kinetic gravity braiding [29]. The Horndeski theory can also be extended further to a more general framework in the language of an effective field theory (EFT). An EFT for dark energy was formulated by Gubitosi *et al.* [30], Gleyzes *et al.*[31], and Bellini and Sawicky [32].

3.4 Global time-translation symmetry-breaking

In the modern perspective of inflation and dark energy are captured by the symmetry breaking of the global time-translation symmetry. This means that Lorentz invariance

of a space-time is partially broken. Quantitatively, the coordinate transformation given as

$$t \to t + \pi(t, \mathbf{x}) \,, \tag{3.4.1}$$

$\pi(t, \mathbf{x})$ breaks time translation symmetry of space-time. Inflationary cosmology is described via this symmetry-breaking from de Sitter space-time. [33]. A similar formulation is formulated at the present energy scales of the Universe [30, 34] (detail discussions are shown in Appendix.B. Below a symmetry breaking scale, it is possible to formulate an effective field theory. EFT is phenomenologically useful to test various models of inflation, dark energy, or modified gravity.

3.5 Summary

We briefly highlight the problems that can be a signature for new understanding of the space-time symmetry and the foundation of gravity. In the rest of this part of the thesis, we argue the specific cases. We consider such a general framework of modified gravity theories in Chapter. 4. In Chapter. 5, we study a case when local Lorentz invariance is broken in gravity in the inflationary Universe.

Chapter 4

Observationally-viable scalar-tensor theories

We consider the phenomenology of scalar-tensor theories at cosmological distances. Scalar-tensor theories are familiarly known as one of the extensions of Einstein gravity, which respect general covariance whereas containing one scalar degree of freedom in addition to normal massless tensor. A novel property of the scalar field is its ability to change the cosmic expansion and growth rate of structures either faster or slower. Another aspect of scalar tensor theories is that the scalar field modifies gravitational interactions as the expansion. When the scalar field couples on Ricci tensor or another geometrical quantity such as Einstein tensor, called this case as "non-minimal coupling", gravitational interactions between massless/massive matters. As a consequence of non-minimal coupling, the equivalence principle is no longer respected, leading crucial differences from Einstein gravity. Throughout this chapter, we discuss cosmological phenomenology of the scalar-tensor theories, showing how possible to distinguish the scalar-tensor theories from the concordance Einstein gravity. Important remarks are given as follows.

- A scalar field is compatible to the cosmological principle; i.e., homogeneity and isotropy are still viable in scalar-tensor theories.
- Equivalence principle would be broken due to non-trivial interactions with the massless spin-2 graviton.
- Observational constraints on scalar-tensor theories are to be expected.

4.1 Covariant theories beyond Einstein's gravity

We consider the mathematical structure of covariant theories as extensions of Einstein gravity.

4.1.1 Conformal and disformal transformation

The main idea beyond Einstein gravity is to introduce another dynamical scaling into a theory. It comes up with the conformal or disformal transformation. The conformal transformation has been known as

$$g_{\mu\nu} \longrightarrow \tilde{g}_{\mu\nu} = \Omega^2(x) g_{\mu\nu} \,, \tag{4.1.1}$$

Since the operator of the conformal transformation $\Omega^2(x)$ is common in all the metric components, the transformed line element $d\tilde{s}^2$ is proportional to ds^2,

$$ds^2 \longrightarrow d\tilde{s}^2 = \Omega^2(x) ds^2 \,, \tag{4.1.2}$$

This results in the preservation of causal structure of a theory before and after the conformal transformation.

The disformal transformation is defined as

$$g_{\mu\nu} \longrightarrow \tilde{g}_{\mu\nu} = g_{\mu\nu} + \Gamma(x) v_\mu v_\nu \,, \tag{4.1.3}$$

where v_μ is a covariant vector which is either time-like, null, or space-like. With any configuration of v_μ, the point is that the line element is given as

$$d\tilde{s}^2 = ds^2 + \Gamma(x) v_\mu v_\nu dx^\mu dx^\nu \,, \tag{4.1.4}$$

Physical consequences of conformal and disformal transformation is

- Conformal transformation changes, while leaving the structure of the null geodesics unchanged.
- Disformal transformation change the shape of the null geodesics and the associated light cones.

As firstly introduced in J. Bekenstein 1993 [35], the WEP should be satisfied as long as we consider that all the matters are *universally coupled* [36]. In that case, it is required that $\Omega(x)$ and $\Gamma(x)$ only depends on some invariant quantities under general

covariance. A popular choice is introducing a scalar field ϕ, and its canonical kinetic term $X = -g^{\mu\nu}\partial_\mu\phi\partial_\nu\phi/2$, i.e., $\Omega(x) = \Omega(\phi, X)$ and $\Gamma(x) = \Gamma(\phi, X)$.

Note that the diffeomorphism invariance still keeps in both transformations. In this chapter, we consider a specific type of the conformal and disformal transformation by a scalar degree of freedom. After the construction of a theory in the family of the conformal and disformal transformations, the theory is not fully guaranteed as a physically sensible, leading further inspection of dynamical instability of the Hamiltonian.

4.2 Kinematic bounds in gravity

We briefly review a couple of types of covariant scalar-tensor theories. The variation of scalar-tensor theories appears as the theories are required the conditions whether or not the Hamiltonian is bounded, i.e., the degeneracy conditions. The degeneracy conditions are required for constructing a theory in order to a ghost degree of freedom from being dynamical at any energy scale. The types of scalar tensor theories are determined by what condition for the degeneracy is imposed. The kinematic theory often requires certain criteria for theories such that a physical state realised in a theory is stable in its dynamical time. The well known criteria are that (1) the Hamiltonian is bounded from the minimum, (2) kinetic energy for dynamical mode should not be negative. (1) and (2) guarantee that a system considered is kinetically stable. Such criteria would be applied for gravity theories as well.

4.2.1 Ostrogradosky's instabilities

As is often the case, the Lagrangian only argues with q and $\dot{q}$; $L(q, \dot{q})$. Generally speaking, this statement is replaced by the absent of the higher time derivative of q. Let us think the second derivative of q, i.e., $\ddot{q}$. By pointing out that the linear dependency of $\ddot{q}$ does not lead the higher derivative dependency on the Euler - Lagrange equation, it is crucial to consider the quadratic or other dependencies of $\ddot{q}$. Then the condition is written as

$$\frac{\partial^2 L}{\partial \ddot{q}^2} \neq 0\,, \tag{4.2.1}$$

This is called the non degeneracy condition. Under the non degeneracy condition, the Euler-Lagrange equation is

$$\frac{d^2}{dt^2}\frac{\partial L}{\partial \ddot{q}} - \frac{d}{dt}\frac{\partial L}{\partial \dot{q}} + \frac{\partial L}{\partial q} = 0\,, \tag{4.2.2}$$

$$Q_1 = q\,,\ Q_2 = \dot{q}\,,\ P_1 = \frac{\partial L}{\partial \dot{q}} - \frac{d}{dt}\frac{\partial L}{\partial \ddot{q}}\,,\ P_2 = \frac{\partial L}{\partial \ddot{q}}\,, \tag{4.2.3}$$

These combinations of variables satisfy the Hamilton Jacobi equations; $\dot{P}_i = -\partial H/\partial Q_i$ and $\dot{Q}_i = \partial H/\partial P_i$ from the Hamiltonian $H(Q_1, Q_2, P_1, P_2)$,

$$H(Q_1, Q_2, P_1, P_2) = P_1 Q_2 + P_2 \mathcal{Q}(Q_1, Q_2, P_2) - L(Q_1, Q_2, \mathcal{Q}(Q_1, Q_2, P_2))\,, \tag{4.2.4}$$

where we solve $\ddot{q}$ via

$$\ddot{q} = \mathcal{Q}(Q_1, Q_2, P_1)\,, \tag{4.2.5}$$

which is allowed from the non-degeneracy condition in Eq. (4.2.1). Then we will see that the Hamiltonian is linearly dependent on the canonical momentum $P_i (i = 1, 2)$. As a result, it is not guaranteed that the Hamiltonian possesses its minima. What if the minima of the Hamiltonian does not exist leads is that spontaneous decay of the dynamical system into instability, which should be avoidable for dynamical analysis. Not that this instability should be respected whether or not we work in classical or quantum mechanics. In Einstein gravity looks violating for the non degeneracy condition since the Ricci curvature R depends on the second derivative of the metric, but the terms appears only at linear order and behave as the surface terms, being irrespective to the equation of motion. Hence, we would expect that the extension of the degeneracy conditions leads to a new class of theories without violating the analytical mechanical limitation. In particular, the insertion of an additional degree of freedom can avoid the non degeneracy of the Lagrangian with specific form of the degeneracy condition. Hereafter, let us show the cases with a scalar degree of freedom.

4.3 The Lovelock's theorem

A strong conclusion is obtained from the David. Lovelock's simple mathematical theorem called "Lovelock theorem". We investigate the whole picture of how we construct gravity theory with the essential compositions needed for modelling gravity. The Lovelock theorem states that

(a) A^{ij} is symmetric, i.e.,

$$A^{ij} = A^{ji}\,, \tag{4.3.1}$$

(b) A^{ij} is a concomitant of the metric tensor g_{ab} and its first two derivatives, i.e.,

$$A^{ij} = A^{ij}(g_{ab}; g_{ab,c}, g_{ab,cd}) \,, \tag{4.3.2}$$

(c) A^{ij} is divergence free, i.e.,

$$A^{ij}_{;j} = 0 \,, \tag{4.3.3}$$

(d) A^{ij} is linear in the second derivatives of g_{ab}
To satisfy the conditions (a)-(d), A^{ij} is determined as

$$A^{ij} = aG^{ij} + bg^{ij} \,, \tag{4.3.4}$$

for the arbitrary coefficients a and b is the unique expression of A^{ij}. The Lovelock's theorem states a strong constraint to develop gravity theory. To break the Lovelock's theorem, one of the following statements should be needed,

- The dimension of a spacetime is higher than four
- The local general covariance is broken
- The higher derivatives with the higher curvature terms are included
- An extra degree of freedom is coupled to gravity

Note that the equivalence principle is not implicitly broken. It is known that

4.4 Specific scalar-tensor theories

We consider scalar-tensor theories that have been known. These theories are made by satisfying the dynamical stability of their Hamiltonian, i.e., degeneracy conditions, while breaking the Lovelock's statement, which is firstly porposed by G. W. Horndeski in 1974 [25]. Decades after the original work of G. W. Horndeski [25], Horndeski theory was rediscovered in the construction of general formulation for modification of gravity [37, 26]. A few years later, though, Horndeski theory is not a unique extension of gravity, resulting in the construction of Gleyzes-Langlois-Piazza-Vernizzi (GLPV) theory [38]. Since GLPV theory is written in ADM formalism, Hamiltonian is well-defined and conditions for avoiding Ostrogradosky instability are transparently given (see in detail in Appendix. A). In 2015, Degenerated Higher-Order Scalar-Tensor (DHOST) theory was proposed as the most general scalar-tensor theory without Hamiltonian instability by D. Langlois and K.Noui [39, 40].

4.4.1 Horndeski theory

One of the oldest theories with the extra scalar field is Horndeski theory [41, 26]. The covariant Lagrangian of the Horndeski theory is given as [1],

$$\mathcal{L} = \sum_{i=2}^{5} \mathcal{L}_i \,. \tag{4.4.1}$$

where

$$\mathcal{L}_2 = G_2(\phi, X)\,, \tag{4.4.2}$$

$$\mathcal{L}_3 = -G_3(\phi, X)\Box\phi\,, \tag{4.4.3}$$

$$\mathcal{L}_4 = G_4(\phi, X)R + G_{4X}(\phi, X)\left[(\Box\phi)^2 - \phi_{;\mu\nu}\phi^{;\mu\nu}\right]\,, \tag{4.4.4}$$

$$\begin{aligned}\mathcal{L}_5 = {} & G_5(\phi, X)G_{\mu\nu}\phi^{;\mu\nu} \\ & - \frac{1}{6}G_{5X}(\phi, X)\Bigg[(\Box\phi)^3 - 3\Box\phi_{;\mu\nu}\phi^{;\mu\nu} \\ & \qquad + 2\phi_{;\mu}{}^{;\nu}\phi_{;\nu}{}^{;\lambda}\phi_{;\lambda}{}^{;\mu}\Bigg]\,.\end{aligned} \tag{4.4.5}$$

Here $;_\mu$ is a covariant derivative and $X = -\phi_{;\mu}\phi^{;\mu}/2$, the canonical kinetic energy density of ϕ. The Lagrangian does not plague with the higher order derivatives of the scalar field, ending up with the equations of motion include up to the second derivative. The Horndeski theory widely include specific types of theories. The Horndeski theory includes not only the quintessence [42, 43] and nonlinear kinetic theory [42, 43], but also many specific theories: $f(R)$ theories [27], covariant Galileons [37, 44], and kinetic gravity braiding [29]. However, it has been known that the Horndeski theory is not the most general scalar-tensor theory.

4.4.2 DHOST theory

The Degenerated Higher Order Scalar Tensor (DHOST) theory is the most general scalar-tensor theory currently found. The DHOST theory is firstly discovered by D. Langlois and K. Noui 2015 [39], and successively investigated by J. B. Achour *et al.* [45] and H. Motohashi *et al.* in the different context [46]. The covariant Lagrangian is

[1] $G_2(\phi, X)$ is often written $K(\phi, X)$ in literature.

given as

$$L = f_0(\phi, X) + f_1(\phi, X)\Box\phi + f_2(\phi, X)R + C^{\mu\nu\rho\sigma}_{(2)}\phi_{;\mu\nu}\phi_{;\rho\sigma} + f_3(\phi, X)G_{\mu\nu}\phi^{;\mu\nu} + C^{\mu\nu\rho\sigma\alpha\beta}_{(3)}\phi_{;\mu\nu}\phi_{;\rho\sigma}\phi_{;\alpha\beta}\,, \tag{4.4.6}$$

$$C^{\mu\nu\rho\sigma}_{(2)}\phi_{;\mu\nu}\phi_{;\rho\sigma} = \sum_{A=1}^{5} a_A(\phi, X)L^{(2)}_A\,, \tag{4.4.7}$$

where the quadratic order is given as

$$L^{(2)}_1 = \phi_{;\mu\nu}\phi^{;\mu\nu}\,,\ L^{(2)}_2 = (\Box\phi)^2\,,\ L^{(2)}_3 = \Box\phi\phi^{;\mu}\phi^{;\nu}\phi_{;\mu\nu}$$
$$L^{(2)}_4 = \phi^{;\mu}\phi_{;\mu\rho}\phi^{;\rho\nu}\phi_{;\nu}\,,\ L^{(2)}_5 = (\phi^{;\mu}\phi^{;\nu}\phi_{;\mu\nu})^2\,, \tag{4.4.8}$$

and the cubic order is given as

$$C^{\mu\nu\rho\sigma\alpha\beta}_{(3)}\phi_{;\mu\nu}\phi_{;\rho\sigma}\phi_{;\alpha\beta} = \sum_{A=1}^{10} b_A(\phi, X)L^{(3)}_A \tag{4.4.9}$$

$$L^{(3)}_1 = (\Box\phi)^3\,,\ L^{(3)}_2 = \Box\phi\phi_{;\mu\nu}\phi^{;\mu\nu}\,,\ L^{(3)}_3 = \phi_{;\mu\nu}\phi^{;\nu\rho}\phi^{;\mu}_{;\rho}\,,\ L^{(3)}_4 = ,(\Box\phi)^2\phi^{;\mu}\phi_{;\mu\nu}\phi^{;\nu}$$
$$L^{(3)}_5 = \Box\phi\phi_{;\mu}\phi^{;\mu\nu}\phi_{;\nu\rho}\phi^{;\rho}\,,\ L^{(3)}_6 = \phi_{;\mu\nu}\phi^{;\mu\nu}\phi_{;\rho}\phi^{;\rho\sigma}\phi_{;\sigma}\,,\ L^{(3)}_7 = \phi_{;\mu}\phi^{;\mu\nu}\phi_{;\nu\rho}\phi^{;\rho\sigma}\phi_{;\sigma}\,,$$
$$L^{(3)}_8 = \phi_{;\mu}\phi^{;\mu\nu}\phi_{;\nu\rho}\phi^{;\rho}\phi_{;\sigma}\phi^{;\sigma\lambda}\phi_{;\lambda}\,,\ L^{(3)}_9 = \Box\phi(\phi_{;\mu}\phi^{;\mu\nu}\phi_{;\nu})^2\,,\ L^{(3)}_{10} = (\phi_{;\mu}\phi^{;\mu\nu}\phi_{;\nu})^3\,, \tag{4.4.10}$$

The crucial difference from Horndeski theory is that DHOST theory has the higher order derivative operators $L^{(2)}_{3,4,5}$ and $L^{(3)}_{4-10}$ respectively shown in Eqs. (4.4.8) and (4.4.10) with the arbitrary coefficients depending on ϕ and X. while keeping the second order of equations of motion. To achieve this, the "degeneracy conditions" are imposed, successfully avoiding the Ostrogradosky instability [40].

GLPV theory

GLPV theory is understood as a peculiar subclass of DHOST theory. Although it might be transparent in logic to derive GLPV theory from DHOST theory, we explain GLPV theory based on the original proposal of GLPV theory,i.e. J. Gleyzes *et al.* 2014

[38] The Lagrangian of GLPV theory is given as

$$\mathcal{L} = \sum_{i=2}^{5} \mathcal{L}_i \,, \tag{4.4.11}$$

$$L_2 = G_2(\phi, X) \,, \tag{4.4.12}$$

$$L_3 = -G_3(\phi, X)\Box\phi \,, \tag{4.4.13}$$

$$\begin{aligned} L_4 = {} & G_4(\phi, X)R + G_{4X}(\phi, X)[(\Box\phi)^2 - \phi^{;\mu\nu}\phi_{;\mu\nu}] \\ & + F_4(\phi, X)\epsilon^{\mu\nu\rho}_{\ \ \ \sigma}\epsilon^{\mu'\nu'\rho'\sigma}\phi_{;\mu}\phi_{;\mu'}\phi_{;\nu\nu'}\phi_{;\rho\rho'} \,, \end{aligned} \tag{4.4.14}$$

$$\begin{aligned} L_5 = {} & G_5(\phi, X)G_{\mu\nu}\phi^{;\mu\nu} - \frac{1}{6}G_{5X}[(\Box\phi)^3 - 3\Box\phi\phi_{;\mu\nu}\phi^{;\mu\nu} + 2\phi_{;\mu\nu}\phi^{;\mu\sigma}\phi^{\nu}_{\ \sigma}] \\ & + F_5(\phi, X)\epsilon^{\mu\nu\rho\sigma}\epsilon^{\mu'\nu'\rho'\sigma'}\phi_{;\mu}\phi_{;\mu'}\phi_{;\nu\nu'}\phi_{;\rho\rho'}\phi_{\sigma\sigma'} \,, \end{aligned} \tag{4.4.15}$$

The theory space of the scalar-tensor theories are schematically shown in Fig. 4.1. The main message here is that DHOST theory includes Horndeski theory and GLPV theory.

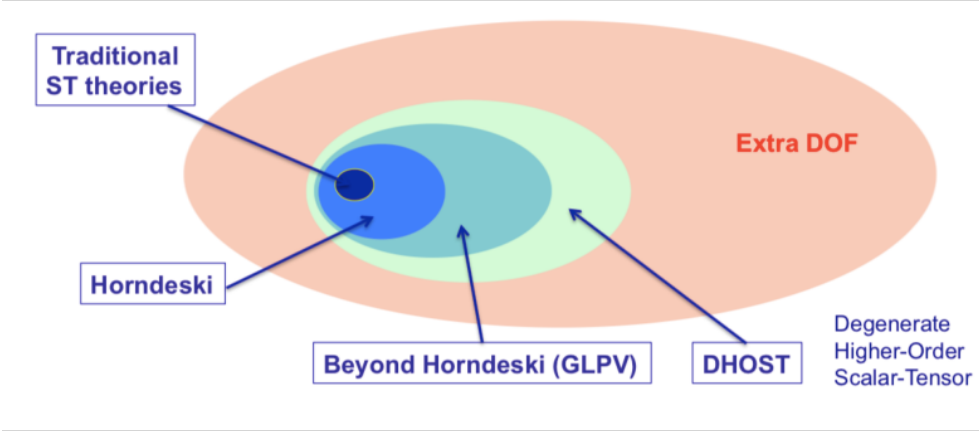

Figure 4.1. The landscape of scalar-tensor theories shown in [47]

4.5 Observational constraints of scalar-tensor theories

Observational constraints for constructing a viable model in scalar-tensor theories are important to be considered. We pick up significant conditions currently obtained by observations.

4.5.1 The late-time acceleration

As is already known, the expansion of the Universe is accelerating at late-time Universe. From the first direct measurement of the cosmic accelerating expansion with type-Ia supernovae [9, 8], subsequent observations of the cosmic microwave background (CMB) and surveys of large scale structure (LSS) have strongly suggested that the ΛCDM model is the best explanation to describe the cosmic acceleration. [7, 16]. Nowadays, however, modified gravity is one of candidates to explain the late-time cosmic acceleration. As is different from the ΛCDM model or well-known models such as quintessence [19] and the nonlinear kinetic term of a scalar field [42, 43], modified gravity changes gravitational interactions between matters while accounting for the cosmic acceleration. In comparison to the local tests of gravity suggesting Einstein gravity fits to experiments and observations, gravity at cosmological scales are less understood. Therefore, it is interesting to consider the possible modification of gravity at cosmological scales by the additional scalar field, providing a solution the cosmic acceleration.

4.5.2 Observation of GW170817 and GRB170817A

Very recently, LIGO and VIRGO detected a binary neutron star (BNS) merger named GW170817 [48]. This event is special because a few gamma-ray telescopes simultaneously caught the signal of a short gamma-ray burst, GRB170817A, and it was identified as the electromagnetic transient counterpart of GW170817. By using the difference of the arrival times between GW170817 and GRB170817A, they obtained a stringent constraint on δ_g down to $-7.0 \times 10^{-16} \lesssim \delta_g \lesssim 3.0 \times 10^{-15}$[49]. This means that the propagation of gravitational waves almost the same as the speed of light. Therefore, the observation of GW170817 and its electro-magnetic counterpart, i.e., GRB170817A has provided important constraints on gravity theories.

Modification of Gravitational-Wave propagation at cosmological scales

We briefly introduce how GW is deformed during propagation because of the modification of gravity. This argument was originally proposed in Saltas *et al.* [50] and recently

it has been extended by Nishizawa to a general framework to test gravity theories [51]. The propagation equation of GW is generally given by

$$h_{ij}'' + (2+\nu)\mathcal{H}h_{ij}' + (c_T^2 k^2 + a^2\mu^2)h_{ij} = a^2\Gamma\gamma_{ij}\,, \tag{4.5.1}$$

where h_{ij} is a tensor perturbation (GW) and $'$ denotes the derivative with respect to conformal time. In Eq. (4.5.1) there are four time-dependent parameters ν, c_T, μ, and Γ. ν is the Planck mass run rate, c_T is the phase velocity of a GW and μ is the graviton mass. Γ denotes extra sources generating GW. We assume that the gravitons are massless [2] and there is no source, i.e. $\mu = 0$ and $\Gamma = 0$. In the case that ν, c_T are slowly varying functions with a cosmological timescale, the solution of Eq. (4.5.1) is given in [51] as

$$h = \mathcal{C}_{\rm MG} h_{\rm GR}\,, \tag{4.5.2}$$

where

$$\mathcal{C}_{\rm MG} \equiv e^{-\mathcal{D}} e^{-ik\Delta T}\,, \tag{4.5.3}$$

$$\mathcal{D} \equiv \frac{1}{2}\int^{\tau} d\tau' \nu\mathcal{H}\,, \tag{4.5.4}$$

$$\Delta T \equiv \int^{\tau} d\tau' \delta_g\,. \tag{4.5.5}$$

In Eq. (4.5.5) we replace $1-c_T$ with the deviation parameter δ_g. $\mathcal{D}$ and ΔT correspond to the amplitude damping index and additional time delay of GW, respectively. We see that the damping parameter ν only appears in GW amplitude, while δ_g and μ are both involved in the GW phase. In order to measure the arrival time difference between a GW and a photon, δ_g is small enough to make the time delay shorter than the timescale of GW observations. We consider the case when δ_g is small. Note that $\mathcal{D}$ and ΔT are the observables given after integrating all effects between emission and detection. However, we are now interested in the case that all the quantities vary in the cosmological timescale. In such a case it is justified to use the Taylor expansion with respect to $H_0\tau_{LB}$ as given in Eq. (4.6.5). As we introduced in Sec. II, ν and δ_g are the observational parameters that are model independent. With the definitions of

[2] Mass of gravitons should not be given without thoughts of instability, as the mass for gauge fields can induce unstable degree of freedoms. More careful consideration are shown in literature, e.g.[52, 53]

the time evolution of ν and δ_g as

$$\nu = \nu_0 - \nu_1 H_0 \tau_{LB} \,, \tag{4.5.6}$$

$$\delta_g = \delta_{g0} - \delta_{g1} H_0 \tau_{LB} \,, \tag{4.5.7}$$

expanding up to the next-to-leading order in $H_0\tau_{LB}$ gives the approximated expressions of Eqs. (4.5.4) and (4.5.5) as

$$\mathcal{D} \simeq \frac{1}{2}\left\{\nu_0 \ln(1+z) - \frac{\nu_1}{2}(H_0\tau_{LB})^2\right\} \,, \tag{4.5.8}$$

$$\Delta T \simeq \frac{1}{H_0}\left\{\delta_{g0} H_0 \tau_{LB} - \frac{\delta_{g1}}{2}(H_0\tau_{LB})^2\right\} \,. \tag{4.5.9}$$

We now give observational constraints on ν_0, ν_1, δ_{g0}, and δ_{g1} from the detection of GW170817 and GRB170817A. The reason to choose this GW event is that the redshift of the GW is independently measured from the optical follow-up observation of NGC4993 [54], which resolves the degeneracy between the redshift and the luminosity distance in the GW observation. For the observables, $\mathcal{D}$ and ΔT, we have to take into account their estimation errors. In the case of measuring the arrival time difference, errors arise due to the accuracy of time resolution and intrinsic time delay at the source. As mentioned in the paper [55], the time resolution is sufficient so that we ignore the timing error and consider only the arrival time difference. As we see in [48], the arrival time difference is measured as 1.7s, which gives the upper bound on c_T. We also set the intrinsic time delay at the source to 10s to obtain the lower bound of c_T.

The constraint on ν is given by comparison between the observed luminosity distance and the computed one using redshift determined by optical observations. As shown in [48], the observed luminosity distance is given with error as 40^{+8}_{-14}Mpc, corresponding to the redshift is $z \sim 0.008$. In this case, $H_0\tau_{\rm LB} \sim z$ is a good approximation, being independent with the cosmological parameters. ΔT, on the contrary, explicitly depends on the Hubble constant. We assume that $H_0 = 67.8 {\rm kms}^{-1}{\rm Mpc}^{-1}$. By substituting $z = 0.008$ and $H_0 = 67.8 {\rm kms}^{-1}{\rm Mpc}^{-1}$ into Eqs. (4.5.8) and (4.5.9), obtaining Eqs. (4.5.10) and (4.5.11) and Figs. 4.2 and 4.3.

If we take the cases that $\nu_1 = 0$ or $\delta_{g1} = 0$, we obtain the constraints on ν_0 and δ_{g0} as

$$-75.3 \leq \nu_0 \leq 78.4 \,, \tag{4.5.10}$$

$$-4.7 \times 10^{-16} \leq \delta_{g0} \leq 2.2 \times 10^{-15} \,. \tag{4.5.11}$$

ν_0 is too loose to constrain the gravity theories, but being bounded in the finite value.

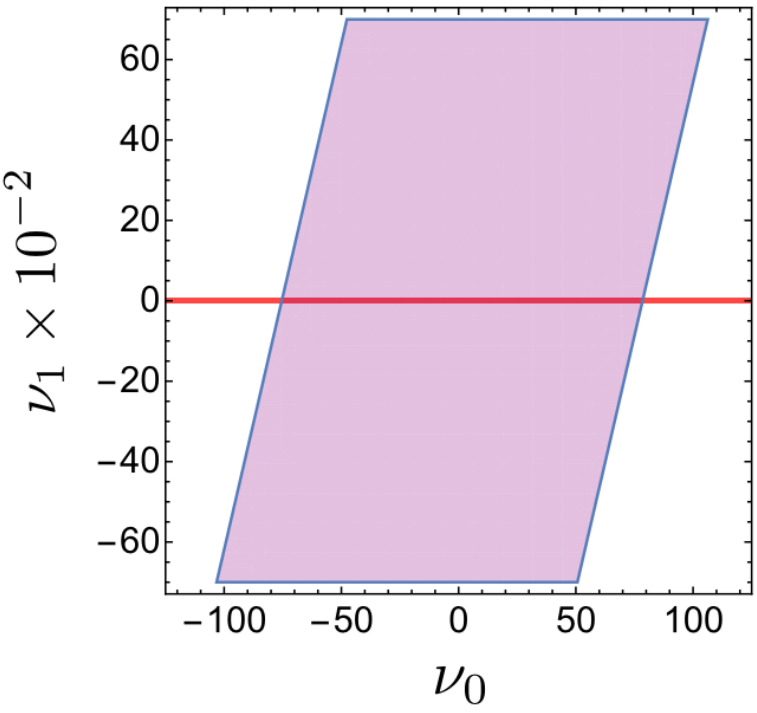

Figure 4.2. Observational constraint on ν_0 and ν_1 by GW170817. The width of the coloured region is given at a 1σ confidence level of the GW observation. The red solid line is $\nu_1 = 0$.

On the other hand, δ_{g0} is well determined enough to exclude the models. The time variation of ν and δ_g, i.e., ν_1 and δ_{g0} respectively, are almost unconstrained, because the only one event is observed. Note that the ΛCDM model, i.e., $\nu = 0$, $\delta_g = 0$, is observationally consistent to these constraints. Note that the ΛCDM model explains all the observational features

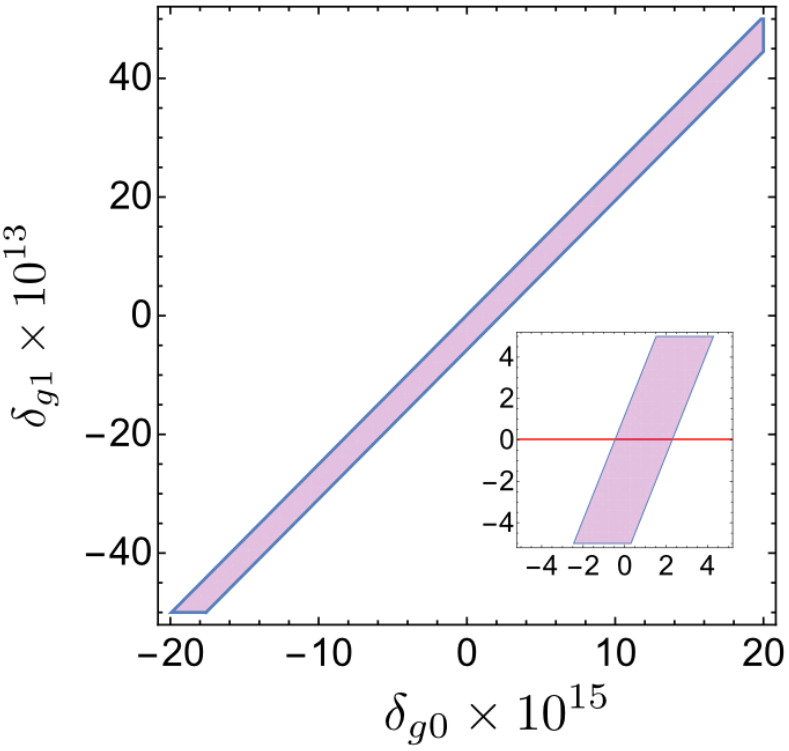

Figure 4.3. Observational constraint on δ_0 and δ_1 by GW170817/GRB170817A. The width of the coloured region is given between the lower and upper bounds. Inset: the enlarged version around the centre of the figure. The width of the coloured region is given at a 1σ confidence level of the GW observation. The red solid line is $\delta_{g1} = 0$.

4.6 Modelling of the observationally-viable scalar-tensor theories

We argue models in scalar-tensor theories so that they satisfy the observational constraints in the previous section; the late-time acceleration, observation of GW170817, and constraints from the early Universe. To create the models under the observational constraints, we assume the following conditions for making a model;

1. The scalar field varies only at late-time Universe, being subdominant in the matter and radiation dominant Universe.
2. The expansion history of the Universe is assumed to be close to that of the ΛCDM model.
3. The background universe should be stable at cosmological scale, i.e., linear instability does not occurs.
4. Scalar-tensor theories are treated as an EFT

The first condition for the scalar field states that the scalar field becomes dynamical at cosmological scales only at late-time. The second condition is to satisfy the current observations of the Hubble expansion. These conditions guarantees that the expansion history of the Universe is not so different from that of the ΛCDM concordance cosmology, being consistent to the BAO or CMB observations. The third condition is theoretical to prevent a background universe modelled in the scalar-tensor theories from being unstable by perturbations on the background. The last condition is to reduce the theories to what phenomenologically interesting. Since we are interested in the deviation from the ΛCDM model, it is not necessarily to consider all the possible choices of arbitrary functions in covariant Lagrangians. We will explain the above four conditions in more detail.

4.6.1 Jordan frame ansatz

For the modelling of modification of gravity, we presume that the gravity minimally couples with the gravity. Specifically this is written with the action as

$$S_{\rm tot} = S_G + \int d^4x\sqrt{-g}\mathcal{L}_m(g_{\mu\nu}, \psi)\,, \tag{4.6.1}$$

where ψ denote any type of the matter fields In the context of the scalar-tensor theories, the Jordan frame ansatz avoids the complications in the followings

- The decay of the scalar field will not cause the additional creation/annihilation of standard model particles
- The physical interpretation of gravitational interactions are simply understood.
- It is easy to control the deviation from Einstein gravity.

Note that Einstein gravity is given at the minimally coupled matter when modelling the gravitational interactions. When it comes to explain the late-time acceleration with the scalar filed, the mass of the scalar field is extremely light, not causing any decay for the baryonic matters but the massless In the Jordan frame, the decay of the scalar field only affects gravitational waves that is the only massless fields coupling with the scalar field. In summary, the Jordan frame ansatz nicely works for the purpose of the measurable deviation from Einstein gravity. Hereafter, we assume the Jordan frame.

4.6.2 Time evolution of scalar field

The challenge is to find the right parametrisation for the evolution of the scalar field for which the Taylor series expansion would be pertinent in the late time universe as well as in the early universe up to ($z \sim 1000$) of the CMB last scattering.

The simple choice of the expansion parameter of the scalar field is the inverse of the redshift. Though that expansion works well only in the high redshift region, $z > 1$, and diverges in the smaller redshift. Another possibility of the Taylor expansion parameter is the scale factor, a, which would work well for $a \leq 1$. But from the physical point of view, the scale factor measures the expansion of the universe. But the time evolution of the scalar field is nothing to do with the size of the universe. Hence it is not a natural choice. Another possibility is the look back (LB) time. The scalar field evolution in terms of the look back cosmic time is valid for the very late time universe, $z < 1$, but the look back time quickly converges around $z = 1$, making it hard to extract the time evolution of the scalar field at $z > 1$. [4]. On the other hand, the conformal time is the local time in each cosmological era, which a scalar field feels. The region of convergence would also include the region $z \geq 1$. Therefore, if we want the time evolution of the scalar field which is valid for both regimes, the late-time (today) as well as the early universe ($z \sim 1000$), then the automatic choice for the expansion of the scalar field evolution is the look back conformal time. We define a flat FLRW Universe

$$ds^2 = -dt^2 + a^2(t)\delta_{ij}dx^i dx^j \,. \tag{4.6.2}$$

Using the look-back conformal time $\tau_{\rm LB}$

$$\tau_{\rm LB}(a) = \int_a^1 \frac{da'}{a'^2 H(a')}\,, \tag{4.6.3}$$

$$H(z) = H_0\sqrt{\Omega_{m0}(1+z)^3 + 1 - \Omega_{m0}}\,. \tag{4.6.4}$$

as a time variable, the time dependence of ϕ is expanded as the Taylor series to the Nth order

$$\phi(\tau_{\rm LB}) = M_\phi \sum_{n=0}^{N} \frac{\phi^{(n)}}{n!}\tau_{\rm LB}^n\,, \tag{4.6.5}$$

where $\phi^{(n)} \equiv d^n\phi/d\tau_{\rm LB}^n$ and M_ϕ is the normalisation of ϕ at $\tau_{\rm LB} = 0$, being unfixed. Hereafter we assume $N = 3$ to make ϕ slowly varying out to higher redshifts. When we take the cosmic expansion in the ΛCDM model $H_{\Lambda{\rm CDM}}(a)$ as in Eq. (4.6.4), the look-back time in Eq. (4.6.3) is expanded around $a = 0$ as

$$\tau_{\rm LB}(a) = \tau_{\rm LB}(0) - \frac{1}{H_0 a_t\sqrt{1-\Omega_{\rm m}}} \times \left\{2\left(\frac{a}{a_t}\right)^{1/2} + \mathcal{O}\left(\left(\frac{a}{a_t}\right)^{7/2}\right)\right\}\,. \tag{4.6.6}$$

Here we introduce the scale factor at which the energy density of matter equals to that of the cosmological constant, $a_t \equiv (\Omega_{\rm m}/(1-\Omega_{\rm m}))^{1/3}$. Notice that $\tau_{LB}(0)$ and a_t are determined once we fix $\Omega_{\rm m}$ and H_0. Hereafter we assume $\Omega_{\rm m} = 0.3080$ to be consistent with the Planck observation of cosmic microwave background (CMB) [56]. Then we obtain $H_0\tau_{LB}(0) \sim 3.27$ and $a_t \sim 0.76$, i. e., $z_t = a_t^{-1} - 1 \sim 0.31$. Equation (4.6.6) gives $\tau_{\rm LB}$ with respect to a for $a \ll a_t$, representing the time in the matter-dominated Universe. The approximation for $\tau_{\rm LB}$ breaks down at $a > a_t$ ($z < z_t$) and may lose an accuracy in computations at low redshifts. For instance, the exact value is $H_0\tau_{\rm LB}(z = 0.1) = 0.10$, while the approximated value from Eq. (4.6.6) is $H_0\tau_{\rm LB}(z = 0.1) = 0.19$. However, the discrepancy in the approximation of τ_{LB} is absorbed by the coefficients $\phi^{(n)}$ and the normalisation of ϕ, causing no inconsistency. We choose the normalisation of ϕ in the following way. Substituting Eq. (4.6.6) into Eq. (4.6.5), we approximate ϕ as

$$\phi(a) \simeq \tilde{M}_\phi\left\{c_\phi^{(0)} + \sum_{n=1}^{N} c_\phi^{(n)}(1 - a^{n/2})\right\}\,. \tag{4.6.7}$$

Here we normalize the coefficients of ϕ with its asymptotic value at $a = 0$, that is, $\phi(\tau_{\rm LB}(0))$ in Eq. (4.6.5) so that

$$\tilde{M}_\phi = M_\phi \frac{\sum_{n=0}^{N} \frac{\phi^{(n)}}{n!} \tau_{\rm LB}^n(0)}{c_\phi^{(0)} + \sum_{n=1}^{N} c_\phi^{(n)}} \,. \tag{4.6.8}$$

Notice that $N = 3$ is the same as in Eq. (4.6.5) to guarantee the smoothness of the functional shape. The time evolution of $\phi(a)$ is controlled by the coefficients $c_\phi^{(n)}(n = 0, 1, 2, 3)$ instead of $\phi^{(n)}$. We assume without loss of generality that the coefficients $c_\phi^{(n)}$ (n=0,1,2,3) span in the range $[-1, 1]$. This is because the energy scale of ϕ, namely, $\tilde{M}_\phi$ determines the normalisation of ϕ. The approximation of ϕ in Eq. (4.6.7) traces the models such that ϕ changes in time at intermediate redshifts, $z \lesssim 10$ as shown in Fig. 4.4. At low redshifts, ϕ diversely fluctuates, depending on the random coefficients. On the contrary, at higher redshifts $z \gtrsim 10$, ϕ converges to its initial value and $\dot{\phi}$ derived from Eq. (4.6.7) by differentiating with respect to t in both sides of the equation universally scales, regardless of the random parameters, as $\dot{\phi}/H \propto -\sqrt{a} \propto -(1+z)^{-1/2}$. Thus, the time evolution of ϕ becomes relatively slower as a redshift increases. In our previous work [4], the applicable range of a redshift was limited to $z \lesssim 1$ and is now extended to higher redshifts due to the different parametrisation of time. Note that even a relatively fast-evolving solution like the tracker solution [57] is marginally included in the truncation $N = 3$. Since, the tracker solution is $\dot{\phi} \propto 1/H \propto t$, then $\phi \propto \tau^2$ at low redshift we can include. On the other hand, in the matter-dominated Universe, since the conformal time and the cosmic time are related by $\tau^n \propto t^{n/3}$, the tracker solution ($n = 6$) might apparently look excluded in our expansion. However, we are interested in the tracker solution after the late matter-dominated era ($z \leq 1$) where the difference between the cosmic time and the conformal time is not large (only a factor of $\mathcal{O}(1)$), the tracker solution is practically captured by our expansion at the order of $n = 2$, even the scalings are different. After all, we claim that our formalism are available at redshifts $z \sim 1$ for models which are already known, capturing wider phenomenological differences of models of cosmic acceleration in DHOST theory.

4.6.3 Consistency and stability conditions

We provide the conditions for the expansion history and the stability of a background universe. We shall call the consistency conditions and stability conditions, respectively. The consistency condition and the stability condition are given as follows.

- 1. Consistency :

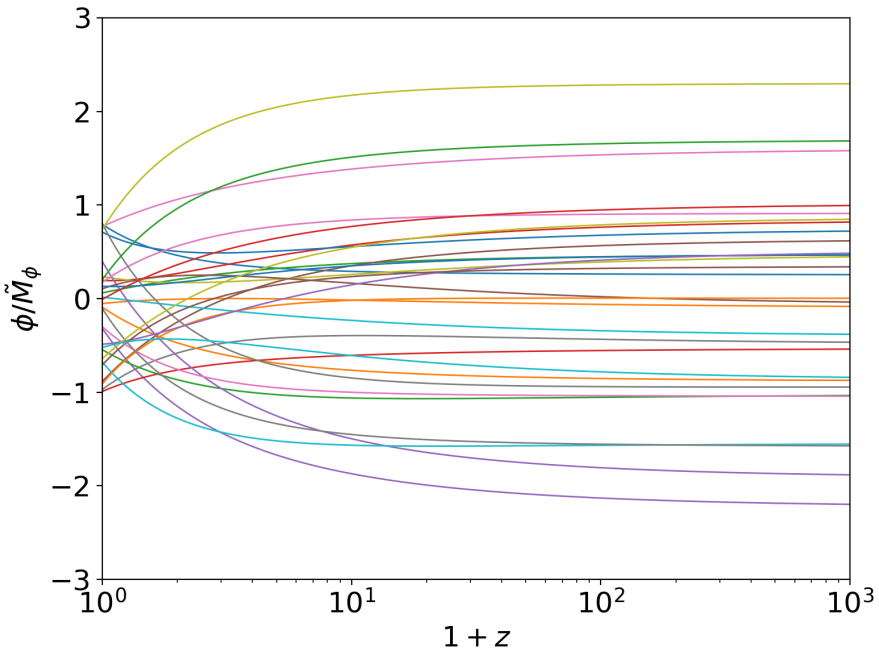

Figure 4.4. Time variation of ϕ with different random coefficients, $c_\phi^{(n)}(n = 0, 1, 2, 3)$.

Collecting the models whose cosmological time evolution are $H_{\rm Horn}$ and $\dot{H}_{\rm Horn}$. $H_{\rm Horn}$ and $\dot{H}_{\rm Horn}$ are given by the Friedmann equations in Eqs. (4.11.8) and (4.11.9) in the Appendix. To obtain $H_{\rm Horn}$ and $\dot{H}_{\rm Horn}$, we substitute $H_{\Lambda\rm CDM}$ and $\phi(t)$ for the right-hand side of Eqs. (4.11.10) and (4.11.11). Then we impose the consistency criteria

$$\left|1 - H_{\rm Horn}/H_{\Lambda\rm CDM}\right| < 20\%\,, \tag{4.6.9}$$

$$\left|1 - \dot{H}_{\rm Horn}/\dot{H}_{\Lambda\rm CDM}\right| < 20\%\,. \tag{4.6.10}$$

Equations. (4.6.9) and (4.6.10) work to select the models that pass the observational bound on the cosmic expansion by assessing the deviation from $H_{\Lambda\rm CDM}$ and $\dot{H}_{\Lambda\rm CDM}$. We choose the allowed range of estimation errors for the Hubble parameter up to 20% based on current variable observations of the Hubble parameter below $z = 0.1$, as shown in Table. I of [58].

- 2. Stability :
  Avoidance of ghost and gradient instabilities for the perturbations of scalar and

tensor modes.

The quadratic action for the scalar and tensor perturbations with the perfect-fluid matter are given in the unitary gauge,

$$S_2 = \int dtd^3xa^3\left[Q_s\left(\dot{\zeta}^2 - \frac{c_s^2}{a^2}(\partial_i\zeta)^2\right) + Q_T\left(\dot{h}_{ij}^2 - \frac{c_T^2}{a^2}(\partial_k h_{ij})^2\right)\right], \tag{4.6.11}$$

where the subscripts s and T represent a scalar and tensor modes in cosmological perturbation, respectively. To evade the ghost and gradient instabilities, the following conditions must be satisfied,

$$Q_s > 0,\ c_s^2 > 0,\ Q_T > 0,\ c_T^2 > 0\,. \tag{4.6.12}$$

Q_s, c_s^2, Q_T, and c_T^2 are specifically given once specifying a scalar-tensor theory. We numerically utilise the consistency and stability conditions to select specific models.

4.7 EFT-like modelling of scalar-tensor theories at cosmological scales

For determining a model in the framework of the scalar-tensor theory, it is necessary to choose the arbitrary functions. Specifically, the four free functions in the covariant form of Horndeski theory, i.e., G_i $(i = 2, 3, 4, 5)$ must be specifically given as a function of ϕ and X. For the purpose of choosing $G_i(i = 2, 3, 4, 5)$, we apply a way of selecting models, as we shall say, "EFT-like modelilng". This means that we expand G_i with respect to ϕ and X at a given energy scale, processing the model - independent analysis. Hereafter, we shall call this just as "EFT modelling".

In the EFT modelling, we parameterise the arbitrary functions $G_i(i = 2, 3, 4, 5)$ in Horndeski theory as

$$G_i^{\rm app}(\phi, X) \equiv \mathcal{G}_i(M_{\rm pl}, \tilde{M}_\phi, H_0)\sum_{m,n=0}^{N_{\rm app}}\frac{g_{i,mn}}{m!n!}\hat{\phi}^m\hat{X}^n\,. \tag{4.7.1}$$

Here $N_{\rm app}$ controls the truncation order for the expansion of the $G_i^{\rm app}$ with respect to $\hat{\phi}$ and $\hat{X}$. $\hat{\phi}$ and $\hat{X}$ are the dimensionless quantities given as $\hat{\phi} \equiv \phi/\tilde{M}_\phi$ and $\hat{X} \equiv$

$\dot{\phi}^2/2H_0^2\tilde{M}_\phi^2$. The dot denotes the derivative with respect to physical time t. We assume that $N_{\rm app} = 3$ to guarantee for $G_i^{\rm app}$ to change slowly in time, compared with the cosmic expansion. $\mathcal{G}_i$ are normalisation factors such as

$$\mathcal{G}_2 = M^4\,,\ \mathcal{G}_3 = \frac{M^4}{\tilde{M}_\phi H_0^2}\,,\ \mathcal{G}_4 = \frac{M^4}{H_0^2}\,,\ \mathcal{G}_5 = \frac{M^4}{\tilde{M}_\phi H_0^4}\,, \tag{4.7.2}$$

where $M \equiv \sqrt{\tilde{M}_\phi H_0}$. These normalisation factors are determined in the way that the Lagrangian density of the system is of the order of $\tilde{M}_\phi^2 H_0^2 = M^4$.

The philosophy of the EFT modelling is the rationality such that the ΛCDM model should emerge as a consequence of the decoupling limit of the scalar field in the scalar-tensor theory with the conventional matter. If we take the limit where the scalar field is cosmologically static, i.e., $\dot{\phi} \to 0$, leading G_i are all constant from Eq. (4.7.1). This identifies a cosmological model to the ΛCDM parametrisation. After all, the EFT model affirmatively works for selecting an appropriate model for the cosmic expansion in the scope of the physics at cosmological scales, i.e., the lowest energy scale we have currently probed.

4.8 Monte-Carlo sampling of models in Horndeski theory

In this section we provide a numerical modelling of Horndeski theory independent of specific models. As we mentioned in Sec. 1, the current observational analyses for Horndeski theory are only limited to specific models. This is because Horndeski theory is too general to investigate. Consequently, one can hardly extract information for which models are relatively favoured from others under observational constraints. To tackle this difficulty, we perform a Monte Carlo simulation with a suitable parametrisation independent of specific models. We classify models in Horndeski theory into subgroups, depending on which arbitrary functions G_i play a role in accelerating the cosmic expansion. To this end, we now compute all physical quantities by randomly drawing all the coefficients from a uniform distribution, $[-1, 1]$, with a Monte Carlo method. As shown in Fig. 4.5, we filter the solutions by the following two conditions.

As shown in Fig. 4.5, the consistency and stability conditions are numerically imposed. For the computation of these conditions, we substitute $H = H_{\Lambda\rm CDM}$, $\dot{H} = \dot{H}_{\Lambda\rm CDM}$ in the quantities. Although we should use $H_{\rm Horn}$ to compute the quantities in Eq. (4.6.12), the difference of the quantities stays within observational errors. Hence the systematic misestimation of the stability condition associated with the choice of the Hubble parameter is negligibly small to sample consistent models.

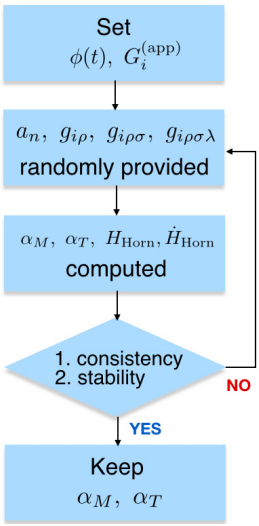

Figure 4.5. The procedure to extract observationally reliable models with Monte Carlo simulation

4.8.1 Equations of motion in Horndeski theory

The equations of motion on a flat FLRW universe in the framework of Horndeski theory is originally derived in T. Kobayashi, M. Yamaguchi, and J. Yokoyama 2011[26]. Perturbative expansion with matters for Horndeski theory is firstly derived in A. De Felice and S. Tsujikawa 2012 [59] and for GLPV theory by J. Gleyzes 2016[60]. After that, another formulation has been proposed in more simplified and physically-transparently by E. Bellini and I. Sawicki 2014 [32], which is commonly used for the tests of cosmological surveys. We follow the notation of the Friedmann equations and the equation of motion of a scalar field based on E. Bellini and I. Sawicki 2014 [32] for convenience of discussion. The Friedman equations in Horndeski theory are given by

$$3M_*^2H^2 = \rho_m + \mathcal{E}\,, \tag{4.8.1}$$

$$M_*^2(2\dot{H} + 3H^2) = -p_m - \mathcal{P}\,, \tag{4.8.2}$$

$\mathcal{E}$ and $\mathcal{P}$ are given by

$$\begin{aligned}
&\mathcal{E} \\
&= -G_2 + 2X(G_{2X} - G_{3\phi}) \\
&+ 6\dot{\phi}H(XG_{3X} - G_{4\phi} - 2XG_{4\phi X}) \\
&+ 12H^2X(G_{4X} + 2XG_{4XX} - G_{5\phi} - XG_{5\phi X}) \\
&+ 4\dot{\phi}H^3X(G_{5X} + XG_{5XX})\,, \qquad (4.8.3) \\
&\mathcal{P} \\
&= G_2 - 2X(G_{3\phi} - 2G_{4\phi\phi}) \\
&+ 4\dot{\phi}H(G_{4\phi} - 2XG_{4\phi X} + XG_{5\phi\phi}) \\
&- M_*^2\alpha_B H\frac{\ddot{\phi}}{\dot{\phi}} - 4H^2X^2G_{5\phi X} + 2\dot{\phi}H^3XG_{5X}\,. \qquad (4.8.4)
\end{aligned}$$

The equation of motion for the scalar field is given as

$$\dot{n} + 3Hn = \mathcal{P}_\phi\,, \qquad (4.8.5)$$

where

$$\begin{aligned}
n \equiv &\dot{\phi}(G_{2X} - 2G_{3\phi}) + 6HX(G_{3X} - 2G_{4\phi X}) \\
&+ 6H^2\dot{\phi}(G_{4X} + 2XG_{4XX} - G_{5\phi} - XG_{5\phi X}) \\
&+ 2H^3X(3G_{5X} + 2XG_{5XX})\,, \qquad (4.8.6)
\end{aligned}$$

and

$$\begin{aligned}
\mathcal{P}_\phi \equiv\, & G_{2\phi} - 2XG_{3\phi\phi} + 2\ddot{\phi}(XG_{3\phi X} + 3H\dot{\phi}G_{4\phi X}) + 6\dot{H}G_{4\phi} \\
&+ 6H^2(2G_{4\phi} + 2XG_{4\phi X} - XG_{5\phi\phi}) + 2H^3\dot{\phi}XG_{5\phi X}\,, \qquad (4.8.7)
\end{aligned}$$

Physically, n denotes the current associate with the scalar field, whereas $\mathcal{P}_\phi$ is the charge sourced by the motion of the scalar field[3].

The EFT parameters are given in α parametrisation in Bellini and Sawacki [32] and [61]. We adopt the notation of [61]. The time-evolving parameters , $\alpha_{M,K,B,T}$ are derived with the free functions as

[3]The notation of n and $\mathcal{P}_\phi$ corresponds to J and P in T. Kobayashi *et al.* 2012, respectively.

$$M_*^2 \equiv 2(G_4 - 2XG_{4X} + XG_{5\phi} - \dot{\phi}HXG_{5X})\,, \tag{4.8.8}$$

$$HM_*^2\alpha_M \equiv \frac{d}{dt}M_*^2\,, \tag{4.8.9}$$

$$\begin{aligned} H^2M_*^2\alpha_K \equiv{}& 2X(G_{2X} + 2XG_{2XX} - 2G_{3\phi} - 2XG_{3\phi X}) \\ &+ 12\dot{\phi}XH(G_{3X} + XG_{3XX} - 3G_{4\phi X} - 2XG_{4\phi XX}) \\ &+ 12XH^2(G_{4X} + 8XG_{4XX} + 4X^2G_{4XXX}) \\ &- 12XH^2(G_{5\phi} + 5XG_{5\phi X} + 2X^2G_{5XXX}) \\ &+ 4\dot{\phi}XH^3(3G_{5X} + 7XG_{5XX} + 2X^2G_{5XXX})\,, \end{aligned} \tag{4.8.10}$$

$$\begin{aligned} HM_*^2\alpha_B \equiv{}& -\dot{\phi}(XG_{3X} - G_{4\phi} - 2XG_{4\phi X}) \\ &- 4XH(G_{4X} + 2XG_{4XX} - G_{5\phi} - XG_{5\phi X}) \\ &- \dot{\phi}XH^2(3G_{5X} + 2XG_{5XX})\,, \end{aligned} \tag{4.8.11}$$

$$M_*^2\alpha_T \equiv 2X(2G_{4X} - 2G_{5\phi} - (\ddot{\phi} - \dot{\phi}H)G_{5X})\,. \tag{4.8.12}$$

$$Q_s = \frac{M_*^2 D}{2(1+\alpha_B)^2}, \tag{4.8.13}$$

$$\begin{aligned} c_s^2 = \frac{2(1+\alpha_B)}{H^2D}\Bigg[&\dot{H} + H^2\alpha_B(1+\alpha_T) \\ &- H^2(\alpha_M - \alpha_T) + 2H\dot{\alpha}_B + \tilde{\rho}_m + \tilde{p}_m\Bigg]\,, \end{aligned} \tag{4.8.14}$$

$$D \equiv \alpha_K + 6\alpha_B^2\,,$$

while

$$Q_T = \frac{M_*^2}{8}\,, \tag{4.8.15}$$

$$c_T^2 = 1 + \alpha_T\,, \tag{4.8.16}$$

To avoid the theoretical instabilities, we should impose the condition that $Q_s > 0$, $c_s^2 > 0$, $Q_T > 0$, and $c_T^2 > 0$.

4.8.2 The effect of G_4 and G_5

The functions G_4 and G_5 play significant roles for α_T and α_M. In fact, one can see that α_T and α_M are determined solely by G_4 and G_5 in Eqs. (4.8.26) and (4.8.27). In addition, G_4 and G_5 can control the cosmic accelerating expansion. Because of their importance, we firstly perform our simulation while leaving G_4 and G_5 nontrivial and

setting $G_2 = 0 = G_3$.

Parameter distribution in different expansion history

Firstly we see how the different histories of cosmic expansion affect the model distribution on the α_T - α_M plane. Here we refer to the cosmic expansion in the EdS universe. We now obtain the distribution in the case of the EdS just by replacing $H_{\Lambda\mathrm{CDM}}$ and $\dot{H}_{\Lambda\mathrm{CDM}}$ in Eqs. (4.6.9) and (4.6.10) with those of the EdS model, H_{EdS} and $\dot{H}_{\mathrm{EdS}}$, respectively. Figure 2 shows how distinctively the models distribute on the α_T-α_M plane under two different histories of the cosmic expansion. Moreover, to realise the cosmic expansion close to the case in the ΛCDM model with G_4 and G_5, either α_T or α_M must be $\mathcal{O}(1)$. This result is expected from the analytic estimation of Lombriser and Taylor [62], but the shape of our distribution is different in detail from theirs. The dots are very sparse at the top left or bottom right, where either α_T or α_M is extremely small. The main reason for this is due to the random sampling of models from all possible models. In other words, the models that have tiny values of α_M and α_T need fine-tuning to realise the cosmic expansion in the same way as the ΛCDM model.

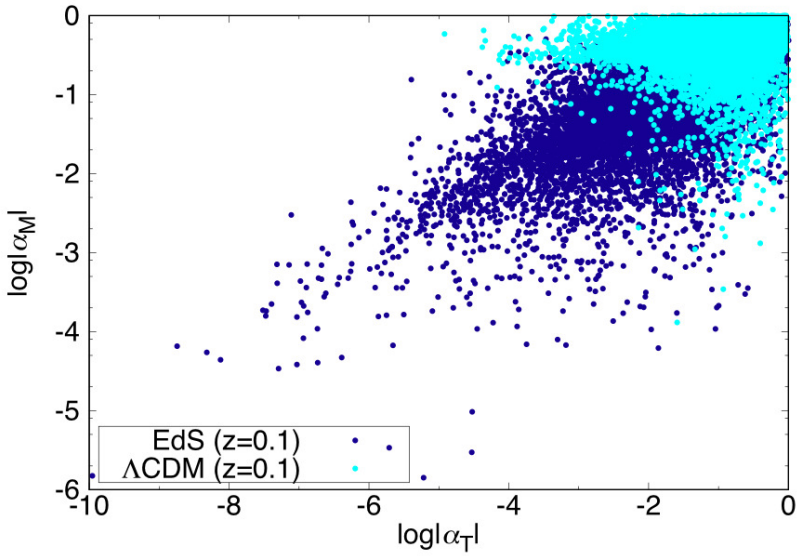

Figure 4.6. Distribution of the models in the α_T-α_M plane with different cosmic expansion histories. The ΛCDM model (cyan dots) and the EdS model (dark blue dots) are considered. We collect the models in Horndeski theory via the consistency condition in Eqs. (4.6.9) and (4.6.10), comparing the Hubble parameter of models with those of ΛCDM or EdS.

Model classification on the α_T-α_M plane in general cases

We now allow all the model parameters to vary; namely G_2 and G_3 are both nonzero. The parameters in Eqs. (4.6.5) and (4.7.1) are now provided at random. What we show in this section is how the models belonging to the different subclasses of Horndeski theory are distributed on the α_T-α_M plane. For instance, quintessence and the scalar field with nonlinear kinetic theory are exactly at the point of $\alpha_T = 0 = \alpha_M$, while $f(R)$ theory is on the α_M axis ($\alpha_T = 0$). We now classify the models into four categories, as shown in Table. I. Based on the classification, we carry out the Monte Carlo simulation and obtain the distributions of each subclass in Fig. 4.7.

Subclass of Horndeski theory	Parameters of $G_i^{(\mathrm{app})}$	Models	Refs.
(I) $G_4 + G_5$	$G_2, G_3 = 0$	Self acceleration	[62]
		Quintessence	[19]
(II) $G_4 + G_5 + G_2$	$g_2, g_{2X}, g_{2\phi\phi} \neq 0$	nonlinear kinetic theory	[42]
		$f(R)$ theories	[27, 63]
(III) $G_4 + G_5 + G_3$	$G_3 \neq 0$	Cubic Galileons	[64, 65]
(IV) Cov.Gal	$g_{2X}, g_{3X}, g_{4XX}, g_{5XX} \neq 0$	Covariant Galileons	[37, 44]

Table 4.1. Division of subclasses with parameters in $G_i^{(\mathrm{app})}$ and corresponding theories

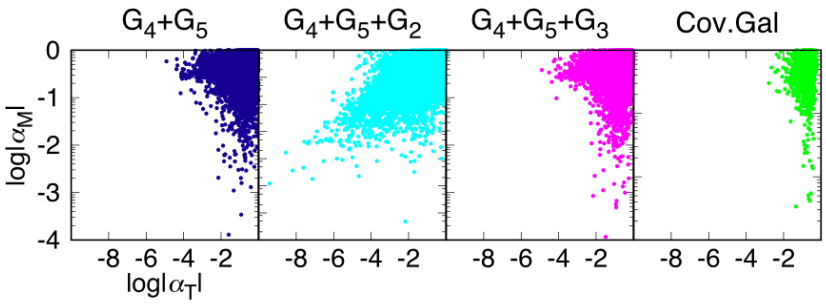

Figure 4.7. Distribution of models in each subclass shown in Table. I on $\alpha_T - \alpha_M$ plane.

As we see in Fig. 4.7, the models except the subclass (II) are distributed in the domain with large α_T. This is because in those cases G_4 and G_5 mainly drive the cosmic accelerating expansion and α_T consequently becomes large. In the subclass (II), on the contrary, the models diagonally concentrate toward the area in which both α_T and α_M are small. This is because G_2 in turn plays a role in accelerating the

cosmic expansion, which relaxes the constraints on G_4 and G_5. In this subclass, we also find that the models are predicted to align along the diagonal line, $|\alpha_T| \propto |\alpha_M|^2$. We discuss analytically why this feature appears in the following way. First of all, we assume that $\dot{\phi}$ is initially tiny and the time evolution of $\dot{\phi}$ is very slow as $|\ddot{\phi}/H\dot{\phi}| \ll 1$. In this case, we expand G_i as

$$G_i(\phi, X) \simeq G_i(\phi_0, X_0) - G_{i\phi}(\phi_0, X_0)\dot{\phi}_0\tau_{LB}\,, \tag{4.8.17}$$

where the subscript 0 denotes the values at the present time. Note that we use the fact that the difference between the look-back conformal time τ_{LB} and the look-back cosmic time t_{LB} is at higher order of Taylor expansion in time, i.e. $\tau_{LB} \simeq a^{-1}t_{LB} \simeq (1 + H_0 t_{LB})^{-1}t_{LB} \simeq t_{LB}$ .Hereafter we simplify the expressions $G_i(\phi_0, X_0) = G_{i,0}$ and $G_{i\rho}(\phi_0, X_0) = G_{i\rho,0}$, where $\rho = \phi$ or X. In the same way as in Eq. (4.8.17), we obtain the observable parameters α_M and α_T from Eqs. (4.8.25) − (4.8.27) as

$$\alpha_M \simeq \frac{G_{4\phi,0}}{G_{4,0}}\dot{\phi}_0\,, \tag{4.8.18}$$

$$\alpha_T \simeq \frac{2(G_{4\phi,0} - G_{5\phi,0})}{G_{4,0}}X_0\,, \tag{4.8.19}$$

Considering $X_0 = \dot{\phi}_0^2/2$, we obtain the relation between α_M and α_T as

$$\frac{\alpha_T}{\alpha_M^2} \simeq \frac{G_{4,0}(G_{4X,0} - G_{5\phi,0})}{{G_{4\phi,0}}^2} = \frac{g_4(g_{4X} - g_{5\phi})}{{g_{4\phi}}^2}\,. \tag{4.8.20}$$

Equation. (4.8.20) is only valid if $g_{4\phi} = 0$. The second equality is obtained from Eq. (4.7.1). Since in our computation the model parameters are given by constants at random, we see that models are distributed along the line of $|\alpha_T| \propto |\alpha_M|^2$, which corresponds to a diagonal line on the α_T-α_M plane in the logarithmic scale. Our analysis also suggests that the naive parametrisation of αs is not always applicable. In the literature, it is widely accepted that the time evolution of all $\alpha's$ is proportional to the energy density of dark energy, $\alpha = \Omega_{DE}\alpha_i$, where $\Omega_{DE}(t) \equiv \tilde{\mathcal{E}}/3H_0^2$ and α_i is the initial value of α [32]. Indeed, this parametrisation has proved to be valid in Galileon theories [66] and it is supported in cosmological surveys by Bayesian evidence[60]. However, as Linder has pointed out recently, this assumption is not always correct in the case of $f(R)$ gravity [67]. Our results also support this statement. Here we only see the correlation between α_T and α_M, but our technique is easily applicable to investigate the correlations among other parameters, including α_K and α_B.

4.8.3 Constraints on Horndeski theory by GW170817/GRB170817

When we consider the scalar-tensor gravity, ν and δ_g are given as a function of α_M and α_T. Expanding both sides of Eqs. (4.8.28) and (4.8.29) with respect to $H_0\tau_{LB}$ and assuming δ_g to be considerably small, we obtain ν_0, ν_1, δ_{g0}, and δ_{g1} as

$$\nu_0 = \alpha_{M,0}\,, \tag{4.8.21}$$

$$\nu_1 = \frac{\dot{\alpha}_{M,0}}{H_0}\,, \tag{4.8.22}$$

$$\delta_{g0} = -\frac{\alpha_{T,0}}{2}\,, \tag{4.8.23}$$

$$\delta_{g1} = -\frac{\dot{\alpha}_{T,0}}{2H_0}\,. \tag{4.8.24}$$

In Horndeski theory, α_M and α_T are given by

$$M_*^2(t) \equiv 2(G_4 - 2XG_{4X} + XG_{5\phi} - \dot{\phi}HXG_{5X})\,, \tag{4.8.25}$$

$$\alpha_M(t) = \frac{1}{HM_*^2}\frac{dM_*^2}{dt}\,, \tag{4.8.26}$$

$$\alpha_T(t) = \frac{2X(2G_{4X} - 2G_{5\phi} - (\ddot{\phi} - \dot{\phi}H)G_{5X})}{M_*^2}\,. \tag{4.8.27}$$

α_M and α_T are related to the observable parameters ν and δ_g as

$$\nu = \alpha_M\,, \tag{4.8.28}$$

$$\delta_g = 1 - \sqrt{1+\alpha_T}\,. \tag{4.8.29}$$

Note that $\delta_g \simeq -\alpha_T/2$ if δ_g is small. Substituting $\phi(t)$, the Hubble parameter in Eq. (4.6.3), and all $G_i^{(\mathrm{app})}$ in Eq. (4.7.1) into Eqs. (4.8.25) $-$ (4.8.27), we can compute α_M and α_T as a function of redshift.

Converting the model parameters in the previous section to those in Eqs. (4.8.21) - (4.8.24), we obtain the distributions of the observable parameters as shown in Fig. 4.8. Similar to Fig. 4.8, Fig. 4.2 shows that the effect of the G_4 and G_5 functions is distinguishable in both parameters ν and δ_g, while Fig. 4.8 additionally shows the information about the time evolution of the models in terms of ν_1 and δ_{g1}. The model space of Horndeski theory after GW170817 is significantly reduced into the quadratic order of the second derivative of ϕ. By taking into account the constraints $|\delta_{g0}| \lesssim 10^{-15}$, the right column in Fig. 4.8 tells that the models we construct are significantly excluded.

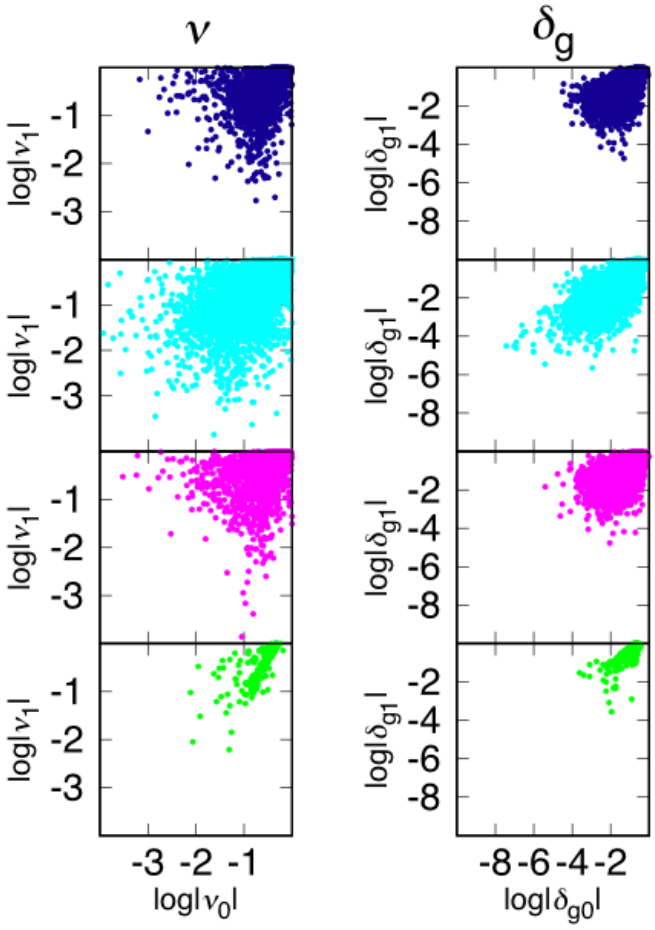

Figure 4.8. Model distributions on the observable parameter plane for the subclasses shown in Table. I. Each colour of the dots corresponds to that in Fig. 4.7.

4.9 Horndeski theory after GW170817

The constraint from the simultaneous observation of GW170817 and GRB170817A is robust on α_T as $|\alpha_T| \lesssim 10^{-15}$, practically $\alpha_T = 0$. In Horndeski theory, $\alpha_T = 0$ has resulted in $G_{4X} = 0$ and $G_5 = 0$. Once imposing $G_{4X} = 0$ and $G_5 = 0$, the Lagrangian in Eq. (4.4.5) is reduced to

$$\mathcal{L}_{c_g^2=1} = P(\phi, X) + Q(\phi, X)\Box\phi + F(\phi)R\,, \tag{4.9.1}$$

where we define $G_2 = P(\phi, X)$, $G_3 = -Q(\phi, X)$, and $G_4 = F(\phi)$. Although the action in Eq. 4.9.1 is rather simple than the Lagrangian in Eq. (4.4.5), it significantly changes the law of gravity via $Q(\phi, X)$ and $F(\phi)$. This Lagrangian is interesting at cosmological scales because it is capable of making the cosmic acceleration. We construct the models that explain the cosmic expansion history.

4.9.1 Friedmann equations

The Friedman equations in Horndeski theory are given by

$$3M_*^2H^2 = \rho_m + \mathcal{E}\,, \tag{4.9.2}$$
$$M_*^2(2\dot{H} + 3H^2) = -p_m - \mathcal{P}\,, \tag{4.9.3}$$

$\tilde{\mathcal{E}}$ and $\tilde{\mathcal{P}}$ are given by

$$\mathcal{E} = -P + 2X(P_X + Q_\phi) + 6\dot{\phi}H(XP_X - F_\phi)\,, \tag{4.9.4}$$
$$\mathcal{P} = P + 2X(P_\phi + 2F_{\phi\phi}) + 4\dot{\phi}HF_\phi - M_*^2\alpha_B H\frac{\ddot{\phi}}{\dot{\phi}}\,. \tag{4.9.5}$$

$\alpha_{M,K,B}$ are derived with P, Q, and F as

$$M_*^2 \equiv 2F\,, \tag{4.9.6}$$
$$HM_*^2\alpha_M \equiv \frac{d}{dt}M_*^2\,, \tag{4.9.7}$$
$$H^2M_*^2\alpha_K \equiv 2X(P_X + 2XP_{XX} + 2Q_\phi + 2XQ_{\phi X}) - 12\dot{\phi}XH(Q_X + XQ_{XX})\,, \tag{4.9.8}$$
$$HM_*^2\alpha_B \equiv \dot{\phi}(XQ_X + F_\phi)\,, \tag{4.9.9}$$

$$Q_s = \frac{M_*^2 D}{2(1+\alpha_B)^2}, \tag{4.9.10}$$

$$c_s^2 = \frac{2(1+\alpha_B)}{H^2 D}\left[\dot{H} + H^2\alpha_B - H^2\alpha_M + 2H\dot{\alpha}_B + \tilde{\rho}_m + \tilde{p}_m\right], \tag{4.9.11}$$

$$Q_T = \frac{M_*^2}{8}, \tag{4.9.12}$$

$$c_T^2 = 1, \tag{4.9.13}$$

$$D \equiv \alpha_K + 6\alpha_B^2,$$

To avoid the theoretical instabilities, we should impose the condition that $Q_s > 0$, $c_s^2 > 0$, $Q_T > 0$.

4.9.2 Gravitational couplings at cosmological scales

When one considers the fluctuations of a scalar field on a given cosmological background, the scalar field acquires the mass M. For a canonical field with a potential $V(\phi)$, M^2 is nothing but the second derivative of V with respect to ϕ, $V_{\phi\phi}$. However, M arises not only from V in P but also from Q and F (see Eq. (35) in [68] for the exact expression of M). When M is much larger than the Hubble scale H, the scalar field fluctuation does not propagate at cosmological scales. On the contrary, when $M \sim H$, the fluctuation affects the cosmic expansion. Since we are interested in the case when the scalar field fluctuations significantly modify the gravitational force at cosmological scales in accordance with the late-time acceleration of the Universe, we consider the case of $M \sim H_0$, where H_0 is the Hubble constant.

In particular, under the quasi-static approximation (QSA), we ignore all dynamical terms in the equations of motion. Then the Poisson and lensing equations are given by [69, 70]

$$k^2\Psi \simeq -4\pi G_{\rm matter}(k,\tau)\delta\rho_{\rm m}\,, \tag{4.9.14}$$

$$k^2(\Psi+\Phi) \simeq -8\pi G_{\rm light}(k,\tau)\delta\rho_{\rm m}\,, \tag{4.9.15}$$

where τ is the conformal time, $\delta\rho_{\rm m}$ is the density fluctuation of matter.

Hence it is convenient to divide into two cases: super-Compton limit ($k/a \ll M$)

and sub-Compton limit ($k/a \gg M$). According to [68, 71], the couplings at the super-Compton scales become

$$G_{\rm matter} = G_{\rm light} = G_{\rm N}\frac{M_{\rm pl}^2}{M_*^2}\,, \tag{4.9.16}$$

while at the sub-Compton scales

$$G_{\rm matter} = G_{\rm N}\frac{M_{\rm pl}^2}{M_*^2}(1+\beta_\xi^2)\,, \tag{4.9.17}$$

$$G_{\rm light} = G_{\rm N}\frac{M_{\rm pl}^2}{M_*^2}\left[1+\beta_\xi^2+\sqrt{\frac{2}{c_S^2 D}}\frac{\alpha_M\beta_\xi}{2}\right]\,, \tag{4.9.18}$$

where β_ξ is

$$\beta_\xi = -\sqrt{\frac{2}{c_S^2 D}}\,(\alpha_M-\alpha_B)\,. \tag{4.9.19}$$

Here and hereafter we use $M_{\rm pl}$ to denote the reduced Planck mass. Particularly, the function β_ξ plays an important role to distinguish the gravitational couplings. This difference is originated from the fluctuations of a scalar field.

4.9.3 Model distributions

From Eqs. (4.9.16)-(4.9.18), we obtain $G_{\rm matter} = G_{\rm light}$ at the super-Compton scales, while $G_{\rm light}$ and $G_{\rm matter}$ are not equivalent at the sub-Compton scales. To see these behaviors, it is useful to see the correlation between $G_{\rm matter}$ and $G_{\rm light}$. In addition to that, we are interested in how α_M is distributed and related to $G_{\rm matter}$ and $G_{\rm light}$. In Figs. 4.9 and 4.10, we distribute the models filtered by the conditions in Sec. 4.9 and show α_M in colour on the $G_{\rm light}$-$G_{\rm matter}$ plane at different redshifts for two representative models of Horndeski theory.

At first glance, there is little difference between the Horndeski Lagrangian with/ without the Q function. This explicitly shows that the Q term does not play any significant role to distribute models in the parameter space.

At the super-Compton scales in Fig. 4.9, all the models are aligned along the diagonal line, while at the sub-Compton scales in Fig. 4.10, the off-diagonal scatter is apparent. This trend at sub-Compton scales is expected since the fluctuations of a scalar field become significant. The offset trend is traced back to the third term in Eq. (4.9.18).

For convenience to discuss the offset trend, we introduce the gravitational slip

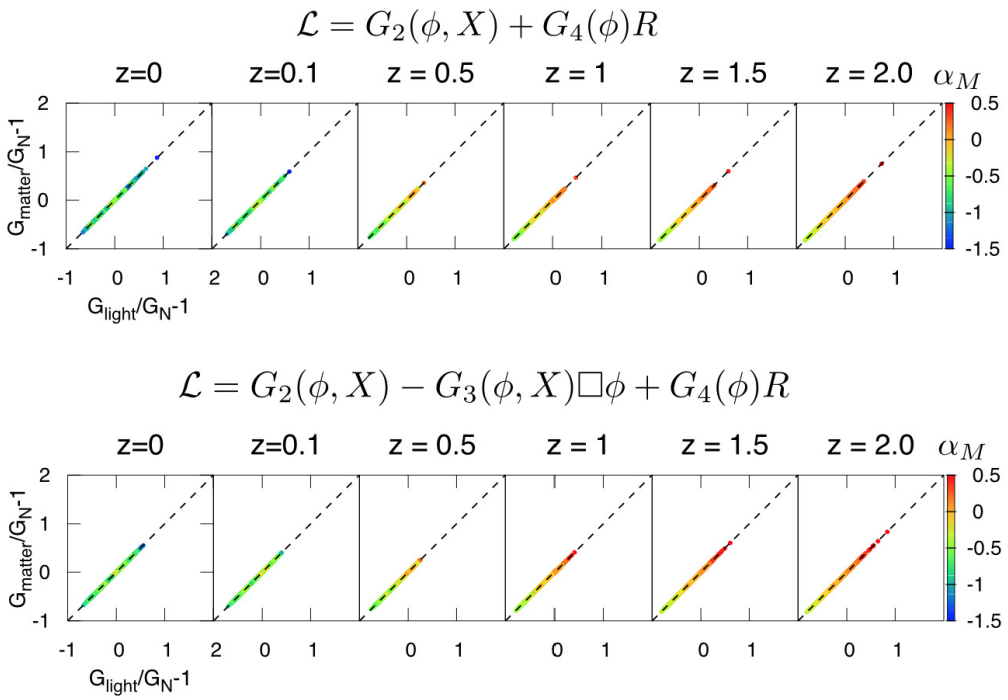

Figure 4.9. Time evolution of the correlation between $G_{\rm light}$ and $G_{\rm matter}$ at super-Compton limit. The colour bar shows the value of α_M. The diagonal dashed lines show $G_{\rm matter} = G_{\rm light}$, i.e. $\Delta\gamma = 0$. Top: models without Q term. Bottom: models with Q term. The range of α_M covers over 95% of all the filtered models.

parameter γ [72, 73, 74][4] as

$$\Phi = \gamma\Psi\,, \tag{4.9.20}$$

where Φ and Ψ are the linear perturbations of the space-time metric. In general relativity, $\gamma = 1$, while in general theories of modified gravity, $\gamma \neq 1$. Therefore, $\gamma \neq 1$ explicitly captures the modification of gravity. We further introduce the deviation parameter $\Delta\gamma \equiv \gamma - 1$. Let us focus on the sub-Compton scales. By using Eqs. (4.9.14), (4.9.15), and (4.9.20), $\Delta\gamma$ relates to the gravitational couplings as

$$\frac{G_{\rm light}}{G_{\rm matter}} = 1 + \frac{\Delta\gamma}{2}\,, \tag{4.9.21}$$

[4]In the literature [75, 76, 77], the gravitational slip parameter has different definitions.

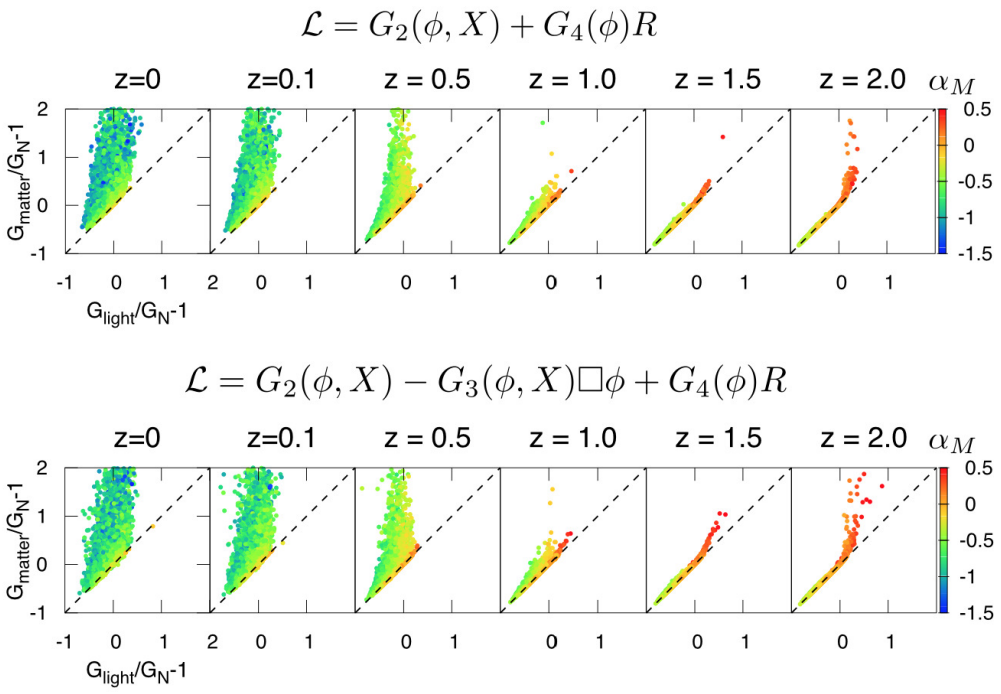

Figure 4.10. Time evolution of the correlation between $G_{\rm light}$ and $G_{\rm matter}$ at sub-Compton limit. The colour shows the value of α_M. The diagonal dashed lines show $G_{\rm matter} = G_{\rm light}$, i.e. $\Delta\gamma = 0$. Top: models without Q term. Bottom: models with Q term. The range of α_M covers over 95% of all the filtered models.

and from Eqs. (4.9.17) and (4.9.18),

$$\Delta\gamma = \sqrt{\frac{2}{c_S^2 D}}\frac{\alpha_M \beta_\xi}{1+\beta_\xi^2}\,. \tag{4.9.22}$$

When $\Delta\gamma = 0$, the offset disappears and there are two different branches $\alpha_M = 0$ or $\beta_\xi = 0$. From Eq. (4.9.19), the latter is the case of $\alpha_B = \alpha_M$, known as No Slip Gravity [78].

Taking a closer look at low redshifts below $z = 1$ in Fig. 4.10, the offset trend we observe implies $\Delta\gamma < 0$, consequently $\alpha_M\beta_\xi < 0$ from Eq. (4.9.22). To understand the condition $\alpha_M\beta_\xi < 0$, we recall the relation among α_M, α_B, and Q, which comes from Eqs. (4.9.7) and (4.9.9),

$$\alpha_B = \frac{\alpha_M}{2} + \frac{\dot\phi X Q_X}{2HF}\,. \tag{4.9.23}$$

The case when $Q = 0$ (the top panels in Fig. 4.10), we obtain $\alpha_B = \alpha_M/2$. In this case, by substituting β_ξ in Eq. (4.9.19) for Eq. (4.9.22) and using $\alpha_B = \alpha_M/2$, $\Delta\gamma$ becomes

$$\Delta\gamma = -\frac{\alpha_M^2}{c_S^2 D(1+\beta_\xi^2)}\,. \tag{4.9.24}$$

Since we impose the stability conditions, $c_S^2 > 0$ and $D > 0$, $\Delta\gamma < 0$ is always satisfied for a non-zero α_M. Consequently, the offset scatters above the diagonal line, as seen in the top panels of Fig. 4.10.

The opposite case $\Delta\gamma > 0$ with a nonzero Q is also possible in principle. However, the bottom panels of Fig. 4.10 in the presence of Q show no trend of $\Delta\gamma > 0$. To have a positive $\Delta\gamma$, the second term on the right-hand side in Eq. (4.9.23) should be negative and dominate the first term. In other words, ϕ should decrease in time as rapid as the cosmic expansion. However, this is not the case, indicating that the models such that ϕ changes rapidly is less supported by our filtering conditions we imposed. The absence of the contribution from the Q term in Eq. (4.9.23) is because of the small value of X. In fact, the derivative of Q with respect to X and the multiplication of X in the term $\dot{\phi}XQ_X/2HF$ bring the suppression factor proportional to $\hat{X}^{3/2}$. The smallness of $\hat{X}$ is due to the filtering conditions on the cosmic expansion history in Eqs. (4.6.9) and (4.6.10). As explicitly shown in Fig. 4.11, the filters in Eqs. (4.6.9) and (4.6.10) preferentially choose the models with smaller magnitude of $\hat{X}$. This is because the time variation of the energy density on the right-hand side in Eq. (4.11.8) is slow to keep the agreement with the ΛCDM model. For these reasons, the models with $\Delta\gamma > 0$ do not appear.

The interesting feature is the signature of α_M. We clearly see that the trend $\alpha_M \lesssim 0$ at low redshifts, that is, M_*^2 decreases in time. In addition, the magnitude of α_M is of the order of 0.1. At the super-Compton scales, the models with negative α_M have smaller $G_{\rm matter}$ and $G_{\rm light}$, namely, M_*^2 larger than $M_{\rm pl}^2$ from Eq. (4.9.16). On the other hand, at the sub-Compton scales, the values of $G_{\rm matter}$ and $G_{\rm light}$ distribute more widely from smaller to larger and the offset scatter significantly correlates with the negative values of α_M, unlike the super-Compton case. This difference arises since the magnitude of β_ξ is larger as that of α_M is larger. In other words, $G_{\rm matter}$ and $G_{\rm light}$ at the sub-Compton scales are significantly diversified by the larger magnitude of α_M, explicitly breaking the equivalence principle of gravity.

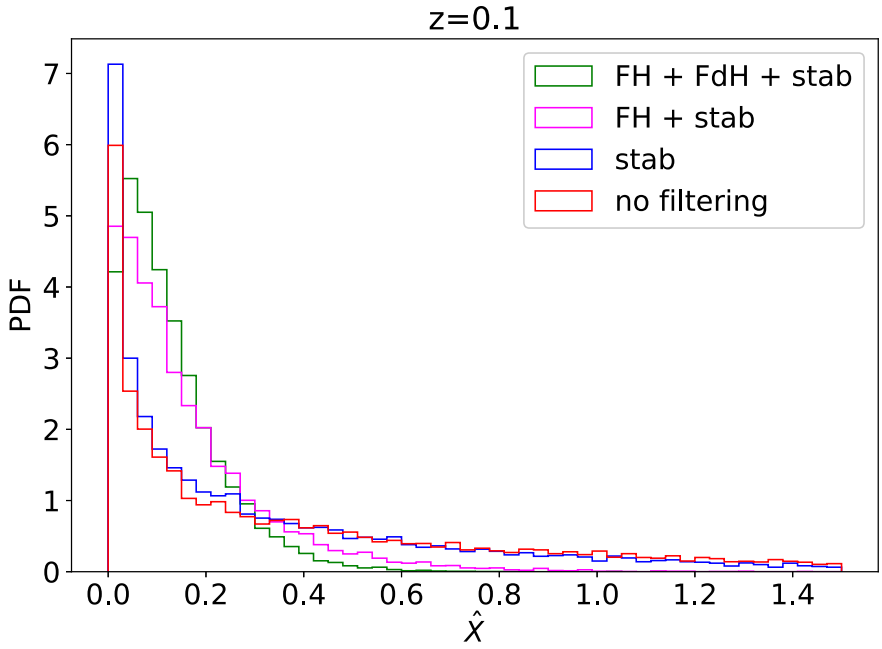

Figure 4.11. The probability distribution of $\hat{X}$, showing the roles of the filters at $z = 0.1$. In the legend, "FH", "FdH", and "stab" denote the filters in Eqs. (4.6.9), (4.6.10), and (4.6.12), respectively. "no filtering" denotes the distribution without any filter.

4.9.4 Negative sign of α_M

Remarkably, the origin of the negative value of α_M is the conditions that the cosmic expansion history should be similar to that of the ΛCDM model. As shown in Fig. 4.12, the consistency conditions for $H_{\rm Horn}$ and $\dot{H}_{\rm Horn}$ are essential to bias α_M toward the negative side as the redshift becomes smaller. Looking at the Friedmann equation in Eq. (4.11.8) divided by $3H^2$ for the both sides of the equation, we obtain

$$1 = \frac{V_{\rm eff}}{3M_*^2H^2} + \frac{\rho_m}{3M_*^2H^2} + \mathcal{O}(\hat{X})\,, \tag{4.9.25}$$

where we omit the kinetic terms and define $V_{\rm eff}$ as

$$V_{\rm eff} = -3M_*^2H^2\alpha_M + V(\phi)\,. \tag{4.9.26}$$

Here $V(\phi)$ denotes the terms in G_2 depending only on ϕ. When the Universe is accelerating and the kinetic energy $\hat{X}$ is small, i. e., the second and last terms in

Eq. (4.9.25) are negligible, $V_{\rm eff} \sim 3M_*^2H^2$. The both terms in Eq. (4.9.26) equivalently contribute to $V_{\rm eff}$ because there is no prior knowledge about which term is more significant than the other. Therefore, it is probabilistically reasonable to assume $-3M_*^2H^2\alpha_M \sim V(\phi) \sim 0.5V_{\rm eff} > 0$. As a result, α_M stays negative.

The other evidence for $\alpha_M < 0$ is the signature of $\dot{H}$. It is useful to present an additional equation for $\dot{H}$ from Eqs. (4.11.8) - (4.11.11) as

$$\begin{aligned}(2+\alpha_M)M_*^2\dot{H} = &-HM_*^2\dot{\alpha}_M + H^2M_*^2\alpha_M(1-\alpha_M) \\ &- 2X(P_{2X}+2Q_\phi) + 6\dot{\phi}HXQ_X \\ &+ (\alpha_M - 2\alpha_B)\frac{M_*^2H\ddot{\phi}}{\dot{\phi}} - \rho_{\rm m} - p_{\rm m}\,,\end{aligned} \tag{4.9.27}$$

where we replaced $F_{\phi\phi}$ with $\dot{\alpha}_M$ by using the relation

$$\dot{\alpha}_M = H\left\{\frac{4XF_{\phi\phi}}{H^2M_*^2} + \left(\frac{\ddot{\phi}}{H\dot{\phi}} - \frac{\dot{H}}{H^2}\right)\alpha_M - \alpha_M^2\right\}. \tag{4.9.28}$$

From Fig. 4.12, we find that the time variation of α_M with redshifts is small, i.e., $|\dot{\alpha}_M/H\alpha_M| \ll 1$. Since $\dot{\alpha}_M$ is negligibly small, we can drop the term with $\dot{\alpha}_M$ from Eq. (4.9.27) and obtain

$$(\alpha_M+2)\frac{\dot{H}}{H^2} = \alpha_M - \frac{\rho_m}{H^2M_*^2} + (\text{kinetic terms for } \phi)\,, \tag{4.9.29}$$

where we omit α_M^2 and take $p_{\rm m} = 0$. When the second and last terms in Eq. (4.9.29) are negligibly small compared to α_M, namely, corresponding to the epoch when the Universe is accelerating with the slow-rolling scalar field, the signature of the $\dot{H}$ is the same as $\alpha_M/(\alpha_M+2)$. Since the range of α_M is $|\alpha_M| < 1$ in Fig. 4.12, the consistency condition in Eq. (4.6.10) selects $\dot{H} < 0$ and consequently $\alpha_M < 0$.

We comment the following two points on the negativeness of α_M. Firstly, we can show that the signature of α_M does not affect the condition $c_S^2 > 0$ at the leading order. By substituting Eq. (4.9.27) into Eq. (4.9.11), we obtain

$$c_s^2 = \frac{2X(P_X+2Q_\phi)/H^2M_*^2 + 3\alpha_M^2/2 + \Delta}{\alpha_K + 6\alpha_B^2}\,, \tag{4.9.30}$$

where Δ in the numerator denotes

$$\Delta = (\alpha_M - 2\alpha_B)\left\{\frac{\dot{H}}{H^2} - \frac{\ddot{\phi}}{H\dot{\phi}} + 4 - \frac{\alpha_M - 2\alpha_B}{2}\right\} + \frac{\dot{\alpha}_M - 2\dot{\alpha}_B}{H}\,. \tag{4.9.31}$$

Under the approximation $\hat{X} \ll 1$ obtained from the conditions in Eqs. (4.6.9) and (4.6.10) (more directly see Fig. 4.11), we obtain the following equations from Eqs. (4.9.23) and (4.8.10),

$$\alpha_B = \frac{\alpha_M}{+}\mathcal{O}(\hat{X}^{3/2})\,, \tag{4.9.32}$$

$$\alpha_K = \frac{2X(P_X + 2Q_\phi)}{H^2 M_*^2} + \mathcal{O}(\hat{X}^{3/2}), \tag{4.9.33}$$

By using Eqs. (4.9.32) and (4.9.33), c_S^2 is given by

$$c_S^2 = 1 + \mathcal{O}(\hat{X}^{1/2})\,, \tag{4.9.34}$$

where we use $\alpha_K + 6\alpha_B^2 = \mathcal{O}(\hat{X})$ and $\Delta = \mathcal{O}(\hat{X}^{3/2})$. The formula in Eq. (4.9.34) explicitly states that the condition $c_S^2 > 0$ is nothing to do with the value of α_M. Secondly, one might consider that the negative α_M or the decrease of M_*^2 seem to be counter-intuitive as a behaviour of the cosmic acceleration because a larger gravitational coupling could decelerate the Universe more by stronger gravitational attraction. However, we find that M_* larger than $M_{\rm pl}$ is realised in the filtered solutions. As a result, $G_{\rm matter}$ and $G_{\rm light}$ remain smaller than the Newton constant at the super-Compton scale. In Fig. 4.13, at low redshifts, M_*^2 mostly stays larger than $M_{\rm pl}^2$, while α_M is negative. Therefore, $\alpha_M \lesssim 0$ and weaker gravitational couplings are compatible.

Finally, we mention that the gravitational slip parameter $\Delta\gamma$ is positively correlated with α_M, as we see in Fig. 4.14. More quantitatively, both of $\Delta\gamma$ and α_M are of the order of -0.1 at $z = 0$.

4.9.5 Current observational constriants on Horndeski theory

Although in the model of the Horndeski theory in Eq. (4.10.8), the Vainshtein mechanism produces the Newtonian law of gravity at small scales, whereas the time variation of the gravitational couplings are allowed at cosmological scales [79]. However, the direct measurements of the gravitational couplings with local astronomical objects can give the constraint on the present value of α_M, denoted by α_{M0}, by connecting a local

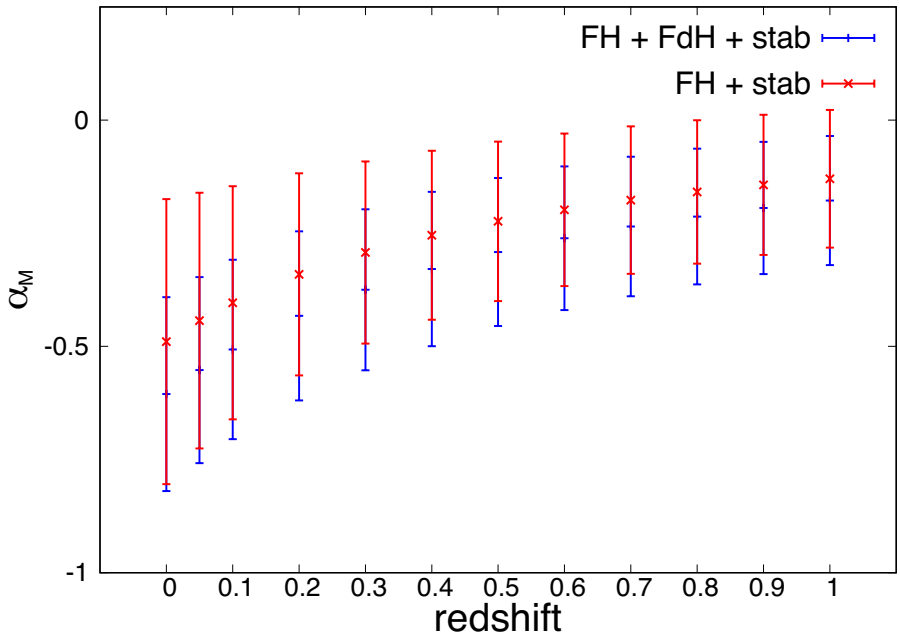

Figure 4.12. The effect of the consistency filters. The points at the middle of the lines represent the mean values. The ranges of the lines correspond to the standard deviation. Note that the stability conditions are already imposed on the both cases. The legends "FH" and "EdH", and "stab" denote the filters in Eqs. (4.6.9), (4.6.10), and (4.6.12), respectively.

solution of a scalar field to a cosmological solution. For instance, the observations of the binary pulsars [80] and the lunar laser ranging experiments [81] currently give the constraints[5] $|\dot{G}/G| \approx 0.02 H_0$. As pointed out by [79], these observations directly measure α_M, namely $|\alpha_{M0}| < 0.02$, which gives the tightest constraint on α_M so far. As we discussed in this paper, the GW observation can constrain α_M at the order of 0.01, which is comparable with the local measurements such as the binary pulsar and the lunar laser ranging. More importantly, the observation of GW propagation does not rely on gravity at local scales but can measure modification of gravity at cosmological scales directly. Potentially, the GW observation allows us to measure not only the time dependence of α_M but also the scale dependence. For these reasons, the GW observation combined with the local measurements is significant to check the consistency of a gravity theory over the wide ranges of space and time.

[5]The upper limit can be stronger by one order of magnitude by assuming the advanced models of the lunar core rotation for lunar laser ranging [82] and of solar mass loss for Mercury's ephemeris [83].

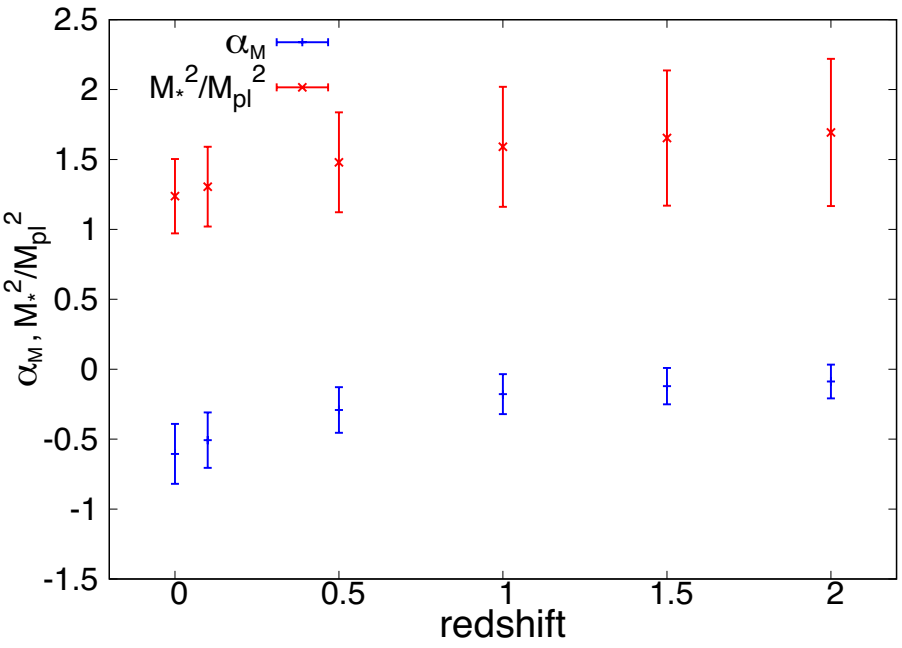

Figure 4.13. The ranges of α_M and $M_*^2/M_{\rm pl}^2$ at $z = 0, 0.1, 0.5, 1.0, 1.5$, and 2.0. The mean value and the standard deviation are shown.

It is known that cosmological observations also put bounds on the gravitational couplings. For instance, the gravitational constant G is constrained at the time of the Big Bang nucleosynthesis, $|1 - G/G_N| < 20\%$ [84, 85]. Moreover, G has been constrained by the detailed analyses of the CMB anisotropy [86, 87, 88]. However, these constraints are implicitly based on that the equivalence principle of gravity holds through the past of the Universe, which is in general not the case among the modified gravity theories. Recently, the constraint on α_{M0} has been obtained from the CMB observation by Planck [74], by jointly analyzing the galaxy survey data [89] and the recent cosmic shear measurement data by KiDS and GAMA observations [90]. In these studies, the violation of the equivalence principle is taken into account by implementing $G_{\rm matter}$ and $G_{\rm light}$ for cosmological perturbations. The current stringent bound on α_{M0} is $|\alpha_{M0}| < 0.04$ [74]. However, in order to put the bounds on $G_{\rm matter}$, $G_{\rm light}$, and α_M by cosmological observations, it is crucial to assume simple forms of the time evolutions for them, except for specific models such as the Jordan-Brans-Dicke theory [91, 92]. In this sense, it is difficult to compare the constraining power of these cosmological observations with GW observations. In addition, the simple parametrization may be problematic in that it cannot cover the whole parameter space of the Horndeski theory.

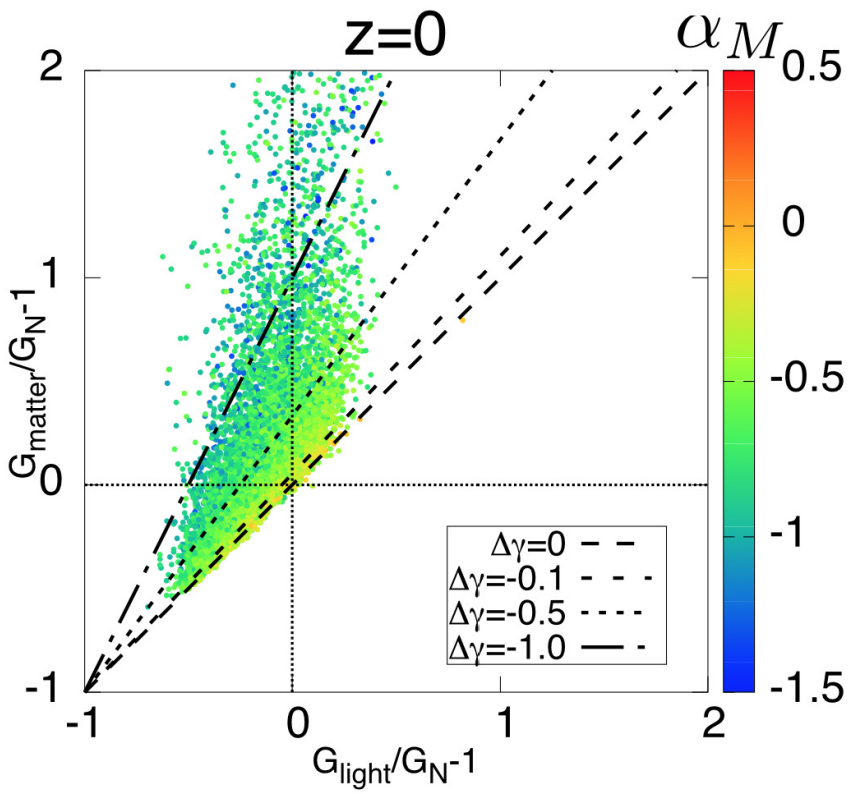

Figure 4.14. The contour plot of $\Delta\gamma$ on the $G_{\rm matter} - G_{\rm light}$ plane at $z = 0$.

4.9.6 Concluding remarks

We have done the numerical search of the models in Horndeski theory which successfully explain the cosmic expansion history of the Universe. We found that

- It is significantly distinguished in α_M and α_T whether the cosmic expansion is described by Einstein-de Sitter or the ΛCDM models.
- $|\alpha_T| < 10^{-15}$ by the simultaneous observation of GW170817 and GRB170817A crucially requires that $G_{4X} = 0$ and $G_5 = 0$.
- Horndeski theory with $\alpha_T = 0$ predicts the negative α_M and $G_{\rm matter} \gtrsim G_{\rm light}$ at low redshift.
- Lunar Laser Ranging experiment give the most stringent constraints on α_M, $|\alpha_{M0}| \simeq 0.01$ for the rest of Horndeski theory with $\alpha_T = 0$.

4.10 DHOST theory after GW170817

We briefly summarise the DHOST framework after GW170817/GRB170817A, i.e., $c_g = 1$, and introduce the EFT parametrization of the DHOST theory. We utilise the numerical simulation that had been developed for the Horndeski theory. Then the distributions of the models in the space of the EFT parameters are presented.

The covariant form of DHOST theory obeying $c_g = c$ has four arbitrary free functions. In the effective field theory (EFT) description of the DHOST theory [93], this framework is expressed in terms of additional time-dependent parameters in the linear perturbations from the ΛCDM model.

Let us consider the general DHOST action [39, 94, 95],

$$S = \int d^4x \sqrt{-g}\,\mathcal{L}\,, \tag{4.10.1}$$

where the DHOST Lagrangian, $\mathcal{L}$ is defined as the sum of the following four parts,

$$\mathcal{L} = \mathcal{L}_{\rm g} + \mathcal{L}_\phi + \mathcal{L}_{\rm oth} + \mathcal{L}_{\rm m}\,, \tag{4.10.2}$$

with

$$\mathcal{L}_{\rm g} \equiv F(\phi, X)R\,, \tag{4.10.3}$$

$$\mathcal{L}_\phi \equiv \sum_{i=1}^{5} A_i(\phi, X)\mathcal{L}_i\,, \tag{4.10.4}$$

$$\mathcal{L}_{\rm oth} \equiv P(\phi, X) + Q(\phi, X)\Box\phi\,, \tag{4.10.5}$$

where $X \equiv -\nabla_\mu\phi\nabla^\mu\phi/2$, and the $\mathcal{L}_\phi$ contains all possible contractions of a scalar field of the quadratic polynomial degree in second-order derivatives of the scalar field, i.e., $\phi_{\mu\nu}$ with

$$\begin{aligned}&\mathcal{L}_1 = \phi_{\mu\nu}\phi^{\mu\nu}\,, \quad \mathcal{L}_2 = (\Box\phi)^2\,, \quad \mathcal{L}_3 = (\Box\phi)\phi^\mu\phi_{\mu\nu}\phi^\nu\,,\\ &\mathcal{L}_4 = \phi^\mu\phi_{\mu\rho}\phi^{\rho\nu}\phi_\nu\,, \quad \mathcal{L}_5 = (\phi^\mu\phi_{\mu\nu}\phi^\nu)^2\,.\end{aligned} \tag{4.10.6}$$

The matter Lagrangian, $\mathcal{L}_{\rm m}$, is minimally coupled to the metric, $g_{\mu\nu}$. We are using the short hand notations $\phi_\mu = \nabla_\mu\phi$, $\phi_{\mu\nu} = \nabla_\mu\nabla_\nu\phi$.

Among the degenerate classes of DHOST theory, only dubbed class I does not suffer from the gradient instability [93]. One could enlarge DHOST theory by adding the cubic, quartic or quintic dependencies on $\phi_{\mu\nu}$ to the action (4.10.2). For fulfilling the constraint on the speed of the GW, $c_g^2 = c^2$, independent of any background, $A_1 = 0$

for the quadratic polynomial degree of DHOST theory given in Eq. (4.10.2), and all cubic or higher polynomial degrees should be vanished, hence not discussed here.

The degeneracy conditions, which ensures the absence of the Ostrogradsky ghost of the class I DHOST theory after the GW170817 event are

$$\begin{aligned} A_1 &= -A_2 = 0\,, \\ A_4 &= \frac{1}{2F}\left[3{F_X}^2 - 2(F - XF_X)A_3 - X^2A_3^2\right]\,, \\ A_5 &= -\frac{1}{F}\left(F_X + XA_3\right)A_3\,, \end{aligned} \tag{4.10.7}$$

where $F_X = \partial F/\partial X$.

The corresponding Lagrangian of the Class I DHOST theory after GW170817 event is

$$L^{\rm DHOST}_{c_g=1} = P + Q\,\Box\phi + F\,R + A_3\phi^\mu\phi^\nu\phi_{\mu\nu}\Box\phi + A_4\phi^\mu\phi_{\mu\nu}\phi_\lambda\phi^{\lambda\nu} + A_5(\phi_\mu\phi^{\mu\nu}\phi_\nu)^2\,. \tag{4.10.8}$$

Viable ($c_g = c$) GLPV theory can be identified as the above DHOST theory with the following mapping (using GLPV notation of [38]):

$$F = G_4\,, \quad A_3 = -A_4 = -\frac{G_{4X}}{X}\,, \quad A_5 = 0\,. \tag{4.10.9}$$

We call it as GLPV limit in rest of the article.

Horndeski theory is included in DHOST theory as well as GLPV theory. Viable ($c_g = c$) Horndeski theory can be classified from Eq. (4.10.9) by further setting

$$F_4 = 0 = F_X = G_{4X}\,, \tag{4.10.10}$$

which restrict $G_4 = G_4(\phi)$. We call Eqs. (4.10.9) and (4.10.10) as Horndeski limit in our remaining paper. Hereafter we call the theories given by the Lagrangian in Eq. (4.10.8) DHOST theory simply, and use it as our generalised framework in this article.

4.11 Numerical formulation of DHOST theory

The characteristic behaviours of the aforementioned EFT parameters can be understood if one could find the cosmological solution of the scalar field, ϕ and gravitational perturbations of the full DHOST theory. But the cosmological solution of the full DHOST theory for general arbitrary functions in all redshift regimes is unsolved yet.

The full numerical solution is neither studied yet nor computationally cheap. But we are interested in studying the maximum possible range of models which is acceptable by the observation in a model-independent way. Therefore, first, we approximate the scalar field, ϕ, and the arbitrary free functions, P, Q, F, A_3 [6] by using Taylor series expansion without solving the background Friedmann equations of the system. Then we will check the stability and consistency with the observations of those solutions.

4.11.1 Characteristic parameters

Modification of GR can be in both, background as well as perturbations. In this section, we parameterise the cosmological perturbations in the DHOST theory, which capture the modifications from GR in the linear perturbations. We adopt the low-energy single-field EFT of DE and MG parametrisations which describes a cosmological background evolution and the linear perturbations around it [30, 97, 98]. These minimal EFT parameters, α_M, α_K, α_B, α_H, and β_1 represent the observational deviation of a model in the DHOST theory from the ΛCDM model in the linear regime [32, 93]. In this article, we are considering the detuning of the extrinsic curvature parameter, $\alpha_L = 0$ for the degeneracy class [93]. The excess tensor speed parameter is set to $\alpha_T = 0$ since we consider the DHOST theory with $c_g = 1$. It is worth mentioning that $\alpha_{K,B,M}$ parameters are shared with the Horndeski theory. Therefore our purpose here is to figure out the deviations from the Horndeski theory in the DHOST theory. In order to see the differences, it is convenient to express those EFT parameters into two parts:

$$\alpha^{\rm DHOST}_{M,K,B} = \alpha^{\rm Horn}_{M,K,B} + \alpha^{\rm res}_{M,K,B}\,, \tag{4.11.1}$$

where $\alpha^{\rm Horn}_{M,K,B}$ characterises the Horndeski theory with $c_g = 1$, and $\alpha^{\rm res}_{M,K,B}$ characterises the deviations from the Horndeski theory. We compute the EFT parameters of the DHOST theory in Appendix. A.2.2 and the expressions are given below. The running of the effective Planck mass $M_* = \sqrt{2F}$ is given as

$$\alpha_M = \frac{1}{HF}\frac{dF}{dt} \quad = \quad \alpha^{\rm Horn}_M + \alpha^{\rm res}_M\,, \tag{4.11.2}$$

where

$$\alpha^{\rm Horn}_M \equiv \frac{\dot\phi F_\phi}{HF}\,,\ \alpha^{\rm res}_M \equiv \frac{\dot X F_X}{HF}\,. \tag{4.11.3}$$

[6] It has been already known that the constraints so that gravitons do not decay into scalar field is obtained[96]. We will take into account this as 'A3eq0$_{c_g=1}$' model in Table. 4.2

Here and hereafter, the dot in $\dot{\phi}$ denotes the time derivative with respect to the cosmic time. The effective Planck mass does not change in time when $\alpha_M = 0$. The parameter α_M becomes nonzero in general for modified gravity theories with a non-minimal coupling to matter. Above expressions explain that $\alpha_M^{\rm res}$ vanishes in the Horndeski limit, $F_X = 0$, and one can recover Horndeski theory from the DHOST theory.

$$\alpha_B^{\rm Horn} \equiv \frac{\dot{\phi}(Q_X X + F_\phi)}{2FH}\,, \tag{4.11.4}$$

$$\alpha_B^{\rm res} \equiv \frac{1}{2FH}\left[4HXF_X + 2\dot{\phi}XF_{\phi X} + \dot{\phi}\ddot{\phi}\left\{2X(F_{XX} + A_3 + A_{3X}X) + 3(F_X + A_3 X)\right\}\right]. \tag{4.11.5}$$

Notice that $\alpha_B^{\rm res} = 0$ when $F_X = 0$ for the Horndeski theory.

The parameter α_K, commonly appearing in the EFT parameters, is also computed in the DHOST theory and denotes the coefficient of the scalar perturbation. Since we use α_K only for assessing the stability conditions throughout this paper, we omit the specific expression of α_K here (see Appendix. A.2.2 for the explicit form of α_K). Beside the aforementioned $\alpha_{M,K,B}^{\rm res}$, two additional EFT parameters associated to the deviations of the DHOST$_{c_g=1}$ theory from the Horndeski theory are α_H and β_1 expressed as

$$\alpha_H = -\frac{2XF_X}{F}\,, \tag{4.11.6}$$

$$\beta_1 = \frac{X(F_X + A_3 X)}{F}\,. \tag{4.11.7}$$

Notice that $\beta_1 = 0$ in the GLPV limit in Eq. (4.10.9), and $\alpha_H = 0 = \beta_1$ in the Horndeski limit in Eq. (4.10.10).

The summary of the characteristic EFT parameters of the DHOST theory are shown in Table I. As we discuss in Sec. 4.12, we propose a method to distinguish the theories within the DHOST$_{c_g=1}$ theory via $\alpha_{M,B,H}$ and β_1.

4.11.2 Equations of motion

The Friedman equations of the DHOST theory was firstly derived in [99], just after the full derivation was completed for the GLPV theory [31]. We independently derived the Friedmann equations in [1] as

$$3M_*^2H^2 = \rho_m + \mathcal{E}\,, \tag{4.11.8}$$

$$M_*^2(2\dot{H} + 3H^2) = -p_m - \mathcal{P}\,, \tag{4.11.9}$$

where the effective mass, $M_*^2 = 2F$. ρ_m and p_m are the background energy density and pressure of all the matter components together, while $\mathcal{E}$ and $\mathcal{P}$ are the background energy density and pressure of the dark energy, which are defined as

$$
\begin{aligned}
\mathcal{E} &= 4F_X\dot{\phi}^2 + 6F_X\dot{\phi}^2\dot{H} \\
&\quad +6\left(-F_\phi\dot{\phi} - \frac{1}{2}Q_X\dot{\phi}^3 + \left(-F_X\dot{\phi} + \left(-A_3 + \frac{3}{2}\frac{{F_X}^2}{F}\right)\dot{\phi}^3 + \frac{3}{2}A_3\frac{F_X}{F}\dot{\phi}^5 + \frac{3}{8}\frac{A_3^2}{F}\dot{\phi}^7\right)\ddot{\phi}\right)H \\
&\quad +2\left(\left(-A_3 + \frac{3}{2}\frac{{F_X}^2}{F}\right)\dot{\phi}^3 + \frac{3}{2}A_3\frac{F_X}{F}\dot{\phi}^5 + \frac{3}{8}\frac{A_3^2}{F}\dot{\phi}^7\right)\dddot{\phi} \\
&\quad +\left(\left(-A_3 + \frac{3}{2}\frac{{F_X}^2}{F}\right)\dot{\phi}^2 + \left(-A_{3X} + \frac{9}{2}A_3\frac{F_X}{F} - \frac{3}{2}\frac{{F_X}^3}{F^2} + 3\frac{F_X F_{XX}}{F}\right)\dot{\phi}^4\right. \\
&\quad \left.+6\left(\frac{5}{16}\frac{A_3^2}{F} + \frac{A_{3X}F_X}{4F} - A_3\frac{{F_X}^2}{4F^2} + A_3\frac{F_{XX}}{4F}\right)\dot{\phi}^6 + \left(\frac{3}{4}\frac{A_3A_{3X}}{F} - \frac{3}{8}\frac{A_3^2F_X}{F^2}\right)\dot{\phi}^8\right)\ddot{\phi}^2 \\
&\quad \left(\left(-A_{3\phi} - 3\frac{{F_X}^2F_\phi}{F^2} + 6\frac{F_XF_{\phi X}}{F}\right)\dot{\phi}^4\right. \\
&\quad \left.+3\left(\frac{A_{3\phi}F_X}{F} - A_3\frac{F_XF_\phi}{F^2} + A_3\frac{F_{\phi X}}{F}\right)\dot{\phi}^6 - \frac{3}{4}\left(2\frac{A_3A_{3\phi}}{F} + \frac{A_3^2F_\phi}{F^2}\right)\dot{\phi}^8\right)\ddot{\phi} \\
&\quad +(P_X + Q_\phi)\dot{\phi}^2 - P\,, \qquad (4.11.10) \\
\mathcal{P} &= \frac{1}{2F}\left[4\left(F_\phi\dot{\phi} + F_X\dot{\phi}\ddot{\phi}\right)H + 2F_X\dot{\phi}\ddddot{\phi}\right. \\
&\quad +\left(2F_X + \left(A_3 + 3\frac{F_X}{F} + 2F_{XX}\right)\dot{\phi}^2 - \frac{3}{2}A_3\frac{F_X}{F}\dot{\phi}^4 - \frac{3}{8}\frac{A_3^2}{F}\dot{\phi}^6\right)\ddot{\phi}^2 \\
&\quad \left.+2\left(F_\phi + (2F_{\phi X} + \frac{1}{2}Q_X)\dot{\phi}^2\right)\ddot{\phi} + (2F_{\phi\phi} + Q_\phi)\,\dot{\phi}^2 + P\right]. \qquad (4.11.11)
\end{aligned}
$$

We indicate the appearance of $\dot{H}$ and $\dddot{\phi}$ in the above Friedmann equations. By using the spatial component of the Einstein equation, one can eliminate the $\dot{H}$ and $\dddot{\phi}$ in the temporal component if necessary, and rewrite the second order Friedmann equations as mentioned in [100, 101]. Here we are keeping $\dot{H}$ and $\dddot{\phi}$ in the equation without substitution because the higher derivatives would not give any trouble in our numerical computation.

By using the formula Eq. (4.6.6), the evolution of $\phi(a)$ is rewritten as

$$
\hat{\phi} \equiv \phi(a)/\tilde{M}_\phi = c_0 + \sum_{i=1}^{3} c_i(1 - a^{i/2})\,. \qquad (4.11.12)
$$

where $\tilde{M}_\phi$ is the normalisation at $a = 0$. We assign that the coefficients c_i are utterly random in the range $[-1, 1]$. Note that we are precisely sampling $c_\phi^{(n)}$ in Eq. (37) of [2].

The dimensionless arbitrary functions as a function of time are

$$\hat{\mathcal{A}}_i^{(\rm app)} \equiv \frac{\mathcal{A}_i^{(\rm app)}(\phi, X)}{\mathcal{A}_i(\Lambda_P, \Lambda_Q)} = a_i + \sum_{\rho=\hat{\phi},\hat{X}} a_{i,\rho}\rho + \sum_{\rho,\sigma=\hat{\phi},\hat{X}} \frac{a_{i,\rho\sigma}}{2}\rho\sigma + \sum_{\rho,\sigma,\lambda=\hat{\phi},\hat{X}} \frac{a_{,i\rho\sigma\lambda}}{6}\rho\sigma\lambda\,, \tag{4.11.13}$$

where $\hat{X} \equiv -\dot{\phi}^2/\tilde{M}_\phi^2 H^2$. $\mathcal{A}_i^{(\rm app)}(\phi, X)$ with $i = 1, 2, 3, 4$ represent the DHOST theory functions, P, Q, F, or A_3, respectively. H_0 is the Hubble constant of today. $\tilde{M}_\phi$ and $\mathcal{A}_i(\Lambda_P, \Lambda_Q)$ are the normalisation factors to make ϕ and $\mathcal{A}_i^{(\rm app)}(\phi, X)$ dimensionless,

$$\mathcal{A}_1 = \Lambda_P^4\,,\ \mathcal{A}_2 = \frac{\Lambda_P^4}{\Lambda_Q^3}\,,\ \mathcal{A}_3 = \frac{\Lambda_P^8}{\Lambda_Q^6}\,,\ \mathcal{A}_4 = \frac{1}{\Lambda_Q^6}\,, \tag{4.11.14}$$

where $\Lambda_P \equiv (\tilde{M}_\phi H_0)^{1/2}$ and $\Lambda_Q \equiv (\tilde{M}_\phi H_0^2)^{1/3}$, respectively describing the dynamical energy scale of ϕ and the cut-off scale of non-linearity of ϕ at the present Hubble scale, H_0. Note that the cosmic acceleration realises since $\mathcal{E}$ is at the order of the cosmic critical density, $M_{\rm pl}^2 H_0^2$.

The above expressions are valid for the both, the late and early Universe. The model coefficients, c_i ($i = 0, 1, 2, 3$) and a_i ($i = 1, 2, 3, 4$), are the inputs in the numerical program, which are randomly chosen in the range of [-1,1]. This choice of the range is motivated by our normalisation in Eqs. (4.11.12) and (4.11.13). A particular set of values of a_i ($i = 1, 2, 3, 4$) in Eq. (4.11.13) represents a model within the framework of the DHOST theory, and a set of c_i in Eq. (4.11.12) represents the time evolution of the scalar field in that model. Given the expressions of $\phi(a)$ and $\mathcal{A}_i^{(\rm app)}(a)$, we would able to evaluate all EFT parameters, $\alpha_{M,B,H}$, and β_1, mentioned in the previous section by using Eqs. (4.11.12) and (4.11.13).

4.11.3 Filtering through the consistency and stability conditions

We check the following consistency and stability conditions at redshifts, $z = 0$, 0.1, 0.5, 1.0, 1.5, and 2.0, where the constraints on the Hubble parameter exist [58].

(i) **Consistency conditions:** In the previous section, we arbitrarily produced the numerical solution of ϕ without solving the Friedmann equation. Therefore, we will filter only the models which can consistently produce the Hubble parameter, H, and its time variation, $\dot{H}$, within the observational error, 20% deviation from the ΛCDM model (Table I of [58]).

We substitute $H_{\Lambda\rm CDM}$ and $\phi(t)$ in the right-hand sides of Eqs. (4.11.8) and (4.11.9)

which give $H_{\rm DHOST}$ and $\dot{H}_{\rm DHOST}$. Then we check two following consistency filters for the Hubble parameter(FH) and the derivative of the Hubble parameter (FdH),

$$\text{FH}: \left|1 - H_{\rm DHOST}/H_{\Lambda\rm CDM}\right| < 20\%\,, \tag{4.11.15}$$

$$\text{FdH}: \left|1 - \dot{H}_{\rm DHOST}/\dot{H}_{\Lambda\rm CDM}\right| < 20\%\,. \tag{4.11.16}$$

These consistency conditions guarantee the evolution of $\phi(\tau_{LB})$ within the observational ranges of the Hubble parameter and its changes.

(ii) **Stability conditions:** For ensuring the linear scalar and tensor perturbations are free from ghost and gradient instabilities, we pass through the stability conditions [99],

$$\begin{aligned} &A_{\tilde{\zeta}} + \frac{\rho_m + p_m}{M_*^2 H^2}\frac{3\beta_1(2+3c_{\rm m}^2\beta_1)}{(1+\alpha_B - \dot{\beta}_1/H)^2} > 0\,, \\ &B_{\tilde{\zeta}} + \frac{\rho_m + p_m}{M_*^2 H^2}\left(\frac{1+\alpha_H+\beta_1}{1+\alpha_B-\dot{\beta}_1/H}\right)^2 < 0\,,\ M_*^2 > 0\,. \end{aligned} \tag{4.11.17}$$

All the aforementioned quantities are derived and defined in the Appendix A.2.2 (see Eqs. (A.2.30) and (A.2.31)). Please note that the inclusion of matter changes the stability conditions, since matter itself may introduce the instability. Linear stability may also depend on the chosen basis of scalar perturbations and particularly on nonzero α_H and β_1. Detailed discussion is in Appendix A.2.2.

4.12 Discriminating theories via the distributions of characteristic parameters

In this section, we will demonstrate the correlations among the characteristic parameters; α_M, α_B, α_H, and β_1, introduced in Sec. 4.11.1, and present the model distributions in the parameter space as a function of redshifts z in the range of $0 \leq z \leq 2$ by using the numerical techniques explained in the previous section 4.11. The model distribution is shown for each subgroup of the DHOST theory summarised in Table 4.2 and is interpreted based on the order-of-magnitude estimation. The essential ingredients for the estimation are the slow time-evolution of ϕ, i.e. $|\hat{X}| \ll 1$, and the expansions of the arbitrary functions in Eq. (4.11.13).

Theory $c_g = 1$	arbitrary functions			linear parameters					
				α_M		α_B		α_H	β_1
	$F(\phi)$	F_X	A_3	$\alpha_M^{\rm Horn}$	$\alpha_M^{\rm res}$	$\alpha_B^{\rm Horn}$	$\alpha_B^{\rm res}$		
Horneski$_{c_g=1}$	✔	0	0	✔	0	✔	0	0	0
GLPV$_{c_g=1}$	✔	✔	$A_3 = -F_X/X$	✔	✔	✔	✔	✔	0
A3eq0$_{c_g=1}$	✔	✔	0	✔	✔	✔	✔	✔	$\beta_1 = -\alpha_H/2$
DHOST$_{c_g=1}$	✔	✔	✔	✔	✔	✔	✔	✔	✔

Table 4.2. Distinction of the theories with $c_g = 1$ by EFT parameters and arbitrary functions.

4.12.1 Time evolution of characteristic parameters

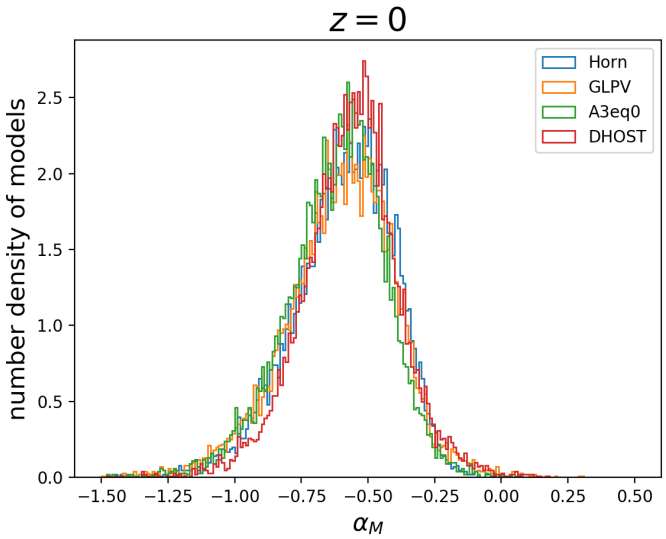

Figure 4.15. The model distribution in α_M at $z = 0$ with the bin size $\Delta\alpha_M = 0.01$. The solid colour lines represent Horndeski (blue), GLPV (orange), A3eq0 (green), and DHOST (red), respectively. This is the enlarged version of the top left panel in Fig. 4.16.

By using the expansions of $\hat{\phi}$ and $\hat{\mathcal{A}}_i^{(\rm app)}$ in Eqs. (4.11.12) and (4.11.13), we get the

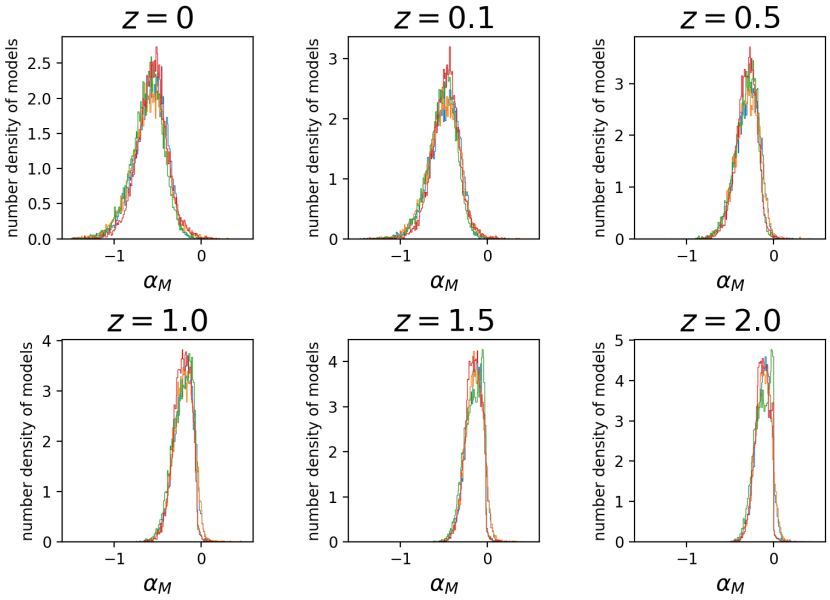

Figure 4.16. The model distribution in α_M at different redshift from $z = 2.0$ to $z = 0$ with the bin size $\Delta\alpha_M = 0.01$. The colours are the same as in Fig. 4.15

order of the α_M from Eqs. (4.11.3) and (4.11.2),

$$\alpha_M^{\rm Horn} = \mathcal{O}(|\hat{X}|^{1/2})\,, \quad \alpha_M^{\rm res} = \mathcal{O}(|\hat{X}|)\,, \tag{4.12.1}$$

$$\alpha_M = \alpha_M^{\rm Horn}\left(1 + \mathcal{O}(|\hat{X}|^{1/2})\right) \tag{4.12.2}$$

$$\simeq \alpha_M^{\rm Horn} \qquad \text{since} \quad |\hat{X}| \ll 1. \tag{4.12.3}$$

Since the order of α_M of DHOST theories is the same as the Horndeski$_{c_g=1}$ theory, α_M parameter is almost identical. Indeed, the indistinguishability of α_M is confirmed from the distribution of α_M at all different redshifts, $z = 0\,, 0.1\,, 0.5\,, 1\,, 1.5\,, 2.0$ in the Figs. 4.15 and 4.16.

Figs. 4.15 and 4.16 show that α_M has a peak around $\alpha_M \sim -0.5$ at all redshifts. For the interpretation of the negative value, the Friedmann equation (4.11.10) helps us understand it intuitively from the point of view of energy balance. The energy density of DHOST theory from Eq. (4.11.8) is

$$\mathcal{E} = V_{\rm eff} + \mathcal{O}(|\hat{X}|)M^4\,, \tag{4.12.4}$$

$$\text{with} \quad V_{\rm eff} \equiv V(\phi) - 3M_*^2H^2\alpha_M^{\rm Horn}\,. \tag{4.12.5}$$

Here we recall $M^4 = M_{\rm Pl}^2 H^2$, the critical density associating with the cosmic expansion. The potential $V(\phi)$ is the sum over the ϕ dependence terms in $\mathcal{E}$. By inserting the approximated $\mathcal{E}$ into Eq. (4.11.10), we express the Friedmann equation as

$$1 = \frac{V_{\rm eff}}{3M_*^2 H^2} + \frac{\rho_m}{3M_*^2 H^2} + \mathcal{O}(|\hat{X}|)\,. \tag{4.12.6}$$

The matter density is negligible during the cosmic acceleration, resulting in $V_{\rm eff} \sim 3M_*^2 H^2$. Because the model are sampling by random coefficients, there is no preference which term in $V_{\rm eff}$ is significant at the same order in $\hat{X}$, ending up with $-3M_*^2 H^2 \alpha_M^{\rm Horn} \sim V \sim 0.5 V_{\rm eff} > 0$. The negative value α_M has already been encountered in our previous investigation of the Horndeski theory [2] under the assumption of $|\hat{X}| \ll 1$. In summary, α_M does not tell the difference between DHOST theory from the Horndeski theory in the observations.

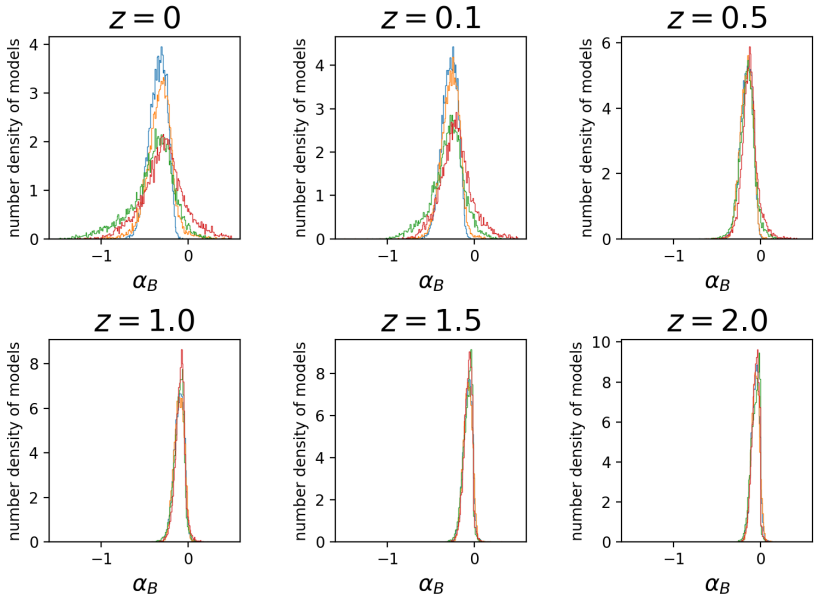

Figure 4.17. The model distribution in α_B with the bin size $\Delta\alpha_B = 0.01$. The colours are the same as in Fig. 4.15

In contrary, Fig. 4.17 shows that the theories are distinguishable in α_B at lower redshifts, while being hard to distinguish at the redshifts above $z = 1.0$. The values of α_B for the theories are biased toward the negative side at all the redshifts. The locations of the peaks of all the distributions are almost identical for all the theories.

In more detail, the distribution for the GLPV theory in orange is almost identical to that of the Horndeski theory. The distributions of the A3eq0 theory in green and the DHOST theory in red are widely scattered around the peak of distribution of the Horndeski theory.

The reason of the scattering is understood from Eq. (4.11.4) as follows. The first term of $\alpha_B^{\rm Horn}$, $\dot\phi Q_X X/2FH$, is of the order of $\mathcal{O}(|\hat{X}|^{3/2})$ and the second term $\dot\phi F_\phi/2FH$ is exactly the same as $\alpha_M^{\rm Horn}/2$ and is of the order of $\mathcal{O}(|\hat{X}|^{1/2})$. One can derive the order of the α_B from Eqs. (4.11.4) and (4.11.5),

$$\alpha_B^{\rm Horn} =\mathcal{O}(|\hat{X}|^{1/2})\,, \quad \alpha_B^{\rm res} = \mathcal{O}(|\hat{X}|)\,, \tag{4.12.7}$$

$$\alpha_B = \frac{\alpha_M^{\rm Horn}}{2}\left(1+\mathcal{O}(|\hat{X}|^{1/2})\right)\,, \tag{4.12.8}$$

The leading term of Eq. (4.12.8) is $\alpha_M^{\rm Horn}$, which is negative. Therefore, α_B is biased to the negative values in Fig. 4.17. The difference in α_B arises from the second term in Eq. (4.12.8), which is of the order of $\mathcal{O}(|\hat{X}|^{1/2})$. Earlier, we saw that the theories are hardly distinguishable in α_M. Therefore, the locations of the distribution peaks in α_B are almost identical α_M.

We interpret the broader distributions of the A3eq0 theory and the DHOST with the help of Eq. (4.12.8). The distributions of the two theories look like the superposition of the two components: the principal component making the peak of the distribution in the Horndeski theory and the random component around the peak. It is worth noting that the subleading contribution of $\alpha_B^{\rm res}$ in α_B is quantitatively larger than $\alpha_M^{\rm res}$ in α_M because the dimensionless coefficients multiplied by the terms HXF_X and $\dot\phi\ddot\phi F_X$ in $\alpha_B^{\rm res}$ are relatively larger.

The variance of α_M and α_B decrease as a redshift increases, because the time evolution of ϕ is slower at higher redshifts where matter starts to dominate, i.e., $|\hat{X}| \propto \dot\phi^2/H^2 \propto H^{-2/3}$, and the magnitudes of α_M and α_B are roughly given by $\alpha_M = \mathcal{O}(|\hat{X}|^{1/2})$ and $\alpha_B = \mathcal{O}(|\hat{X}|^{1/2})$.

Beyond Horndeski parameters: α_H and β_1

The models distributions in α_H and β_1 are shown in Figs. 4.18 and 4.19, respectively. At first glance, α_H is evenly scattered around zero for the three plotted theories. The A3eq0 and the DHOST are distributed almost identically in α_H. In the GLPV theory, the models are highly concentrated around zero due to the condition for the GLPV theory, i.e., $4F_X + A_3X = 0$. Using this relation in the definition of α_H in Eq. (4.11.6), we have $\alpha_H = -2XF_X/F = A_3X^2/2F = \mathcal{O}(|\hat{X}|^2)$.

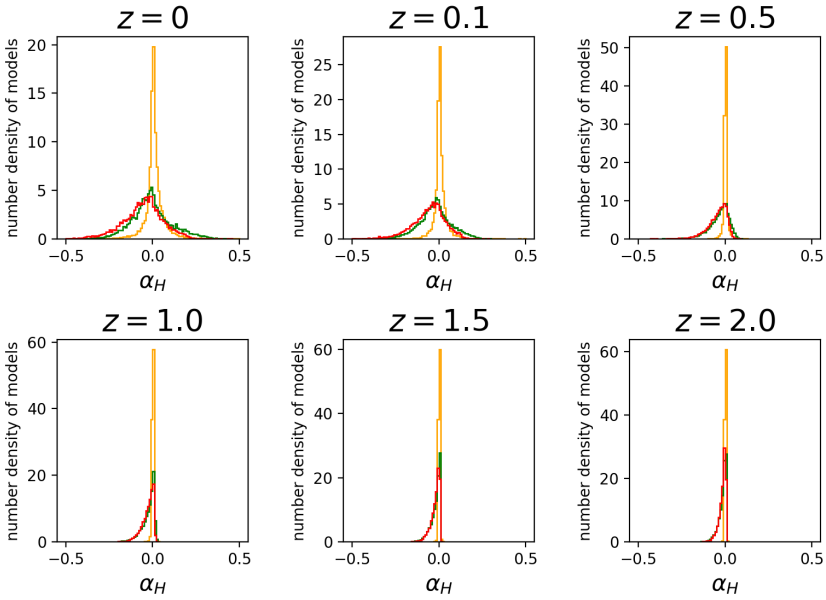

Figure 4.18. The model distribution in α_H with the bin size $\Delta\alpha_H = 0.01$. The colours are the same as in Fig. 4.15. We do not plot the Horndeski theory in which $\alpha_H = 0$.

Consequently, the models in the GLPV theory are peaked sharply at $\alpha_H = 0$. For the other theories, A3eq0 and DHOST, $\alpha_H = \mathcal{O}(|\hat{X}|)$ still keeps the distributions peaked at $\alpha_H = 0$, in contrast to $\alpha_M = \mathcal{O}(|\hat{X}|^{1/2})$ and $\alpha_B = \mathcal{O}(|\hat{X}|^{1/2})$, merely because of a higher order contribution.

The other beyond-Horndeski parameter β_1 is shown in Fig. 4.19 and has a subtle difference in the distributions between A3eq0 and DHOST. This is because the function which discriminate A3eq0 and DHOST is A_3, whose term is always subleading in β_1, e.g., $A_3X^2/F = \mathcal{O}(|\hat{X}|^2)$. From Eqs. (4.11.6) and (4.11.7), we obtain the relation

$$\alpha_H = -2\beta_1 + \mathcal{O}(|\hat{X}|^2)\,. \tag{4.12.9}$$

After all, α_H and β_1 are dependent up to the order of $\mathcal{O}(|\hat{X}|)$. The difference begins to arise at the higher orders than $\mathcal{O}(|\hat{X}|)$.

We summarise the following remarks. For all the theories in Table. 4.2, α_M hardly tells the differences among the theories via Eq. (4.12.2). In contrast, α_B gives the significant discrimination among the theories. This is because $\alpha_B^{\rm res}$ contains multiple terms. α_H is generally $\mathcal{O}(|\hat{X}|)$, and α_H and β_1 always correlates via Eq. (4.12.9). Throughout the features of α_M, α_B, α_H, and β_1, the terms associated with A_3 are

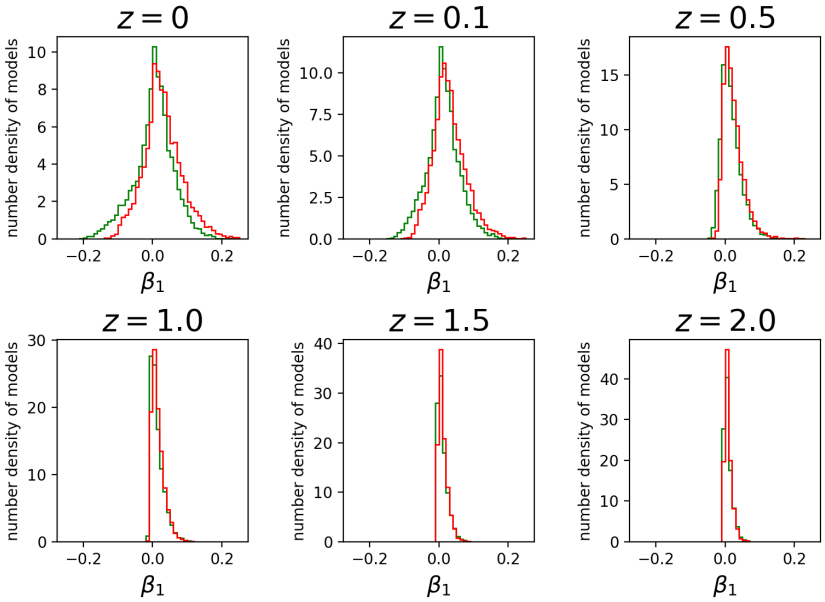

Figure 4.19. The model distribution in β_1 with the bin size $\Delta\beta_1 = 0.01$. The colours are the same as in Fig. 4.15. We do not plot the Horndeski theory and the GLPV theory in which $\beta_1 = 0$.

always negligible. Interestingly, we find specific features in the GLPV theory, $\alpha_B \approx \alpha_B^{\rm Horn}$ and $\alpha_H \approx 0$. These state that the condition $4F_X + A_3X = 0$ for the GLPV theory selects out a fine-tuned theory from the DHOST theory as a model for the cosmic acceleration.

4.12.2 Correlations between characteristic parameters

We further investigate the differences among the theories via correlations among the four characteristic parameters, α_M, α_B, α_H, and β_1. Since α_H is related to β_1 via Eq. (4.12.9), we study the correlations among three parameters, α_M, α_B, and β_1.

Figure 4.20 shows the model distributions in three dimensional parameter space composed of α_M, α_B, and β_1 in the DHOST and A3eq0 theories. Firstly, in the left panel, we confirm that the distributions of α_M and α_B for different values of β_1 in different colours are stretched along the line whose inclination is approximately 2 and clearly form the layers in parallel to a black line. In the right panel, the model distributions in the A3eq0 theory are shown. The features discussed above on the left panel also hold on the right except for that the distribution is slightly biased to smaller

α_B and smaller β_1.

One can find the following relations by expanding the analytic forms of the α_M, α_B, and β_1 given in Eqs. (4.11.3), (4.11.4), and (4.11.7) up to the leading and next-to-leading orders in $\hat{X}$.

$$\mathcal{O}(|\hat{X}|^{1/2}):\ \alpha_M^{\rm Horn} = 2\alpha_B^{\rm Horn}\,, \tag{4.12.10}$$

$$\mathcal{O}(|\hat{X}|):\ \alpha_M^{\rm res} = \frac{2}{3}\alpha_B^{\rm res} - \frac{4}{3}\beta_1\,. \tag{4.12.11}$$

The inclination of the black line and the coloured layers are originated from Eq. (4.12.10). The inclination of the stretched distributions coincides with the coefficient in Eq. (4.12.11). The continuous change of the colour is characterised by the second term in Eq. (4.12.11).

The negative sign in front of the term $4\beta_1/3$ precisely explains that the larger (smaller) values of β_1 locate at the top right (bottom left). Comparing both the panels in Fig. 4.20, we could not distinguish them other than a slightly broadened distribution of β_1. However, the DHOST and A3eq0 theories indeed deviate from the Horndeski theory (away from the black line).

The domain of α_B with $\beta_1 \neq 0$ is significantly distinguishable. Discriminating the GLPV theories from the Horndeski theory is difficult, since $\alpha_B \approx \alpha_B^{\rm Horn}$, $\alpha_H \approx 0$, and $\beta_1 = 0$ are satisfied.

Theoretically, the difference of the Horndeski theory from the rest of the theories in α_B is characterized by $\alpha_B^{\rm res}$. By using the estimation in Eqs. (4.12.2), (4.12.10) and (4.12.11) and considering the indistinguishability of the thories in α_M, we find that $\alpha_B - \alpha_M/2$ is the main component that discriminates the Horndeski theory from GLPV, A3eq0, and DHOST$_{c_g=1}$ theory. Since Eqs. (4.12.9), (4.12.10), and (4.12.11) reduce the six parameters $(\alpha_M, \alpha_M^{\rm Horn}, \alpha_B, \alpha_B^{\rm Horn}, \alpha_H, \beta_1)$ into three parameters, we conclude that $(\alpha_M, \alpha_B - \alpha_M/2, \beta_1)$ is a useful parameter to discriminate the DHOST$_{c_g=1}$ theory from the Horndeski theory.

4.12.3 Redshift evolution of α_M, $\alpha_B - \alpha_M/2$, and β_1

As found in Sec.4.12.2, the set of parameters $(\alpha_M, \alpha_B - \alpha_M/2, \beta_1)$ is a well-motivated selection of parameters to discreminate the DHOST$_{c_g=1}$ theory from the Horndeski theory. We give the redshift evolution of the parameter $(\alpha_M, \alpha_B - \alpha_M/2, \beta_1)$ in the models in the Horndeski theory and DHOST$_{c_g=1}$ theory.

In Fig.4.21, the redshift evolutions of the filtered models in the Horndeski theory (left) and the DHOST$_{c_g=1}$ theory (right). At first glance, the trend of redshift evolution is similarly monotonic in the both theories. Taking a more closer look, in the

comparison of the Horndeski theory and the DHOST$_{c_g=1}$ theory , the models in the DHOST$_{c_g=1}$ theory slightly diversify in their evolution to steeper or milder extent, while the range of α_M does not significantly change in the both theories. To diagnose the difference between the two theories, let us see $\alpha_M^{\rm res}$ of the models in the DHOST$_{c_g=1}$ theory in Fig. 4.22. As we see at $z < 1$, $\alpha_M^{\rm res}$ have oscillations. Since in Horndeski theory $\alpha_M^{\rm res} = 0$, this oscillatory behaviour propagates as a pure signal of the DHOST$_{c_g=1}$ theory.

In Fig. 4.23, $\alpha_B - \alpha_M/2$ fluctuates in $z < 2$ and swiftly converges to zero in higher redshifts, which is mutual in the both theories. In contrast to α_M, we clearly find that the range of $\alpha_B - \alpha_M/2$ significantly differentiate the Horndeski and the DHOST$_{c_g=1}$ theory at $z \lesssim 1$. Moreover, the evolution of $\alpha_M - \alpha_B/2$ in the DHOST$_{c_g=1}$ theory is more oscillatory than the Horndeski counterpart. In Fig. 4.24, β_1 shows also the conversion to zero at $z > 2$. We observe that the initial value of β_1 is less than 0.1 in the shown models. Although the absolute value of β_1 is small, β_1 oscillatorily evolves in redshift.

In terms of the distinguighment of the DHOST$_{c_g=1}$ theory and the Horndeski theory in $\alpha_B - \alpha_M/2$ or β_1, we predict that an observation at $z < 2$ is crucial to inspect the theories. Moreover, oscillatory features of the parameters are generally expected in the DHOST$_{c_g=1}$ theory, which can suggest that the parametrisation of α_M, $\alpha_B - \alpha_M/2$, and β_1 should take into account for the oscillation properly.

Figures 4.25 and 4.26 show the cumulative probabilities of α_M and α_B for each theory, respectively. In Fig. 4.25, more than 90% of the models for all the theories are distributed in $-1 < \alpha_M < -0.2$, and there are few distinguished features in the shape of the lines for the corresponding theories. On the other hand, in Fig. 4.26, we notice that the model distributions in $\alpha_B < -1$ or $\alpha_B > 0.5$ is almost similar among the four theories, but in $-1 < \alpha_B < 0.5$ the distribution of the Horndeski theory is peculiarly different from the other three theories. Thus it is able to say that a test of α_B in observations is very likely to discriminate the Horndeski theory from the other three theories in Table 4.2.

Theoretically, the difference of the Horndeski theory from the rest of the theories in α_B is characterised by $\alpha_B^{\rm res}$. By using the estimation in Eqs. (4.12.2), (4.12.10) and (4.12.11) and considering the indistinguishability of the theories in α_M, we find that $\alpha_B - \alpha_M/2$ is the main component that discriminates the Horndeski theory from GLPV, A3eq0, and DHOST theory.

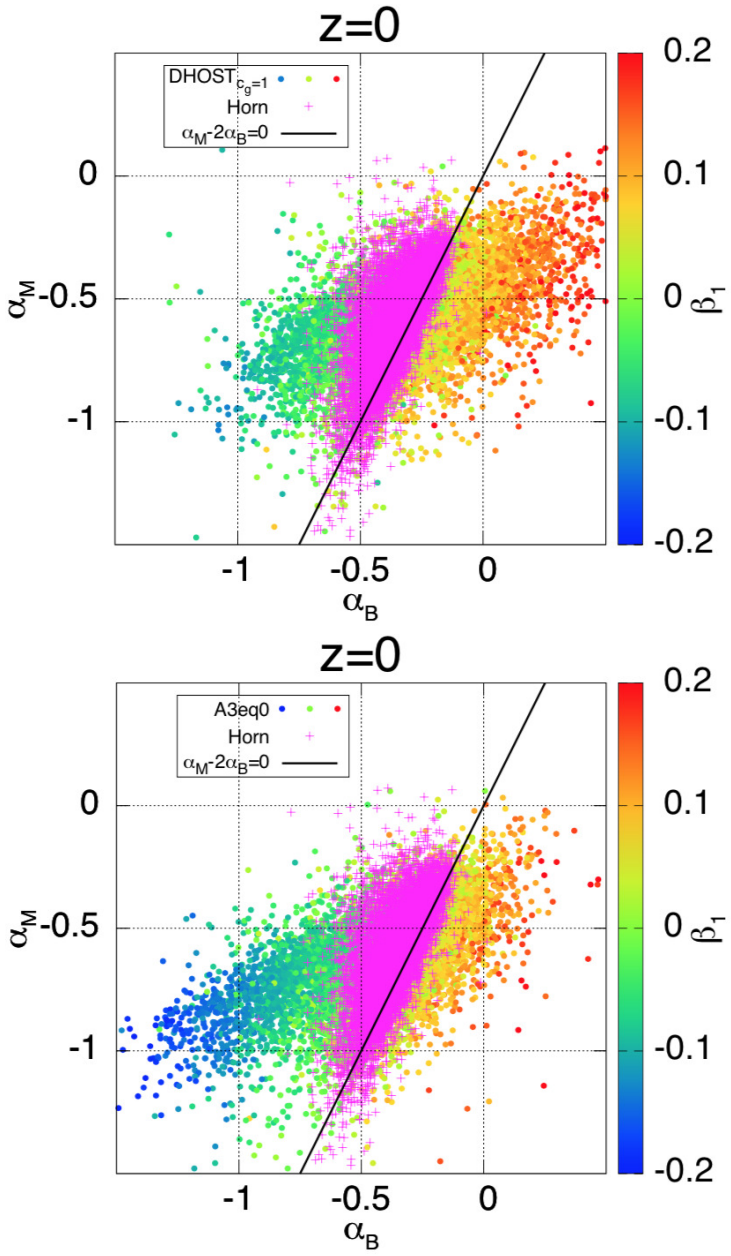

Figure 4.20. Correlations among α_M,α_B, and β_1. The panels show the distribution of models in the DHOST$_{c_g=1}$ theory (left) and the A3eq0 theory (right), respectively. The cross points in magenta show the distribution of the Horndeski theory, which is overlapped partially with the distribution of the DHOST$_{c_g=1}$ and A3eq0 theories.

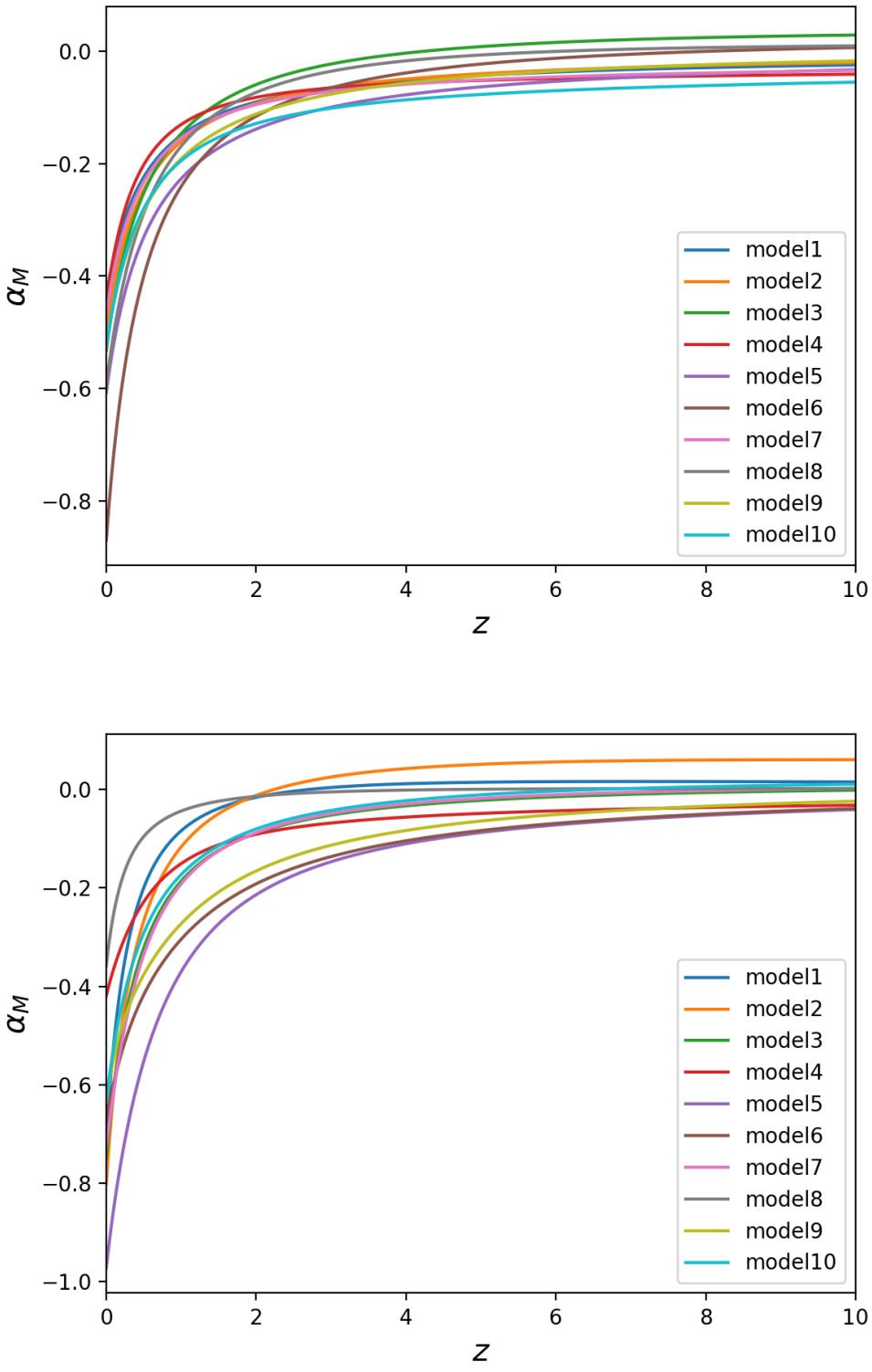

Figure 4.21. The time evolution of α_M in Horndeski theory (left) and DHOST$_{c_g=1}$ theory (right). 10 models of 10^4 generated models for each theory are arbitrary selected shown in the range of redshift $0 \leq z \leq 10$.

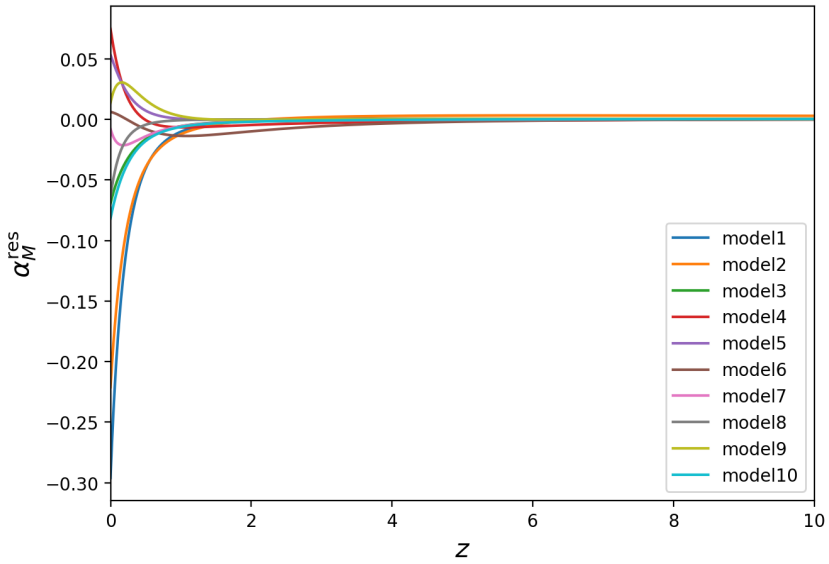

Figure 4.22. The time evolution of $\alpha_M^{\rm res}$ in DHOST$_{c_g=1}$ theory. 10 models of 10^4 generated models are arbitrary selected shown in the range of redshift $0 \leq z \leq 10$.The same models as in Fig. 4.21 are plotted.

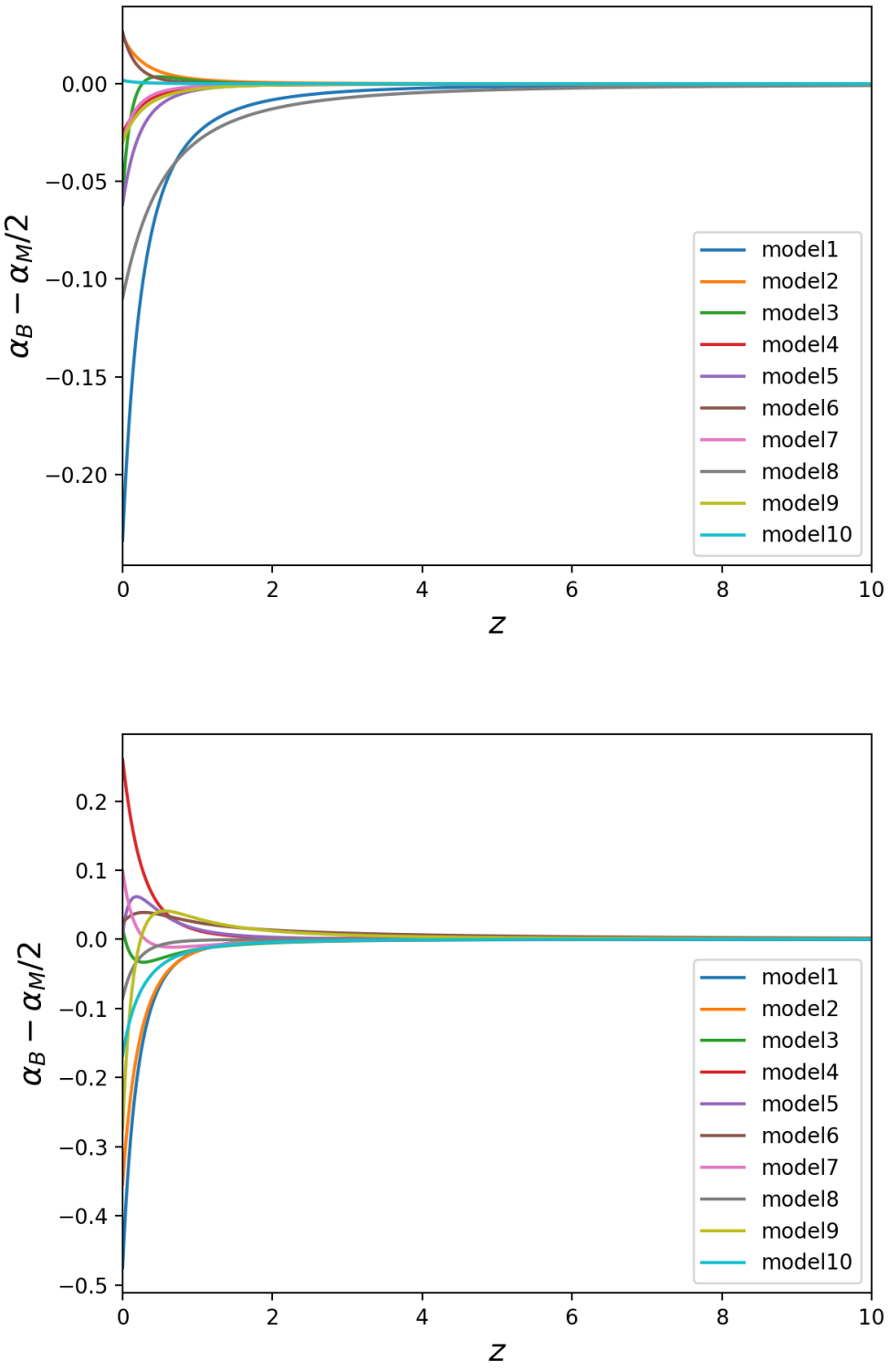

Figure 4.23. The time evolution of $\alpha_B - \alpha_M/2$ in Horndeski theory (left) and DHOST$_{c_g=1}$ theory (right). 10 models of 10^4 generated models for each theory are arbitrary selected shown in the range of redshift $0 \leq z \leq 10$. The same models as those in Fig. 4.21 are plotted.

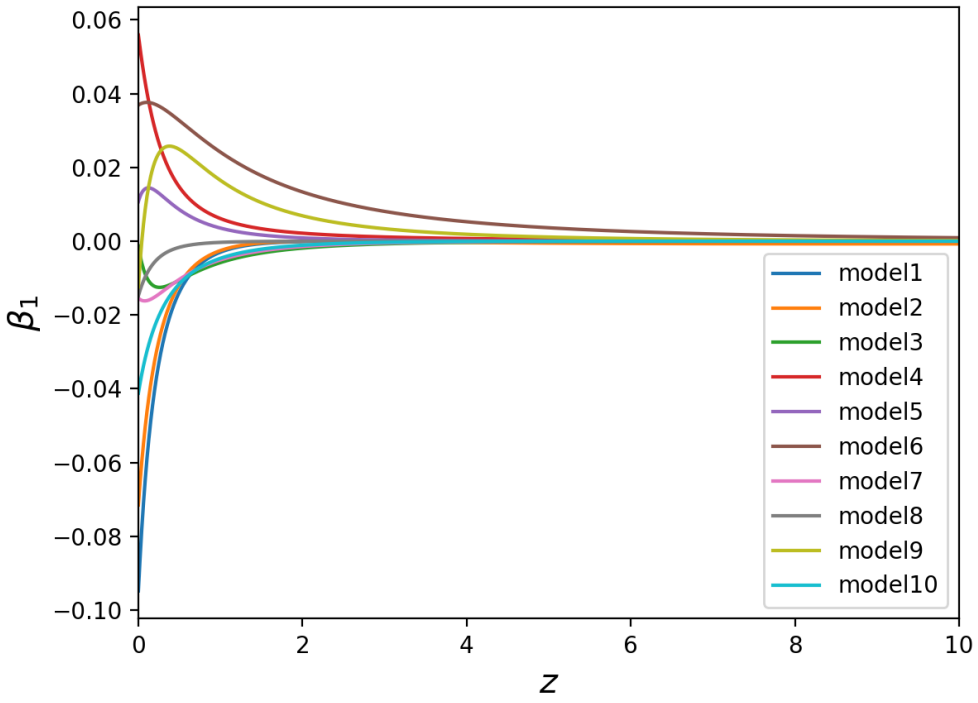

Figure 4.24. The time evolution of β_1 in DHOST$_{c_g=1}$ theory. 10 models of 10^4 generated models are arbitrary selected shown in the range of redshift $0 \leq z \leq 10$.The same models as in Fig. 4.21 and Fig. 4.23 are plotted.

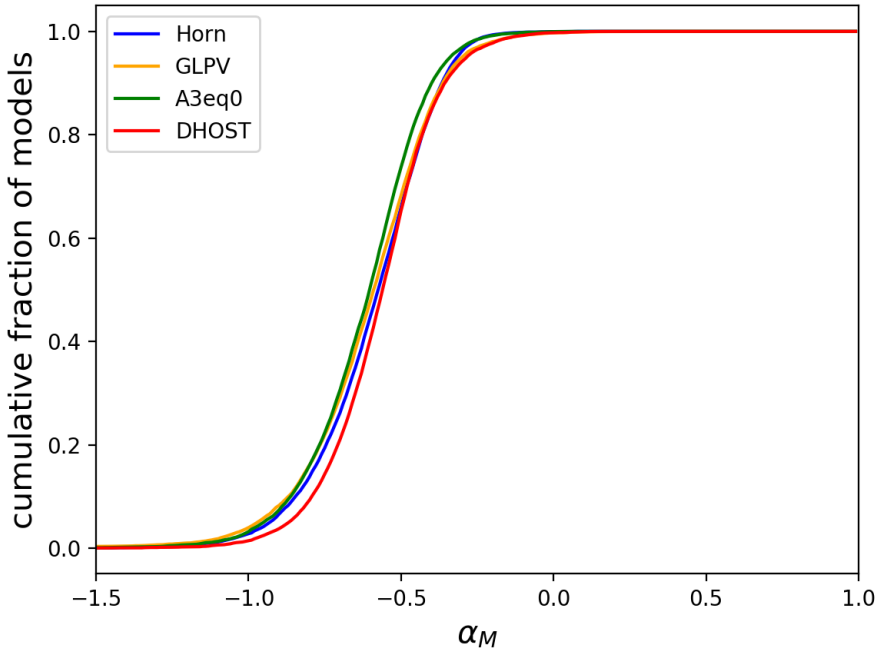

Figure 4.25. The cumulative probabilities of α_M.

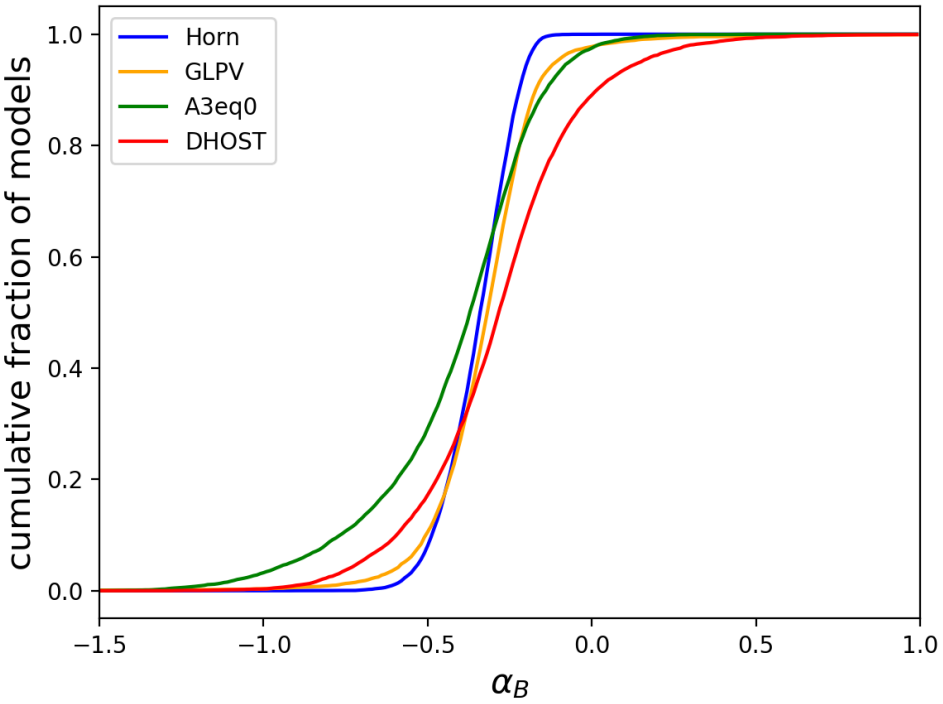

Figure 4.26. The cumulative probabilities of α_B.

4.12.4 Other constraints on DHOST theory

In the following discussion, we comment on the impact of our results on the existing parameterization, and constraints on the DHOST theory.

- The condition for evading graviton decay obtained in [96] is $A_3 = 0$, i.e, $\alpha_H + 2\beta_1 = 0$. Indeed the A3eq0 theory is precisely the theory when we apply the constraint from the no graviton decay. However, the impact of graviton decay constraint is very insignificant, at least at cosmological scales, when the DE field is rolling slowly. Because, the terms associated to A_3 in α_B in Eq. (4.11.5) and β_1 in Eq. (4.11.7), are very small which is the order of $\mathcal{O}(|\hat{X}|^2)$ under the slow-rolling assumption, $|\hat{X}| \ll 1$. Indeed, Fig. 4.20 shows that the difference between A3eq0 (right) and DHOST (left) theories are very insignificant, i.e., $A_3 = 0$ leads to a slight shift towards the left in the distribution of the model parameters.

- The remaining DHOST models after the constraint of the no graviton decay ($\alpha_H + 2\beta_1 = 0$) are principally characterized by α_M, $\alpha_B - \alpha_M/2$ and β_1. Let us mention the current constraints on the present values of these parameters. α_M is currently bounded at small scales; $|\alpha_M| = \mathcal{O}(10^{-2})$ [80, 81, 82], only when the screening mechanism are realized. α_M and α_B has been constrained in the Horndeski theory at cosmological scales [102, 103, 104, 90], typically $|\alpha_M|, |\alpha_B| = \mathcal{O}(10^{-1})$, whereas has yet to be constrained in the DHOST theory. References [105, 100] claimed that the measurement of the orbital decay rate of the Hulse - Taylor binary pulsars constrains up to $|\beta_1| = \mathcal{O}(10^{-3})$. Moreover, the simultaneous fitting of the X-ray and lensing profiles of galaxy clusters could reaches at $|\beta_1| = \mathcal{O}(10^{-1})$ as mentioned in [105]. In our simulation, $|\beta_1| = \mathcal{O}(10^{-1})$ is allowed at lower redshifts as shown in Fig. 4.19. If we assume that β_1 at local scales could be extrapolated to cosmological scales, the Hulse-Taylor pulsar rules out almost all the extended Horndeski models in Fig. 4.20. On the other hand, our models are still compatible with the constraint on β_1 from galaxy clusters.

- The paper [106] claims that the instability of dark energy can be induced by the kinetic - braiding interaction in the system of a compact binary. The instability is evaded if the kinetic - brading term in the Lagrangian is dropped off. In the Horndeski theory, $Q(\phi, X) \sim 0$ is obtained, resulting in $\alpha_M - \alpha_B/2 \sim 0$ from Eqs. (4.8.26) and (4.11.4). In the DHOST theory, however, $\alpha_M - \alpha_B/2$ still deviates from zero due to the effects from $F(\phi, X)$, even after setting $Q(\phi, X) \sim 0$. This may indicate that the parameter $\alpha_B - \alpha_M/2$ is significant to probe the DHOST theory.

- The redshift evolutions of $(\alpha_M, \alpha_B - \alpha_M/2, \beta_1)$ in the DHOST theory show the oscillatory features that are hardly realized in the Horndeski theory. The parametrization for the time evolution of α_M and α_B in cosmology is often assumed to be monotonic in literature, such as $\alpha_{M,B}(z) = \alpha_{M,B}(z=0)\times(1-\Omega_{\rm m}(z))$ in [39] or $\alpha_{M,B}(z) = \alpha_{M,B}(z=0)\times(1+z)^{-\beta}$ in [74, 103]. Such parametrizations may approximately work for the Horndeski theory as confirmed in this paper and [2], but is no longer valid in the DHOST theory because of the oscillations.

After all, our predictions in the DHOST theory are still worth being tested by observations at cosmological scales. For observations, the cosmological perturbations need to be studied further in the DHOST theory, except for the linear growth of matter in the shift-symmetric case [107]. In addition, it is significant to take into account the oscillatory behavior of $\alpha_B - \alpha_M/2$, or β_1 to trace their redshift evolution and compare with observational data.

4.13 Conclusion

4.13.1 Horndeski theory at cosmological scales

We have discussed constraints on Horndeski theory with GW propagation. We firstly reviewed the general framework for the waveform deformation from modified gravity including the Horndeski theory. Then we numerically formulated the Horndeski theory at the cosmological scale to compute α_M and α_T.

Next, we performed a Monte Carlo simulation that keeps the models consistent with the observations of cosmic expansion. In this procedure, we adopted two criteria; consistency and stability. Carrying out the simulation, we obtained the model distribution on the $\alpha_T - \alpha_M$ plane. Then we found that α_M and α_T have large values in the models including only G_4 or G_5, while including G_2 together with G_4 or G_5 allows both α_M and α_T to be smaller. Thanks to this feature, the models are significantly distinguishable depending on whether or not the models include the function G_2.

Finally, we constrained the Horndeski theory from the simultaneous detection of GW170817 and GRB170817A. We provided the observational bounds for the physical parameters that are involved in GW propagation ;ν_0, ν_1, δ_{g0}, and δ_{g1}. As a result, we found that the constraints on ν_0 and ν_1 are still too weak to distinguish the specific models shown in the Table. I, while those on δ_{g0}, and δ_{g1} are sufficiently strong enough to exclude the models that contain G_4 or G_5 without G_2. Consequently, we concluded that the model space of the Horndeski theory must be significantly reduced to explain the cosmic accelerating expansion and the GW propagation simultaneously. In other

words, in the Horndeski framework the main driver of the cosmic accelerating expansion should be G_2. At present, the models such as quintessence, nonlinear kinetic theory, or $f(R)$ theories are still allowed.

In addition to our work, we comment on the theories other than the Horndeski theory including higher derivatives of a scalar curvature and a scalar field. Our formulation in effect contains those theories because the higher derivative terms become too tiny to be observed at the cosmological scale. This argument agrees with the recent reports just after the detection of GW170817 was announced [108, 109, 110, 111]. However, our work quantitatively discusses how much the fine-tuning of the model is required within the current observational errors. In addition, as shown in Eq. (4.5.10), we obtained for the first time the constraint on the amplitude damping parameter ν by the observation of GW170817. Although the constraint is loose, it plays an important role in further restricting the models whose δ_g is fine-tuned to zero.

In the end, we report on an accidental finding that the parametrization of $\alpha \propto \Omega_{DE}\alpha_i$ is not valid in general. This assumption is now widely used when computing cosmological observables, particularly the CMB angular power spectrum, using Einstein-Boltzmann solvers [112, 113, 114]. Therefore, it is important to revisit the previous constraints on the Horndeski theory that parametrized $\alpha \propto \Omega_{DE}\alpha_i$ and to investigate the application of our simulation to other cosmological observations such as CMB or LSS. We will address this issue in a future publication

4.13.2 Horndeski theory after GW170817

We have studied how modification of gravity, particularly, in Horndeski theory with $c_{\rm T} = 1$, affects the properties of GW propagation. In the former part, we have estimated the measurement errors of the modification parameters with Voyager and the third generation detectors such as CE and ET, showing that

- the measurement errors of the gravity modification parameters, ν and μ, hardly depend on a redshift due to the accumulation effect during propagation,
- a heavier source in general gives a smaller error,
- the future GW observation can reach the measurement error of $\Delta\nu \approx 0.02$, significantly depending on the maximum redshift at which a source redshift can be identified with electromagnetic observations.

In the latter part, we have studied the model distribution of the Horndeski theory with a numerical approach. We performed a Monte Carlo-based numerical simulation and computed $G_{\rm matter}$, $G_{\rm light}$, and α_M. We found that

- $G_{\rm matter} \approx G_{\rm light}$ in the super-Compton case, while $G_{\rm matter} \geq G_{\rm light}$ in the sub-Compton case,

- model-filtering conditions consistent with ΛCDM cosmology preferentially select the negative sign of α_M at lower redshifts $z < 1$, indicating that the observed amplitude of a GW is relatively enhanced.

Thus, the future GW observations can constrain ν in the general formalism of GW propagation and equivalently α_M in the Horndeski theory at the precision of $\mathcal{O}(0.01)$, which is comparable with the local measurements such as the binary pulsars and the lunar laser ranging. The strength of the GW observations is that it does not rely on gravity at local scales but can measure modification of gravity at cosmological scales directly, allowing us to measure not only the time dependence of α_M but also the scale dependence of α_M. In the future, the GW observations combined with the local and cosmological measurements play a significant role to check the consistency of a gravity theory at cosmological distance.

4.13.3 DHOST theory after GW170817

We have numerically investigated the DHOST theory after GW170817, i.e., DHOST$_{c_g^2=1}$ theory with the conventional matter at cosmological scales. We assumed the slow time evolution of the scalar field, $|\hat{X}| \ll 1$, particularly realizing the cosmic expansion of the late-time acceleration and the matter dominant epoch. We numerically computed the conventional EFT parameters, and found that the stable models that explain the cosmic acceleration within the DHOST$_{c_g^2=1}$ theory framework have the following features:

- The Planck mass run rate, α_M, is almost identical in all subclasses of the DHOST$_{c_g=1}$ theory, which makes difficult to distinguish the DHOST$_{c_g=1}$ theory from the Horndeski theory. In general, α_M has a negative value, $\alpha_M \leq -0.1$, as found in the Horndeski theory in [2].

- The kinetic brading parameter, α_B, sensibly distinguishes the theories. In the region that $\alpha_B > -0.1$, the Horndeski theory is clearly distinguished from the DHOST$_{c_g=1}$ theory.

- α_H and β_1 are correlated by $\alpha_H + 2\beta_1 = \mathcal{O}(|\hat{X}^2|)$, which is generically satisfied in the DHOST$_{c_g=1}$ theory. The values of α_H and β_1 in our computation range from -0.2 to 0.2.

- The GLPV theory peculiarly predicts $\alpha_H = \mathcal{O}(|\hat{X}|^2)$, and deviates from the Horndeski theory in α_M and α_B at the order of $\mathcal{O}(|\hat{X}|^2)$. This is due to the condition of $\beta_1 = 0$. This makes the discrimination of these theories difficult.

In conclusion, we note that the correlations among α_M, α_B, and α_H, and β_1 reduce the number of the characteristic parameters to three parameters. We propose that a parameter set of $(\alpha_M, \alpha_B - \alpha_M/2, \beta_1)$ is the principal set to discriminate the subdivision of the DHOST$_{c_g=1}$ theory. We find that the common parameters α_M and $\alpha_B - \alpha_M/2$ in the Horndeski and DHOST$_{c_g=1}$ theories can differ by the oscillatory features in their redshift evolutions. Our prediction on $(\alpha_M, \alpha_B - \alpha_M/2, \beta_1)$ can provide a broad opportunity to test the DHOST$_{c_g=1}$ theory for the cosmological surveys such as cosmic shear measurements [115, 116, 117, 118, 119, 120] and upcoming GW observations [2, 121]. We will address the constraints on $(\alpha_M, \alpha_B - \alpha_M/2, \beta_1)$ quantitatively from the different observations in the future work.

Chapter 5

Inflation without Lorentz invariance

The Lorentz invariance is one of the most fundamental properties of physics. Although the Lorentz invariance occasionally confirmed by the Michealson-Morley interferometric experiment in 1901, that resulted in the perpetual change of the classical Newtonian dynamics, leading the development of the electromagnetism, the special relativity, and the general relativity. The Lorentz invariance healthily accommodates with the quantum mechanics, i.e., unitarity of the time evolution, and non-trivially confines the types of elementary particles by its mathematical symmetry. Experimentally, a number of experiments and observations have verified that the Lorentz invariance in particle physics is truly evident. In particular, the constraint of the Lorentz invariance in the electromagnetic physics, was tightly obtained, as shown in Fig. (5.1). Deviations from Lorentz invariance are tightly constrained in the Standard Model sector [122, 123, 124]. Hence, the verification of the Lorentz invariance is prominently established.

When it comes to the local Lorentz invariance, which is subgroup of the diffeomorphism invariance of gravity theories, the experiments and observation for testing it is much less than the that of global Lorentz invariance. This is partially because the cut-off scale of the Einstein gravity is located at the Planck scale 10^{19}GeV, at which the energy is well above from the range we can probe in. Nonetheless, a number of observations at low energies such as Solar System tests [124, 125], pulsar timing [126, 127, 128, 129], cosmology [130, 131, 132, 133, 134, 135, 136] and direct detection of the gravitational waves [137, 138, 49, 139].

In the cosmological context, the break of the Lorentz invariance is significant. As discussed in the EFT of inflation [33] (or brief summary in Appendix. B), the inflaton can be understood as a Nambu-Goldstone bosons induced by the spontaneous symmetry

breaking of the global time translation invariance of de Sitter spacetime. In other words, the inflaton is created by the break of the (global) Lorentz invariance. Then one naively wonders whether or not the local Lorentz invariance of space-time is sustained in the inflationary universe. To think of this much further, a theoretical framework to describe such phenomena in an appropriate sense of physics.

It has been acknowledged that the mechanisms in the absence of the local Lorentz invariance actually exist, i.e., the ghost condensation, the Aether field, or the anisotropic scaling of space and time. We further make use of such Lorentz-violating physics as a solution to the UV completion of gravity, specifically the renormalisability of gravity. Interestingly, the renormalisability of gravity can be achieved by introducing anisotropic scaling law of space and time, as P.Horava firstly showed in 2009 [140]. This is called Hořava-Lifshitz gravity. In this Chapter, we focus on the Hořava-Lifshitz gravity and exhibit the phenomenology in Hořava-Lifshitz gravity.

By contrast the theories investigated in Chapter 4, Hořava - Lifshitz gravity explicitly breaks diffeomorphism invarinace between space and time. Therefore, it is significant to argue independently whether or not the Hořava-Lifshitz gravity is consistent to the experimental and observational constraints on gravity.

5.1 Gravity without local general covariance

The general covariance, or the diffeomorphism invariance, is one of the essential status of the gravity theories. To be more general, however, the break of the general covariance can be realized as an possible extension of the gravity theories. Moreover, it has been less tested in phenomenology whether or not the gravitational interactions respect the general covariance. Hence the construction of gravity theories without general covariance is an important question to look into. In this section, we summarise the theories that virtually general covariance.

5.1.1 Ghost condensation

A well-known mechanism of breaking the general covariance is Ghost condensation [141]. The ghost condensation is found to be a general realisation of a spontaneous symmetry breaking of general covariance, sometimes noted as the Higgs mechanism in gravity. As is often the case, we start with a vacuum such that an underlining scalar field has a trivial vacuum expectation value,i.e.,

$$\langle \phi \rangle = 0 \tag{5.1.1}$$

When we consider the scalar field whose kinetic term is opposite. With the metric configuration $g_{\mu\nu} = (-,+,+,+)$, the kinetic term is given as

$$S_\phi = \int d^4x\sqrt{-g}\left[+\frac{1}{2}g^{\mu\nu}\partial_\mu\phi\partial_\nu\phi + \dots\right], \tag{5.1.2}$$

By imposing the shift symmetry, i.e., $\phi \to \phi + a$, there are only the derivative interactions in the action Eq. (5.1.2). Then action is written as

$$S = \int d^4x\sqrt{-g}M^4P(X)\,, \tag{5.1.3}$$

where $X = g^{\mu\nu}\partial_\mu\phi\partial_\nu\phi$ is the canonical kinetic term of the scalar field, and $P(X)$ is an arbitrary dimensionless function of X. Note that this is the most general action that realises the shift symmetry. With the FLRW metric

$$ds^2 = -dt^2 + a^2(t)d\Omega^2\,, \tag{5.1.4}$$

where $d\Omega^2$ is the spatial metric for a maximally symmetric 3-dimensional space. When the scalar field only depends on the time t, the equation of motion of the scalar field is derived as

$$\partial_t[a^3P'(\dot\phi^2)\dot\phi] = 0\,, \tag{5.1.5}$$

By integrating Eq. (5.1.5) and we obtain

$$\dot\phi P'(\dot\phi^2) = \frac{const.}{a^3(t)}\,, \tag{5.1.6}$$

In the expanding universe, the long range limit is given by $a \to \infty$. Then we have two fixed points,

$$\dot\phi = 0,\ P'(\dot\phi^2) = 0\,, \tag{5.1.7}$$

The stability around the two fixed points are derived. In particular, the second fixed point is stabilised whenever the condition $P''(\dot\phi^2) > 0$ is satisfied. When we take that the scalar field to be a time coordinate with the excitation π, i.e., $\phi = M^2t + \pi$, the second fixed point is able to be stabilised from the higher derivative operator,

$$\left\langle\dot\phi\right\rangle = M^2 \neq 0\,, \tag{5.1.8}$$

can be stabilised via the higher derivative

$$S \sim \int d^4x \left[\frac{1}{2}\dot{\pi}^2 - \frac{1}{2M^2}(\nabla^2\pi)^2 + \dots \right] \tag{5.1.9}$$

The dispersion relation of the excitation is given as

$$\omega^2 \sim \frac{k^4}{M^2}\,, \tag{5.1.10}$$

At this phase, the background with the scalar field with wrong sign of the kinetic term is stable. Since the dispersion relation suggest that the propagation speed of π is $c_\pi^2 \sim k^2/M^2$, causing the break of the Lorentz symmetry breaking.

5.1.2 Einstein-Aether theory

The Einstein Aether theory is a covariant theory with a time-like vector field that breaks local Lorentz symmetry. The action is given as

$$S = \frac{1}{16\pi G}\int d^4x\sqrt{-g}\left(R + \mathcal{K}^{ab}{}_{mn}\nabla_a n^m \nabla_b n^n + \lambda(n^a n_a + 1)\right), \tag{5.1.11}$$

where

$$\mathcal{K}^{ab}{}_{mn} = c_1 g^{ab}g_{mn} + c_2\delta^a_m\delta^b_n + c_3\delta^a_n\delta^b_m - c_4 n^a n^b g_{mn}\,, \tag{5.1.12}$$

where the coefficients $c_i (i = 1, 2, 3, 4)$ are free constants typically at the order of unity. Then the Gauss - Godazzi identity is given as

$$R = {}^{(3)}R + K_{\mu\nu}K^{\mu\nu} - K^2 + 2\nabla_\mu(Kn^\mu - n^\rho\nabla_\rho n^\mu)\,, \tag{5.1.13}$$

The covariant derivative of the Aether field u_a is given as

$$\nabla_a n_b = K_{ab} + n_a v_b\,, \tag{5.1.14}$$

v_b denotes the acceleration vector that satisfies $n^c\nabla_c n_a = -v_a$. Note that the acceleration vector v_a is perpendicular to n^a, i.e., $v^a n_a = 0$. By replacing $\nabla_a n_b$ with Eq. (5.1.14) and inserting R with Eq. (5.1.13) in the action Eq. (5.1.11), we obtain the

$$S = \frac{1}{16\pi G}\int d^4x\sqrt{-g}\left[(1+c_{13})K_{\mu\nu}K^{\mu\nu} - (1-c_2)K^2 - c_{14}v_a v^a\right], \tag{5.1.15}$$

where $c_{13} \equiv c_1 + c_3$ and $c_{14} \equiv c_1 + c_4$. Since c_{13} and c_2 are independently chosen, this theory is a theory such that the propagation speed of the gravitational waves are not identical to the speed of light. As shown later, this theory is nothing but the non-projectable Hořava - Lifshitz theory at the anisotropic scaling index z is given by $z = 1$. In fact in the ADM form, $n_a dx^a = -Ndt$, $n^a \partial_a = (1/N, -N^i/N)$, v_a is obtained as $v^a \partial_a = (0, \gamma^{ij}\partial_j N/N)$, which is precisely equivalent to $z = 1$ non projectable Hořava - Lifshitz gravity.

5.1.3 Anisotropic scaling in space and time

The origin of the general covariance is the equivalence of space and time. The realisation of the equivalence is formulated in the Lorentz invariance by keeping the causal structure of physical theory. Once we admit that the space and time is no longer the same, an instant consequence is that the break of the Lorentz invariance.

The realization for such a theory is the Horava Lifshitz gravity The local Lorentz invariance is broken.

- The review of Horava Lifshitz gravity from my master thesis (and its review papers)

$$t \to b^z t\,,\ \mathbf{x} \to b\mathbf{x}\,, \tag{5.1.16}$$

The diffeomorphism of the theory

$$t \to \tilde{t} = \tilde{t}(t)\,,\ \mathbf{x} \to \tilde{\mathbf{x}} = \tilde{\mathbf{x}}(x)\,, \tag{5.1.17}$$

The metric is given as

$$ds^2 = -N^2 c^2 dt^2 + g_{ij}(dx^i + N^i dt)(dx^i + N^i dt)\,, \tag{5.1.18}$$

The action is given as

$$S_{HL} = \frac{M_{\rm pl}^2}{2}\int dt d^D x \sqrt{g}\left\{N[K_{ij}K^{ij} - \lambda K^2] + \xi^{(D)}R - 2\Lambda + \alpha v_i v^i + \mathcal{V}\right\}, \tag{5.1.19}$$

where $\mathcal{V}$ denotes the effective potential term that contains the higher curvatures,

$$\mathcal{V} = R^2,\ \Delta R\,,\ R_{ij}R^{ij}\,,\ R_{ijkl}R^{ijkl}\,,\ (a_i a^i)^2, a_i a^i R, \ldots \tag{5.1.20}$$

The anisotropic scaling law defined in Eq. (5.1.16) has a novel property such that

the spatial derivatives are capable of the higher numbers of derivatives while the time derivatives are up to quadratic order, consequently the initial data of dynamics does not induce additional degree of freedom. Moreover, the higher spatial derivative terms play a role to suppress the high energy momenta at smaller scales, satisfying the property of power counting renormalizability. In more detail, we discuss in the Chapter 5.

5.2 Toy model: Lifshitz scalar

Before working with gravity, let us see a toy model of anisotropic scaling in the flat Minkowski spacetime. We introduce a scalar field called Lifshitz scalar. The anisotropic scaling is defined as

$$t \to b^{-z} t\,,\ \mathbf{x} \to b^{-1}\mathbf{x}\,, \tag{5.2.1}$$

That means the space and time differently scales in energy. For the generality, let us consider $1+D$ dimensional spacetime. Since the action principle states that the action should be invariant from energy scaling, the free interaction of the Lifshitz scalar is determined. The action of the Lifshitz scalar is given as

$$S = \frac{1}{2}\int dt d^D x \left(\dot{\phi}^2 - \frac{1}{M^{2(z-1)}}\phi\Delta^z\phi - \mathcal{L}_{\rm int}\right), \tag{5.2.2}$$

The scaling dimension of the kinetic term gives the dynamical scale of ϕ, i.e., $[\phi]$,

$$[\phi] = \frac{D-z}{2}\,, \tag{5.2.3}$$

The interaction term is given by

$$\mathcal{L}_{\rm int}\lambda_n\phi^n\,, \tag{5.2.4}$$

The scaling dimension of the coupling constant $[\lambda_n]$ is

$$[\lambda_n] = D + z - n[\phi]\,, \tag{5.2.5}$$

The contribution in the Lagrangian is

$$\int dt d^D x \phi^n \propto E^{-[\lambda_n]/z}\,, \tag{5.2.6}$$

Notice that $[\lambda_n] \geq 0$ is necessary condition for the finite convergence of interaction

terms in UV regime. Whenever we consider the scaling exponent z in the range $z \geq D$, the second term in Eq. (5.2.5) is always positive regardless of the artbitorary n and thus $[\lambda_n]$ is positive. Therefore, the necessary condition for the renormalisation is given as $z \geq D$.

5.3 Hořava Lifshitz gravity

General relativity (GR) accurately describes all known gravitational phenomena. Still, it has a theoretical flaw: it is not renormalizable [142] and thus cannot be a complete theory of quantum gravity. One way to address this problem is to introduce terms with higher powers of the curvature tensor which make the theory renormalisable [143, 20]. However, if Lorentz invariant, these higher curvature terms lead to loss of unitarity. This motivated P. Hořava to propose a framework to render gravity power-counting renormalisable by abandoning Lorentz invariance [140]. By breaking Lorentz invariance, we can introduce higher spatial derivative terms, while avoiding higher time derivative terms and thus making the theory compatible with unitarity. A key role in the power-counting argument is played by an approximate invariance of the theory at high energies and momenta with respect to the so-called Lifshitz scaling transformations. These stretch space and time by different amount, so they are also often referred to as anisotropic scaling. The dispersion relations of various degrees of freedom at high energies, compatible with anisotropic scaling, have the form $\omega \propto p^z/M_*^{z-1}$, where ω and p are particle's energy and momentum, z is the Lifshitz exponent (z equals the number of spatial dimensions in Hořava's proposal) and M_* is the energy threshold, above which the anisotropic scaling sets in. This framework has received the name of Hořava–Lifshitz (HL) gravity and the so-called projectable subclass of the resulting theories has been rigorously demonstrated to be perturbatively renormalizable [144, 145]. Moreover, in 2 spatial and 1 time dimensions the theory exhibits asymptotic freedom [146] which strongly suggests that it is ultraviolet (UV) complete.

5.3.1 Cosmological perturbations in Hořava-Lifshitz gravity

The discussion is based on the review by S. Mukohyama 2015 The infinitesimal coordinate transformation is given as

$$\delta t = f(t)\,,\ \delta x^i = \xi^i(t,x)\,, \tag{5.3.1}$$

The metric is given as

$$ds^2 = (N^2 - N_i N^i)dt^2 - 2N_i dx^i dt - g_{ij}dx^i dx^j \,, \tag{5.3.2}$$

The gauge structure is given as

$$\delta N = \partial_t(Nf) \,, \tag{5.3.3}$$
$$\delta N^i = \partial_t(N^i f) + \partial_t \xi^i + \mathcal{L}_\xi N^i \,, \tag{5.3.4}$$
$$\delta N_i = \partial_t(N_i f) + g_{ij}\partial_t \xi^j + \mathcal{L}_\xi N_i \,, \tag{5.3.5}$$
$$\delta g_{ij} = f\partial_t g_{ij} + \mathcal{L}_\xi g_{ij} \,, \tag{5.3.6}$$

Projectable version

The projectable version of the Hořava - Lifshitz gravity is a theory given by the following action,

$$S = \frac{M_{\rm pl}^2}{2}\int dt d^3x \sqrt{g} N(K_{ij}K^{ij} - \lambda K^2 - \mathcal{V}[g_{ij}]) \,, \tag{5.3.7}$$

where

$$\begin{aligned}\mathcal{V}_{\rm proj} = &-\xi R + M_{\rm pl}^{-2}(A_1 \Delta R + A_2 R_{ij}R^{ij} + \dots) \\ &M_{\rm pl}^{-4}(B_1 R\nabla^2 R + B_2 R_{ij}R^{j_k}R^{ki} + \dots) \,,\end{aligned} \tag{5.3.8}$$

The symmetry of the projectable version is the rule of coordinate transformation of the lapse function,

$$N \to \tilde{N} = N\frac{\partial t}{\partial \tilde{t}} \,, \tag{5.3.9}$$

The perturbative quantities are

$$N = 1 + \phi(t) \,, \tag{5.3.10}$$
$$N_i = \frac{\partial}{\sqrt{\Delta}} B \,, \tag{5.3.11}$$
$$g_{ij} = \delta_{ij} - 2\left(\delta_{ij} - \frac{\partial_i \partial_j}{\Delta}\right)\psi - 2\frac{\partial_i \partial_j}{\Delta}E \,, \tag{5.3.12}$$

namely in the Minkowski space The Lagrangian of the scalar perturbation at the quadratic order, $\mathcal{L}^{(2)}_{\rm scalar}$ is

$$\mathcal{L}^{(2)}_{\rm scalar} = \frac{M_P^2}{2}\Bigg\{-\dot{\psi}^2 - 2\psi\Delta\psi + 4\psi\sqrt{\Delta}\dot{B} + 4\psi\ddot{E} \\ - (\lambda-1)\left(\sqrt{\Delta}B + \dot{E} + 2\dot{\psi}\right)^2 - \frac{f_1}{M_*^2}(\Delta\psi)^2 - \frac{g_1}{M_*^4}\psi\Delta^3\psi\Bigg\}, \tag{5.3.13}$$

f_1 and g_1 are related to the constant coefficients in Eq. (5.3.8), which are not important for the following discussion. Note that the perturbation of the lapse ϕ drops out due to the projectability condition The hamiltonian constraint is derived as

$$4\dot{\psi} + 2(\lambda-1)(\sqrt{\Delta}B + \dot{E} + 2\dot{\psi}) = 0\,, \tag{5.3.14}$$

By eliminating $\sqrt{\Delta}B$ from Eq. (5.3.13) we obtain

$$\mathcal{L}^{(2)}_{\rm scalar} = \frac{M_P^2}{2}\left\{\frac{2(3\lambda-1)}{\lambda-1}\dot{\psi}^2 - \psi\left(2\Delta + \frac{f_1}{M_*^2}\Delta^2 + \frac{g_1}{M_*^4}\Delta^3\right)\psi\right\}, \tag{5.3.15}$$

To keep the positive kinetic term of ψ yields the necessary condition,

$$\frac{3\lambda-1}{\lambda-1} > 0\,, \tag{5.3.16}$$

The dispersion relation of ψ is

$$\omega^2 = -\frac{\lambda-1}{3\lambda-1}\left(p^2 - \frac{f_1}{2M_*^2}p^4 + \frac{g_1}{2M_*^4}p^6\right), \tag{5.3.17}$$

Here p denotes the norm of the spatial momentum. M_* is the cut of scale at which the contributions of higher derivatives as a result of anisotropic scaling are relevant above M_*. λ controls the propagation speed of ψ at the low energy limit. The general relativity realises when $\lambda = 1$, but it is worth mentioning that the limit of $\lambda \to 1{+}0$ with the respect of the condition Eq. (5.3.16) does not properly recover the general relativity in the linear perturbation, which is due to the disappearance of the spatial derivatives of ψ. It is instantly found that the condition of the positive kinetic energy prohibit the avoidance of the gradient instability, $\omega^2 < 0$ at $p/M_* \lesssim 1$. This causes a pathology when applying in phenomenology. To accommodate with the current stability of the universe at least in the Hubble time scale, $1/H_0$, the instability of ω^2

$$\mathrm{Im}\omega \sim \sqrt{|\lambda-1|}M_* < H_0\,, \tag{5.3.18}$$

which ends up with the upper limit of M_*. Although it is theoretically motivated that M_* is close to the Planck mass scale, M_* could be chosen at any scale. Hence, the bound in Eq. (5.3.18) is still thoughtful. On top of that, the consistency of the Newtonian gravity at the scale of $10\mu m$ [], M_* has a lower limit,

$$M_* > 0.1\mathrm{eV}\,, \tag{5.3.19}$$

In the combination of the conditions in Eqs. (5.3.18) and (5.3.19), λ is constrained as

$$\sqrt{|\lambda - 1|} \lesssim 10^{-61}\,, \tag{5.3.20}$$

The value of λ is unsatisfactory in theoretical modeling. Therefore, the projectable Hořava - Lifshitz gravity is not viable as a model for cosmology.

Non-projectable version

In the framework of the Hořava - Lifshitz gravity, the projectable condition Eq. (5.3.9) is not necessary. The non projectable version of the Hořava - Lifshitz gravity is given by removing the projectable condition Eq. (5.3.9). As a result, an additional operator $a_i \equiv \partial_i N/N$ can appear in the Lagrangian. Specifically in $z = 3$ case,

$$\mathcal{V}_{\mathrm{non-proj}} = \mathcal{V}_{\mathrm{proj}} + C_1 a_i a^i + C_2 R \nabla_i a^i + C_3 a_i \Delta a^i + C_4 \Delta R \nabla_i a^i + C_5 a_i \Delta^2 a^i\,, \tag{5.3.21}$$

The quadratic Lagrangian of the scalar sector is

$$\begin{aligned}\mathcal{L}^{(2)}_{\mathrm{scalar}} = \frac{M_P^2}{2}\Bigg\{ & -\dot{\psi}^2 - 2\psi\Delta\psi + 4\phi\Delta\psi + 4\psi\sqrt{\Delta}\dot{B} + 4\psi\ddot{E} \\ & - (\lambda - 1)\left(\sqrt{\Delta}B + \dot{E} + 2\dot{\psi}\right)^2 + \alpha(\partial_i\phi)^2 \\ & - \frac{f_1}{M_*^2}(\Delta\psi)^2 - \frac{2f_2}{M_*^2}\Delta\phi\Delta\psi - \frac{f_3}{M_*^2}(\Delta\phi)^2 \\ & - \frac{g_1}{M_*^4}\psi\Delta^3\psi - \frac{2g_2}{M_*^4}\phi\Delta^3\psi - \frac{g_3}{M_*^4}\phi\Delta^3\phi\Bigg\}\,,\end{aligned} \tag{5.3.22}$$

where the constants α, f_n, and g_n are related to the coefficients of the terms in the potential $\mathcal{V}_{\mathrm{non-proj}}$. By fixing the gauge $B = 0$ and integrating out the non dynamical fields E and ϕ, we obtain

$$\mathcal{L}^{(2)}_{\mathrm{scalar}} = \frac{M_*^2}{2}\left\{\frac{2(3\lambda - 1)}{\lambda - 1}\dot{\psi}^2 + \psi\frac{P[M_*^{-2}\Delta]}{Q[M_*^{-2}\Delta]}\Delta\psi\right\}\,, \tag{5.3.23}$$

where the polynomials P, Q have the form

$$P[x] = (g_2^2 - g_1 g_3)x^4 - (g_1 f_3 + g_3 f_1 - 2g_2 f_2)x^3 + (f_2^2 - 4g_2 - f_1 f_3 - 2g_3 - g_1\alpha)x^2 - (2f_3 + f_2\alpha + 4f_2)x + (4 - 2\alpha)\,, \tag{5.3.24}$$

$$Q[x] = g_3 x^2 + f_3 x + \alpha\,, \tag{5.3.25}$$

The Lagrangian Eq. (5.3.23) does not plague with the instabilities by the following two conditions. The first is the positivity of the kinetic energy of the system, realising when $\lambda > 1$ in the accommodation with the small deviation from the general relativity. The second is the absence of gradient instability, namely satisfying by the frequency

$$\omega^2 = \frac{\lambda - 1}{2(3\lambda - 1)} \frac{P[-p^2/M_*^2]}{Q[-p^2/M_*^2]}\,, \tag{5.3.26}$$

is positive, $\omega^2 > 0$ at all the spatial momentum p. Equivalently, the condition reads

$$P[x]/Q[x] > 0 \text{ at } x < 0\,, \tag{5.3.27}$$

This condition leads the certain constraints on the coefficients α, f_n, and g_n. In comparison of the inevitable gradient instability in the projectable version, we particularly focus on the condition at $p/M_* \ll 1$. By the truncation of the higher order of p/M_*, we obtain

$$\omega^2 = \frac{\lambda - 1}{3\lambda - 1}\left(\frac{2}{\alpha} - 1\right)p^2\,, \tag{5.3.28}$$

and thus the stability condition requires

$$0 < \alpha < 2\,, \tag{5.3.29}$$

As a result, the theoretical pathology raising in the projectable version does not the case in the non projectable one. It is shown that the low energy limit of the non projectable version is equivalent to the covariant theory with a vector field of a preferred direction of time, so called the Einstein Aether theory.

5.4 Early universe

In the framework of the Hořava-Lifshitz gravity, the scenario of the early universe gives us some insightful features. Let us discuss in the non projectable version of Hořava-Lifshitz gravity, in which we have known no pathology in its theoretical construction. As derived in the previous section, the dispersion relation depends on the energy scale. At the time when the anisotropic scaling index z is given the

$$\omega^2 = c_z^2 p^2 \left(\frac{p}{aM}\right)^{2(z-1)} , \tag{5.4.1}$$

where c_z^2 denotes the coefficient in the dimension of the sound speed which is order of unity, and M denotes the mass scale at which the anisotropic scaling matters, typically given $M \sim M_*$. In the case of $z = 1$, Eq. (5.4.1) is nothing but the normal dispersion relation with non trivial sound speed, by the independence from M. The fluctuation of a canonical scalar field, $\delta\phi$ is normalised by the canonical quantisation, acquiring the norm $1/a\sqrt{2\omega}$ the dimensionless power spectrum of $\delta\phi$ is given at the horizon crossing, i.e, $\omega \sim aH$,

$$\mathcal{P}_{\delta\phi} \equiv \frac{p^3}{2\pi^3}|\delta\phi|^2 = \left(\frac{M}{2\pi}\right)^2 \left(\frac{H}{M}\right)^{(3-z)/z} , \tag{5.4.2}$$

where the scale factor is replaced by solving $\omega \sim aH$ with a. Note that $z = 1$ recovers the normal power spectrum of a canonical field, $(H/2\pi)^2$. Interestingly, $z = 3$ gives the independence from the horizon scale H, realising the scale invariance of the power spectrum. The condition such that the power spectrum is frozen out during the cosmic expansion at $\omega \ll aH$ is that

$$\frac{d}{dt}\left(\frac{a^2H^2}{\omega^2}\right) > 0 , \tag{5.4.3}$$

This condition could be realised not only de Sitter universe, but also one with the power-law expansion. In particular, when $z = 3$, the scale invariance is preserved even in the radiation or matter domination epoch.

5.5 Inflationary universe with Lifshitz scaling

In order to examine the consequences of violation of Lorentz invariance at high energies we study in this paper its effect on cosmic inflation in the early universe. One may

expect that breaking of Lorentz invariance during inflation will leave an imprint on the primordial perturbations generated during inflation. This possibility has been explored in a number of works [141, 147, 148, 149, 150, 151, 152, 153, 154, 155, 156, 157]. In HL gravity, where 4D diffeomorphism (Diff) is reduced to foliation preserving Diff, there appears a scalar degree of freedom in gravity sector, so called khronon. It is tempting to speculate that this additional degree of freedom can play the role of inflaton. However, at the moment this seems to be forbidden due the restrictive structure of the theory. Therefore, to drive inflation, we need to introduce a scalar field, as usual. Then, in general, generation of the primordial scalar perturbation is described by a coupled system for two fields, the inflaton and khronon perturbations.

To provide a prediction of the observable quantities, we need to solve consistently the two field system of the inflaton and khronon, which are coupled with each other during inflation. When 4D Diff is preserved and the universe is dominated by a single component, it is well-known that the adiabatic curvature perturbation ζ stays constant in time after the Hubble crossing (see, e.g., Refs. [158, 159]). On the other hand, in HL gravity the number of scalar degrees of freedom is always greater than one due to the presence of khronon and it is not clear a priori if there exists a conserved variable or not.

The inflaton and khronon are gravitationally coupled even in the absence of a direct interaction between them. In this paper we compute the primordial power spectra by consistently solving the two field models with the inflaton and khronon. The previous studies mostly focused on the regime where the Hubble scale of inflation is low, $H < M_*$, so that the higher derivative terms in the action are unimportant and the theory is described by its infrared (IR) limit. By contrast, in this paper we are interested in the high-energy regime of Lifshitz scaling relevant for the case[1] $H > M_*$. We consider both projectable and non-projectable versions of HL gravity. As discussed in Refs. [160, 161], the khronon sector of the projectable HL gravity suffers from either the gradient instability or the strong coupling in the IR limit. This means that it cannot describe the physics all the way down to low energies, unless inflationary epoch is separated from the later hot universe by a phase transition that eliminates khronon from the spectrum. Still, the projectable version is perfectly well-behaved in the high-energy regime and its study is instructive to make comparison with the non-projectable version.

[1]Recent observation of gravitational waves from neutron star merger in coincidence with the electromagnetic signal [49] points towards an upper bound on the scale M_* in non-projectable HL gravity, $M_* \lesssim 10^{11}$GeV [139]. Hence, in this theory the Lifshitz regime is relevant whenever the inflationary Hubble exceeds 10^{11}GeV.

When the fluctuations are deep inside the Hubble scale, the gravitational interaction is suppressed and we simply have two decoupled Lifshitz scalars. On the other hand, in the super Hubble scales, the gravitational interaction makes the inflaton and khronon coupled. Then one may naively expect that the primordial spectrum will depend on the time evolution of these two fields and we will need to solve the evolution all along also after the Hubble crossing time. Indeed, this is the case for the projectable version. On the other hand, in the non-projectable version, we will find that khronon gets decoupled from the adiabatic curvature perturbation ζ. As a result, ζ is conserved at large scales and the power spectrum of ζ is solely determined by the inflaton. Thanks to the presence of the conserved quantity, we can easily calculate the spectrum of the fluctuation at the end of inflation. Then the consequence of the LV in the spectrum of ζ only stems from the modification of the dispersion relation.

The spectrum of primordial gravitational waves in HL gravity was computed in Ref. [147]. Once the scalar perturbation is obtained, we can also compute the tensor to scalar ratio r. In a 4D Diff invariant theory, there exists a universal relation between r and the tensor spectral tilt n_t, the so-called consistency relation. We will show that this consistency relation can be broken if the primordial perturbations are generated in the anisotropic scaling regime. The violation of the consistency relation provides a signal of LV in the gravity sector in the high energy regime.

This paper is organized as follows. In Sec. 5.6 we describe our setup and review the computation of the power spectrum of the Lifshitz scalar and the gravitational waves generated in the anisotropic scaling regime. In Sec. 5.7 we discuss the behaviour of the khronon perturbation. We show that khronon stays gapless in the projectable version, while it is gapped in the non-projectable version, which leads to the decoupling from the adiabatic mode. In Sec. 5.8 we discuss violation of the consistency relation by inflationary perturbations with Lifshitz scaling. We conclude in Sec. 5.9. Appendices summarise some technical details.

5.6 Primordial perturbations with anisotropic scaling

In this section we describe our setup and briefly summarise the computation of the primordial spectra of the Lifshitz scalar and gravitational waves.

5.6.1 Projectable and non-projectable Hořava gravity

Lagrangian densities

First, we consider the non-projectable version of HL gravity [140] with the extension introduced in [162]. Due to the complexity of the most general Lagrangian in this framework, we restrict only to the terms that contribute to the action at quadratic order in the perturbations around spatially flat backgrounds and that preserve the parity invariance. This restriction is sufficient to capture the qualitative features of the theory. The complete list of these terms is given in [162] and leads to the following Lagrangian density,

$$\begin{aligned}\mathcal{L}_{HG} = N\sqrt{h}\Bigg\{ & \frac{M_*^2}{2}\left[\frac{1}{\alpha_1}K_{ij}K^{ij} - \frac{1}{\alpha_2}K^2 + \frac{1}{\alpha_3}R + \frac{a_i a^i}{\alpha_4}\right] \\ & - \frac{1}{2}\left[\frac{R_{ij}R^{ij}}{\beta_1} + \frac{R^2}{\beta_2} - \frac{R\nabla_i a^i}{\beta_3} + \frac{a_i \Delta a^i}{\beta_4}\right] \\ & - \frac{1}{2M_*^2}\left[\frac{(\nabla_i R_{jk})^2}{\gamma_1} + \frac{(\nabla_i R)^2}{\gamma_2} + \frac{\Delta R \nabla_i a^i}{\gamma_3} - \frac{a_i \Delta^2 a^i}{\gamma_4}\right]\Bigg\}, \end{aligned} \tag{5.6.1}$$

where we used the ADM line element, given by

$$\mathrm{d}s^2 = (N^2 - N_i N^i)\mathrm{d}t^2 - 2N_i \mathrm{d}t\mathrm{d}x^i - h_{ij}\mathrm{d}x^i\mathrm{d}x^j\,. \tag{5.6.2}$$

Here R_{ij}, ∇_i and Δ denote the 3-dimensional Ricci tensor, the covariant derivative with respect to h_{ij} and the covariant Laplacian,

$$K_{ij} = \frac{\dot{h}_{ij} - \nabla_i N_j - \nabla_j N_i}{2N} \tag{5.6.3}$$

is the extrinsic curvature and we have defined a_i as

$$a_i \equiv \frac{\partial_i N}{N}\,. \tag{5.6.4}$$

Here, the dot denotes the derivative with respect to the cosmological time. Note that we included the integration measure in the definition of the Lagrangian density. The terms in the first line of Eq. (5.6.1) describe the low energy part of the action, and the parameters entering it are constrained by the present-day observations[2]. The relation

[2]We assume that during inflation these parameters have the same values as nowadays. This assumption can be relaxed in a more general setup.

between these parameters and the parameters α, λ, ξ introduced in [161] is

$$M_*^2 = M_P^2 \alpha \ , \quad \alpha_1 = \alpha \ , \quad \alpha_2 = \alpha/\lambda \ , \quad \alpha_3 = \alpha/\xi \ , \tag{5.6.5}$$

where M_P is the Planck mass. In what follows, we will write

$$\alpha_1 - \alpha_2 = 2\alpha_1 \bar{\alpha} \, . \tag{5.6.6}$$

We also discuss the projectable version, where the lapse function is postulated to be space-independent,

$$N = N(t) \, . \tag{5.6.7}$$

The action for the projectable version can be obtained simply by dropping the perturbation of the lapse function in the action for the non-projectable version. Then the parameters α_4, β_3, β_4, γ_3, and γ_4 are irrelevant in the projectable theory.

For both the non-projectable and projectable versions, we add as the inflaton a Lifshitz scalar field whose Lagrangian density is given by:

$$\begin{aligned} \mathcal{L}_{inf} = N\sqrt{h}\Bigg\{ & \frac{(\dot{\Phi} - N^i \partial_i \Phi)^2}{2N^2} - \frac{\varkappa_1}{2} \nabla_i \Phi \nabla^i \Phi - \frac{\varkappa_2}{2M_*^2} \nabla_i \nabla_j \Phi \nabla^i \nabla^j \Phi \\ & - \frac{\varkappa_3}{2M_*^4} \nabla_i \nabla_j \nabla_k \Phi \nabla^i \nabla^j \nabla^k \Phi - V(\Phi) \Bigg\} \, . \end{aligned} \tag{5.6.8}$$

In principle, the coefficients $\varkappa_{1,2,3}$ here can be functions of the field Φ which has zero scaling dimension. We concentrate on the case of constant coefficients for simplicity. We assume that the inflaton is minimally coupled to the gravity sector. We will briefly discuss a non-minimally coupled case in Sec. 5.9.

Parameter hierarchy

The Lagrangian density (5.6.1) contains a number of parameters. Here we discuss the hierarchy between them. First of all, we require that the anisotropic scaling sets in before the gravity becomes strongly coupled, assuming

$$0 < \alpha_1 < 1 \, . \tag{5.6.9}$$

Consider now the propagation of gravitational waves in flat spacetime where their dispersion relation is given by

$$\omega^2(p) = p^2 \sum_{z=1}^{3} \varkappa_{\gamma,z} \left(\frac{p}{M_*}\right)^{2(z-1)} , \tag{5.6.10}$$

with

$$\varkappa_{\gamma,1} \equiv \frac{\alpha_1}{\alpha_3} , \qquad \varkappa_{\gamma,2} \equiv \frac{\alpha_1}{\beta_1} , \qquad \varkappa_{\gamma,3} \equiv \frac{\alpha_1}{\gamma_1} . \tag{5.6.11}$$

The coefficient $\varkappa_{\gamma,1}$ determines (the square of) the propagation speed of the gravitational waves at low energies. According to the constraints from the observation of the Hulse-Taylor pulsar [129] and more directly from the detections of the gravitational waves at the two detector sites [137], the propagation speed of the gravitational waves in the IR should be of order of the speed of light, which imposes $\alpha_1 \simeq \alpha_3$. The recent detections of GW170817 and GRB170817A give a tight constraint $|\varkappa_{\gamma,1} - 1| < 10^{-15}$ [49]. (See also Ref. [163] for the constraint on the subluminal propagation of the gravitational waves from the absence of the gravitational Cherenkov radiation.) Next, requiring that the transition from linear dispersion relation to the Lifshitz scaling happens at $p \sim M_*$ we obtain the requirements $\varkappa_{\gamma,2}, \varkappa_{\gamma,3} \simeq 1$. By combining these two conditions, we obtain

$$\alpha_1 \simeq \alpha_3 \simeq \beta_1 \simeq \gamma_1 < 1 . \tag{5.6.12}$$

The conditions described above are common both for the projectable and non-projectable versions.

Let us now turn to khronon. In the projectable version its dispersion relation reads,

$$\omega^2_{pr}(p) = \frac{\alpha_1 \bar{\alpha}}{1+\bar{\alpha}} p^2 \left[-\frac{1}{\alpha_3} + \left(\frac{3}{\beta_1} + \frac{8}{\beta_2}\right)\left(\frac{p}{M_*}\right)^2 + \left(\frac{3}{\gamma_1} + \frac{8}{\gamma_2}\right)\left(\frac{p}{M_*}\right)^4 \right] . \tag{5.6.13}$$

The first term in the square brackets is negative and is responsible for gradient instability in IR. On the other hand, the remaining terms in (5.6.13) can be chosen positive, so that at $p > M_*$ the dispersion relation is well-behaved. Again, setting the transition to Lifshitz scaling at around $p \simeq M_*$ and taking into account (5.6.12) we obtain

$$\alpha_{1,3} \simeq \beta_{1,2} \simeq \gamma_{1,2} < 1 . \tag{5.6.14}$$

Further, for simplicity, requiring that the overall magnitude of the frequency $\omega_{pr}(p)$ in

UV is $\mathcal{O}(1) \times p^z/M_*^{z-1}$ we set $\bar{\alpha} \simeq \mathcal{O}(1)$. To sum up, in the projectable case we will work under the assumptions,

$$\alpha_{1,2,3} \simeq \beta_{1,2} \simeq \gamma_{1,2} < 1\,, \qquad \bar{\alpha} = \mathcal{O}(1) \qquad \text{(projectable)}. \tag{5.6.15}$$

In the non-projectable version, constraints on deviations from Lorentz invariance at low energies require [161]

$$\alpha_1 \ll \alpha_4\,. \tag{5.6.16}$$

The dispersion relation for khronon now becomes more complicated and is given by

$$\omega^2_{npr}(p) = \omega^2_{pr}(p) + \frac{2\alpha_1\bar{\alpha}}{1+\bar{\alpha}}\,p^2\,\frac{\left[-\frac{1}{\alpha_3} + \frac{1}{\beta_3}(\frac{p}{M_*})^2 + \frac{1}{\gamma_3}(\frac{p}{M_*})^4\right]^2}{\frac{1}{\alpha_4} + \frac{1}{\beta_4}(\frac{p}{M_*})^2 + \frac{1}{\gamma_4}(\frac{p}{M_*})^4}\,, \tag{5.6.17}$$

where the second piece comes from integrating out the lapse function N which enters into the action without time derivatives. Setting the transition scale at $p \simeq M_*$ and using Eqs. (5.6.12) and (5.6.16), we obtain

$$\alpha_{1,3} \simeq \beta_{1,2,3} \simeq \gamma_{1,2,3} \ll \alpha_4\,, \qquad \alpha_4 \simeq \beta_4 \simeq \gamma_4\,. \tag{5.6.18}$$

Similarly to the discussion of the projectable version, for simplicity, we assume that $\omega(p)$ becomes $\mathcal{O}(1) \times p^z/M_*^{z-1}$ in UV and obtain

$$\bar{\alpha} \simeq \frac{\gamma_3^2}{\gamma_4\alpha_1} \simeq \frac{\alpha_1}{\alpha_4} \ll 1\,, \tag{5.6.19}$$

where we used Eq. (5.6.16). Notice that the order of $\bar{\alpha}$ in the non-projectable version is different from the one in the projectable version, cf. Eq. (5.6.15). Using Eqs. (5.6.18) and (5.6.19), we find that (the leading term in) the propagation speed of khronon in the IR, $\alpha_1\bar{\alpha}\alpha_4/\alpha_3^2$, is now set to $\mathcal{O}(1)$. Combining all conditions together, we obtain

$$\frac{\alpha_{1,2,3}}{\alpha_4} \simeq \frac{\beta_{1,2,3}}{\beta_4} \simeq \frac{\gamma_{1,2,3}}{\gamma_4} \simeq \bar{\alpha} \ll 1\,, \qquad \alpha_4 \simeq \beta_4 \simeq \gamma_4 \qquad \text{(non-projectable)}. \tag{5.6.20}$$

The parameters which satisfy these conditions are consistent with the experimental data in IR[3] [161].

In summery, the parameter hierarchy (5.6.20) is derived by imposing i) the phenomenological condition in the IR (5.6.16) ii) the simplicity assumption $\omega(p) \simeq \mathcal{O}(1) \times$

[3]We leave aside the question of stability of the parameter hierarchy under radiative corrections.

p^z/M_*^{z-1} in the UV and iii) the other simplicity assumption that khronon and gravitational waves both make transition from the isotropic scaling regime to the anisotropic scaling regime at $p \simeq M_*$.

5.6.2 Background equations

Equations for the inflationary background read,

$$3M_P^2 \frac{1+\bar{\alpha}}{1-2\bar{\alpha}} H^2 = \frac{\dot{\phi}^2}{2} + V\,, \tag{5.6.21}$$

$$\ddot{\phi} + 3H\dot{\phi} + V_\phi = 0\,, \tag{5.6.22}$$

where ϕ is the background value of the inflaton and V_ϕ denotes the derivative of V with respect to ϕ. Positivity of the l.h.s. in the Friedmann equation (5.6.21) requires $\bar{\alpha}$ to be in the range $-1 < \bar{\alpha} < 1/2$. We define the slow-roll parameters,

$$\varepsilon_1 \equiv -\frac{\dot{H}}{H^2} = \frac{1-2\bar{\alpha}}{2(1+\bar{\alpha})} \left(\frac{\dot{\phi}}{M_P H}\right)^2\,, \tag{5.6.23}$$

and

$$\varepsilon_n = \frac{\mathrm{d}\ln \varepsilon_{n-1}}{\mathrm{d}\ln a}\,, \tag{5.6.24}$$

for $n \geq 2$. The expressions for the slow-roll parameters agree with the standard ones up to $\mathcal{O}(\bar{\alpha})$ corrections. Using ε_2 we can express the second derivative of ϕ as

$$\frac{\ddot{\phi}}{H\dot{\phi}} = \frac{\varepsilon_2}{2} - \varepsilon_1\,. \tag{5.6.25}$$

We also define the slow-roll parameters ε_V and η_V as

$$\varepsilon_V \equiv \frac{M_P^2}{2}\left(\frac{V_\phi}{V}\right)^2 = \frac{1-2\bar{\alpha}}{1+\bar{\alpha}}\varepsilon_1 + \mathcal{O}(\varepsilon^2)\,, \tag{5.6.26}$$

$$\eta_V \equiv M_P^2 \frac{V_{\phi\phi}}{V} = \frac{1-2\bar{\alpha}}{1+\bar{\alpha}}\left(2\varepsilon_1 - \frac{\varepsilon_2}{2}\right) + \mathcal{O}(\varepsilon^2)\,, \tag{5.6.27}$$

where $V_{\phi\phi} \equiv \mathrm{d}^2V/\mathrm{d}\phi^2$. In the limit $\bar{\alpha} \to 0$ the relations between $(\varepsilon_1, \varepsilon_2)$ and (ε_V, η_V) agree with those in GR.

5.6.3 Lifshitz scalar in a fixed background

As a warm-up exercise, in this subsection we briefly review the computation of the spectrum of a probe massless scalar field φ in a fixed inflationary background. From now on we will work in conformal time t and denote derivatives with respect to it by primes. The action for Fourier modes of the field reads,

$$S_{scalar} = \frac{1}{2}\int \mathrm{d}t \int \mathrm{d}^3\boldsymbol{p}\, a^2 \left[\varphi'_{\boldsymbol{p}}\varphi'_{-\boldsymbol{p}} - \omega^2_\varphi(t,\, p)\varphi_{\boldsymbol{p}}\varphi_{-\boldsymbol{p}}\right] . \tag{5.6.28}$$

Anisotropic scaling in UV implies modified dispersion relation [150],

$$\frac{\omega^2_\varphi(t,p)}{\mathcal{H}^2} = \frac{p^2}{\mathcal{H}^2}\left[\varkappa_1 + \varkappa_2\left(\frac{p}{aM_*}\right)^2 + \varkappa_3\left(\frac{p}{aM_*}\right)^4\right] , \tag{5.6.29}$$

where $\mathcal{H} = a'/a = aH$. The mode equation is given by

$$\varphi''_p + 2\mathcal{H}\varphi'_p + \omega^2_\varphi\varphi_p = 0\,. \tag{5.6.30}$$

During inflation, we have

$$\mathcal{H} = -1/t\,, \tag{5.6.31}$$

where we have neglected the corrections suppressed by the slow-roll parameters. When the contribution from either of $z = 1,\, 2,\, 3$ dominates the others, using Eq. (5.6.31) and imposing the adiabatic initial condition:

$$\varphi_p(t) \to \frac{1}{a}\frac{1}{\sqrt{2\omega_\varphi}} e^{-i\int \mathrm{d}t\,\omega_\varphi} , \tag{5.6.32}$$

we can solve the mode equation as

$$\varphi_p = \frac{1}{2a}\sqrt{\frac{-\pi t}{z}}\, e^{i\frac{\pi(2\nu+1)}{4}} H^{(1)}_\nu\left[\frac{\sqrt{\varkappa_z}}{z}\frac{p}{\mathcal{H}}\left(\frac{p}{aM_*}\right)^{z-1}\right] , \tag{5.6.33}$$

where the index of the Hankel function is given by

$$\nu = \frac{3}{2z}\,. \tag{5.6.34}$$

At the Hubble crossing, $\omega_\varphi/\mathcal{H} \simeq z$, after which φ ceases to oscillate, we obtain the power spectrum of Lifshitz scalar φ as

$$\mathcal{P}_{LS}(p) \equiv \frac{p^3}{2\pi^2}\left|\varphi_p\right|^2 = \frac{\alpha_1^{\nu(z-1)}}{\varkappa_z^\nu}\frac{(2^\nu\Gamma[\nu])^2}{8\pi^3}z^{\frac{3}{z}-1}M_P^2\left(\frac{H_p}{M_P}\right)^{\frac{3}{z}-1}, \tag{5.6.35}$$

where H_p denotes the Hubble parameter at this time. In order to obtain the power spectrum at the end of inflation, we need to solve the time evolution also after $\omega_\varphi/\mathcal{H} \simeq z$. In the massless case φ stops evolving in time soon after the Hubble crossing. Then Eq. (5.6.35) gives the spectrum of φ at the end of inflation. Notice that, as discussed in Ref. [150], for $z = 3$ the spectrum of Lifshitz scalar is exactly flat. This is a consequence of the fact that for $z = 3$ the scaling dimension of the scalar φ vanishes. If the Lifshitz scalar has a small mass, its evolution must also be traced after the Hubble crossing and the final spectrum in general depends on the details of this evolution.

5.6.4 Gravitational waves

In this subsection we compute the spectrum of the gravitational waves generated during inflation in HL gravity. We consider the metric,

$$N = 1, \quad N_i = 0, \quad h_{ij} = a^2\left(\delta_{ij} + \gamma_{ij}\right) \tag{5.6.36}$$

with the transverse traceless condition on the perturbations:

$$\partial_i\gamma_{ij} = 0\,, \qquad \gamma_{ii} = 0\,. \tag{5.6.37}$$

The quadratic Lagrangian density for the gravitational waves is given by

$$\mathcal{L}_{GW} = \frac{M_*^2}{8\alpha_1}a^2\left[\gamma'^i{}_j\gamma'^j{}_i - \frac{\alpha_1}{\alpha_3}\partial_k\gamma^i{}_j\partial^k\gamma^j{}_i - \frac{\alpha_1}{\beta_1 M_*^2}a^{-2}\partial^2\gamma^i{}_j\partial^2\gamma^j{}_i - \frac{\alpha_1}{\gamma_1 M_*^4}a^{-4}\partial^2\partial_k\gamma^i{}_j\partial^2\partial^k\gamma^j{}_i\right]. \tag{5.6.38}$$

This is the most general form of the Lagrangian for linear tensor perturbations in HL gravity in the absence of parity violation and non-minimal coupling to the inflaton. (See Ref. [147] for the computation of the polarised gravitational wave spectrum in the presence of the parity violation.)

Taking variation with respect to γ_{ij}, we obtain the mode equation for γ_{ij} as usual,

$$\gamma''_{ij\,p} + 2\mathcal{H}\gamma'_{ij\,p} + \omega_\gamma^2\,\gamma_{ij\,p} = 0\,, \tag{5.6.39}$$

where the frequency ω_γ is given by

$$\frac{\omega_\gamma^2(\eta,p)}{\mathcal{H}^2}=\left(\frac{p}{\mathcal{H}}\right)^2\sum_{z=1}^{3}\varkappa_{\gamma,z}\left(\frac{p}{aM_*}\right)^{2(z-1)}\,, \tag{5.6.40}$$

with $\varkappa_{\gamma,z}$ given in Eq. (5.6.11). We quantize the gravitational waves as

$$\gamma_{ij}(x)=\sum_{\lambda=\pm}\int\frac{\mathrm{d}^3\boldsymbol{p}}{(2\pi)^{3/2}}\gamma_p(t)e^{(\lambda)i}{}_j(\boldsymbol{p})e^{i\boldsymbol{p}\cdot\boldsymbol{x}}a_{\boldsymbol{p}}^{(\lambda)}+(\text{h.c.})\,, \tag{5.6.41}$$

where λ is the helicity of the gravitational waves, $e_{ij}^{(\lambda)}$ are the standard transverse and traceless polarization tensors, and $a_{\boldsymbol{k}}^{(\lambda)}$ are the annihilation operators which satisfy

$$\left[a_{\boldsymbol{k}}^{(\lambda)},\,a_{\boldsymbol{p}}^{(\lambda')\dagger}\right]=\delta_{\lambda\lambda'}\delta^{(3)}(\boldsymbol{k}-\boldsymbol{p})\,. \tag{5.6.42}$$

The number of the polarisation in HL gravity is the same as in GR. Imposing the adiabatic initial condition:

$$\gamma_p(t)\to\frac{2}{aM_P}\frac{1}{\sqrt{2\omega_\gamma}}e^{-i\int\mathrm{d}t\,\omega_\gamma}\,, \tag{5.6.43}$$

we obtain the mode functions γ_p as

$$\gamma_p(t)=\frac{1}{M_Pa}\sqrt{\frac{-\pi t}{z}}e^{i\frac{\pi(2\nu+1)}{4}}H_\nu^{(1)}\left[\frac{\sqrt{\varkappa_{\gamma,z}}}{z}\frac{p}{\mathcal{H}}\left(\frac{p}{aM_*}\right)^{z-1}\right]\,, \tag{5.6.44}$$

where the Hankel index ν is given in Eq. (5.6.34). Like in the GR, γ_p is conserved in time for $\omega_\gamma/\mathcal{H}<z$. Using Eq. (5.6.44) we obtain the power spectrum of the gravitational waves as

$$\mathcal{P}_\gamma\equiv\frac{p^3}{\pi^2}\left|\gamma_p\right|^2=\frac{\alpha_1^{\nu(z-1)}}{\varkappa_{\gamma,z}^{\nu}}\frac{(2^\nu\Gamma[\nu])^2}{\pi^3}z^{\frac{3}{z}-1}\left(\frac{H_{p,\gamma}}{M_P}\right)^{\frac{3}{z}-1}\,, \tag{5.6.45}$$

where $H_{p,\gamma}$ denotes the Hubble parameter when $\omega_\gamma/\mathcal{H}\simeq z$.

The spectral index for the gravitational waves is given by

$$n_t\equiv\frac{\mathrm{d}\ln\mathcal{P}_\gamma}{\mathrm{d}\ln p}\simeq-\frac{3-z}{z}\varepsilon_1\,. \tag{5.6.46}$$

In 4D Diff invariant theory, the spectrum of the primordial gravitational waves is generically red-tilted in an inflationary universe with $\varepsilon_1>0$ [164, 165]. By contrast, in HL gravity, for $z=3$, the spectral index n_t vanishes even if $\varepsilon_1\neq0$. This serves as a

distinctive feature of the anisotropic scaling regime of gravity. Since the lapse function is irrelevant to the gravitational waves at the linear order of perturbation, the results of this section apply both to the projectable and non-projectable versions of HL gravity.

5.7 Decoupling and non-decoupling of khronon

In this section, we consider the scalar linear perturbations including the inflaton and metric perturbations. We express the fields as,

$$\Phi(t, \boldsymbol{x}) = \phi(t) + \varphi(t, \boldsymbol{x}) , \quad N = a(1 + \delta N) , \quad N_i = a^2 \partial_i B , \quad h_{ij} = a^2 e^{2\mathcal{R}} \delta_{ij} . \tag{5.7.1}$$

In general relativity, the metric perturbation $\mathcal{R}$ and the fluctuation of the inflaton φ are not independent. By contrast, in HL gravity $\mathcal{R}$ serves an additional scalar degree of freedom, khronon, as a consequence of the lack of 4D Diff invariance. In this section we discuss the evolution of khronon both in the projectable and non-projectable versions of HL gravity. We will find that the khronon behaviour differs qualitatively in these two cases.

5.7.1 Projectable HL gravity

First we consider the projectable version of HL gravity. A review of this version can be found in Ref. [166]. In this case the lapse function is constrained to be homogeneous and does not affect local physics. Setting $\delta N = 0$ and integrating out the non-dynamical field B we find the action,

$$S = \int \mathrm{d}t \int \mathrm{d}^3 \boldsymbol{p} \left[\mathcal{L}_{\mathcal{R}} + \mathcal{L}_{\varphi} + \mathcal{L}_{\mathcal{R}\varphi} \right] , \tag{5.7.2}$$

with

$$\mathcal{L}_{\mathcal{R}} = a^2 M_*^2 \frac{1 + \bar{\alpha}}{\alpha_1 \bar{\alpha}} \left[\mathcal{R}'_{\boldsymbol{p}} \mathcal{R}'_{-\boldsymbol{p}} - \omega_{\mathcal{R}}^2(t, p) \mathcal{R}_{\boldsymbol{p}} \mathcal{R}_{-\boldsymbol{p}} \right] , \tag{5.7.3}$$

$$\mathcal{L}_{\varphi} = \frac{a^2}{2} \left[\varphi'_{\boldsymbol{p}} \varphi'_{-\boldsymbol{p}} - \omega_{\varphi}^2(t, p) \varphi_{\boldsymbol{p}} \varphi_{-\boldsymbol{p}} \right] , \tag{5.7.4}$$

$$\mathcal{L}_{\mathcal{R}\varphi} = a^2 \frac{1 - 2\bar{\alpha}}{\bar{\alpha}} \phi' \varphi_{\boldsymbol{p}} \mathcal{R}'_{-\boldsymbol{p}} . \tag{5.7.5}$$

The frequencies $\omega^2_{\mathcal{R}}$ and ω^2_{φ} are given by

$$\frac{\omega^2_{\mathcal{R}}(t,\,p)}{\mathcal{H}^2} = \frac{\alpha_1\bar{\alpha}}{1+\bar{\alpha}}\left(\frac{p}{\mathcal{H}}\right)^2\left[-\frac{1}{\alpha_3}+\left(\frac{3}{\beta_1}+\frac{8}{\beta_2}\right)\left(\frac{p}{aM_*}\right)^2+\left(\frac{3}{\gamma_1}+\frac{8}{\gamma_2}\right)\left(\frac{p}{aM_*}\right)^4\right], \tag{5.7.6}$$

$$\frac{\omega^2_{\varphi}(t,\,p)}{\mathcal{H}^2} = \left(\frac{p}{\mathcal{H}}\right)^2\left[\varkappa_1+\varkappa_2\left(\frac{p}{aM_*}\right)^2+\varkappa_3\left(\frac{p}{aM_*}\right)^4\right]-\frac{1+\bar{\alpha}}{\bar{\alpha}}\varepsilon_1+\frac{3(1+\bar{\alpha})}{1-2\bar{\alpha}}\eta_V\,. \tag{5.7.7}$$

We observe that in de Sitter universe, where the inflaton is absent, khronon $\mathcal{R}$ behaves as a massless Lifshitz scalar and thus is conserved at super Hubble scales. However, mixing with the inflaton (5.7.5) essentially modifies the dynamics.

Positivity of khronon kinetic energy requires,

$$\frac{1+\bar{\alpha}}{\alpha_1\bar{\alpha}} > 0\,, \tag{5.7.8}$$

which implies that $\mathcal{R}$ suffers from a gradient instability in the IR limit, since $\alpha_3 > 0$. An attempt to suppress this instability by taking the coefficient $\alpha_1\bar{\alpha}/\alpha_3(1+\bar{\alpha})$ to be small leads to strong coupling and invalidates the perturbative description (see a detailed discussion in Ref. [161]). Thus, projectable HL gravity cannot provide a viable low-energy phenomenology in the regime of weak coupling. By analogy with non-Abelian gauge theories, one might envision a scenario where strong coupling occurs only in IR and leads to confinement of khronon at low energies. However, currently there exist no controllable realizations of this scenario. Here we restrict to the anisotropic scaling regime where the second and third terms in the brackets in (5.7.6) dominate, the theory is stable and weakly coupled.

Estimates of various terms in the Lagrangian show that at $\omega_{\mathcal{R}}, \omega_{\varphi} \gg \mathcal{H}\sqrt{\varepsilon}$ the mixing term between $\mathcal{R}$ and φ is negligible and these two fields evolve independently. Assuming that either $z = 2$ or $z = 3$ contribution is dominant and imposing the standard WKB initial condition we find the mode functions for $\mathcal{R}$ and φ,

$$\mathcal{R}_p(t) = \frac{1}{M_P a}\sqrt{\frac{\bar{\alpha}}{1+\bar{\alpha}}}\sqrt{\frac{-\pi t}{8z}}e^{i\frac{\pi(2\nu+1)}{4}}H^{(1)}_{\nu}\left[\frac{\omega_{\mathcal{R}}}{z\mathcal{H}}\right], \tag{5.7.9}$$

$$\varphi_p(t) = \frac{1}{2a}\sqrt{\frac{-\pi t}{z}}e^{i\frac{\pi(2\nu+1)}{4}}H^{(1)}_{\nu}\left[\frac{\omega_{\varphi}}{z\mathcal{H}}\right], \tag{5.7.10}$$

where the Hankel index ν is given by Eq. (5.6.34). We did not write explicitly the arguments of the Hankel functions; they have the same dependence on p and t as those

in Eqs. (5.6.33) and (5.6.44). We have also neglected the slow-roll correction in $\omega_\varphi/\mathcal{H}$, since the momentum dependent contribution dominates it in this regime.

The above solutions cannot be extended to super Hubble evolution where $\omega_\mathcal{R}, \omega_\varphi \lesssim \mathcal{H}\sqrt{\varepsilon}$ and the mixing between $\mathcal{R}$ and φ becomes important. In this regime we have two light Lifshitz scalars, the inflaton and khronon, which are mixed with each other. As in a 4D Diff invariant theory with more than one light scalar fields, in this case we do not find an adiabatic mode which is conserved in time at large scales (see, e.g., Ref. [167]). Then, in order to compute the observed fluctuations, we need to solve the time evolution which can depend on concrete models of the reheating, the transition to the isotropic scaling regime, and so on. As discussed above, this would require also a controllable description of the mechanism that suppresses the IR instability of the theory, which is currently missing. Therefore it appears problematic to provide a robust prediction for primordial scalar power spectrum in the projectable version of HL gravity.

5.7.2 Non-projectable HL gravity

In this subsection we will find that the time evolution of khronon in the non-projectable version is qualitatively different from the one in the projectable version discussed above. In particular, we will show that khronon is decoupled from the adiabatic curvature perturbation ζ at large scales. Because of that, ζ is conserved in time as in the single field model with 4D Diff invariance. Therefore, we can derive a robust prediction for the power spectrum of ζ without solving the detailed evolution after the Hubble crossing.

Mass gap of khronon and anti-friction

In the non-projectable version of HL gravity, upon eliminating the non-dynamical fields B and δN, we obtain the action for $\mathcal{R}$ and φ in the form (5.7.2) with

$$\mathcal{L}_\mathcal{R} = a^2 M_*^2 \frac{1+\bar{\alpha}}{\alpha_1 \bar{\alpha}} \left[(1 - \Omega_1(t,\, p)) \mathcal{R}'_{\boldsymbol{p}} \mathcal{R}'_{-\boldsymbol{p}} - \omega^2_\mathcal{R}(t,\, p) \mathcal{R}_{\boldsymbol{p}} \mathcal{R}_{-\boldsymbol{p}} \right] \ . \tag{5.7.11}$$

5.7.3 Action for $\mathcal{R}$ and φ

The expressions for $\mathcal{L}_\varphi, \mathcal{L}_{\mathcal{R}\varphi}$ are given as follows. Substituting the fields (5.7.1) into the Lagrangian consisting of (5.6.1) and (5.6.8), expanding to second order in perturbations and integrating out the lapse function and the shift vector, we obtain

$$S = \int \mathrm{d}^4 x \mathcal{L} = \int \mathrm{d}t \int \mathrm{d}^3 \boldsymbol{p} \left[\mathcal{L}_\mathcal{R} + \mathcal{L}_\varphi + \mathcal{L}_{\mathcal{R}\varphi} \right] \tag{5.7.12}$$

with

$$\mathcal{L}_{\mathcal{R}} = a^2 M_*^2 \frac{1+\bar{\alpha}}{\alpha_1 \bar{\alpha}} \left[(1-\Omega_1(t,\, p)) \mathcal{R}'_{\boldsymbol{p}} \mathcal{R}'_{-\boldsymbol{p}} - \omega^2_{\mathcal{R}}(t,\, p) \mathcal{R}_{\boldsymbol{p}} \mathcal{R}_{-\boldsymbol{p}} \right] , \tag{5.7.13}$$

$$\mathcal{L}_{\varphi} = \frac{a^2}{2} \left[\left(1 - \frac{\bar{\alpha}\varepsilon_1}{1-2\bar{\alpha}} \Omega_1(t,\, p) \right) \varphi'_{\boldsymbol{p}} \varphi'_{-\boldsymbol{p}} - \omega^2_{\varphi}(\eta,\, p) \varphi_{\boldsymbol{p}} \varphi_{-\boldsymbol{p}} \right] , \tag{5.7.14}$$

$$\begin{aligned} \mathcal{L}_{\mathcal{R}\varphi} = a^2 \Bigg\{ & - \frac{\phi'}{\mathcal{H}} \Omega_1(t,\, p) \varphi'_{\boldsymbol{p}} \mathcal{R}'_{-\boldsymbol{p}} + \left[\frac{1-2\bar{\alpha}}{\bar{\alpha}} (1-\Omega_1(t,\, p)) \phi' + \Omega_1(t,\, p) \frac{\phi'' - \mathcal{H}\phi'}{\mathcal{H}} \right] \varphi_{\boldsymbol{p}} \mathcal{R}'_{-\boldsymbol{p}} \\ & - \phi' \Omega_2(t,\, p) \varphi'_{\boldsymbol{p}} \mathcal{R}_{-\boldsymbol{p}} - \left(\frac{1+\bar{\alpha}}{\bar{\alpha}} \mathcal{H}\phi' + a^2 V_{\phi} \right) \Omega_2(t,\, p) \varphi_{\boldsymbol{p}} \mathcal{R}_{-\boldsymbol{p}} \Bigg\} , \end{aligned} \tag{5.7.15}$$

where the functions $\Omega_{1,2}(t, p)$ have been introduced in (5.7.23), (5.7.24), the frequency $\omega_{\mathcal{R}}$ is given by Eq. (5.7.25) and ω_{φ} is given by

$$\begin{aligned} \frac{\omega^2_{\varphi}(t,\, p)}{\mathcal{H}^2} = & \left(\frac{p}{\mathcal{H}} \right)^2 \left[\varkappa_1 + \varkappa_2 \left(\frac{p}{aM_*} \right)^2 + \varkappa_3 \left(\frac{p}{aM_*} \right)^4 \right] + \frac{a^2 V_{\phi\phi}}{\mathcal{H}^2} - \frac{1+\bar{\alpha}}{\bar{\alpha}} \varepsilon_1 \\ & + \frac{(1+\bar{\alpha})\alpha_1}{2\bar{\alpha} M_*^2} \left(\phi' + \frac{\bar{\alpha}}{1+\bar{\alpha}} \frac{a^2 V_{\phi}}{\mathcal{H}} \right)^2 \frac{\Omega_1(t,\, p)}{\mathcal{H}^2} \\ & - \frac{\alpha_1}{2M_*^2} \frac{1}{(\mathcal{H}a)^2} \left[a^2 \phi' \left(\phi' + \frac{\bar{\alpha}}{1+\bar{\alpha}} \frac{a^2 V_{\phi}}{\mathcal{H}} \right) \frac{\Omega_1(t,\, p)}{\mathcal{H}} \right]' . \end{aligned} \tag{5.7.16}$$

By inspection of various terms in the Lagrangian we can see that $\mathcal{R}$ and φ are decoupled in the limit of large momenta p.

5.7.4 Action for ζ and φ

Using ζ defined in (5.7.47) and eliminating $\mathcal{R}$, we obtain the quadratic action as

$$S = \int \mathrm{d}t \int \mathrm{d}^3 \boldsymbol{p} \left[\mathcal{L}_{\zeta} + \tilde{\mathcal{L}}_{\varphi} + \mathcal{L}_{\zeta\varphi} \right] \tag{5.7.17}$$

with

$$\mathcal{L}_{\zeta} = a^2 M_*^2 \frac{1+\bar{\alpha}}{\alpha_1 \bar{\alpha}} \left[(1-\Omega_1(t,\, p)) \zeta'_{\boldsymbol{p}} \zeta'_{-\boldsymbol{p}} - \omega^2_{\mathcal{R}}(t,\, p) \zeta_{\boldsymbol{p}} \zeta_{-\boldsymbol{p}} \right] , \tag{5.7.18}$$

$$\tilde{\mathcal{L}}_{\varphi} = \frac{a^2}{2} \left[\frac{(1-2\bar{\alpha})\alpha_1}{2(1+\bar{\alpha})\varepsilon_1} \left(1 + \frac{\bar{\alpha}\varepsilon_1}{1-2\bar{\alpha}} \right) \Omega_3(t,\, p) \varphi'_{\boldsymbol{p}} \varphi'_{-\boldsymbol{p}} - \tilde{\omega}^2_{\varphi}(t,\, p) \varphi_{\boldsymbol{p}} \varphi_{-\boldsymbol{p}} \right] , \tag{5.7.19}$$

$$\begin{aligned} \mathcal{L}_{\zeta\varphi} = a^2 \Bigg\{ & M_*^2 \frac{\mathcal{H}}{\phi'} \Omega_3(t,\, p) \left(\zeta'_{\boldsymbol{p}} \varphi'_{-\boldsymbol{p}} - \frac{\phi'' - \mathcal{H}\phi'}{\phi'} \zeta'_{\boldsymbol{p}} \varphi_{-\boldsymbol{p}} \right) - \phi' \Omega_2(t,\, p) \zeta_{\boldsymbol{p}} \varphi'_{-\boldsymbol{p}} \\ & - \left[2M_*^2 \frac{1+\bar{\alpha}}{\alpha_1 \bar{\alpha}} \frac{\mathcal{H}}{\phi'} \omega^2_{\mathcal{R}}(t,\, p) + \left(\frac{1+\bar{\alpha}}{\bar{\alpha}} \mathcal{H}\phi' + a^2 V_{\phi} \right) \Omega_2(t,\, p) \right] \zeta_{\boldsymbol{p}} \varphi_{-\boldsymbol{p}} \Bigg\} , \end{aligned} \tag{5.7.20}$$

where we introduced

$$\Omega_3(t,\,p)=\left(\frac{p}{\mathcal{H}}\right)^2\left[1+\frac{1}{\beta_4}\left(\frac{p}{aM_*}\right)^2+\frac{1}{\gamma_4}\left(\frac{p}{aM_*}\right)^4\right]\Omega_1(t,\,p)\,. \tag{5.7.21}$$

The new expression for the φ-frequency is

$$\begin{aligned}\frac{\tilde{\omega}^2_\varphi(t,\,p)}{\mathcal{H}^2}=&\left(\frac{p}{\mathcal{H}}\right)^2\left[\varkappa_1+\varkappa_2\left(\frac{p}{aM_*}\right)^2+\varkappa_3\left(\frac{p}{aM_*}\right)^4\right]+\frac{1-2\bar{\alpha}}{\varepsilon_1\bar{\alpha}}\frac{\omega^2_{\mathcal{R}}(t,\,p)}{\mathcal{H}^2}\\&-\frac{\alpha_1\bar{\alpha}}{2(1+\bar{\alpha})}\left\{\frac{1-2\bar{\alpha}}{\bar{\alpha}}\varepsilon_1+\left(\varepsilon_1-\frac{\varepsilon_2}{2}\right)^2\right\}\Omega_3(t,\,p)\\&+\frac{1}{(a\mathcal{H})^2}\left\{a^2\mathcal{H}\left[-\Omega_2(t,\,p)+\frac{(1-2\bar{\alpha})\alpha_1}{2(1+\bar{\alpha})\varepsilon_1}\left(\varepsilon_1-\frac{\varepsilon_2}{2}\right)\left(1+\frac{\varepsilon_1\bar{\alpha}}{1-2\bar{\alpha}}\right)\Omega_3(t,\,p)\right]\right\}'\\&+2\left(\frac{1-2\bar{\alpha}}{\bar{\alpha}}+\varepsilon_1-\frac{\varepsilon_2}{2}\right)\Omega_2(t,\,p)-\frac{(1-2\bar{\alpha})\alpha_1}{8(1+\bar{\alpha})}\frac{\varepsilon_2}{\varepsilon_1}(\varepsilon_2-4\varepsilon_1)\Omega_3(t,\,p).\end{aligned} \tag{5.7.22}$$

Notice that all terms in $\mathcal{L}_{\zeta\varphi}$ and $\tilde{\mathcal{L}}_\varphi$ are multiplied by factors of order $\mathcal{O}(X)$ (The decoupling of ζ from φ can be explicitly seen by changing φ to the canonically normalized variable.). This implies that ζ has a constant solution in the long-wavelength limit.

We introduce the functions $\Omega_i(t,\,p)$ with $i=1,\,2$ as

$$\Omega_1(t,\,p)=\left\{1+\frac{\bar{\alpha}\varepsilon_1}{1-2\bar{\alpha}}+\frac{\alpha_1\bar{\alpha}}{2(1+\bar{\alpha})}\left(\frac{p}{\mathcal{H}}\right)^2\left[\frac{1}{\alpha_4}+\frac{1}{\beta_4}\left(\frac{p}{aM_*}\right)^2+\frac{1}{\gamma_4}\left(\frac{p}{aM_*}\right)^4\right]\right\}^{-1}, \tag{5.7.23}$$

$$\Omega_2(t,\,p)=\frac{\alpha_1\bar{\alpha}}{1+\bar{\alpha}}\left(\frac{p}{\mathcal{H}}\right)^2\left[-\frac{1}{\alpha_3}+\frac{1}{\beta_3}\left(\frac{p}{aM_*}\right)^2+\frac{1}{\gamma_3}\left(\frac{p}{aM_*}\right)^4\right]\Omega_1(t,\,p)\,. \tag{5.7.24}$$

In terms of these quantities the frequency $\omega_{\mathcal{R}}$ is expressed as,

$$\begin{aligned}\frac{\omega^2_{\mathcal{R}}(t,\,p)}{\mathcal{H}^2}=&\frac{\alpha_1\bar{\alpha}}{1+\bar{\alpha}}\left(\frac{p}{\mathcal{H}}\right)^2\left[-\frac{1}{\alpha_3}+\left(\frac{3}{\beta_1}+\frac{8}{\beta_2}\right)\left(\frac{p}{aM_*}\right)^2+\left(\frac{3}{\gamma_1}+\frac{8}{\gamma_2}\right)\left(\frac{p}{aM_*}\right)^4\right]\\&+\frac{\Omega_2^2(t,\,p)}{\Omega_1(t,\,p)}-\frac{(a^2\mathcal{H}\Omega_2(t,\,p))'}{a^2\mathcal{H}^2}.\end{aligned} \tag{5.7.25}$$

We observe that the khronon Lagrangian is now much more complicated than in the projectable case. A crucial new feature is the dependence of the coefficient in front of the term with time derivatives in (5.7.11) on the mode momentum. This leads to a

peculiar behavior of khronon in inflationary universe, as we presently discuss.

It is convenient to introduce the notation,

$$X(t,p) \equiv \left(\frac{p}{\mathcal{H}}\right)^2 \left\{1 + \frac{\alpha_4}{\beta_4}\left(\frac{p}{aM_*}\right)^2 + \frac{\alpha_4}{\gamma_4}\left(\frac{p}{aM_*}\right)^4\right\} . \tag{5.7.26}$$

Roughly speaking, this quantity characterises the (square of the) ratio between the frequencies of the perturbations and the Hubble rate (the precise expressions will be given below). In the course of cosmological evolution it goes through four different regimes:

$$\textit{(a)} \qquad X \gg 1/\tilde{\alpha}^2 \, , \tag{5.7.27}$$

$$\textit{(b)} \qquad \varepsilon_1/\tilde{\alpha} \ll X \ll 1/\tilde{\alpha}^2 \, , \tag{5.7.28}$$

$$\textit{(c)} \qquad 1 \ll X \lesssim \varepsilon_1/\tilde{\alpha} \, , \tag{5.7.29}$$

$$\textit{(d)} \qquad X \ll 1 \, . \tag{5.7.30}$$

Recall that in the non-projectable case the parameters are assumed to satisfy the hierarchy (5.6.20). Here and below we symbolically denote the small quantities in the first equation of Eq. (5.6.20) by $\tilde{\alpha}$. Additionally, we will assume for the moment that

$$\varepsilon_1/\tilde{\alpha} \gg 1 \, . \tag{5.7.31}$$

The opposite case will be commented on at the end of the section. Let us consider the above regimes one by one.

(a) $X \gg 1/\tilde{\alpha}^2$. In this case

$$\Omega_1 \simeq \frac{2\alpha_4}{\alpha_1 \bar{\alpha} X} \ll 1 \, , \tag{5.7.32}$$

$$\frac{\omega^2_{\mathcal{R}}}{\mathcal{H}^2} \simeq 2\alpha_1\bar{\alpha}\left(\frac{p}{\mathcal{H}}\right)^2 \frac{\left[-\frac{1}{\alpha_3} + \frac{1}{\beta_3}(\frac{p}{aM_*})^2 + \frac{1}{\gamma_3}(\frac{p}{aM_*})^4\right]^2}{\frac{1}{\alpha_4} + \frac{1}{\beta_4}(\frac{p}{aM_*})^2 + \frac{1}{\gamma_4}(\frac{p}{aM_*})^4} \, . \tag{5.7.33}$$

In the latter expression we recognize the dispersion relation of khronon in flat spacetime (5.6.17) (up to suppressed corrections). In the UV regime, $p > aM_*$, it behaves as a Lifshitz scalar with $z = 3$ and

$$\omega^2_{\mathcal{R}} \simeq \frac{2\gamma_4\alpha_1\bar{\alpha}}{\gamma_3^2} p^2 \Big(\frac{p}{aM_*}\Big)^4 \, ,$$

whereas if $p < aM_*$ (but (5.7.27) still satisfied) it obeys the $z = 1$ scaling,

$$\omega_{\mathcal{R}}^2 \simeq \frac{2\alpha_4\alpha_1\bar{\alpha}}{\alpha_3^2}p^2 \ .$$

Note that in both limiting cases the ratio $\omega_{\mathcal{R}}^2/\mathcal{H}^2$ is of order $X(t,p)$. One can infer that inflaton φ also behaves in this regime as a Lifshitz scalar with dispersion relation (5.6.29). Further, by estimating various terms in the Lagrangian $\mathcal{L}_{\mathcal{R}\varphi}$, Eq. (5.7.15), it is straightforward to check that mixing between modes $\mathcal{R}$ and φ is negligible[4].

The IR limit $p \ll aM_*$ of non-projectable HL gravity is closely related to Einstein-aether theory [168]. Evolution of cosmological perturbations in the latter theory was analyzed in [133] and it was shown that in the short wavelength limit the khronon $\mathcal{R}$ and the fluctuation of the inflaton φ are decoupled from each other, which allows to impose the WKB initial condition as usual. Our analysis provides a generalisation of this result to the UV modes of HL gravity where terms with Lifshitz scaling $z = 2$ and 3 are important.

(b) $\varepsilon_1/\tilde{\alpha} \ll X \ll 1/\tilde{\alpha}^2$. In this regime we have,

$$\Omega_1 \approx 1 - \frac{\alpha_1\bar{\alpha}}{2\alpha_4}X \ ,$$

and the khronon Lagrangian takes the form,

$$\mathcal{L}_{\mathcal{R}} = a^2\frac{M_*^2X(t,p)}{2}\left(\mathcal{R}'_{\boldsymbol{p}}\mathcal{R}'_{-\boldsymbol{p}} - \bar{\omega}_{\mathcal{R}}^2(t,p)\mathcal{R}_{\boldsymbol{p}}\mathcal{R}_{-\boldsymbol{p}}\right) \ .$$

The khronon frequency $\bar{\omega}_{\mathcal{R}}$ now reads,

$$\frac{\bar{\omega}_{\mathcal{R}}^2}{\mathcal{H}^2} = \frac{a^2\left[\frac{m_{k,1}^2}{\alpha_4} + \frac{m_{k,2}^2}{\beta_4}(\frac{p}{aM_*})^2 + \frac{m_{k,3}^2}{\gamma_4}(\frac{p}{aM_*})^4\right]}{\mathcal{H}^2\left[\frac{1}{\alpha_4} + \frac{1}{\beta_4}(\frac{p}{aM_*})^2 + \frac{1}{\gamma_4}(\frac{p}{aM_*})^4\right]} + 2\alpha_1\bar{\alpha}\left(\frac{p}{\mathcal{H}}\right)^2\frac{\left[-\frac{1}{\alpha_3} + \frac{1}{\beta_3}(\frac{p}{aM_*})^2 + \frac{1}{\gamma_3}(\frac{p}{aM_*})^4\right]^2}{\frac{1}{\alpha_4} + \frac{1}{\beta_4}(\frac{p}{aM_*})^2 + \frac{1}{\gamma_4}(\frac{p}{aM_*})^4}, \tag{5.7.34}$$

[4]Strictly speaking, the mixing can be resonantly enhanced if the frequencies $\omega_{\mathcal{R}}(t,p)$ and $\omega_{\varphi}(t,p)$ happen to cross at some specific time. In our analysis, we do not consider this possibility. However, even if the crossing takes place, the mode functions stay in the WKB form and the time evolution remains essentially unchanged after the crossing.

where

$$m_{k,1}^2 \equiv 2\frac{\alpha_4}{\alpha_3}\varepsilon_1 H^2\,, \tag{5.7.35}$$

$$m_{k,2}^2 \equiv 2\beta_4\left(\frac{3}{\beta_1}+\frac{8}{\beta_2}+\frac{1}{\beta_3}\right)H^2\,, \tag{5.7.36}$$

$$m_{k,3}^2 \equiv 2\gamma_4\left(\frac{3}{\gamma_1}+\frac{8}{\gamma_2}+\frac{3}{\gamma_3}\right)H^2\,. \tag{5.7.37}$$

The second term in (5.7.34) is the same as (5.7.33). However, we observe that a new contribution appears which gives the khronon a mass gap. For the regime where terms with a given $z = 1, 2, 3$ dominate the mass is given by $m_{k,z}$. Notice that $m_{k,1}$ is suppressed by the slow-roll parameter compared to $m_{k,2}$ and $m_{k,3}$. Still, within our assumption (5.7.31) all the masses are parametrically larger than the Hubble rate. Note that we can study evolution of $\mathcal{R}$ separately.

Due to the mass gap, the khronon rapidly oscillates. However, unlike one could naively expect, the amplitude of these oscillations does not decay in the Lifshitz regime. When either $z = 2$ or $z = 3$ contribution is dominant and the khronon frequency $\bar{\omega}_{\mathcal{R}}$ is dominated by the mass term, as happens for $X \ll 1/\tilde{\alpha}$, the equation for $\mathcal{R}$ reads,

$$\mathcal{R}'' - 2(z-1)\mathcal{H}\mathcal{R}' + a^2 m_{k,\,z}^2\mathcal{R} = 0\,. \tag{5.7.38}$$

The second term here produces an 'anti-friction'. The canonically normalized mode functions have the form in the WKB approximation,

$$\mathcal{R}(t) = \frac{HM_*^{z-2}}{p^z\sqrt{2m_{k,z}}}\,(a(t))^{z-3/2}\,e^{-i\int \mathrm{d}t a(t) m_{k,z}}\,, \tag{5.7.39}$$

and describe oscillations with a growing amplitude, $|\mathcal{R}_p| \propto a^{z-3/2}$. We are going to see in the next subsection that the growth of khronon perturbations persists also at $X < \varepsilon_1/\tilde{\alpha}$ as long as the modes remain in the Lifshitz regime and stops only when they pass into the isotropic scaling $z = 1$. To stay within the validity of perturbation theory, we will impose the requirement that the amplitude of khronon perturbations remains small throughout the cosmological evolution, $p^{3/2}|R_p| < 1$. This translates into certain conditions on the inflationary parameters that will be discussed below.

Khronon-inflaton mixing

As the modes are further redshifted, the fields $\mathcal{R}$ and φ get mixed and no longer provide a convenient basis for perturbations. To find the appropriate basis, we study

the Lagrangian for $\mathcal{R}$ and φ in the regime: *(c)* $1 \ll X \lesssim \varepsilon_1/\tilde{\alpha}$. We will focus in this subsection on the case when the terms with Lifshitz scaling $z = 2$ or 3 dominate in the dispersion relation. This is true if the inflationary Hubble rate H is bigger than M_*, which is the scenario of primary interest to us. For completeness we consider the case of isotropic scaling, which will be shown in Sec. 5.7.4.

In the Lifshitz regime the leading mixing term is the first contribution in (5.7.15). Simplifying the expressions using the assumed parameter hierarchy and introducing the canonically normalised field

$$\hat{\mathcal{R}} \equiv \sqrt{2\varepsilon_1 + \alpha_1 X/\alpha_4}\, M_P \mathcal{R} \,,$$

we obtain the relevant part of the Lagrangian,

$$\mathcal{L} = \frac{a^2}{2}\big(\hat{\mathcal{R}}'_{\boldsymbol{p}}\hat{\mathcal{R}}'_{-\boldsymbol{p}} - \hat{\omega}^2_{\mathcal{R}}\hat{\mathcal{R}}_{\boldsymbol{p}}\hat{\mathcal{R}}_{-\boldsymbol{p}}\big) + \frac{a^2}{2}\big(\varphi'_{\boldsymbol{p}}\varphi'_{-\boldsymbol{p}} - \omega^2_{\varphi}\varphi_{\boldsymbol{p}}\varphi_{-\boldsymbol{p}}\big) - \frac{a^2}{\sqrt{1+\frac{\alpha_1 X}{2\varepsilon_1\alpha_4}}}\varphi'_{\boldsymbol{p}}\hat{\mathcal{R}}'_{-\boldsymbol{p}} \,, \tag{5.7.40}$$

where ω^2_φ is given by (5.6.29) and

$$\hat{\omega}^2_{\mathcal{R}} = \frac{\omega^2_{\mathcal{R}}}{\bar{\alpha}(\varepsilon_1 + \alpha_1 X/(2\alpha_4))} \,.$$

In deriving these expressions we have neglected contributions of order $\mathcal{H}$ into the frequencies. Note that $\hat{\omega}_{\mathcal{R}}$ is much higher than ω_φ. Indeed, we have

$$\hat{\omega}^2_{\mathcal{R}} \simeq a^2\frac{\alpha_1}{\varepsilon_1\alpha_4}m^2_{k,z}X \simeq \mathcal{H}^2\frac{X}{\varepsilon_1} \gg \mathcal{H}^2 X \simeq \omega^2_\varphi \,. \tag{5.7.41}$$

The Lagrangian (5.7.40) confirms explicitly our previous assertion that at $X \gg \varepsilon_1/\tilde{\alpha}$ the mixing between $\mathcal{R}$ and φ is negligible. On the other hand, we see that at $X \ll \varepsilon_1/\tilde{\alpha}$ it becomes essential. To identify the independent modes we use the substitution,

$$\chi_+ = \varphi\cos\theta - \hat{\mathcal{R}}\frac{\hat{\omega}_{\mathcal{R}}}{\omega_\varphi}\sin\theta \,, \tag{5.7.42}$$

$$\chi_- = \varphi\frac{\omega_\varphi}{\hat{\omega}_{\mathcal{R}}}\sin\theta + \hat{\mathcal{R}}\cos\theta \,, \tag{5.7.43}$$

and find that the mixing term between $\chi_\pm$ disappears provided that[5]

$$\tan 2\theta = \frac{2\omega_\varphi \hat{\omega}_\mathcal{R}}{\hat{\omega}_\mathcal{R}^2 - \omega_\varphi^2} \frac{1}{\sqrt{1 + \frac{\alpha_1 X}{2\varepsilon_1 \alpha_4}}} \,. \tag{5.7.44}$$

Due to (5.7.41) the mixing angle θ is always small and the expressions for the new variables $\chi_\pm$ simplify. At $X \ll \varepsilon_1/\alpha$ they become,

$$\chi_+ = \varphi - \sqrt{2\varepsilon_1} M_P \mathcal{R} \,, \tag{5.7.45}$$

$$\chi_- = \sqrt{2\varepsilon_1} M_P \mathcal{R} + \left(\frac{\omega_\varphi}{\hat{\omega}_\mathcal{R}}\right)^2 \varphi \,, \tag{5.7.46}$$

where we have switched back to the original metric perturbation $\mathcal{R}$. In the expression (5.7.45) we recognise the standard gauge invariant variable

$$\zeta \equiv \mathcal{R} - \frac{\mathcal{H}}{\phi'} \varphi = -\frac{\mathcal{H}}{\phi'} \chi_+ \tag{5.7.47}$$

describing curvature perturbation on the slices of constant inflaton field. The Lagrangian for $\chi_\pm$ reads,

$$\mathcal{L} = \frac{a^2}{2} \left({\chi_+'}^2 - \omega_\varphi^2(t,p) \chi_+^2 \right) + a^2 \frac{\alpha_1 X(t,p)}{4\varepsilon_1 \alpha_4} \left({\chi_-'}^2 - \bar{\omega}_\mathcal{R}^2(t,p) \chi_-^2 \right) \,, \tag{5.7.48}$$

where $\bar{\omega}_\mathcal{R}^2$ is the same as in (5.7.34). We see that χ_+ (or equivalently ζ) inherits the dispersion relation of the inflaton, whereas the second mode χ_- — that of khronon. In other words, in the regime (5.7.29) we still have two independent physical excitations, inflaton and khronon, with their respective dispersion relations (5.6.29), (5.7.34). The corresponding eigenfunctions are connected to the original variables by (5.7.45), (5.7.46). This is illustrated in Fig. 5.3.

We chose the positive frequency mode by imposing the WKB initial condition (see Sec. 5.6.3) in the limit $X \gg \varepsilon_1/\tilde{\alpha}$, where $\mathcal{R}$ and φ are decoupled. Then, since the rotation of the bases (5.7.45) and (5.7.46) does not mix the positive and negative frequency modes, $\chi_\pm$ stay (the positive frequency mode of) the WKB solution for $X \gtrsim 1$.

[5] We again neglect contributions proportional to $\mathcal{H}$ that come from time variation of $\hat{\omega}_\mathcal{R}$, ω_φ, X. These are irrelevant as long as the frequencies of the fields are higher than the Hubble rate.

Khronon-inflaton mixing for $z = 1$

If the inflationary Hubble rate is low, $H < M_*\sqrt{\alpha_1/\varepsilon_1}$, mixing between the inflaton and khronon perturbations occurs in the regime where the dynamics is dominated by the terms with relativistic scaling $z = 1$. In this Appendix, we consider the case with $\varepsilon_1/\alpha > 1$ and the range $X \ll 1/\alpha^2$.

Compared to the Lagrangian (5.7.40) considered in the main text, one should keep an additional mixing contribution, so that the total mixing Lagrangian reads,

$$\mathcal{L}_{\mathcal{R}\varphi} = a^2 \left[-\frac{\varphi'_{\boldsymbol{p}}\hat{R}'_{-\boldsymbol{p}}}{\sqrt{1+\frac{\alpha_1 X}{2\varepsilon_1}}} + \frac{\alpha_1}{\alpha_3}\frac{\mathcal{H}^2 X}{\sqrt{1+\frac{\alpha_1 X}{2\varepsilon_1}}}\varphi_{\boldsymbol{p}}\hat{R}_{-\boldsymbol{p}}\right] . \tag{5.7.49}$$

The quantity X is now given simply by,

$$X = (p/\mathcal{H})^2 ,$$

whereas the fields' frequencies are,

$$\hat{\omega}^2_{\mathcal{R}} = p^2\frac{\alpha_1}{\alpha_3}\frac{1+\frac{\alpha_1\bar{\alpha}}{\alpha_3\varepsilon_1}X}{1+\frac{\alpha_1 X}{2\varepsilon_1}} , \qquad \omega^2_{\varphi} = \varkappa_1 p^2 .$$

At $X \gg \varepsilon_1/\alpha_1$ the fields φ and $\hat{\mathcal{R}}$ are decoupled and have the same velocities as the inflaton and khronon in flat spacetime, whereas at $X \ll \varepsilon_1/\alpha_1$ they become strongly mixed. To diagonalize the Lagrangian in the latter case, we write it in terms of φ and

$$\chi_+ = \varphi - \frac{\hat{\mathcal{R}}}{\sqrt{1+\frac{\alpha_1 X}{2\varepsilon_1}}} .$$

It is straightforward to see that the mixing terms are negligible at $X \ll \varepsilon_1/\alpha_1$. Thus, we conclude that in this regime the decoupled modes are χ_+ (or equivalently ζ, see Eq. (5.7.47)) and φ. Their Lagrangian reads,

$$\mathcal{L} = \frac{a^2}{2}\left(\chi_+'^{\,2} - \frac{\alpha_1}{\alpha_3}p^2\chi_+^2\right) + \frac{a^2\alpha_1}{4\varepsilon_1}\left(\frac{p}{\mathcal{H}}\right)\left[\varphi'^2 - \mathcal{H}^2\frac{2\varepsilon_1}{\alpha_1}\left(\varkappa_1 - \frac{\alpha_1}{\alpha_3}\right)\varphi^2\right] . \tag{5.7.50}$$

It is worth stressing that in this Appendix we have focused on 'sub Hubble' modes, i.e. modes with $X \gg 1$. Nevertheless, we observe that the φ-equation following from the Lagrangian (5.7.50) coincides with Eq. (5.7.59) obeyed by super Hubble isocurvature modes in the $z = 1$ regime. In other words, in the $z = 1$ case the adiabatic and isocurvature modes are described respectively by ζ and φ at all times when $X \ll \varepsilon_1/\alpha_1$.

Note that the velocity of the adiabatic mode is given by $\sqrt{\alpha_1/\alpha_3}$ and coincides with the velocity of gravitons, rather than the velocity of inflaton.

Long wavelength evolution and power spectrum

We have shown that the variables $\chi_\pm$ are independent as long as the frequencies of the modes remain higher than the Hubble rate. As the modes redshift and approach the 'horizon crossing', $X \simeq 1$, the situation gets more complicated due to the terms proportional to $\mathcal{H}$ in the Lagrangian that can no longer be neglected. However, the situation simplifies again for 'super Hubble' modes corresponding to the regime:

(d) $X \ll 1$. In the standard relativistic single field inflation the curvature perturbation ζ is conserved at these scales. All non-derivative terms in the ζ-equation turn out to be suppressed by X, so that we obtain the solution,

$$\zeta = const\ . \tag{5.7.51}$$

This allows to immediately write down the power spectrum for ζ by matching to the amplitude of χ_+ fluctuations at the Hubble crossing, see Eq. (5.7.47),

$$\mathcal{P}_\zeta(p) = \frac{1}{2\varepsilon_{1,p} M_P^2}\, \mathcal{P}_{LS}(p)\,, \tag{5.7.52}$$

where $\mathcal{P}_{LS}(p)$ is the power spectrum of the Lifshitz scalar and $\varepsilon_{1,p}$ is the value of the slow-roll parameter at the Hubble crossing time of the mode p. Explicitly we have,

$$\mathcal{P}_\zeta(p) = \frac{\alpha_1^{\nu(z-1)}}{\varepsilon_{1,p}\varkappa_z^\nu} \frac{(2^\nu \Gamma[\nu])^2}{16\pi^3} z^{\frac{3}{z}-1} \left(\frac{H_p}{M_P}\right)^{\frac{3}{z}-1}\,, \qquad \nu = \frac{3}{2z}\ . \tag{5.7.53}$$

Note that for $z = 3$ the spectrum is independent of the Hubble rate at inflation,

$$\mathcal{P}_\zeta(p) = \frac{1}{8\pi^2}\frac{\alpha_1}{\varepsilon_{1,p}\sqrt{\varkappa_3}}\,, \qquad z = 3\ . \tag{5.7.54}$$

The spectral index is given by

$$n_s - 1 \equiv \frac{\mathrm{d}\ln \mathcal{P}_\zeta}{\mathrm{d}\ln p} = -\frac{3-z}{z}\varepsilon_1 - \varepsilon_2\,, \tag{5.7.55}$$

or alternatively,

$$n_s - 1 = -\frac{3(1+z)}{z}\varepsilon_V + 2\eta_V\ . \tag{5.7.56}$$

For $z = 1$ we recover the standard expressions.

We now analyze the super Hubble behavior of khronon, or 'isocurvature' mode. Despite the fact that the frequency term for φ in the Lagrangian (5.7.19), as well as its mixing with ζ, are suppressed by X, it still evolves non-trivially, because its time derivative term is also proportional to X. When the contributions with Lifshitz scaling $z = 2, 3$ dominate, the equation for φ following from (5.7.19), (5.7.20) simplifies,

$$\varphi'' - 2\mathcal{H}(z-1)\varphi' + a^2 m_{k,z}^2 \big(\varphi + \sqrt{2\varepsilon_1} M_P \zeta\big) = 0 \,. \tag{5.7.57}$$

The combination in brackets in the last term is nothing but $\sqrt{2\varepsilon_1} M_P \mathcal{R}$, which also coincides with χ_-, up to slow-roll suppressed corrections. Also Eq. (5.7.57) is the same as the khronon equation (5.7.38). We conclude that khronon preserves its identity through Hubble crossing. Despite very long wavelength of the modes, they continue to rapidly oscillate with growing amplitude due to anti-friction. The decoupling of ζ and $\mathcal{R}$ now receives an intuitive explanation: these excitations have very different frequencies and therefore cannot mix.

The amplitude of khronon oscillations seizes to grow when the momentum redshifts down to $p/aM_* \simeq 1$. For $\sqrt{\varepsilon_1} \ll p/aM_* \ll 1$ the equation for φ reads,

$$\varphi'' + \beta_4 \frac{p^2 m_{k,2}^2}{M_*^2} \big(\varphi + \sqrt{2\varepsilon_1} M_P \zeta\big) = 0 \,, \tag{5.7.58}$$

and describes pure oscillations of $\mathcal{R}$ with constant amplitude. This is illustrated in Fig. 5.4. Finally, for $p/aM_* \ll \sqrt{\varepsilon_1}$ the φ-equation becomes,

$$\varphi'' + \frac{2\mathcal{H}^2 \varepsilon_1}{\alpha_1} \Big(\varkappa_1 - \frac{\alpha_1}{\alpha_3}\Big) \varphi = 0 \,. \tag{5.7.59}$$

First, we notice that φ has completely decoupled from ζ. This is consistent with the result of [133] which studied inflation in the $z = 1$ limit of HL gravity and identified the independent modes in the super Hubble regime as ζ and $\delta\mathcal{N} = (\mathcal{H}/\phi')\varphi$. The latter has geometric interpretation of the difference in the number of e-foldings between the surfaces of constant inflaton (i.e. constant density) and constant khronon. Second, the nature of solutions to (5.7.59) depends on the sign of the combination in brackets which has the physical meaning of the difference between (the squares of) the low-energy velocities of the inflaton, $c_\varphi^2 \equiv \varkappa_1$, and graviton $c_\gamma^2 \equiv \alpha_1/\alpha_3$ (see Eqs. (5.6.11), (5.6.29)). If it is positive, the mode φ performs rapid oscillations with the physical frequency $\omega_\varphi/a \simeq H\sqrt{\varepsilon_1/\alpha_1} \gg H$ and the amplitude decaying as $a^{-1/2}$. On the other

hand, if $\varkappa_1 < \alpha_1/\alpha_3$, the solutions to (5.7.59) exhibit an exponential runaway behavior, signaling an instability. These two cases are illustrated in Fig. 5.4. To avoid instability, we will assume that $\varkappa_1 > \alpha_1/\alpha_3$.

Equation (5.7.59) has been derived under the assumption that the low-energy velocities of inflaton and graviton differ by a factor of order one. Alternatively, one can impose the requirement that this difference should be small, $c_\varphi^2 - c_\gamma^2 = \mathcal{O}(\alpha)$, which corresponds to an emergence of approximate Lorentz invariance at low energies. In this case one must retain additional contributions of the same order in the expression (5.7.22) for the frequency of φ, so that the φ-Lagrangian becomes,

$$\tilde{\mathcal{L}}_\varphi = a^2 \frac{\alpha_1}{4\varepsilon_1}\left(\frac{p}{\mathcal{H}}\right)^2\left[\varphi'^2 - \mathcal{H}^2\,\varepsilon_1\left(1 - \frac{\varepsilon_2}{2\varepsilon_1} + \frac{2(c_\varphi^2 - c_\gamma^2)}{\alpha_1} + \frac{3c_k^2}{c_\gamma^2}\right)\varphi^2\right], \tag{5.7.60}$$

where $c_k^2 \equiv 2\alpha_1\bar{\alpha}/\alpha_3^2$ is the low-energy velocity of the khronon. Upon proper translation of notations, this coincides with the Lagrangian for the isocurvature mode obtained in [133]. From (5.7.60) we see that the isocurvature mode evolves slowly with the rate suppressed by the slow-roll parameter ε_1. This behavior is also illustrated in Fig. 5.4.

Even if the isocurvature mode does not develop instability at late times, it initially grows due to anti-friction, see Eq. (5.7.57) and Fig. 5.4. By the time the growth terminates the power spectrum of $\mathcal{R}$ reaches

$$\mathcal{P}_\mathcal{R}\Big|_{a=p/M_*} = \frac{H^2}{4\pi^2 m_{k,z} M_*} \simeq \frac{H}{4\pi^2 M_P}\,. \tag{5.7.61}$$

For the validity of the linearized theory developed above we must require that the perturbations of $\mathcal{R}$ do not exceed unity. Then we obtain an upper bound on the inflationary Hubble scale,

$$H < 4\pi^2 M_P\,. \tag{5.7.62}$$

This constraint is somewhat unexpected, as a priori HL gravity should be applicable also at trans-Planckian energies[6]. In fact, the requirement (5.7.62) may be too restrictive. It follows from consideration of metric perturbations with very long wavelengths. Unlike in GR, we cannot use a space-dependent reparameterization of time to remove this perturbation completely. However, *space-independent* time reparametrisations are still a symmetry of HL gravity and can be used to remove the fluctuation $\mathcal{R}$ at any given point. This suggests that coupling of khronon to other physical degrees

[6]Recall, in particular, that for $z = 3$ the power spectra of the curvature perturbation ζ and the gravitational waves γ do not depend on the Hubble scale, so their perturbative calculation does not require sub-Planckian energies.

of freedom should involve spatial derivatives and its almost homogeneous fluctuation, even with a large amplitude, should not have any effect locally. This property is indeed satisfied by the Lagrangian (5.7.20) describing dynamics of ζ and khronon at super Hubble scales. We have also verified that in pure de Sitter universe the growth of $\mathcal{R}$ does not lead to divergence of local gauge invariant observables constructed out of the metric h_{ij}, such as the extrinsic curvature K and $K^i_j K^j_i$ and the spatial Ricci scalar R. For instance, the linear perturbation of the trace part of the extrinsic curvature is given by

$$\delta K = K - 3H = -\frac{1-2\bar{\alpha}}{\bar{\alpha}}\left[(1-\Omega_1)\dot{\mathcal{R}} - \Omega_2 H\mathcal{R}\right] \propto a^{-(z+\frac{3}{2})}\,. \tag{5.7.63}$$

These arguments indicate that the constraint (5.7.62) may be avoided by a more careful treatment where the growth of super Hubble khronon fluctuations is absorbed by an appropriate field redefinition. This study is, however, beyond the scope of the present paper.

Before concluding this section, let us describe what happens if the slow-roll parameter ε_1 is the smallest quantity in the setup,

$$\varepsilon_1/\alpha_1 \ll 1\,. \tag{5.7.64}$$

In this case the perturbations $\mathcal{R}$ and φ are decoupled all the way through the Hubble crossing down to $X \simeq \varepsilon_1/\alpha$. After that, the good variables are ζ and φ. As before, ζ is conserved, whereas the evolution of φ is described by Eqs. (5.7.57), (5.7.58), (5.7.59), (5.7.60). The power spectrum of ζ is determined by matching it to the fluctuations of the inflaton and khronon at $X \simeq \varepsilon_1/\alpha$. It is easy to see that the inflaton fluctuations dominate, so the spectrum is still given by (5.7.53) (leaving aside a small correction due to the damping of the inflaton perturbations between the Hubble crossing and $X \simeq \varepsilon_1/\alpha$). Note that for $z = 3$ the hierarchy (5.7.64) is actually not viable, as it would imply that the power spectrum is larger than unity, see Eq. (5.7.54).

5.8 Violation of consistency relation

In the previous section, we computed the power spectra of the adiabatic curvature perturbation ζ and the primordial gravitational waves in the anisotropic scaling regime of HL gravity. In particular, we have shown that in the non-projectable case ζ is conserved at super Hubble scales during inflation, despite the presence of an isocurvature scalar perturbation. The intuitive explanation of this conservation is that the isocurvature mode, associated to the shift of khronon, is locally unobservable and its

interaction with ζ is suppressed by spatial derivatives. This suggests that ζ will not be affected by the isocurvature mode at super Hubble scales also after the end of inflation. Indeed, conservation of ζ at super Hubble scales has been demonstrated for rather general matter content in the low-energy limit ($z = 1$) of non-projectable HL gravity in Refs. [133, 151]. We will proceed under the assumption that this also holds between the end of inflation and the time when the universe enters into the isotropic scaling regime. Below we discuss a signal of the Lifshitz scaling in the primordial spectra.

5.8.1 Consistency relation in 4D Diff invariant theories

Before discussing the primordial spectra generated in the anisotropic scaling regime, let us review the discussion in theories encompassed by the Effective Field Theory (EFT) of inflation [33] where the inflaton background breaks 4D Diff invariance down to time-dependent spatial Diff. We follow Ref. [164, 165]. Within EFT of inflation, the quadratic action for the gravitational waves is given by

$$S_{\gamma\gamma} = \frac{1}{8}\int \mathrm{d}t\, \mathrm{d}^3\boldsymbol{x}\, a^2\, \frac{M_P^2}{c_\gamma^2}\left[(\gamma'_{ij})^2 - c_\gamma^2(\partial_k\gamma_{ij})^2\right]. \tag{5.8.1}$$

In the presence of a time-dependent inflaton background which breaks Lorentz invariance and time-translations, the parameters M_P and c_γ can deviate from their vacuum values and can vary with time. However, one can always set these parameters to fixed values by a redefinition of the metric. Indeed, performing the disformal transformation:

$$g_{\mu\nu} \mapsto g_{\mu\nu} + (1 - c_\gamma^2(t))n_\mu n_\nu\,, \tag{5.8.2}$$

where n_μ is the unit vector orthogonal to the constant-inflaton slices, and successively performing the conformal transformation to the Einstein frame,

$$g_{\mu\nu} \mapsto c_\gamma^{-1}(t)\frac{M_P^2(t)}{M_{P,0}^2}g_{\mu\nu}\,, \tag{5.8.3}$$

we can set the graviton speed c_γ to unity and M_P^2 to constant. The equivalence between the Einstein frame and the Jordan frame for the gravitational waves was explicitly confirmed in Ref. [164, 165]. The price to pay is that these transformations also alter the sector of scalar perturbations. For instance, if the propagation speed of the inflaton c_s is 1 in the original frame, after the above disformal transformation which sets c_γ to 1, the sound speed c_s is changed into $c_s = c_\gamma^{-1}$.

After inflation, the non-minimal coupling introduced by the inflaton should disappear. Therefore, it is reasonable to calculate the primordial spectra in the Einstein

frame for the gravitational waves. Then the spectrum for the gravitational waves is given by the standard expression and depends only on the ratio of inflationary Hubble scale and Planck mass. Besides, one obtains the well-known consistency relation

$$n_t = -\frac{r}{8c_s}\,, \tag{5.8.4}$$

which relates the spectral index for the gravitational waves n_t and the tensor to scalar ratio r. (The sub leading contribution to the consistency relation in the slow-roll approximation can be found, e.g., in Ref. [169].) In a Lorentz invariant theory the velocity of any excitation cannot exceed unity, $c_s \leq 1$, which implies a bound,

$$-n_t \geq \frac{r}{8}\,. \tag{5.8.5}$$

This is a robust prediction of (single field) EFT of inflation. Moreover, when c_s is smaller than 1 the equilateral non-Gaussianity is enhanced by $1/c_s^2$ (see, e.g., Refs. [170, 171, 172]). Thus, a deviation from equality in (5.8.5) should be accompanied by large non-Gaussianity.

5.8.2 Violation of consistency relation in Hořava–Lifshitz gravity

We now discuss the primordial spectra generated in gravity with anisotropic scaling. In this case the symmetry breaking pattern is different: there are no 4D Diff to start with, but only the reduced symmetry of foliation-preserving Diff, that is further broken to time-dependent spatial Diff by the inflaton background. The velocity of graviton depends now on the wavenumber p, so one cannot set it to unity by the disformal transformation which globally changes the time component of the metric. This means that the modified dispersion relation physically changes the spectrum of the gravitational waves. In particular, the relation between the power spectrum $\mathcal{P}_\gamma$, Eq. (5.6.45), and the inflationary Hubble rate is no longer straightforward: it depends on the scaling exponent z and other parameters of the theory. For $z = 3$ the tensor power spectrum does not depend on H at all. On the other hand, a robust prediction for $z = 3$ is vanishing of the tensor spectral index, $n_t = 0$.

Using Eqs. (5.6.45) and (5.7.53), at the leading order in the slow-roll approximation,

we obtain the tensor-to-scalar ratio as[7]

$$r \equiv \frac{\mathcal{P}_\gamma}{\mathcal{P}_\zeta} \simeq 16\varepsilon_1 \left(\frac{\varkappa_z}{\varkappa_{\gamma,z}}\right)^{\frac{3}{2z}} . \tag{5.8.8}$$

Exceptionally, for $\varkappa_z = \varkappa_{\gamma,z}$ the tensor-to-scalar ratio is given by the standard expression irrespective of the value of z. Using Eqs. (5.6.46) and (5.8.8), we obtain the modified consistency relation for the primordial perturbations in the anisotropic scaling regime as

$$n_t \simeq -\frac{3-z}{z}\frac{r}{16}\left(\frac{\varkappa_{\gamma,z}}{\varkappa_z}\right)^{\frac{3}{2z}} . \tag{5.8.9}$$

We see that n_t and r are still related linearly, but the coefficient depends on z, $\varkappa_z$, and $\varkappa_{\gamma,z}$. Clearly, this can violate the lower bound (5.8.5) on $-n_t$ obtained in Lorentz invariant theories.

5.9 Concluding remarks

HL gravity contains an additional scalar degree of freedom in the gravity sector, khronon, corresponding to fluctuations of the preferred time foliation. Therefore, a minimal model of inflation possesses two scalar degrees of freedom: the inflaton and khronon. These two fields are coupled gravitationally. In the small scale limit, as usual, the gravitational interaction is suppressed and we simply have two decoupled Lifshitz scalar fields. Naively, one may expect that in the large scale limit, the gravitational interaction becomes important and these two fields start to be coupled. This is indeed the case in the projectable version of HL gravity. The inflaton and khronon stay nearly gapless modes which are bi-linearly coupled. Then the adiabatic curvature perturbation ζ is generically not conserved at large scales.

On the other hand, the situation is crucially different in the non-projectable version.

[7] Equations (5.6.45) and (5.7.53) directly give

$$r = 16\varepsilon_1 \left(\frac{\varkappa_z}{\varkappa_{\gamma,z}}\right)^{\frac{3}{2z}} \left(\frac{H_{p,\gamma}}{H_p}\right)^{\frac{3}{z}-1} . \tag{5.8.6}$$

For $\varkappa_z \neq \varkappa_{\gamma,z}$, the Hubble crossing times for the adiabatic perturbation does not necessarily coincide with the one for the gravitational waves and the Hubble parameters at these times are related as

$$\frac{H_{p,\gamma}}{H_p} \simeq \left(\frac{\varkappa_z}{\varkappa_{\gamma,\,z}}\right)^{\frac{\varepsilon_1}{2z}} . \tag{5.8.7}$$

In the anisotropic scaling regime, khronon acquires the effective mass m_K, which is much larger than the Hubble scale, well before Hubble crossing time. It then decouples from the adiabatic mode ζ and does not leave any impact on the power spectrum of ζ, which is conserved at super Hubble scales. The power spectrum of ζ is simply given by that of the Lifshitz scalar with the multiplicative factor $1/(2\varepsilon_1 M_P^2)$. The decoupled khronon rapidly oscillates, with the amplitude of the oscillations growing exponentially due to anti-friction. The growth persists until the mode enters into the regime of isotropic scaling as a consequence of the redshift of its momentum. We need a more careful consideration to see if this exponential growth can or cannot affect observable quantities.

One remaining question is whether the decoupling between the adiabatic mode ζ and khronon is a robust feature of non-projectable HL gravity also beyond the restricted setup considered in this paper. We have focused on the linear order in perturbations. The physical interpretation presented in Sec. 5.7.2 suggests that the decoupling will also persist at non-linear orders. We postpone an explicit analysis of this issue, as well as of primordial non-Gaussianity, to a future work. In this paper we assumed the minimal coupling of the inflaton to the gravity sector. One may wonder whether a non-minimal interaction can prevent the decoupling of khronon. Recall that khronon gets gapped due to a peculiar structure of the coefficient in front of the (quadratic) time derivative term in the action. Thus, to make khronon gapless, the non-minimal coupling should modify the time derivative terms. The only contribution that can change the time derivative terms under the assumption of foliation-preserving Diff and time reversal symmetry is the term with $K\dot{\Phi}/N$. However, this can be removed by a redefinition of the metric $h_{ij} \to \Omega^2(\Phi)h_{ij}$ and $N \to \Omega^3(\Phi)N$. Therefore, we expect that the decoupling between ζ and khronon takes place generically in the non-projectable version of HL gravity with the time reversal symmetry in the anisotropic scaling regime. It may be interesting to study if this decoupling takes place also in the case when the time reversal symmetry is broken, e.g. by a term with $\sqrt{h}\,\dot{\Phi}/N$.

We also pointed out that the consistency relation between the tensor to scalar ratio r and the tensor spectral index n_t, which holds in the general single field EFT of inflation, can be violated by the primordial perturbations generated during the anisotropic scaling regime. If the primordial gravitational waves are detected, the value of r will give the lower bound on $-n_t$ in Lorentz invariant theory. A violation of this bound will indicate violation of Lorenz invariance in the early universe.

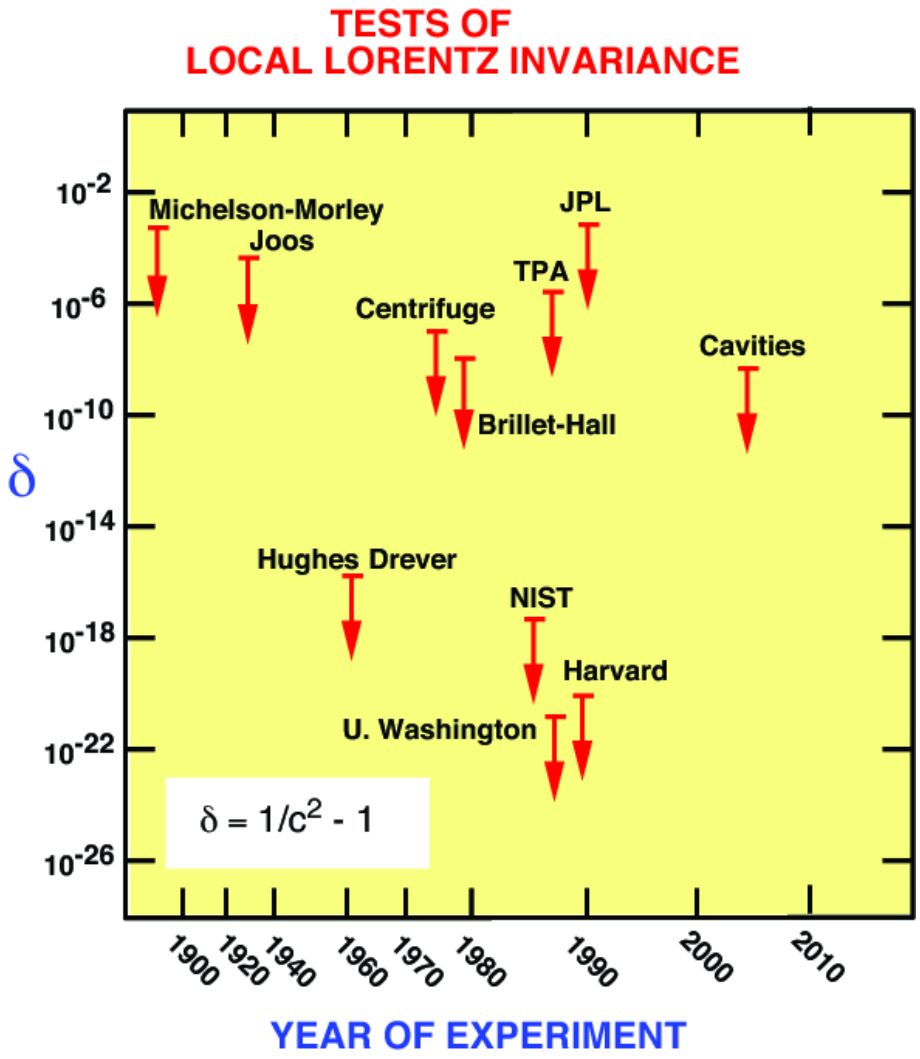

Figure 5.1. The observational constraints on the Lorentz invariance

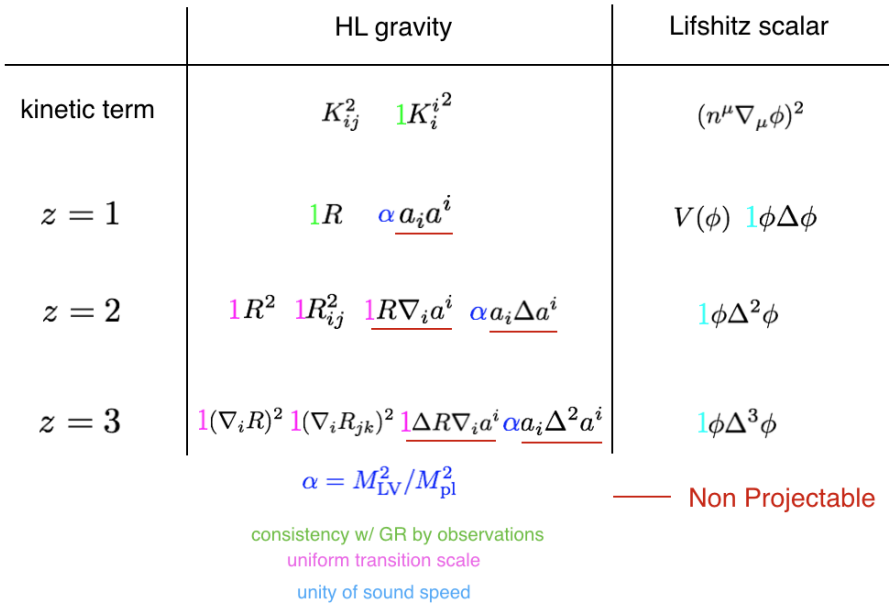

Figure 5.2. The summary table of parameter hierarchy

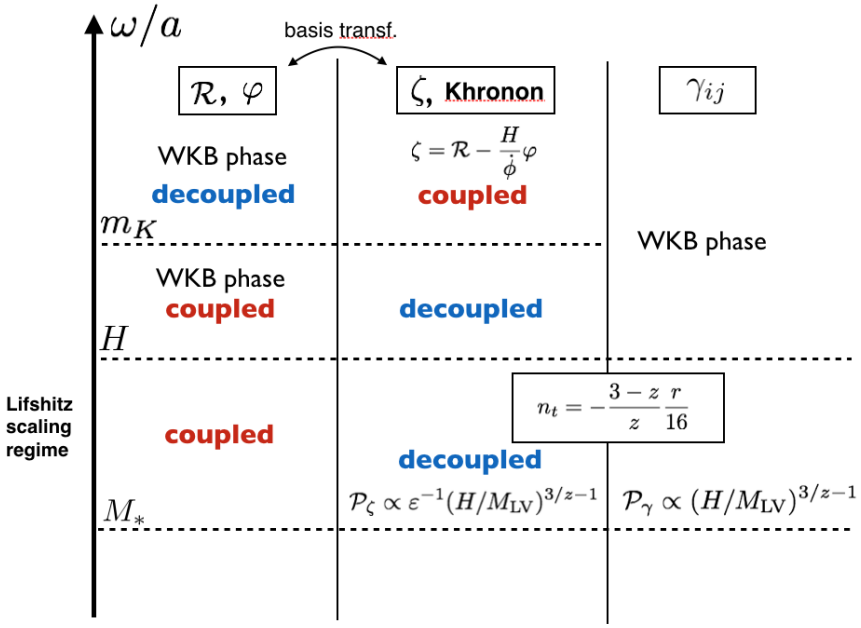

Figure 5.3. Summary of the time evolution of the fluctuations. The central axis denotes the quantity $X(t,p)$ introduced in Eq. (5.7.26).

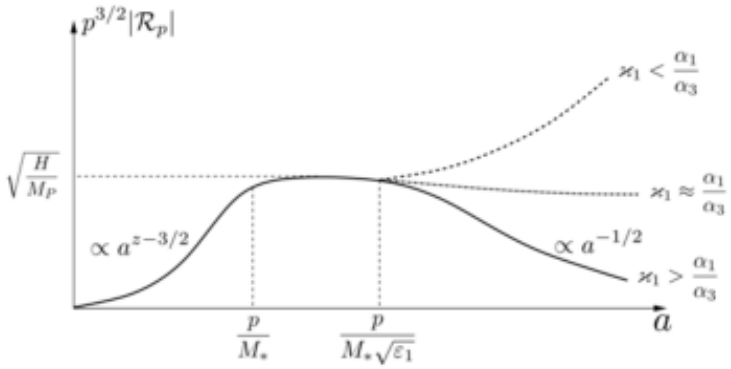

Figure 5.4. The amplitude of a khronon mode with conformal momentum p as a function of the scale factor. It grows in the Lifshitz regime and reaches the value $\sqrt{H/M_P}$. Then it remains constant till $a \sim p/M_*\sqrt{\varepsilon_1}$, where the mode enters into the $z = 1$ scaling. The subsequent evolution depends on the relation between velocities of the inflaton and graviton characterized by the parameters $\varkappa_1$ and α_1/α_3, as explained in the main text.

Chapter 6

Testing gravity with CMB lensing

The cosmic structures existing in today's Universe, i.e., the planets, stars, galaxies, and the large structure have grown from the initial seeds buried in the early Universe. The crucial driver of the cosmic structure formation is gravity. For the large scale structure, gravity affects the speed of the cosmic growth of the structures both in locally and distantly. As a local scale, less than 1Mpc the gaseous objects or dark matters freely falls in a gravitational potential self produced by them. In the distant scale, typically 100Mpc where the cosmic expansion well dominates the coherent motion of the galaxies, the cosmic growth of the gravitational potentials being further deepened or shallower in cosmological time-scale. The cosmic expansion generates the two effects on the gravitationally evolved structures; gravitational redshifts and the growth rate of the potential. The gravitational redshifts are differently known as the Kaiser effect [173, 174] and the Fingers of God effect [175]. These effects was directly measured by 2dF galaxy survey [176], successively confirmed by SDSS survey [177]. Nowadays people call it as the redshift space distortions. On the other hand, the growth speed of the structure formation mainly change the amplitude and clustering degree of the galaxies.

Provided the gravitational interactions are normally given by the Einstein's general relativity in the past 10 billion years, the redshift space distortions and the growth rate of the structure are directly trace the matter clustering. However, if the law of gravity in the past deviates from the Einstein's gravity, the growth of the structure accumulate the change of gravitational law in the cosmological time scale. As predicted in Chapter 4 the change of the additional scalar intermediate causes the observationally significant features on observable quantities.

Observationally, the decode of the modification of gravity and the matter clustering is hard to distinguish. By combining the clustering information and the light deviation by gravitational lensing, however, enables in principle us to disentangle the effects of the gravity from those of the matters. In particular, the time lapse of the cosmic structures carry abundant information of cosmology.

We develop the methodology of testing gravity at high redshifts. We consider the gravitational lensing of CMB by the massive radio galaxies, aiming to measure the growth history of the large scale structure at $z > 1$. We provide all-sky data of radio surveys and develop the method of how we properly assign the number distribution and the galaxy bias of radio sources. We identify the main difficulty for the extraction of growth history of the large scale structure with the existing data of galaxy and radio surveys, and CMB-lensing by Planck 2015, discussing possible removals of such difficulty in future radio and galaxy surveys.

6.1 CMB lensing

We review the CMB lensing based on A. Lewis and A. Challinor 2006 [178] . The small notations are changed, as fitted to the entire thesis. We consider that the metric perturbations in the conformal Newtonian gauge with a flat FLRW background space-time is given as

$$ds^2 = -a^2(\eta)(1+2\Psi)d\eta^2 + a^2(\eta)(1-2\Phi)\delta_{ij}dx^i dx^j\,, \tag{6.1.1}$$

Due to the conformal invariance of a null geodesic on which photons are at motion, the certain conformal transformation so that the spatial metric is nothing but that of the background makes the derivation of formulae for the photon propagation easier. The metric after this transformation is obtained as

$$ds^2 = -a^2(1+4\Psi_W)d\eta^2 + a^2\delta_{ij}dx^i dx^j\,, \tag{6.1.2}$$

where the Weyl potential Ψ_W [1] is defined as

$$\Psi_W \equiv \frac{\Psi+\Phi}{2} \tag{6.1.3}$$

Note that when modified gravity theory is presented, the Weyl potential should reflect that the modification of the gravitational strength for a photon by comparison to the

[1] Ψ_W is often called the Weyl potential because the general linear scalar-mode of the Weyl tensor.

Newton potential computed via the Poisson equation for a photon propagation[2],

$$\nabla^2\Psi_W = 4\pi G_{\rm N} a^2(\bar{\rho}_m\delta + \Pi)\,, \tag{6.1.4}$$

Whenever the anisotropic stress Π is negligible smaller than the density contrast, the Weyl potential Ψ_W is solely determined by the density fluctuation of the matter in the universe. Hereafter, we treat that $\Pi = 0$. $\bar{\rho}_m$ is represented as

$$\bar{\rho}_m = \frac{3H_0^2}{8\pi G_{\rm N} c^2}\Omega_m\,, \tag{6.1.5}$$

Let us consider the CMB lensing. On the way through that a CMB photon passes, the deflection by a local gravitational potential bends the trajectory of a photon. By the fact that we can only know from which angle in the line of sight the photons come from, then the physical information of the CMB photons, i.e., the black-body temperature, polarisation, or the energy injection are all different of the values that suppose to be observed along the line of sight. We represent this fact for the temperature fluctuations. The CMB photons that we actually measures along the line of sight $\hat{\mathbf{n}}$ are $\tilde{T}(\hat{\mathbf{n}})$ given through

$$\tilde{T}(\hat{\mathbf{n}}) = T(\hat{\mathbf{n}} + \nabla\psi)\,, \tag{6.1.6}$$

where $T(\hat{\mathbf{n}})$ is the original temperature fluctuation of the CMB photons without any deflection effect. We call $\nabla_{\hat{\mathbf{n}}}\psi$ as the deflection vector. The integral of the Weyl potential on the line of sight provides you the total deflection vector $\nabla_{\hat{\mathbf{n}}}\psi$. i.e., the gradient of a scalar potential;ψ along the line of sight is given as

$$\psi(\hat{\mathbf{n}}) = -2\int_0^{\chi_*} d\chi \frac{\chi_* - \chi}{\chi_* \cdot \chi}\Psi_W(\chi\hat{\mathbf{n}}; \eta_0 - \chi)\,, \tag{6.1.7}$$

Here ψ is called the lensing potential and χ_* represents the co-moving coordinate at the last scattering surface. Hereafter we omit the subscript and argument $\hat{\mathbf{n}}$ from the derivatives. The schematic image is shown here.

The lensing convergence is defined by

$$\nabla^2\psi = -2\kappa\,, \tag{6.1.8}$$

[2]In modified gravity theories, Poisson equation of a photon is generally obtained in a form Eq. (4.9.15)

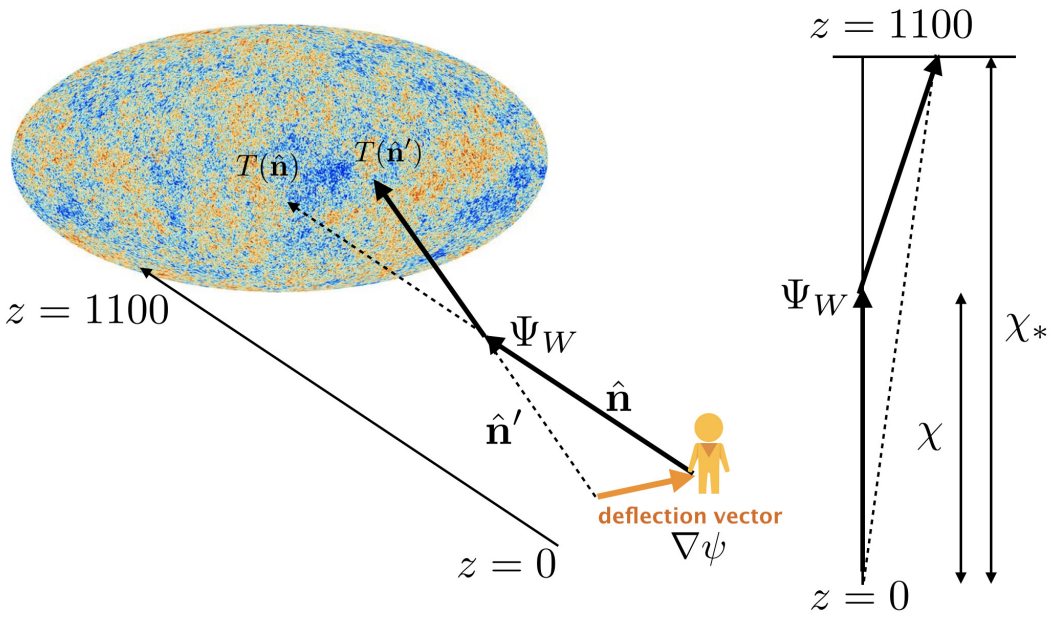

Figure 6.1. The schematic image of CMB lensing

κ is the magnification of CMB flux. By operating Laplacian onto Eq. (6.1.7) and using Eqs. (6.1.8) and (6.1.4), κ is obtained as

$$\kappa = \frac{3H_0^2\Omega_{\mathrm{m}0}}{2c^2}\int_0^{\chi_*} d\chi\delta(\chi)\frac{\chi(\chi_*-\chi)}{a\chi_*} \equiv \int d\chi\delta(\chi)K_\kappa(\chi)\,, \tag{6.1.9}$$

We explicitly see that the density contrast δ is related to κ. Note that K_κ is a kernel function that gives the probability of lensing events at a certain co-moving distance. The dependency of a cosmological model appears in the relation of redshift and co-moving distance and the temporal growth of δ.

6.2 Wide area CMB lensing tomography

CMB lensing is in principle able to measured by cross-correlating with the matter distribution of the Universe. This is reasonable because a gravitational potential at a local environment which induces gravitational lensing on CMB photons is given by the Poisson equation in Eq. (6.1.4). It is able to measure the growth speed of large scale structure in different redshift intervals. We briefly summarise a study that has been done by J. A. Peacock and M. Bilicki 2018 [179]. As argued in [179], in the correlation of the CMB or galaxies, the angular correlations are

$$C_{ab}(\ell) = 4\pi \int d\ln k \Delta^2(k) \int d\chi K_a j_\ell(k\chi) \int d\chi K_b j_\ell(k\chi)\,, \tag{6.2.1}$$

where $\Delta^2(k) \equiv (k^3/2\pi^2)\mathcal{P}_\delta(k)$ is the dimensionless power spectrum of matter density contrast. The Limber approximation is applied, obtaining the shorthanded form of the angular correlation as

$$\frac{\ell(\ell+1)}{2\pi} C_{ab} = \frac{\pi}{\ell} \int d\chi \Delta^2(\ell/\chi)\chi K_a(\chi) K_b(\chi)\,, \tag{6.2.2}$$

where $K_{a,b}$ are kernel functions of tracers of matter density contrast. For instance, galaxies well trace the density contrast in the Universe. We use CMB lensing kernel and the distribution of galaxies.

$$K_g(\chi) \equiv -b(z)\frac{c}{H(z)}\frac{dn(z(\chi))}{dz}\,, \tag{6.2.3}$$

where we use the defnition of the co-moving distance, i.e., $d\chi/dz = -c/H(z)$. We follow that the galaxy bias $b(z)$ is scale-independent, as shown in [180]. Note that the determination of the redshift distribution of galaxies is essential. To compute the matter power specrum $\Delta^2(k)$, we use CLASS [181], a publicly-available Einstein-Boltzmann solver of CMB. For simplicity, we set the background cosmology to the ΛCDM model as default in CLASS,i.e., $(h, \Omega_{\rm m0}h^2, \Omega_{\rm b}h^2, A_s, n_s, \tau_{\rm reio}) = (0.67556, 0.142412, 0.022032, 2.215\cdot 10^{-9}, 0.965, 0.0925)$. We switch on HALOFIT approximation in CLASS to be accurate to the non-linear scale above $0.1h{\rm Mpc}^{-1}$.

6.3 Pseudo estimator of angular power spectrum

When dealing real data, it is often a case that an area of the sky that is observed is incompletely covered all the sky, e.g., foreground emissions, instrumental barriers,

limitation of survey time. This causes a loss of astrophysical information. It is known that an artificial mask on the observed signal is an efficient way to remove noises on the true signal. The price to pay is that we cannot see all the sky, generating statistical uncertainties and some systematic noises.

6.3.1 Fair sample hypothesis

Fair sample hypothesis states that signals in different parts of the sky we observe are assumed to be generated by a same random process. This hypothesis ensures that the average of a signal such as CMB temperature fluctuation or galaxy distributions over the areas we are able to observe are considered as different realisations of cosmological information. Thanks to the central limit theorem, statistical errors shrink to the true distributions of physical parameters we want to test. As it has been conclusively established, the measurement of CMB anisotropy almost reaching to the cosmic variance limit. We rely on the fair sample hypothesis, assuming that the distribution of radio samples in different part of the sky would trace same randomness of density fluctuations.

6.3.2 Pseudo angular power spectrum

The fair sample hypothesis enables us to obtain physical parameters in cosmology via statistical estimators. One of the popular estimators is called pseudo power angular power spectrum [182] which is defined as

$$C_{ab}(\text{pseudo}) \equiv \frac{1}{f_{\text{sky}}} C_{ab}(\text{masked})\,, \tag{6.3.1}$$

where f_{sky} is the sky fraction, which depends on the actual set-up. The mathematical derivation of this formula is shown in Appendix. C.1. We apply the mask for the Planck 2015 lensing, whose sky fraction is $f_{\text{sky}} = 0.68$. For sampling the we use HEALPix [183, 184], which provides the pixelisation of the sky and compute the angular power spectra.

By using the data of the Planck 2015 for the CMB lensing convergence [3], we demonstrate the computation of angular auto power spectrum of CMB convergence. As Fig. 6.3 shows, the noise dominates at higher multipoles in $C_{\kappa\kappa}$. Therefore, we use a model prediction of $C_{\kappa\kappa}$ in the measurements of the cross power spectrum between radio galaxies and CMB lensing convergence.

[3] for the data, please read the link; https://pla.esac.esa.int/

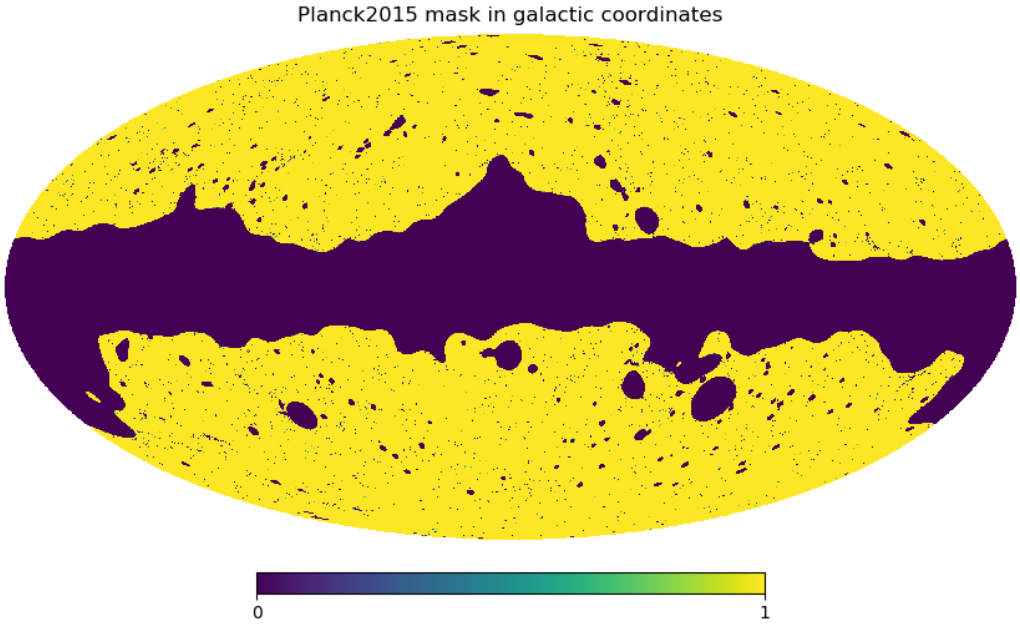

Figure 6.2. Planck 2015 mask for lensing

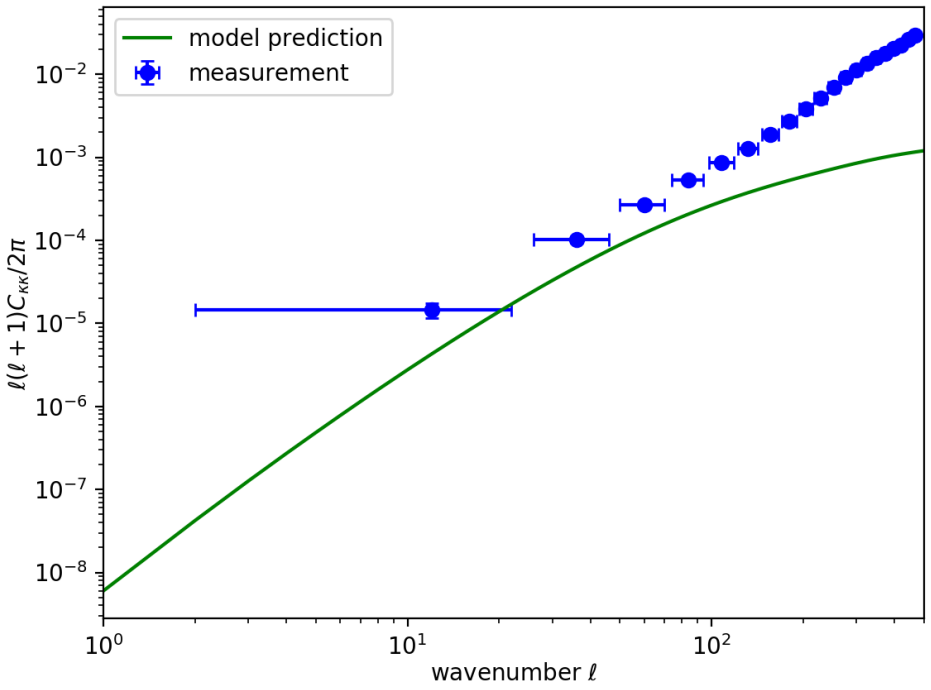

Figure 6.3. Angular power spectrum of CMB lensing (convergence). The blue dot is the real data measured and the green line is the theoretical prediction by the ΛCDM model with $(h, \Omega_{\mathrm{m}0}h^2, \Omega_{\mathrm{b}}h^2, A_s, n_s, \tau_{\mathrm{reio}}) = (0.67556, 0.142412, 0.022032, 2.215 \cdot 10^{-9}, 0.965, 0.0925)$

6.4 The massive radio galaxies

The massive radio galaxies are radio-loud galaxies observed in radio bands. It is believed that the radio galaxies are bright in radio waves because radio emission is energised by active galactic nucleis at the centre of the galaxies, which generates enormous outflow of energy. The luminosity of a radio galaxy at 500 MHz is typically $L_{500}(\text{rest}) > 10^{27}\text{W Hz}^{-1}$[185].

Observationally, the radio galaxies are identified as a point source in the sky as they are distant from us. Currently, tens of millions sources are found in the previous radio surveys, e.g., NRAO VLA Sky Survey (NVSS)[186], Sydney University Molonglo Sky Survey (SUMSS)[187], and VLA FIRST survey[188]. The spectroscopy of radio galaxies is done for 132 galaxies in CENSORS [189, 190], but the rest of radio galaxies are not positioned in redshift space.

Clustering of radio galaxies in NVSS catalog was firstly argued in [191, 192], obtaining non-zero angular correlation between the radio galaxies. The angular cross-correlation with CMB temperature fluctuations is obtained as non-zero value by K. Smith *et al.* 2007 [193], evidently showing that the radio galaxies are indeed a source of gravitational lensing. The other measurement of the angular cross power between a radio catalogue and CMB lensing is obtained with data of FIRST and Acatama Cosmology Telescopes (ACT) [194]. At present, however, the theoretical predictability of the cross power is very limited by uncertainty of radio galaxy bias and the redshift distributions of radio galaxies. To improve theoretical predictions, it is necessary to obtain the bias and the redshift distribution accurately.

The massive radio galaxies are good tracers at higher redshifts at $z > 1$, where the matter components dominate the Universe, determining the expansion history the and structure formation. The growth history of the, typically parametrised by $\sigma_8(z)$ that gives the amplitude of the structure formation is less known at $z > 1$. The main difficulty to measure σ_8 is that we have less tracers that accurately distributes in the redshift space.

Survey	frequency	flux cut	beam size
NVSS	1.4GHz	$\geq$ 6mJy	45 arcsec
SUMSS	843GHz	$\geq$ 8mJy	45 arcsec
CENSORS	1.4GHz	$>$ 7.5mJy	45 arcsec

Table 6.1. Data for radio galaxies

The combination of the tabled data covers over 80% of all the sky,i.e., the sky

fraction is $f_{\rm sky} = 0.823$.

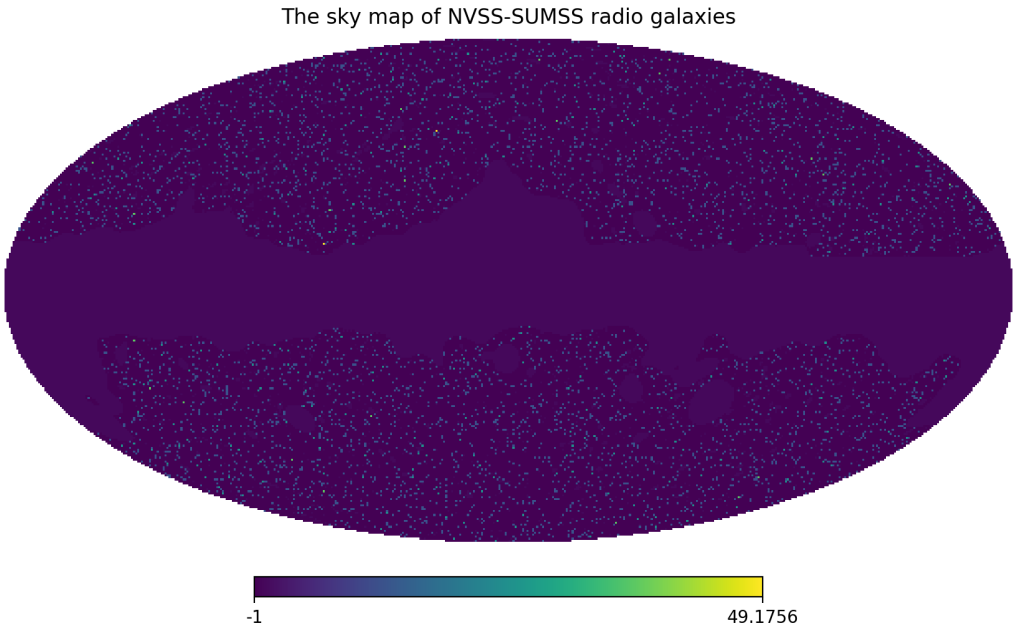

Figure 6.4. The sky map of NVSS-SUMSS radio galaxies. The number distribution is shown.

6.5 Estimated redshift distribution of radio sources

We try to estimate the redshift distribution of the radio galaxies in NVSS and SUMSS with the optical galaxies in Kilo Square Degree Survey (KiDS)[4]. We assume that the radio galaxies locates in galaxy clusters and member galaxies in a cluster can be seen in the catalogs of optical galaxies.

6.5.1 KiDS optical galaxies

KiDS optical galaxies provide the completed catalog of optical galaxies in a wide range of redshifts. Since KiDS is an imaging survey, the redshift of the KiDS galaxies is not spectroscopically but photometrically measured. As [195] shows, the uncertainty of redshifts of KiDS galaxies is $\langle \delta z/(1+z) \rangle < 4 \times 10^{-5}$ and the scatter is $\sigma(\delta z/(1+z)) < 0.019$.

The survey area is shown in Fig. 6.5. For the purpose of estimating the redishift distribution of the radio galaxies, we apply DR1, DR2, and DR3 data of KiDS galaxies.

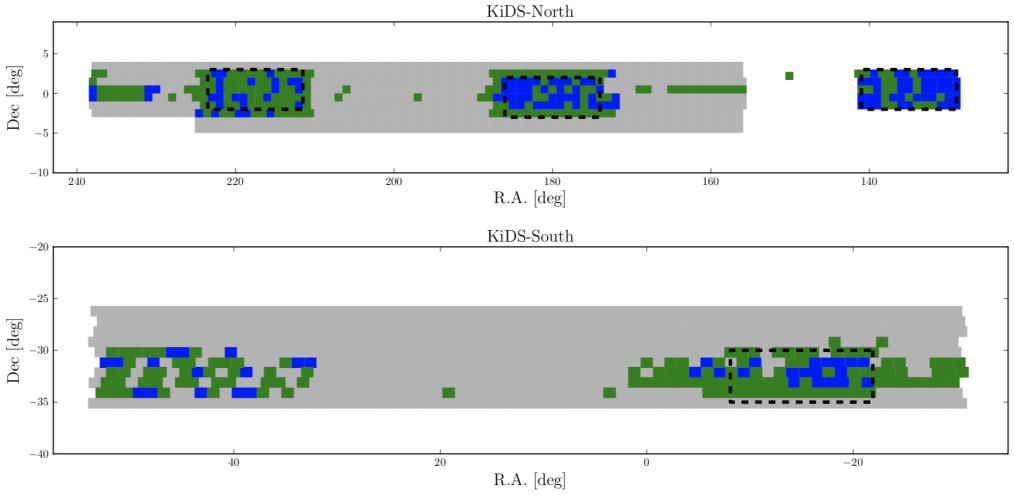

Figure 6.5. Sky distribution of survey tiles released in KiDS-ESO-DR3 (green) and in the previous releases KiDS-ESO-DR1 and -DR2 (blue). The multi-band source catalogue covers the combined area (blue + green) and the full KiDS area is shown in grey. Top: KiDS-North. Bottom: KiDS- South. Black dashed lines delineate the locations of the GAMA fields; the single pointing at RA=150° is centered at the COSMOS/CFHTLS D2 field. Referred from Figure 1 in J. T. A. de Jong *et al.* [196]

[4] `http://kids.strw.leidenuniv.nl/`

6.5.2 Stacking analysis

Practically, we stack the position of optical galaxies for each radio galaxies at certain range of angles, picking up the optical galaxies that could be associating with the radio samples.

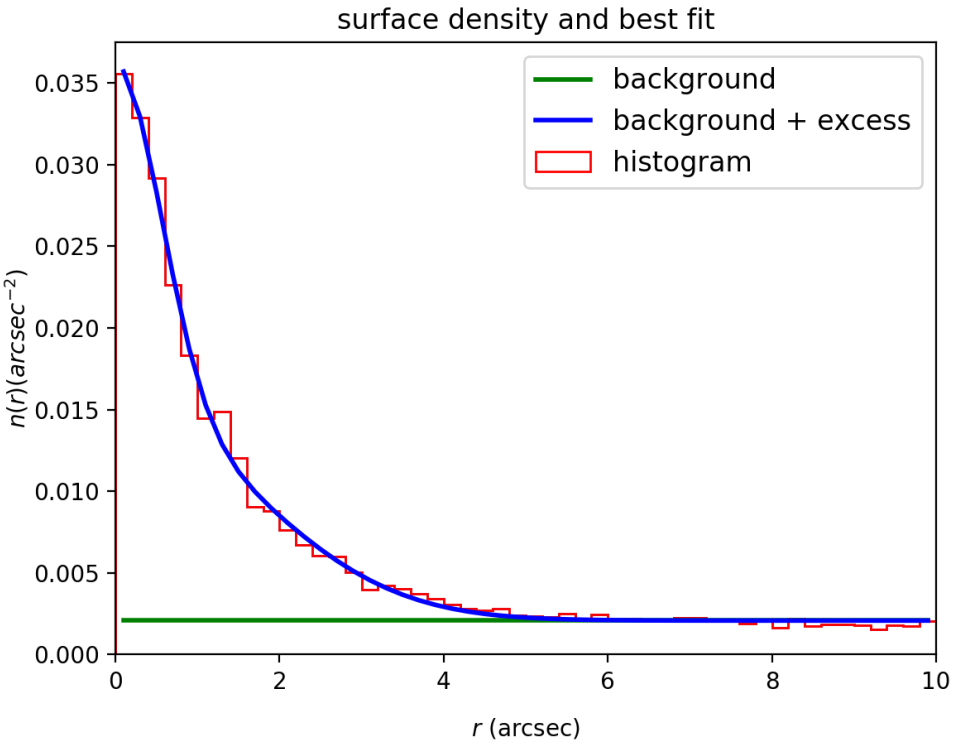

Figure 6.6. Radial number density of KiDS galaxies stacked around a radio sources

The stacked distribution of KiDS galaxies is shown in Fig. 6.6. We see that a significant concentration of the stacked KiDS galaxies around a radio galaxies, roughly $r \lesssim 4$as. The radial number density in Fig. 6.6 is fitted by the following function,

$$n(r) = n_0 \left(1 + \alpha_1 e^{-r^2/2\sigma_1^2} + \alpha_2 e^{-r^2/2\sigma_2^2}\right) , \tag{6.5.1}$$

The best fit value is $(n_0, \alpha_1, \alpha_2, \sigma_1, \sigma_2) = (2.080 \cdot 10^{-3}, 10.29, 6.037, 0.3053, 2.957)$. We find that the background component appears at as the best-fitted line of the background well fits at $r \gtrsim 6$as. We conclude that the member galaxies associating with the radio galaxies are included within $r < 4$as, and the background galaxies are well picked up at $r > 6$as.

In order to remove the background distribution of the KiDS galaxies, we select the KiDS galaxies in range of $r > 10$as where the background components dominates as shown in Fig. 6.6, obtaining the histogram of the background KiDS galaxies in redshifts. The redshift distribution of the KiDS galaxies inferred as the ones in the concentration are shown in Fig. 6.7.

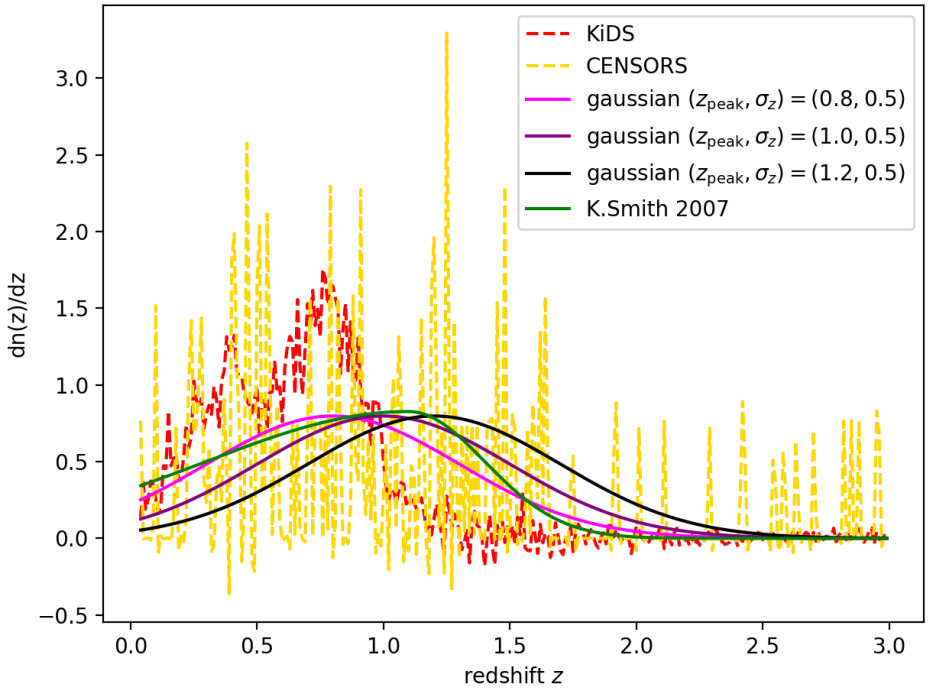

Figure 6.7. Various redshift distributions. All the redshift distributions are obtained by interpolation at quadratic order. Note that the distribution of CENSORS is sometimes crossing to negative due to the interpolation.

In Fig. 6.7, we find that the redshift distribution of the radio galaxies estimated by KiDS (red solid line) is more peaky at $z \lesssim 1$ and smaller at $z \gtrsim 1$ than the other distributions. This might imply that we miss the radio galaxies at $z > 1$ by the stacking analysis. One possibility to explain the feature of the red solid line is that the contamination of the KiDS galaxies which are not accompanied with the radio galaxies as the members of clusters. We check this in terms of the distribution of KiDS galaxies in I-band magnitude space, which is shown in Fig. 6.8. Fig. 6.8 shows an another perspective to check how the selected galaxies in the stacking distribution are distributed in its I-band magnitude. We find that the KiDS galaxies within 4as

from radio positions are bias to lower magnitude, i.e., more brighter galaxies. This can indicate that the selected galaxies that locate 4as from radio positions are likely to be the foreground galaxies for distant radio sources. Hence we conclude that we should be doubtful to use the stacked KiDs galaxies as a tracer of the radio galaxies distributions in redshift space. Hereafter, we use the redshift distribution of radio galaxies estimated by K. Smith *et al.* 2007 [197].

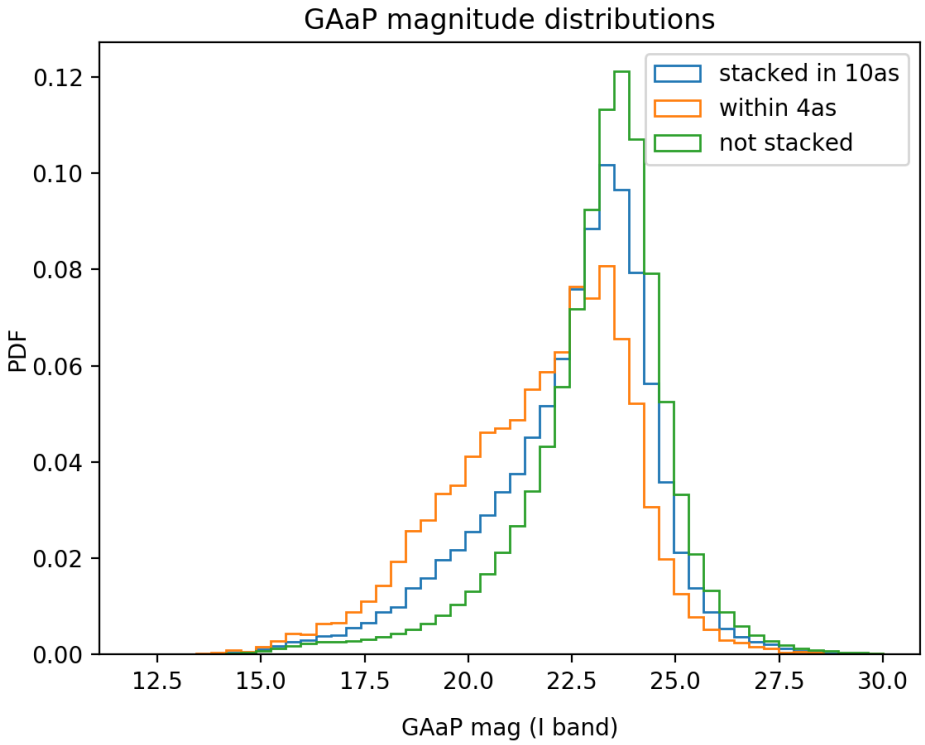

Figure 6.8. I-band magnitude of KiDS galaxies

6.6 Angular power spectra of radio galaxies and CMB lensing

We compute the angular power spectra of the radio galaxies in NVSS and SUMSS and Plack 2015 CMB lensing. Theoretical predictions of the kernel function of the radio galaxies are computed with the fidutial ΛCDM model (specifically given in Sec. 6.2) and the redshift distribution of K. Smith *et al.* 2007 [197]. We assume that bias parameter of the radio galaxies stays constant. To measure the angular power spectra of the radio galaxies, it is important to consider the shot noise subtraction which dominates the real signals at higher multipoles. What is crucial is that the radio signals from a massive galaxy are double or more image. In number counting, the multiple images cause the miscounting of the true number of radio galaxies. Especially, the subtraction for shot noise is crucially incorrect once the multiple sources are included.

6.6.1 Modelling for contamination of double images

For computing the power spectrum, it is often the case that we treat a galaxy from observation as a single source. In the most of the previous surveys, the treatment efficiently works for cosmological measurements. When we use a data of radio surveys, however, the situation, the prescription with a single image sometimes fails. There are two reasons. Firstly the radio emission from a galaxy is continuum of synchrotron radiation, only providing contour map of radio intensity. Some radio signals from nearby radio galaxies is hard to be resolved as point source. Secondly, radio signals spot off from the centre of mass of a galaxy, mainly coming from the relativistic jet outflow. The jet is tightly beamed until stopping at some distance where inter galactic medium bumps with the jet. Typically the jet has several times larger in its width than the size of a galaxy. The brightness of the bumped regions is peculiarly highest in radio signals, therefore most of radio signals have a couple of bright spots well separated in resolution. For this reason, from analyses with radio signals could cause the overestimation of the number of galaxy. In this section we provide a prescription for the overestimation of the number of radio galaxies.

$$\delta_{\rm radio} = \frac{N_1\delta_1 + 2N_2\delta_2}{N_1 + 2N_2}\,, \tag{6.6.1}$$

$$\left\langle \delta^2_{\rm radio} \right\rangle = \frac{N_1^2\left\langle\delta_1^2\right\rangle + 4N_1N_2\left\langle\delta_1\delta_2\right\rangle + 4N_2^2\left\langle\delta_2^2\right\rangle}{(N_1+2N_2)^2} \tag{6.6.2}$$

Notice that δ_1 and δ_2 is not independent. Then we assume the linear response to the density fraction δ_m as $\delta_i = \bar{b}\beta_i\delta_m$ $(i = 1, 2)$[5]. Then we obtain

$$\delta_{\rm radio} = \bar{b}\delta_m \times \{\beta_1(1-2f) + 2\beta_2 f\} \,, \tag{6.6.3}$$

$$\left\langle \delta^2_{\rm radio} \right\rangle = \bar{b}^2 \left\langle \delta^2_m \right\rangle \times \{\beta_1(1-2f) + 2\beta_2 f\}^2 \,, \tag{6.6.4}$$

where $f \equiv N_2/(N_1 + 2N_2)$ denotes the fraction of the doubles. We choose $\bar{b} = 1$ and define $b = \beta_1(1-2f) + 2\beta_2 f$.

Then the noise terms are formulated as

$$\delta_{\rm shot} = \frac{N_1\delta_{{\rm shot},1} + 2N_2\delta_{{\rm shot},2}}{N_1 + 2N_2} \,, \tag{6.6.5}$$

$\langle\delta_1\rangle = 0 = \langle\delta_2\rangle$, $\langle\delta_{\rm shot}\rangle = 0$. For the variance of $\delta_{\rm shot}$, $\left\langle\delta^2_{\rm shot}\right\rangle$, the statistical independence of δ_1 and δ_2 leads the elimination of the cross correlation between δ_1 and δ_2.

$$\left\langle \delta^2_{\rm shot} \right\rangle = \frac{N_1^2 \left\langle \delta^2_{{\rm shot},1} \right\rangle + 4N_2^2 \left\langle \delta^2_{{\rm shot},2} \right\rangle}{(N_1 + 2N_2)^2} \,, \tag{6.6.6}$$

$$\left\langle \delta^2_{{\rm shot},i} \right\rangle = \frac{1}{N_i} \ (i = 1, 2) \,, \tag{6.6.7}$$

and we obtain

$$\left\langle \delta^2_{\rm shot} \right\rangle = \frac{1+2f}{N_1 + 2N_2} \,, \tag{6.6.8}$$

where again $f \equiv N_2/(N_1 + 2N_2)$ denotes the fraction of the doubles.

$$C_{gg}^{\rm pseudo} = \frac{1}{f_{\rm sky}} C_{gg}^{\rm data} - 4\pi \frac{1+2f}{N_1 + 2N_2} \,, \tag{6.6.9}$$

In summary, we develop the formula that takes into account the systematises effects of the doubles in the number fluctuation of the radio galaxies and the shot noise. Remarkably, the effect of the doubles is prominent in the shot noise while the power spectrum less suffers with the doubles.

[5]In reality, the doubles is more relevant in the lower redshifts since the image is closer enough to recognize the double images. In cases the linear bias evolves in time, $\beta_1 \neq \beta_2$ is reasonably expected. Although the offset of a position from the centre of mass from the radio sources should be taken into account, but the bias factors almost degenerate with the offset effect.

Then we fit the parameters by using galaxy auto power. We choose $\bar{b} = 1$. $f_{\rm sky}(N_1 + 2N_2) = 833,564$ and $f = 0.153$. The sky fraction is given as $f_{\rm sky} = 0.823$.

$dn(z)/dz$	b
KiDS	1.14
CENSORS	1.07
K.Smith 2007	1.58

Table 6.2. Fitted parameters

In Fig. 6.10, the data points shows two peaks at $\ell \sim 180$ and $\ell \sim 300$, which does not fit with the theoretical predictions.

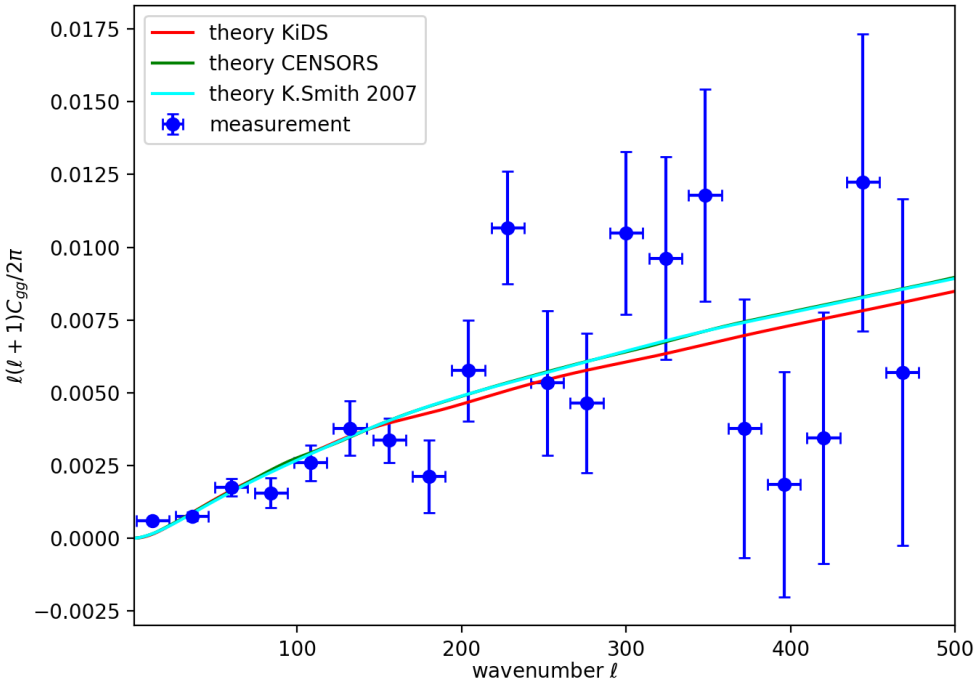

Figure 6.9. The comparison of theory and data (shot noise subtracted) in auto correlation of the radio galaxies

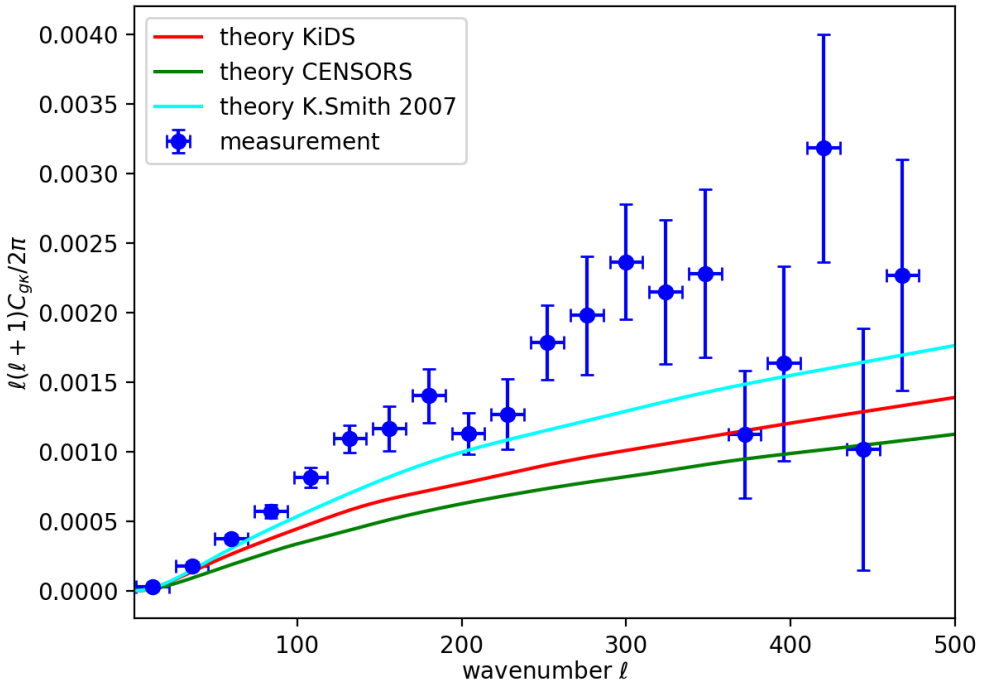

Figure 6.10. The comparison of theory and data in cross power correlation of the CMB lensing and radio galaxies

6.7 Angular cross-power of radio galaxy with low z optical galaxies

We test the three different redshift distributions in Table. 6.6.1 by using angular cross-power with low z galaxies. We use the optical galaxies in 2MASS Photometric Redshift catalogue (2MPZ)[6] [198], WISE×SuperCOSMOS (WI×SC)[7] [199], and the photometric redshift catalogue of Sloan Digital Sky Survey (SDSS DR12)[8] [200], all of whose positions are well measured in redshift space.

6.7.1 Redshift distributions of optical galaxies

We use the redshift distributions of 2MPZ, WI×SC, and SDSS DR12 optical galaxies, those which are well investigated in J. A. Peacock and M. Biliki 2018 [179]. The distributions are shown in Fig. 6.11 and 6.12. We confirm that the redishift distribution successfully reproduces. The redshift distribution of the galaxies in 2MPZ - WI×SC or SDSS DR12 are given as

The value of the biases for 2MPZ, WI×SC, and SDSS DR12 galaxies are given in Table. 6.7.1[9]

[6] `http://ssa.roe.ac.uk//TWOMPZ`

[7] `http://ssa.roe.ac.uk/WISExSCOS.`

[8] `http://www.sdss.org/dr12/algorithms/photo-z/`

[9] Note that the best-fitted values of the biases are obtained by assuming a different fiducial cosmology [179]. This may not cause the problems for our results because the uncertainty of the cosmological parameters is at most percent level difference.

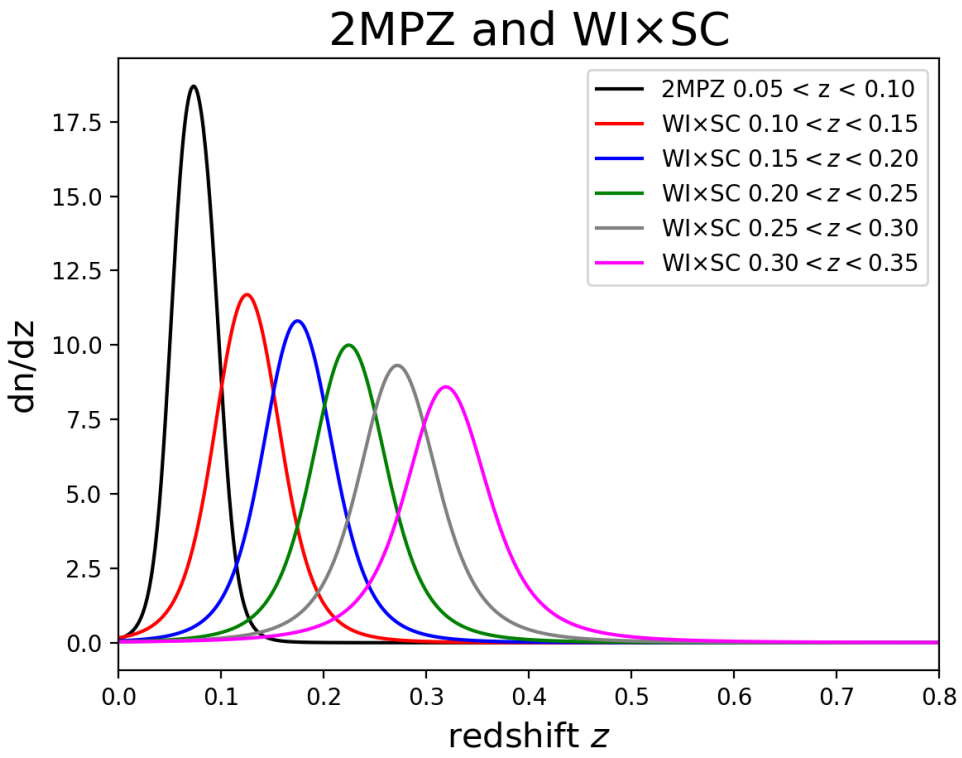

Figure 6.11. The redshift distribution of 2MPZ-WI×SC galaxies

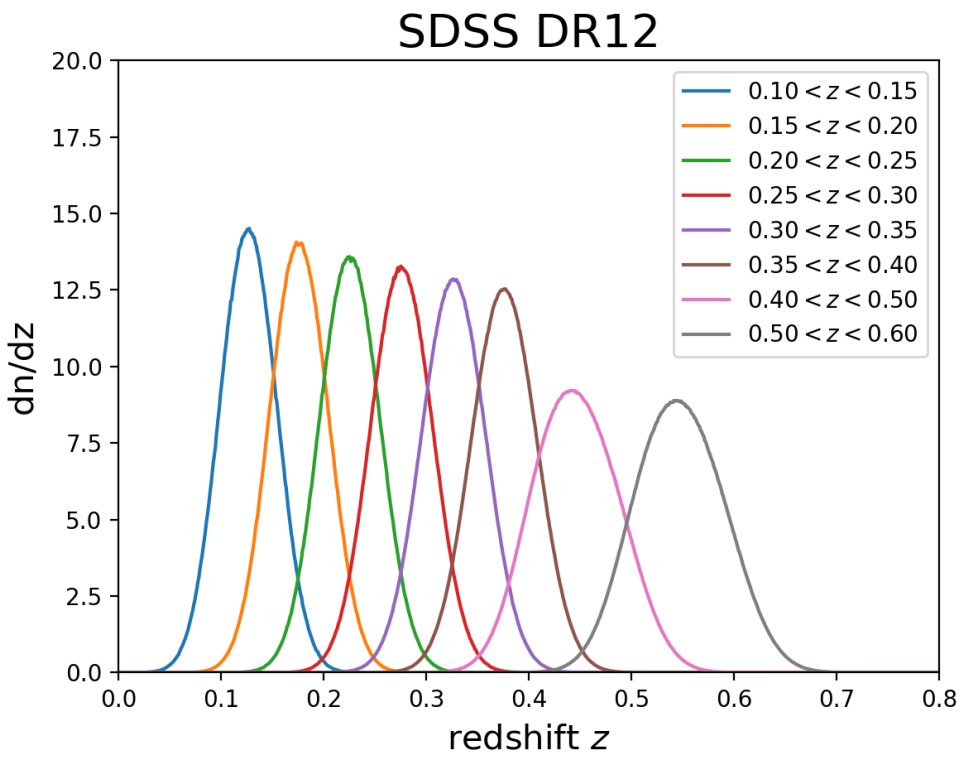

Figure 6.12. The redshift distribution of SDSS DR12 galaxies

Dataset	z	$b(z)$
2MPZ	0.075	1.182±0.009
WI×SC	0.125	1.086±0.007
WI×SC	0.175	1.126±0.007
WI×SC	0.225	1.144±0.013
WI×SC	0.275	1.206±0.009
WI×SC	0.325	1.548±0.018
SDSS	0.125	0.915±0.010
SDSS	0.175	0.894±0.006
SDSS	0.225	0.909±0.007
SDSS	0.275	0.902±0.009
SDSS	0.325	0.888±0.013
SDSS	0.375	0.966±0.020
SDSS	0.450	0.980±0.019
SDSS	0.550	1.245±0.011

Table 6.3. Bias for 2MPZ, WI×SC, and SDSS DR12

6.7.2 Theoretical predictions

We apply the redshift distributions and biases of 2MPZ, WI×SC, and SDSS DR12 galaxies for optical galaxies. We select a model of radio kernel with K. Smith 2007.

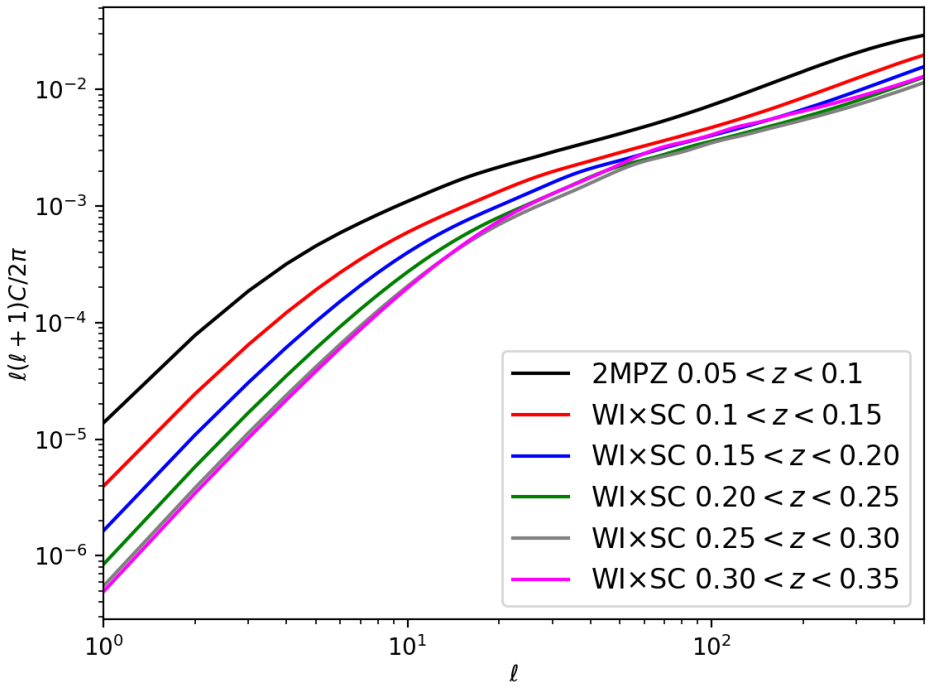

Figure 6.13. Model prediction of the cross-power spectrum between NVSS-SUMSS and 2MPZ-WI×SC galaxies

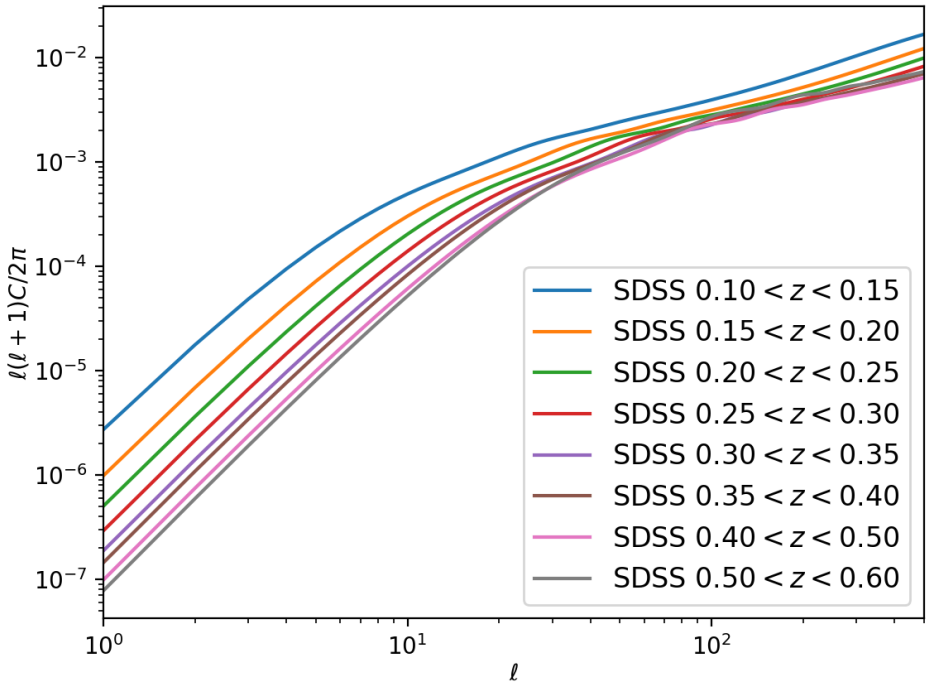

Figure 6.14. Model prediction of the cross-power spectrum between NVSS-SUMSS and SDSS DR12 galaxies

6.7.3 Comparison models with real data

We compute the theoretical prediction of the three models and the data.

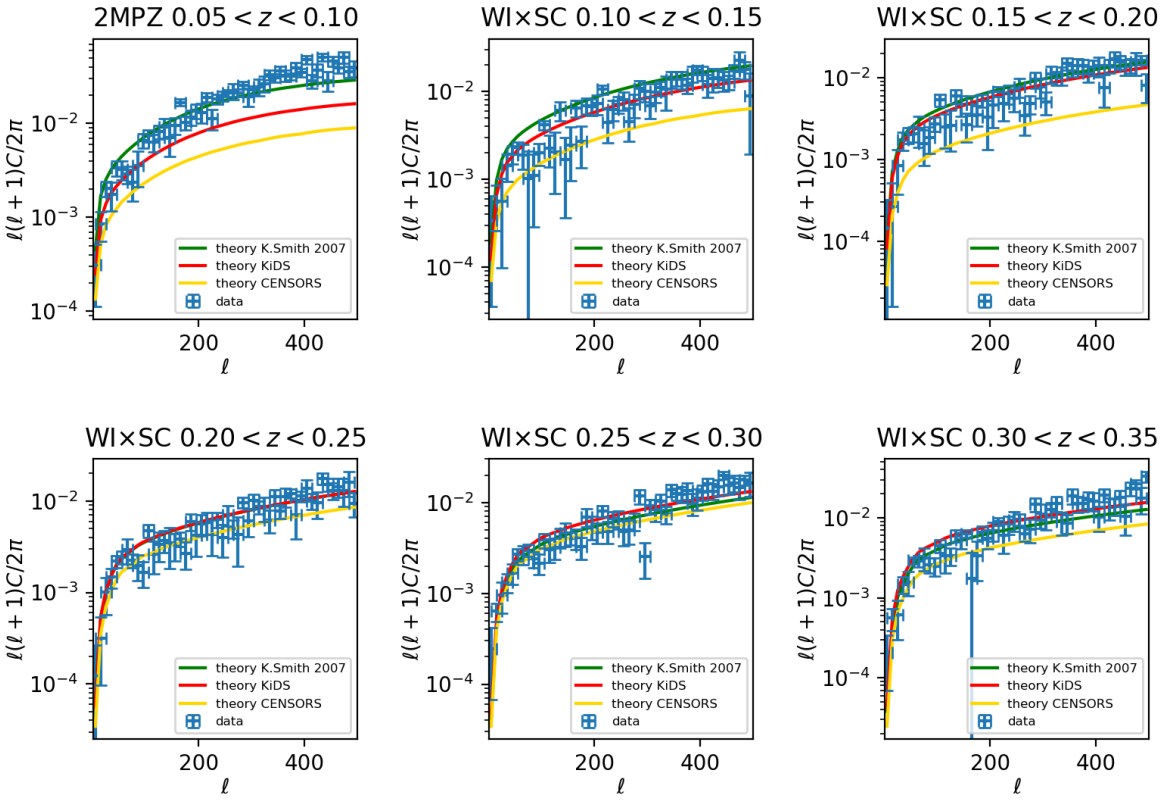

Figure 6.15. Comparison of data and theory in the model prediction of the cross power spectrum between NVSS-SUMSS and 2MPZ-WI×SC

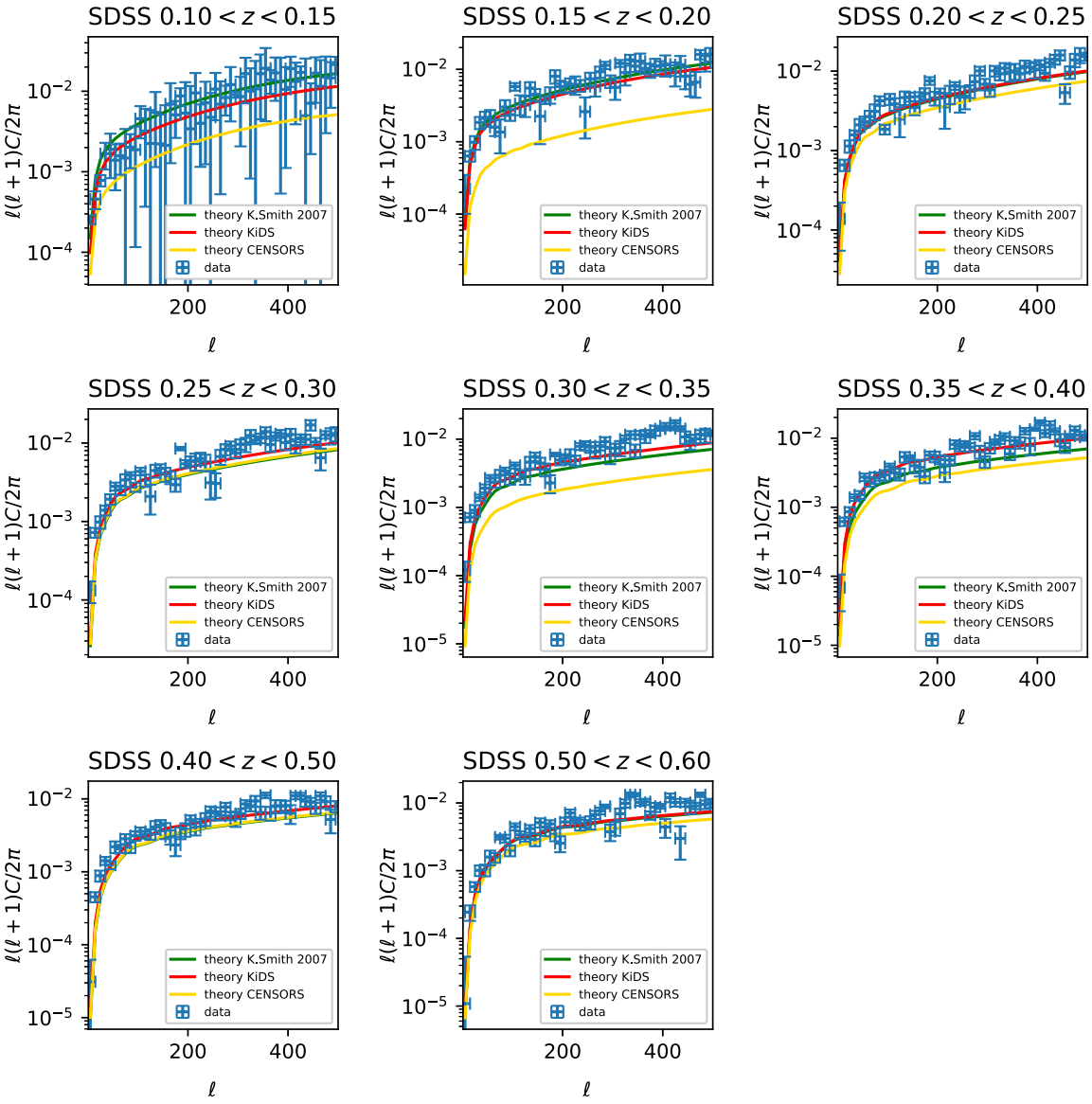

Figure 6.16. Comparison of data and theory in the cross power spectrum between NVSS-SUMSS and SDSS DR12

In Figs. 6.15 and 6.16, we find that the model predictions of K. Smith 2007 and KiDS are well fitted in the errors of the data, while CENSORS deviates from the data points frequently. The model of KiDS is off the data $0.05 < z < 0.1$ with 2MPZ. The lowest redshift bin with 2MPZ data shows that K.Smith 2007 is well fitted in comparison to KiDS and CENSORS. Since we already know from Fig. 6.7 that the redshift distributions of the three models are almost identical, we conclude that the bias parameter should be around $b = 1.58$ below $z < 0.1$. The rest of the redshift bins shows slight differences for the models. This indicates that the detail of the three models does not significantly change the predictability of the measured signals.

6.8 Normalised correlation coefficient

We test the three different models in Table. 6.6.1 by the normalized correlation coefficient,

$$r_{g\kappa} \equiv \frac{C_{g\kappa}}{\sqrt{C_{gg}C_{\kappa\kappa}}}\,, \tag{6.8.1}$$

One imediately notice that this estimator is independent from any constant scaling factors, e.g., H_0, $\Omega_{\rm m0}$, and a constant bias. Since we assume that the bias is constant for the three models, $r_{g\kappa}$ directly trace the difference of the redshift distributions.

Fig. 6.17 shows the comparison with For reference, we plot three other Gaussian models of redshift distribution that are previously shown in Fig. 6.7. We find that the KiDS and CENSORS are not fitted with the measured data points. K. Smith 2007 is more close to the data points. Interestingly, the model predictions are closer to the data as the positions of the peaks move to higher redshifts. None of the models are well fitted much with oscillatory structures at $\ell \sim 150$ and $\ell \sim 320$. Note that the oscillatory features should be identical to those in Fig. 6.10.

6.9 Conclusions

We measured the angular cross-power between the radio galaxies in NVSS-SUMSS catalogs and CMB lensing in Planck 2015. We tried determining the redshift distribution of the radio galaxies by the stacking analysis of KIDS DR1-3 galaxies. Then we measure the angular cross-power between NVSS-SUMSS radio galaxies and 2MPZ-WISE×SuperCOSMOS (WI×SC)-SDSS DR12 optical galaxies. We compare the cross power spectrum with the measurements and found the followings,

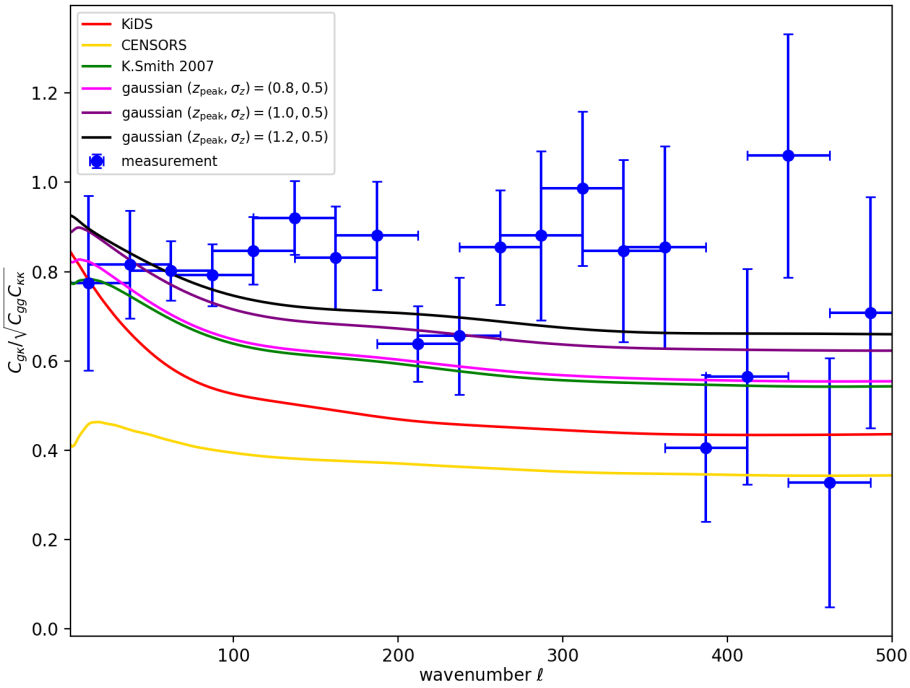

Figure 6.17. Correlation coefficient between radio galaxy and CMB lensing. The dots and lines show the measurement and the theoretical predictions, respectively. The data points are plotted with the auto-correlation of the radio galaxy estimated with $dn(z)/dz$ of K. Smith 2007.

- The estimated redshift distribution by KIDS galaxies has peaks at $z \lesssim 1$, and damps over $z \gtrsim 1$. This can be caused by the contamination the foreground KiDS galaxies in lower redshifts.

- The angluar auto power spectrum of the radio galaxies and the formula shot noise is modelled to deal with the multiple images of radio sources for one radio galaxy. We obtained the best-fitting parameters for three different redshift distributions; KIDS, K. Smith 2007, and CENSORS. We find that the fraction of double images are universally given as $f = 0.153$ irrespective to the redishift distributions, whereas the bias parameters fluctuates. .

- The angular cross power between the radio galaxies and the well-measured optical galaxies in redshift range $0.05 < z < 0.6$ shows that the model of K. Smith 2007

is the best to explain the data. We conclude that the bias should be close to $b = 1.58$ at redshift $z < 0.1$

In conclusion, the determination of the redshift distribution of radio galaxies should be more considered. For testing gravity and cosmological models, more information to constrain the models. Nevertheless, we confirmed that the NVSS-SUMSS data at $z \lesssim 0.6$, where the data is overlapped with 2MPZ, WI×SC, and SDSS DR12, is consistent with the ΛCDM concordance concordance cosmology. We will continue the work to measure more reliable information at $z \gtrsim 0.6$.

Chapter 7

Conclusions

"What makes the desert beautiful is that somewhere it hides a well."
The Little Prince, Antoine de Saint-Exupery

Framework for testing the fundamental principles in gravitation and cosmology are essential to forgo into the better understanding of physics and the Universe itself. Any possibility to go beyond the standard understanding of gravity, i.e., Einstein's general relativity in cosmology should be tested in existing and forthcoming observations. Since the cosmic acceleration was discovered via SN-Ia supernovae, one can reconsider the law of gravity at cosmological scales. In theoretical perspective, the UV incompleteness of Einstein gravity motivate to construct a theory that is regular at high energy scales. In this approach, the control of the higher curvature terms with respect to general covariance could be a problematic issue.

A starting point to think gravity more than Einstein gravity is to add an extra degree of freedom in gravity sector. Then one wonders how large the extension beyond the standard gravitation and cosmology are possible. It has been known that the theories with a scalar field is hugely extensible in mathematical and analytic ways, resulting in obtaining abundant knowledge of gravity e.g., Horndeski theory, or its conformal/disformal extensions, i.e., the DHOST theory. Phenomenologically, however, the theoretical predictions of such theories must be viable to explain the primordial initial conditions, observed expansion history of the Universe, and structure formation. Until recently, cosmological modelling of gravity theories has been limited in some specific types of theories, leaving the vast of theory space to be constrained.

In light of observational cosmology, the role of the extra degree of freedom is significant, especially to explain the cosmic acceleration. As concisely described in Quintessence field, a light scalar field succeeds in realising an accelerating universe.

Theoretical interests in these models are to consider the shift symmetry, the scalar field is massless. The tracker solution is obtained when we respect the shift symmetry (or Galileon symmetry). However, these assumptions are claimed to be hypothetical because the assumptions might model-dependent and it is not observationally proven unlike the gauge symmetries in standard model of particle physics. Therefore, it is important to reduce the assumptions as much as possible; more model-independent or observationally-supported ways of probe theory space.

As argued in Chapter. 4, we investigate a wide range of models with the assumption that the scalar field is slowly changing in comparison to the Hubble time scale. The slow-rolling scalar field is viable because we know that the ΛCDM model, which is obtained in the limit of $\dot{\phi} = 0$, well describes the cosmic expansion history of the Universe. Although it is rough to estimate cosmological evolution, but it is meaningful to investigate at low redshifts. We found that the universal correlation laws between characteristic parameters such as EFT parameters $\alpha_{M,K,B,T,H}$ that specify physical features of scalar-tensor theories are analytically and numerically derived , being consistent with the observational constraints of the cosmic expansion history. We succeeded in predicting various signatures of scalar-tensor theories deviating from the ΛCDM concordance cosmology. In the forthcoming observations, those predictions are able to be tested by cosmic shear, CMB lensing, or gravitational-wave observations.

For the initial conditions of the Universe, what we have known by observations is that the inflationary cosmology with a single scalar field well match with the observations of CMB anisotropy. As the constraints by WMAP and Planck data prove, the initial condition of the Universe is almost adiabatic and primordial tensor modes are well suppressed below several percent level in comparison to the primordial scalar fluctuations. Since the most of inflation models with the single scalar field satisfies the adiabaticity and suppression of tensor modes only by assuming slow-roll conditions. This raises a possibility to test whether or not the fundamental principles of physics is still satisfied in the inflationary Universe. The most violent way to break Einstein gravity is to break the local Lorentz invariance of space-time itself. Despite a simple thinking it seems, constructing such a theory is hard to accommodate without spoiling physical concepts, i.e., unitarity, causality, energy conservation, etc. Ghost condensation or Horáva-Lifshitz gravity are well-defined gravity theories to realise cosmology without the local Lorentz invariance.

The price to pay for the violation of local Lorentz invariance is to introduce an extra scalar degree of freedom , Khronon, in the Universe. One can expect whether Khronon breaks the adiabaticity or suppression of primoridial gravitational waves despite the

slow-roll conditions work. In Chapter. 6, in the framework of Hořava-Lifshitz gravity, we found that the adiabaticity and suppression of the primordial gravitational waves are still obtained, thanks to the mass gap of Khronon that is higher than typical inflationary energy scale. This suggests that the violation of local Lorentz invariance could not be falsified by the current observations of CMB. The spectrum of the primordial gravitational waves only tells a signature of the violation of local Lorentz invariance.

The visualisation of the growth of Large Scale Structure (LSS) allows us to verify the law of gravity at cosmological scales. Gravitational lensing via LSS evidently shows the geometrical nature of gravity, and thus it is possible to test gravity theories. CMB lensing is a good phenomenon for testing gravity because it is directly based on the fundamental principles of gravity, even when non-linear regime of structure formation is taken into account. In other words, theoretical prediction of CMB lensing is straightforward. Extracting the signal of CMB lensing, however, it is inevitable to take into account the properties of tracers, i.e., galaxies. At present, it is possible to know distribution of galaxies in redshift space has been well known in the whole sky, e.g., 2MPZ, WISE×SuperCOSMOS (WI×SC), or SDSS DR12. A weak point of these whole sky map of galaxies is that the redshifts are shallow,i.e., $z \lesssim 0.6$. Further investigation in higher redshift, i.e., $z > 1$, will be significant. This can be achieved by measuring CMB lensing signals from massive radio galaxies toward the tests of gravity in higher redshifts.

In Chapter 6, we developed the methodology to measure CMB lensing via radio galaxies in NVSS-SUMSS catalogue being sensitive for tomographic scanning. We confirmed that the simple estimation of the redshift distribution of radio galaxies is not fully established. In the range of redshift $0 \lesssim z \lesssim 0.6$, the cross-power spectrum between the 2MPZ, WISE×SuperCOSMOS (WI×SC), or SDSS DR12 and radio galaxies shows that the different types of redshift distributions are less significant to explained the measured signals. A promising findings is that we measured the cross-correlation between lensing convergence of CMB by Planck 2015 and the clustering of radio samples with less statistical errors compared to the previous measurement in K. Smith *et al.* 2007. Interestingly, we confirmed some fluctuating features in the cross power between the radio galaxies and CMB lensing, which may tells us more information of the redshift distribution and the bias of the radio galaxies. We will update more findings in future.

In the forthcoming decades, we will reach to great opportunities to develop cosmology in observations at unprecedented level of precision. It will be exciting if we can see

any signature of new physics, deepening our understanding of the Universe. We hope to get a new unknown which Prof. Stephen Hawking would have not expected.

Appendix A

Formalism of the scalar-tensor theory in numerical simulation

Contents:

- selection of the seed theory: the ΛCDM model
- perturbative expansion of conformal/disformal transformation

The Lagrangian of the seed theory is given by

$$S_{\rm seed} = \int d^4x\sqrt{-g}\left\{\frac{M_{\rm pl}^2}{2}R - \Lambda_0^4\right\}, \tag{A.0.1}$$

With the FLRW metric, we obtain the Friedmann Universe with the cosmological constant Λ_0^4,

$$3M_{\rm pl}^2H^2 = \Lambda_0^4\,, \tag{A.0.2}$$
$$M_{\rm pl}^2(2\dot{H} + 3H^2) = \Lambda_0^4\,, \tag{A.0.3}$$

ending up with the De Sitter solution is obtained. We rewrite Eq. (A.0.1) into the ADM form for convenience, and obtain

$$S_{\rm seed} = \int d^4xN\sqrt{\gamma}\left\{\frac{M_{\rm pl}^2}{2}\left(K_{ij}K^{ij} - K^2 + {}^{(3)}R\right) - \Lambda_0^4\right\}, \tag{A.0.4}$$

where $K_{ij} \equiv \frac{\dot{\gamma}_{ij} - \nabla_i N_j - \nabla_j N_i}{2N}$ is the extrinsic curvature and ${}^{(3)}R$ is the 3 dimensional Ricci scalar.

A.1 Conformal/disformal transformation

A.1.1 Conformal transformations

Conformal transformation is defined as

$$g_{\mu\nu} \to C(\phi, X) g_{\mu\nu}\,, \tag{A.1.1}$$

Characteristics. The strength of gravitational couplings are adjusted, while the Lorentz symmetry is kept for all the massless fields, such as photon, graviton, or a massless scalar field.

A.1.2 Disformal transformations

$$g_{\mu\nu} \to C(\phi, X) g_{\mu\nu} + D(\phi, X)\partial_\mu\phi\partial_\nu\phi\,, \tag{A.1.2}$$

The inverse transformation is given by

$$g^{\mu\nu} \to C^{-1}(\phi, X) g^{\mu\nu} - \frac{1}{C(\phi, X) - D(\phi, X)X}\frac{D(\phi, X)}{C(\phi, X)}\partial^\mu\phi\partial^\nu\phi\,, \tag{A.1.3}$$

Disformal coupling changes the propagation speed of the massless particle depending on its gravitational interaction.

The frame transformation is given by

$$g_{\mu\nu} \to g_{\mu\nu} = C(\phi, X)\tilde{g}_{\mu\nu} + D(\phi, X)\partial_\mu\phi\partial_\nu\phi\,, \tag{A.1.4}$$

Here we define that $X \equiv -g^{\mu\nu}\partial_\mu\phi\partial_\nu\phi/2$. We assume that the background is a flat FLRW universe,i.e., $N_i = 0$ and $\gamma_{ij} = a^2\delta_{ij}$ we impose the unitary gauge $\partial_i\phi = 0$. Then we instantly obtain $X = \dot{\phi}^2/2N^2$.

$$N = \sqrt{C + 2DX}\tilde{N}\,, \tag{A.1.5}$$

$$\sqrt{\gamma} = C^{3/2}\sqrt{\tilde{\gamma}}\,, \tag{A.1.6}$$

$$K_{ij} = \frac{C}{\sqrt{C + 2DX}}\left(\tilde{K}_{ij} + \frac{\dot{C}}{NC}\tilde{\gamma}_{ij}\right)\,, \tag{A.1.7}$$

$$^{(3)}R = \frac{1}{C}{}^{(3)}\tilde{R}\,, \tag{A.1.8}$$

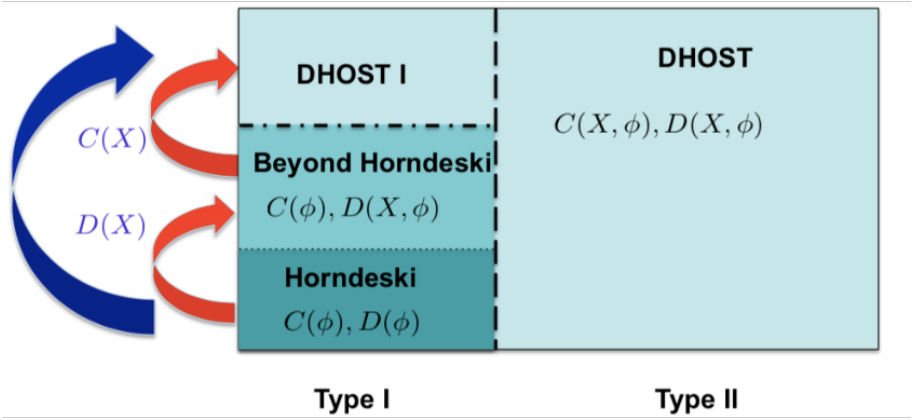

Figure A.1. Structure of the conformal/disfomal chains of scalar-tensor theories shown in []

Then the seed action is expressed in terms of the transformed frame as

$$S = \int d^4x\tilde{N}\sqrt{\tilde{\gamma}}\left[\frac{M_{\rm pl}^2}{2}\left\{\frac{1}{C+2DX}(\tilde{K}_{ij}\tilde{K}^{ij}-\tilde{K}^2)-\frac{1}{C}{}^{(3)}\tilde{R}\right\}-\Lambda_0^4\sqrt{C+2DX}C^{3/2}\right.$$
$$\left.-M_{\rm pl}^2\left\{\frac{2\dot{C}/NC}{C+2DX}\tilde{K}+\frac{3}{C+2DX}\left(\frac{\dot{C}}{NC}\right)^2\right\}\right], \tag{A.1.9}$$

The propagation speed of GW is $c_T^2 = C/(C+2DX)$. According to the simultaneous observations of GW170817 and GRB170817A gives a novel condition $D=0$, meaning D is tightly pinned down to the trivial value. With $D=0$ the action in Eq. (A.1.9) is simplified as

$$S = \int d^4x\tilde{N}\sqrt{\tilde{\gamma}}\left[\frac{M_{\rm pl}^2}{2C}(\tilde{K}_{ij}\tilde{K}^{ij}-\tilde{K}^2-{}^{(3)}\tilde{R})-\Lambda_0^4C^2\right.$$
$$\left.-M_{\rm pl}^2\left\{\frac{2\dot{C}}{NC^2}\tilde{K}+\frac{3}{C}\left(\frac{\dot{C}}{NC}\right)^2\right\}\right], \tag{A.1.10}$$

A.1.3 Correspondence of covariant and ADM action

In the ADM expression, the effective action described in the unitary gauge is more accessibly simplified. Observationally, since the complication of the EFT formalism is not important, it is preferred to choose what types of functions realize the changes of phenomenological quantities. In fact as we will see the following formulations, the functions that would be phenomenologically important are defined. In addition to such a simplification, the structure of the specific theories such as the Horndeski theory or are formalized in covariant way. Here let us introduce a popular prescription to map the covariantly-given theories to the EFT form. Here we follow J.Gleyzes in 2014 [61]. The Gauss - Goddazi equation is given as

$$ {}^{(4)}R = {}^{(3)}R - K^2 + K_\mu K^\mu + 2\nabla_\mu (K n^\nu - n^\rho \nabla_\rho n^\mu) \,, \tag{A.1.11} $$

The action L_4 then changes to

$$ L_4 = B_4 {}^{(4)}R + (A_4 + B_4)(K^2 - K_{\mu\nu}K^{\mu\nu}) - 2B_4 \nabla_\mu (K n^\mu - \dot{n}^\mu) \,, \tag{A.1.12} $$

By recalling $\dot{n}_\mu = h^\nu_\mu \nabla_\nu X/(-2X)$,

$$ K^2 - K_{\mu\nu}K^{\mu\nu} = \frac{(\Box\phi)^2 - \phi_{\mu\nu}\phi^{\mu\nu}}{2X} - \frac{\nabla_\mu X (K n^\mu - \dot{n}^\mu)}{X} \,, \tag{A.1.13} $$

Finally L_4 is obtained as

$$ \begin{aligned} L_4 =& B_4 {}^{(4)}R + \frac{B_4 + A_4}{2X}[(\Box\phi)^2 - \phi_{\mu\nu}\phi^{\mu\nu}] \\ &+ \frac{B_4 + A_4 - 2X B_{4X}}{2X^2}(\phi^\mu \phi^\nu \phi_{\mu\nu} \Box\phi - \phi^\mu \phi_{\mu\nu}\phi_\lambda \phi^{\lambda\nu}) \\ &+ (C_4 + 2X C_{4X})\Box\phi - 2X C_{4\phi} \,, \end{aligned} \tag{A.1.14} $$

Then L_5 is given as a similar way Gauss Godazzi relation for the Ricci scalar is given as

$$ R_{\mu\nu} = ({}^{(4)}R_{\mu\nu})_{||} + (n^\sigma n^{\rho (4)}R_{\mu\sigma\nu\rho})_{||} - K K_{\mu\nu} + K_{\mu\sigma}K^\sigma_\nu \,, \tag{A.1.15} $$

$$
\begin{aligned}
&A_5(K^3 - 3KK_{\mu\nu} + K_{\mu\nu}K^{\mu\rho}K_\rho^\nu) \\
&= -A_5(2X)^{-3/2}[(\Box\phi)^3 - 3\Box\phi_{\mu\nu}\phi^{\mu\nu} + 2\phi_{\mu\nu}\phi^{\nu\rho}\phi_\rho^\mu] \\
&\quad + 3A_5(2X)^{-3/2}\left[+\phi^\rho\nabla_\rho X(K^2 - K_{\mu\nu}K^{\mu\nu}) - 2(2X)^{3/2}(K\dot{n}_\mu\dot{n}^\mu - K_{\mu\nu}\dot{n}^\mu\dot{n}^\nu)\right],
\end{aligned}
\tag{A.1.16}
$$

We define an auxiliary function, F_5, such that it satisfies $F_5/4X + F_{5X}/2 = -A_5(2X)^{-3/2}$. By integrating by parts the lastt line in Eq. (A.1.16), the equation changes to

$$
\begin{aligned}
&A_5(K^3 - 3KK_{\mu\nu}K^{\mu\nu} + 2K_{\mu\nu}K^{\mu\rho}K_\rho^\nu) \\
&= -A_5(2X)^{-3/2}[(\Box\phi)^3 - 3\Box\phi\phi_{\mu\nu}\phi^{\mu\nu} + 2\phi_{\mu\nu}\phi^{\nu\rho}\phi_\rho^\mu] \\
&\quad - 3A_5(2X)^{-3/2}\sqrt{2X}\left[\frac{1}{2}(K^3 - 3KK_{\mu\nu}K^{\mu\nu} + 2K_{\mu\nu}K^{\mu\rho}K_\rho^\nu) + K^{\mu\nu}n^\sigma n^{\rho(4)}R_{\mu\sigma\nu\rho}\right. \\
&\quad \left. - 3Kn^\sigma n^{\rho(4)}R_{\sigma\rho} + \dot{n}^\sigma n^{\rho(4)}R_{\sigma\rho}\right] - XF_{5\phi}(K^2 - K_{\mu\nu}K^{\mu\nu}),
\end{aligned}
\tag{A.1.17}
$$

The second term is computed as

$$
\begin{aligned}
B_5K_{\mu\nu}G^{\mu\nu} =& B_5\left[K_{\mu\nu}{}^{(4)}G^{\mu\nu} + K_{\mu\nu}n_\sigma n_\rho{}^{(4)}R^{\mu\sigma\nu\rho} - Kn_\sigma n_\rho{}^{(4)}R^{\sigma\rho}\right. \\
&\left. + \frac{1}{2}(K^3 - 3KK_{\mu\nu}K^{\mu\nu} + 2K_{\mu\nu}K^{\mu\rho}K_\rho^\nu)\right],
\end{aligned}
\tag{A.1.18}
$$

We define that $G_5 \equiv -\int dX B_{5X}(2X)^{-1/2}$ and by integrating by parts, we obtain

$$
\begin{aligned}
B_5K_{\mu\nu}G^{\mu\nu} =& G_5\phi_{\mu\nu}{}^{(4)}G^{\mu\nu} + \left(G_{5\phi} + \frac{B_{5\phi}}{\sqrt{2X}}\right)\phi_\mu\phi_\nu{}^{(4)}G^{\mu\nu} \\
&+ B_5\left[\frac{1}{2}(K^3 - 3KK_{\mu\nu}K^{\mu\nu} + 2K_{\mu\nu}K^{\mu\rho}K_\rho^\nu)\right. \\
&\left. + K_{\mu\nu}n_\sigma n_\rho{}^{(4)}R^{\mu\sigma\nu\rho} - Kn_\sigma n_\rho{}^{(4)}R^{\sigma\rho} + \dot{n}_\mu n_\nu{}^{(4)R^{\mu\nu}}\right],
\end{aligned}
\tag{A.1.19}
$$

The Gauss Godazzi relations for the Einstein tensor $G_{\mu\nu}$ is given as

$$
n_\mu n_\nu{}^{(4)}G^{\mu\nu} = \frac{1}{2}({}^{(3)}R + K^2 - K_{\mu\nu}K^{\mu\nu}),
\tag{A.1.20}
$$

The Lagrangian L_5 is then given as

$$\begin{aligned} L_5 =& G_5\phi_{\mu\nu}{}^{(4)}G^{\mu\nu} - A_5(2X)^{-3/2}[(\Box\phi)^3 - 3\Box\phi\phi_{\mu\nu}\phi^{\mu\nu} + 2\phi_{\mu\nu}\phi^{\nu\rho}\phi^{\mu}_{\rho}] \\ &+ (3A_5 + XB_{5X})\left[\frac{1}{2}(K^3 - 3KK_\mu K^{\mu\nu} + 2K_{\mu\nu}K^{\mu\rho}K^{\nu}_{\rho})\right] \\ &+ X\left(G_{5\phi} + \frac{B_{5\phi}}{\sqrt{2X}}\right){}^{(3)}R + XG_{5\phi}(K^2 - K_\mu K^{\mu\nu})\,, \end{aligned} \tag{A.1.21}$$

By combining the terms from the cubic interaction of the galileon, the Lagrangian L_5 is finally written as

$$\begin{aligned} L_5 =& G_5{}^{(4)}G_{\mu\nu}\phi^{\mu\nu} - (2X)^{-3/2}A_5[(\Box\phi)^3 - 3\Box\phi\phi_{\mu\nu}\phi^{\mu\nu} + 2\phi_{\mu\nu}\phi^{\nu\rho}\phi^{\mu}_{\rho}] \\ &- \frac{XB_{5X} + 3A_5}{(2X)^{5/2}}[(\Box\phi)^2\phi_\mu\phi_\nu\phi^{\mu\nu} - 2\Box\phi\phi_\mu\phi^{\mu\nu}\phi_{\nu\rho}\phi^{\rho} - \phi_{\mu\nu}\phi^{\mu\nu}\phi_\rho\phi_\lambda\phi^{\rho\lambda} + 2\phi_\mu\phi^{\mu\nu}\phi_{\nu\rho}\phi^{\rho\lambda}\phi_\lambda] \\ &+ C_5{}^{(4)}R + C_{5X}[(\Box\phi)^2 - \phi_{\mu\nu}\phi^{\mu\nu}] + (D_5 + 2XD_{5X})\Box\phi - 2XD_{5\phi}\,, \end{aligned} \tag{A.1.22}$$

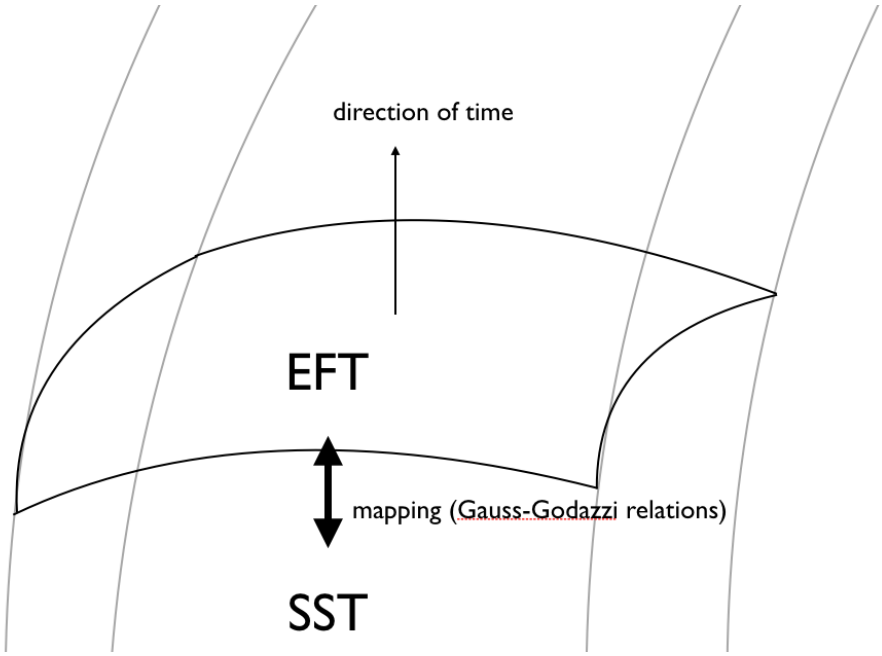

Figure A.2. Image of the correspondence between EFT and scalar-tensor theories (SST)

A.1.4 Covariant/ADM form of Lagrangian

This is a note for the reference of the computation.

- I should write here the expression of the covariant and the ADM form of the Lagrangian.

The computation of $f(\phi, X)\Box\phi$ term.

$$\begin{aligned}
\int d^4x\sqrt{-g}f(\phi,X)\Box\phi &= -\int d^4x\sqrt{-g}\nabla^\mu\phi\nabla_\mu f\,, \\
&= -\int d^4x\sqrt{-g}\nabla^\mu\phi(\nabla_\mu\phi f_\phi + \nabla_\mu X f_X)\,, \\
&= -\int d^4x\sqrt{-g}(-2Xf_\phi - 2XVf_X)\,, \\
&= -\int d^4x\sqrt{-g}(-2Xf_\phi + 2X(AK+\Box\phi)f_X)\,, \\
\therefore \int d^4x\sqrt{-g}(f+2Xf_X)\Box\phi &= 2\int d^4x\sqrt{-g}Xf_\phi - 2\int d^4x\sqrt{-g}AXf_XK\,,
\end{aligned} \tag{A.1.23}$$

where $X = -\nabla_\mu\phi\nabla^\mu\phi/2$ and $V = n^\mu\nabla_\mu A$. The correspondence between the covariant form and the ADM form is thus

$$\begin{aligned}
G_3(\phi,X) &= f + 2Xf_X\,, \\
f &= -\int dX A_3(2X)^{3/2}\,,
\end{aligned} \tag{A.1.24}$$

A.2 Effective Field Theory approach for gravity

A.2.1 EFT with broken space-time symmetry

Preferred frame

In covariant theories, it is arbitrary to take a time coordinate. Under the existence of a scalar field that supports time-like motion, one can take a specific time coordinate such that the scalar field only depends on time, i.e., $\phi = \phi(t)$. More specifically, we choose the direction of time for

$$n_\mu \equiv -\frac{\partial_\mu\phi}{\sqrt{-g^{\rho\sigma}\partial_\rho\phi\partial_\sigma\phi}}\,, \tag{A.2.1}$$

where $n_\mu n^\mu = -1$ is satisfied. The simplest choice of the time coordinate could be $\phi = t$, which is called the unitary gauge. In the unitary gauge the time-like vector n_μ

is simplified as

$$n_\mu = -\frac{\delta^0_\mu}{\sqrt{-g^{00}}}\,, \tag{A.2.2}$$

It is possible to contract tensors by n_μ, leading g^{00} or R^{00} components in the action. The dynamics of a spacetime is projected via the extrinsic curvature,

$$K_{\mu\nu} \equiv h^\sigma_\mu \nabla_\sigma n_\nu\,, \tag{A.2.3}$$

where $h_{\mu\nu} = g_{\mu\nu} + n_\mu n_\nu$ is the projection tensor on the surface perpendicular to n_μ. At first glance, the specification of the time coordinate to the unitary gauge looks violated to the general covariance, which is in parallel to the case of the Einstein-Aether theory where the general covariance is no longer respected. However, the general covariance would recover by a induced degree of freedom by time translation, called Stuckelberg trick. As the diffeomorphism invariance is kept, it is possible to change the time coordinate $t \to t + \pi(x)$ while $\mathbf{x} \to \mathbf{x}$ for spatial coordinate. By considering this peculiar time translation, every time-dependent function transforms along,

$$A(t) \to A(t+\pi) = A(t) + \dot{A}(t)\pi + \frac{1}{2}\ddot{c}(t)\pi^2 + \dots\,, \tag{A.2.4}$$

This coordinate transformation also change the tensor components,

$$g^{00} \longrightarrow g^{00} + 2g^{0\mu}\partial_\mu\pi + g^{\mu\nu}\partial_\mu\pi\partial_\nu\pi\,, \tag{A.2.5}$$

$$g^{0i} \longrightarrow g^{0i} + g^{\mu i}\partial_\mu\pi\,, \tag{A.2.6}$$

$$\delta K_{ij} \longrightarrow \delta K_{ij} - \dot{H}\pi h_{ij} - \partial_i\partial_j\pi\,, \tag{A.2.7}$$

$$\delta K \longrightarrow \delta K - 3\dot{H}\pi - a^{-2}\nabla^2\pi\,, \tag{A.2.8}$$

As a result, we recover the diffeomorphism invariant action helped by the new degree of freedom $\pi(x)$.

The EFT expansion

Under the unitary gauge condition, a general Lagrangian is given as

$$S = \frac{1}{2}\int d^4x\sqrt{-g}\Big[M_{\rm pl}^2 f(t) - 2\Lambda(t) - 2c(t)g^{00} + M_2^4(t)(\delta g^{00})^2 - \bar{m}_1^3(t)\delta g^{00}\delta K - \bar{M}_2^2\delta K^2 - \bar{M}_3^2(t)\delta K^\nu_\mu \delta K^\mu_\nu + \lambda_1\delta R^2 + \mu_1^2(t)\delta g^{00}\delta R + m_2^2(t)h^{\mu\nu}\partial_\mu g^{00}\partial_\nu g^{00} + \dots\Big] \quad \text{(A.2.9)}$$

where $\delta g^{00} = -1 + g^{00}$. Each coefficients in front of the geometrical operators are generally time-dependent functions, which is consequently expected by the break of the time translation symmetry of a background. The covariant form of the action recovers by the Stuckelberg trick,

$$S = \frac{1}{2}\int d^4x\sqrt{-g}\Big[F(\pi)R - Z(\pi)(\partial\pi)^2 - 2V(\pi) + a_1(\pi)(\partial\pi)^4 + a_2(\pi)(\partial\pi)^2\Box\pi + a_3(\pi)(\Box\pi)^2 + \dots\Big], \quad \text{(A.2.10)}$$

where the coefficients on the operators are given by the combination of the ones in Eq. (A.2.9), which are not important to see the explicit form of the coefficients here.

A.2.2 The derivation of the EFT parameters and stability conditions

In this Appendix, we further argue the EFT parameters and the stability conditions in the Class Ia DHOST theory [1]. Throughout the Appendix, we work on in the ADM formalism.

A.2.3 EFT description of the Class Ia DHOST theory

Taking the metric in the ADM form,

$$ds^2 = -N^2dt^2 + g_{ij}(dx^i + N^i dt)(dx^j + N^j dt)\,. \quad \text{(A.2.11)}$$

[1] The main arguments should be applicable in more general class of the DHOST theory such that $A_1 = -A_2 \neq 0$.

We define that a time-like vector, n^μ, orthogonal to the foliation as $n^\mu\partial_\mu = (1/N, -N^i/N)$. The covariant action in Eq. (4.10.8) is converted to the ADM form. To realise this conversion we take the time-like vector n^μ proportional to the gradient of ϕ,

$$\nabla_\mu\phi = -An^\mu\,, \tag{A.2.12}$$

where $A \equiv n^\mu\nabla_\mu\phi$. The time derivative of A, V, is defined as

$$V \equiv n^\mu\nabla_\mu A\,, \tag{A.2.13}$$

and the total action is given as

$$S = \int dtd^3x N\sqrt{g}\mathcal{L}\,, \tag{A.2.14}$$

$$\begin{aligned}\mathcal{L} = {} & P + Q_2AK + F(R + K_{ij}K^{ij} - K^2) - 2F_\phi AK + \left[-2(A_3+A_4)X + 4A_5X^2\right]V^2 \\ & - 2(F_X + A_3X)AKV + 2(F_X - A_4X)\partial_iA\partial^iA\,,\end{aligned} \tag{A.2.15}$$

where $g = \det g_{ij}$ and $Q_2(\phi, X)$ satisfies $Q = Q_1 + 2XQ_{1X}$ with $Q_1 \equiv -\int dX(2X)^{3/2}Q_2(\phi, X)$. Then we impose the unitary gauge condition,i.e, $\nabla_i\phi = 0$, and the flat FLRW metric such that $g_{ij} = a^2\delta_{ij}$. By following the notation in [93] the quadratic action is given as

$$\begin{aligned}S^{(2)}_{\rm EFT} = {} & \int dtd^3x a^3\frac{M^2}{2}\left\{\delta K_{ij}\delta K^{ij} - \delta K^2 + \left(\frac{\delta\sqrt{h}}{a^3}R + \delta_2R\right) + (1+\alpha_H)R\delta N\right. \\ & \left. + H^2\alpha_K\delta N^2 + 4H\alpha_B\delta N\delta K + 4\beta_1\delta K\delta V + \beta_2\delta V^2 + \beta_3v_iv^i\right\},\end{aligned} \tag{A.2.16}$$

where δV and a_i are given as

$$\delta V \equiv (\delta\dot{N} - N^i\partial_iN)/N\,, \tag{A.2.17}$$

$$v_i \equiv \partial_iN/N\,, \tag{A.2.18}$$

Since the second term of δV in Eq. (A.2.17) is at the second order of the perturbations, the relation $\delta V = \delta\dot{N}$ is enough for computing the EFT parameters. As a consequence of the degeneracy conditions, β_2 and β_3 must satisfy the following conditions,

$$\beta_2 = -6\beta_1^2\,,\ \beta_3 = -2\beta_1[2(1+\alpha_H) + \beta_1]\,, \tag{A.2.19}$$

Here we derive α_B and α_K in the following way. In the unitary gauge, $A = \dot{\phi}/N$ and $V = \ddot{\phi}/N^2$ at the background, both of which contains lapse function. Provided $N = \bar{N} + \delta N$, we obtain the perturbed V as

$$V = \frac{\ddot{\phi}}{\bar{N}^2}\left(1 - 2\frac{\delta N}{\bar{N}}\right) - \frac{\dot{\phi}}{\bar{N}^2}\delta\dot{N}\,, \tag{A.2.20}$$

Note that the second term in the first bracket in Eq. (A.2.20) contributes to the perturbation of the Lagrangian with respect to the lapse function, consequently changing $\alpha_{K,B}$. Importantly, the last term in Eq. (A.2.20) does not only appear with $\beta_{1,2,3}$, but also with α_K by the cross multiplication of the second term in the bracket and the last terms in V^2. We discuss this more specifically in the next paragraph. Hereafter we set $\bar{N} = 1$.

To obtain the explicit forms of $\alpha_{K,B}$ from the Lagrangian in Eq.—(A.2.15), we apply the same computational strategy given in [38]. According the expansion shown in Eq. (4.6.11), α_B is formally given as

$$\alpha_B = \frac{2H\mathcal{L}_{SN} + \mathcal{L}_{KN}}{4H\mathcal{L}_{\mathcal{S}}}\,, \tag{A.2.21}$$

where $\mathcal{L}_a \equiv= \partial\mathcal{L}/\partial a$ and $\mathcal{S} \equiv K_{ij}K^{ij}$. The straightforward computation of Eq. (A.2.21) with the choice $N = 1$ gives an explicit result in Eqs. (4.11.4) to (4.11.5). α_K on the contrary is more subtle to be computed. During the perturbation in terms of δ_N from Eq. (A.2.15) to Eq. (4.6.11), the term $\delta N\delta\dot{N}$ appears from the term icluding V^2 and AV. By taking the partial integral on this term, the additional terms should be in α_K. We explicitly treat the contribution from $\delta N\delta\dot{N}$ by the second term of the following equation,

$$\alpha_K = \frac{2\mathcal{L}_N + \mathcal{L}_{NN}}{2H^2L_{\mathcal{S}}} - \frac{\dot{B} + 3HB}{H^2\mathcal{L}_{\mathcal{S}}}\,, \tag{A.2.22}$$

where B is given as

$$\begin{aligned} B \equiv 4\dot{\phi}\ddot{\phi}X\left\{3(A_3 + A_4) - 8A_5X + (A_{3X} + A_{4X})X - 2A_{5X}X^2\right\} \\ + 6HX\left\{2X(F_{XX} + A_{3X}X + A_3) + 3(F_X + A_3X)\right\}\,, \end{aligned} \tag{A.2.23}$$

Notice that if we take the condition for the GLPV theory, i .e. $F_X + A_3X = 0$, $A_3 + A_4 = 0$ and $A_5 = 0$ follow, leading $B = 0$. In the conformal frame where we are working, the form of α_K and α_B are determined, but it becomes complicated since $\delta N\delta\dot{N}$ exists by the choice of the conformal frame such that the scale factor obeys

the Friedmann equations in Eqs. (4.11.8) and (4.11.9). By computing the first term in Eq. (A.2.22), we obtain,

$$\alpha_K^{\rm Horn} = \frac{1}{H^2F}\left\{X(P_X + 2XP_{XX} - Q_\phi - 2XQ_{\phi X}) - 6\dot{\phi}HX(Q_X + XQ_{XX})\right\}, \tag{A.2.24}$$

$$\begin{aligned}\alpha_K^{\rm res} = &-\frac{12(XF_X + 4X^2F_{XX})}{F} - \frac{12\dot{\phi}X(3F_{\phi X} + 2XF_{\phi XX})}{HF} \\ &- 2V^2\left(2\tilde{\beta}_2 + 5X\tilde{\beta}_{2X} + 2X^2\tilde{\beta}_{2XX}\right) + 6HAV\left(3\tilde{\beta}_1 - 3X\tilde{\beta}_{1X} + 2X^2\tilde{\beta}_{1XX}\right) \\ &- \frac{\dot{B} + 3HB}{2H^2F},\end{aligned} \tag{A.2.25}$$

where we define $\tilde{\beta}_1 \equiv -2F\beta_1/X$ and $\tilde{\beta}_2 \equiv -F\beta_2/2X$.

A.2.4 Stability conditions without matters

To derive the stability conditions for the perturbations, we derive the scalar and tensor perturbation. We start with the metric perturbation in the scalar sector. The metric is given as

$$g_{00} = -(1+\delta N)^2,\ g_{0i} = g_{i0} = a^2\partial_i\chi,\ g_{ij} = a^2(1+2\zeta)\delta_{ij}\,, \tag{A.2.26}$$

In the expansion of the quadratic action is specifically given as,

$$\begin{aligned}S^{(2)} = \int dtd^3xa^3\frac{M_*^2}{2}\Bigg\{&-6\dot{\zeta}^2 + 12\beta_1\dot{\zeta}\delta\dot{N} + \beta_2\delta\dot{N}^2 + 12H\left[(1+\alpha_B)\dot{\zeta} - \beta_1\delta\dot{N}\right]\delta N \\ &H^2(\alpha_K - 6 - 12\alpha_B)\delta N^2 + 4\left[\dot{\zeta} - \beta_1\delta\dot{N} - H(1+\alpha_B)\delta N\right]\partial^2\chi \\ &\frac{1}{a^2}\left[2(1+\alpha_T)(\partial_i\zeta)^2 + 4(1+\alpha_H)\partial_i\zeta\partial_i\delta N + \beta_3(\partial_i\delta N)^2\right]\Bigg\},\end{aligned} \tag{A.2.27}$$

The scalar perturbation is diagonalized with the quantity

$$\tilde{\zeta} \equiv \zeta - \beta_1\delta N\,, \tag{A.2.28}$$

with

$$S_{\tilde{\zeta}} = \int dt d^3x a^3 \frac{M_*^2}{2} \left[A_{\tilde{\zeta}} \dot{\tilde{\zeta}}^2 + B_{\tilde{\zeta}} \frac{(\partial_i \tilde{\zeta})^2}{a^2} \right], \tag{A.2.29}$$

where ψ is the curvature perturbation in the spatial metric. Notice that $\tilde{\zeta}$ is not gauge invariant quantity. Basic quantities that appear in the action in Eq. (A.2.29) are the coefficient on the kinetic terms and on the gradient term, $A_{\tilde{\zeta}}$ and $B_{\tilde{\zeta}}$, respectively. In the class I-a DHOST theory $A_{\tilde{\zeta}}$ and $B_{\tilde{\zeta}}$ are given as,

$$A_{\tilde{\zeta}} = \frac{1}{(1+\alpha_B - \dot{\beta}_1/H)^2} \left[\alpha_K + 6\alpha_B^2 - \frac{6}{a^3 H^2 M_*^2} \frac{d}{dt}(a^3 H M_*^2 \alpha_B \beta_1) \right], \tag{A.2.30}$$

$$B_{\tilde{\zeta}} = 2 - \frac{2}{a M_*^2} \frac{d}{dt} \left[\frac{a M_*^2 (1+\alpha_H + \beta_1)}{H(1+\alpha_B) - \dot{\beta}_1} \right], \tag{A.2.31}$$

$$C_{\tilde{\zeta}} = 0\,, \tag{A.2.32}$$

$$\alpha = \alpha_K + 6\alpha_B^2 - \frac{6}{a^3 H^2 M_*^2} \frac{d}{dt}(a^3 H M_*^2 \alpha_B \beta_1)\,, \tag{A.2.33}$$

Then the stability conditions for the scalar perturbation is given as

$$A_{\tilde{\zeta}} > 0\,,\ B_{\tilde{\zeta}} < 0\,, \tag{A.2.34}$$

Then we consider the tensor sector. The spatial part of the metric is relevant,

$$g_{ij} = a^2(\delta_{ij} + h_{ij})\,. \tag{A.2.35}$$

After perturbing the action in Eq. (A.2.15) we obtain the quadratic action for the tensor sector,

$$S_h^{(2)} = \int dt d^3x a^3 \frac{M_*^2}{2} \left[\dot{h}_{ij}^2 - (\partial_k h_{ij})^2 \right], \tag{A.2.36}$$

To avoid the ghost instability for the tensor perturbation,

$$M_*^2 > 0\,, \tag{A.2.37}$$

is necessary.

For the purpose of considering the Universe at late time, it is inevitable to take into account a matter. In other words, it is necessary to derive the stability conditions by

including a matter other than the condition in Eq. (A.2.34).

A.2.5 Gradient instability with a fixed matter frame

We assume a matter component we look into is described by a barotropic perfect fluid,i.e, $p_m = p_m(\rho_m)$. The behaviour of a barotropic perfect fluid is well mimicked by a massless scalar field minimally coupled to gravity[201]. Although in detail the physical property of a massless scalar field is not exactly the same as that of a perfect fluid at certain situations[202], most of the properties are similarly followed. In our paper, we consider a massless scalar field as a matter by assuming in matching situations discussed in [201].

According to Gleyzes et al [203], the stablity conditions in the Beyond Horndeski theory are different from the Horndeski theory by nonzero α_H. On top of that, in the DHOST theory, the stability conditions are also distinguishable from the beyond Horndeski theory. Here we discuss the additional contribution in the DHOST theory to measure any difference of from the beyond Horndeski theory. For simplicity, we argue the matter with the scalar field which minimally couples to gravity as

$$S_m = \int d^3x dt N\sqrt{h} P(Y,\sigma)\ , Y \equiv g^{\mu\nu}\partial_\mu\sigma\partial_\nu\sigma = -\frac{(\dot\sigma - N^i\partial_i\sigma)^2}{N^2} + h^{ij}\partial_i\sigma\partial_j\sigma\,, \tag{A.2.38}$$

Notice that the inhomogeneity of σ exists in the unitary gauge. Then $\sigma = \sigma_0 + \delta\sigma$ and perturbs the action in Eq. (A.2.38) the quadratic perturbation of the matter reads

$$S_m^{(2)} = \int d^3x dt a^3 \left\{ \frac{\delta\sqrt{h}}{a^3}\delta N P + \left(\frac{\delta\sqrt{h}}{a^3} + \delta N\right)(P_Y\delta_1 Y + P_\sigma\delta\sigma) \right. \\ \left. + P_Y\delta_2 Y + \frac{P_{YY}}{2}\delta_1 Y^2 + P_{Y\sigma}\delta_1 Y\delta\sigma + \frac{P_{\sigma\sigma}\delta\sigma^2}{2}\right\}, \tag{A.2.39}$$

with

$$\frac{\delta\sqrt{h}}{a^3} = 3\zeta\,, \tag{A.2.40}$$

$$\delta_1 Y = 2\dot\sigma_0^2\delta N - 2\dot\sigma_0\delta\dot\sigma\,, \tag{A.2.41}$$

$$\delta_2 Y = -3\dot\sigma_0^2\delta N^2 - \delta\dot\sigma^2 + 4\dot\sigma_0\delta\dot\sigma\delta N + 2\dot\sigma_0\partial_i B\delta\partial^i\sigma + h^{ij}\partial_i\sigma\partial_j\sigma\,, \tag{A.2.42}$$

Under the existence of the matter, the momentum constraint reads

$$\delta N = \frac{1}{H(1+\alpha_B)-\dot{\beta}_1}\left(\dot{\tilde{\zeta}} + \frac{\rho_m + p_m}{2M^2}\frac{\delta\sigma}{\dot{\sigma}_0}\right), \tag{A.2.43}$$

Then we introduce the quantity $Q_\sigma \equiv \delta\sigma - (\dot{\sigma}_0/H)\tilde{\zeta}$. Note that Q_σ is not a gauge invariant variable if $\beta_1 \neq 0$. Inserting δN in Eq. (A.2.43) and replacing ζ into $\tilde{\zeta}$ and $\delta\sigma$ to Q_σ, the whole quadratic action reads

$$S^{(2)} = \int dtd^3xa^3\left(\tilde{\mathcal{L}}_{\tilde{\zeta}} + \tilde{\mathcal{L}}_{Q_\sigma} + \tilde{\mathcal{L}}_{\tilde{\zeta}Q_\sigma} + (\text{non derivative terms})\right), \tag{A.2.44}$$

where

$$\tilde{\mathcal{L}}_{\tilde{\zeta}} = \frac{M_*^2}{2}\left\{\tilde{A}_{\tilde{\zeta}}\dot{\tilde{\zeta}}^2 + \tilde{B}_{\tilde{\zeta}}\frac{(\partial_i\tilde{\zeta})^2}{a^2}\right\}, \tag{A.2.45}$$

$$\tilde{\mathcal{L}}_{Q_\sigma} = -\frac{P_Y}{c_m^2}\left(\dot{Q}_\sigma^2 - c_m^2\frac{(\partial_i Q_\sigma)^2}{a^2}\right), \tag{A.2.46}$$

$$\tilde{\mathcal{L}}_{\tilde{\zeta}Q_\sigma} = -\frac{2\dot{\sigma_0}P_Y}{c_m^2(H(1+\alpha_B)-\dot{\beta}_1)}\left((\alpha_B - \dot{\beta}_1/H)\dot{\tilde{\zeta}}\dot{Q}_\sigma - c_m^2(\alpha_B - \dot{\beta}_1/H - \alpha_H - \beta_1)\frac{\partial_i\tilde{\zeta}\partial_i Q_\sigma}{a^2}\right) \tag{A.2.47}$$

$$\tilde{A}_{\tilde{\zeta}} = A_{\tilde{\zeta}} + \frac{(\rho_m + p_m)}{H^2M_*^2c_m^2}\left(\frac{H\alpha_B - \dot{\beta}_1}{H(1+\alpha_B)-\dot{\beta}_1}\right)^2, \tag{A.2.48}$$

$$\tilde{B}_{\tilde{\zeta}} = B_{\tilde{\zeta}} - \frac{\rho_m + p_m}{M_*^2H^2}\left(1 - \frac{2(1+\alpha_H+\beta_1)}{1+\alpha_B-\dot{\beta}_1/H}\right) \tag{A.2.49}$$

$$\tilde{C}_{\tilde{\zeta}} = C_{\tilde{\zeta}} = 0\,, \tag{A.2.50}$$

Here $\rho_m + p_m = -2\dot{\sigma}_0^2P_Y$ and the sound speed of the matter is given as $c_m^2 \equiv P_Y/(P_Y - 2\dot{\sigma}_0^2P_{YY})$. To derive the stability conditions we rewrite the quadratic action in Eq. (A.2.44) as

$$S^{(2)} = \int dtd^3xa^3\frac{M_*^2}{2}\left(\dot{\mathbf{x}}^T\mathcal{K}\dot{\mathbf{x}} + \frac{\partial_i\mathbf{x}^T\mathcal{G}\partial_i\mathbf{x}}{a^2}\right), \tag{A.2.51}$$

where $\mathbf{x} \equiv (\tilde{\zeta}, Q_\sigma)$, and

$$\mathcal{K} = \begin{pmatrix} \tilde{A}_{\tilde{\zeta}} & A(\alpha_B - \dot{\beta}_1/H) \\ A(\alpha_B - \dot{\beta}_1/H) & -2P_Y/M_*^2c_m^2 \end{pmatrix}, \tag{A.2.52}$$

$$\mathcal{G} = \begin{pmatrix} \tilde{B}_{\tilde{\zeta}} & -Ac_m^2(\alpha_B - \dot{\beta}_1/H - \alpha_H - \beta_1) \\ -Ac_m^2(\alpha_B - \dot{\beta}_1/H - \alpha_H - \beta_1) & 2P_Y/M_*^2 \end{pmatrix} , \tag{A.2.53}$$

where

$$A = \frac{-2\dot{\sigma}_0 P_Y}{HM_*^2 c_m^2(1 + \alpha_B - \dot{\beta}_1/H)} . \tag{A.2.54}$$

To avoid the ghost and gradient instabilities of a cosmological solution, it is required that the eigenvalues of $\mathcal{K}$ are positive, and the eigenvalues of $\mathcal{G}$ are negative. Since $\mathcal{K}$ and $\mathcal{G}$ are a symmetric matrix, the necessarry and sufficient conditions of the stability is,

$$\mathrm{Tr}(\mathcal{K}) > 0 \text{ and } \det(\mathcal{K}) > 0 , \tag{A.2.55}$$

$$\mathrm{Tr}(\mathcal{G}) < 0 \text{ and } \det(\mathcal{G}) > 0 , \tag{A.2.56}$$

Eqs. (A.2.55) and (A.2.56) with the null energy condition of the matter,i.e.,$P_Y < 0$ give the condition that

$$A_{\tilde{\zeta}} > 0, \ B_{\tilde{\zeta}} + \frac{\rho_m + p_m}{M_*^2 H^2} \left(\frac{1 + \alpha_H + \beta_1}{1 + \alpha_B - \dot{\beta}_1/H} \right)^2 < 0 , \tag{A.2.57}$$

Note that the condition exactly recovers the same as the condition in Eq. (A.2.34) when the matter is ignored,i.e, decoupling limit of the matter from gravity.

In a recent literature of cosmology of the DHOST theory, the stability conditions with the matter have been derived [100]. However, the conditions make a difference from what we derived in Eq. (A.2.57). What a preference of our derivation is the conditions in Eq. (A.2.57) is continuously applicable toward the super horizon initial conditions by tracing $\tilde{\zeta}$ and Q_σ. In fact, $\tilde{\zeta}$ and Q_σ recovers their gauge invariance in the case of the beyond Horndeski, i.e, $\beta_1 = 0$. In fact, the conditions in the paper [100] leads the same expression in the limit of $\beta_1 = 0$. However, we admit that the variation of the stability conditions are crucial for cosmology.

A.2.6 Dependence on basis of linear perturbations for stability conditions

We show how a choice of the basis for the cosmological perturbation varies the observable quantities we are interested in. We pick up the three different choices of the bases;

stab wom,*stab wm1*, and *stab wm2*,respectively.

$$\text{stab wom} : A_{\tilde{\zeta}} > 0,\ B_{\tilde{\zeta}} < 0\,,\ M_*^2 > 0\,, \tag{A.2.58}$$

$$\text{stab wm1} : A_{\tilde{\zeta}} > 0,\ B_{\tilde{\zeta}} + \frac{\rho_m + p_m}{M_*^2 H^2}\left(\frac{1+\alpha_H+\beta_1}{1+\alpha_B-\dot{\beta}_1/H}\right)^2 < 0\,,\ M_*^2 > 0\,, \tag{A.2.59}$$

$$\begin{aligned}\text{stab wm2} : A_{\tilde{\zeta}} + \frac{\rho_m + p_m}{M_*^2 H^2}\frac{3\beta_1(2+3c_m^2\beta_1)}{(1+\alpha_B-\dot{\beta}_1/H)^2} > 0\,,\\ B_{\tilde{\zeta}} + \frac{\rho_m + p_m}{M_*^2 H^2}\left(\frac{1+\alpha_H+\beta_1}{1+\alpha_B-\dot{\beta}_1/H}\right)^2 < 0\,,\ M_*^2 > 0\,,\end{aligned} \tag{A.2.60}$$

Fig. A.3 provide how the three filtering methods for the stability conditions affect the posterior distribution of the characteristic parameters. Fig. A.3 quantitatively shows that the difference of the bases are ineffective to change the distributions of the characteristic parameters. In comparison between the top and bottom figure, we confirm that the choice of the basis makes little differences in the range of redshifts we are interested in.

In the deep era of matter dominant or radiation dominant epoch in the past Universe, the difference of the basis for the stability conditions could be more serious issue left. In fact the additional terms that appears on the stability coefficients without the matter could be compatible in the matter dominant epoch, namely $\rho_m/3M_*^2H^2$.To deal with the analysis for the stability conditions in those epoch, we might need a more sophisticated and careful analysis. This point, however, is beyond the scope of this paper. Hence, we conclude that a chose of the basis for the stability condition of the scalar fluctuation and the matter fluctuation are less important with the assumptions we take; the slow rolling scalar field and intermediate redshifts up to $z = 2$. Hereafter we prefer the basis as following the one in M.Chrisostomi *et al.* 2019 [100], in which the details of the models have been investigated.

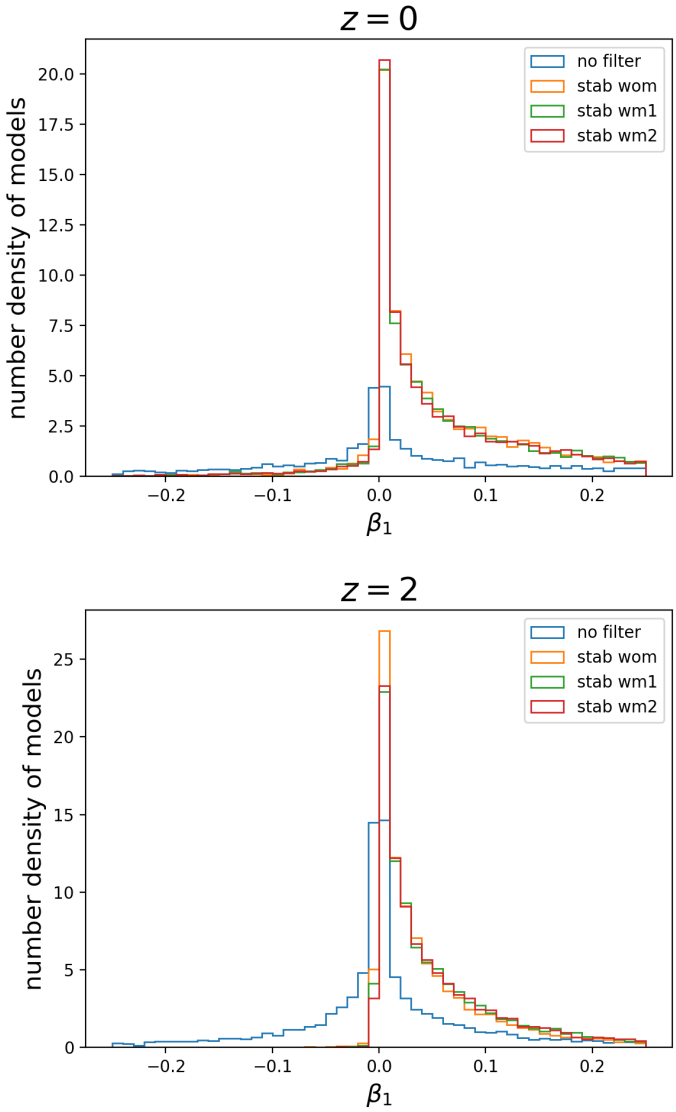

Figure A.3. Filter dependence in the model distributions.The panels show the redshift $z = 0$ and $z = 2$.

Appendix B

Standard theory of inflation

In this appendix, we review the orthodox scenario of an inflationary universe.

B.1 The background spacetime

The system of the equations of motion are derived via the action principle with the action

$$S_\phi = \int d^4x\sqrt{-g}\left(-\frac{1}{2}g^{\mu\nu}\bigtriangledown_\mu\phi\bigtriangledown_\nu\phi - V(\phi)\right). \tag{B.1.1}$$

When the Einstein gravity is considered, the action of gravity sector $S_{\rm G}$ is equivalent to the Einstein Hilbert action $S_{\rm EH}$, and thus the total action including the gravity sector and the scalar filed sector S is shown in

$$S = S_{\rm EH} + S_\phi = \int d^4x\sqrt{-g}\left(\frac{{M_P}^2}{2}R - \frac{1}{2}g^{\mu\nu}\bigtriangledown_\mu\phi\bigtriangledown^\nu\phi - V(\phi)\right). \tag{B.1.2}$$

Next, we utilise the variation principle, deriving the equations of motions

$$\begin{aligned}
&G_{\mu\nu} = \frac{T_{\mu\nu}}{{M_P}^2},\\
&T_{\mu\nu} \equiv -\frac{2}{\sqrt{-g}}\frac{\delta S_\phi}{\delta g^{\mu\nu}} = \bigtriangledown_\mu\phi\bigtriangledown_\nu\phi - g_{\mu\nu}\left(\frac{1}{2}\bigtriangledown_\rho\phi\bigtriangledown^\rho\phi - V(\phi)\right),\\
&g^{\mu\nu}\bigtriangledown_\mu\bigtriangledown_\nu\phi + V_\phi = 0,
\end{aligned} \tag{B.1.3}$$

By assuming the cosmological principle for the background scalar field, namely the scalar field only varies in time, we obtain

$$H^2 = \frac{1}{3{M_P}^2}\left(\frac{\dot{\phi}^2}{2} + V(\phi)\right), \tag{B.1.4}$$

$$\ddot{\phi} + 3H\dot{\phi} + V_\phi = 0\,, \tag{B.1.5}$$

Note that we obtain the dynamical evolution of the scalar field by solving Eqs. (B.1.4) and (B.1.5)

B.2 Slow-roll condition

We impose the condition for the scalar field so that the inflation takes place. We define the parameters for clarifying the dynamics of indlation

$$\epsilon_H \equiv -\frac{\dot{H}}{H^2} = \frac{\dot{\phi}^2}{2{M_P}^2},$$
$$\eta_H \equiv -\frac{\ddot{\phi}}{H\dot{\phi}}, \tag{B.2.1}$$

ϵ_H and η_H describes the conditions for the slow-roll inflation. The condition for the cosmic acceleration is given in terms of the slow-roll parameter ϵ_H as

$$(0 \leq)\, \epsilon_H < 1 \tag{B.2.2}$$

During Eq. (B.2.2) is satisfied, inflation occurs. We define the N-folding number N_* at which the inflation begins. By the Taylor expansion of the Hubble parameter around $N = N_*$, we obtain

$$\frac{1}{H} = \frac{1}{H_*}\left(1 + \epsilon_{H*}(N - N_*) + \frac{1}{2}\frac{d\epsilon_H}{dN}_* (N - N_*)^2 + O((N - N_*)^3)\right),$$
$$\frac{d\epsilon_H}{dN}_* = 2({\epsilon_{H*}}^2 - \epsilon_{H*}\eta_{H*}). \tag{B.2.3}$$

When the inflation occurs exponentially, the Hubble parameter is almost constant during $\Delta N = N_{\rm inf} - N_*$. For the purpose of solving the horizon problem of the Universe,

$\Delta N \lesssim 60$ are required. Then ϵ_{H*} and η_{H*} are conditioned as

$$\epsilon_{H*} \sim \frac{1}{\Delta N} \ll 1,$$
$$\eta_{H*} \sim \frac{1}{\Delta N} \ll 1, \tag{B.2.4}$$

Note that these conditions are sufficient for the condition for inflation, i.e., Eq. (B.2.2). These conditions are called as the slow-roll condition, and we call ϵ_{H*} and η_{H*} as the slow-roll parameters (Slow Roll Parameters; SRP). The slow-roll conditions are essential to construct the phenomenology of inflation. The conditions in Eq. (B.2.4) are equivalently translated to another choice of the parameters as

$$\epsilon_V \equiv \frac{{M_P}^2}{2}\left(\frac{V_\phi}{V}\right)^2,$$
$$\eta_V \equiv {M_P}^2\frac{V_{\phi\phi}}{V}, \tag{B.2.5}$$

ϵ_V and η_V are called the potential slow-roll parameters. The slow roll parameters in Eqs. (B.2.1) and (B.2.5) linearly correlate as

$$\epsilon_H = \epsilon_V + O(\mathrm{SRP}^2),$$
$$\eta_H = \eta_V - \epsilon_V + O(\mathrm{SRP}^2). \tag{B.2.6}$$

B.3 Quantum fluctuation during inflation

One of the biggest features of inflation theory is that quantum fluctuations generate initial density fluctuations that become the seeds of the structure of the universe. When the initial density fluctuations enter the interior of the particle horizon again, they change into various fluctuations. Specifically, the initial fluctuation that entered the particle horizon before clearing is converted to fluctuation of baryon and gravity potentials. During this period, baryons and photons are strongly coupled. Consequently, when the universe eventually cools and clears up ($z_{ls} \sim 1100$), the effects of initial fluctuations are encoded into the temperature fluctuations and polarization of CMB.

Fortunately, we are able to measure CMB very precisely. Therefore, it is possible to retrieve the component of the initial fluctuation by CMB observation and search for whether or not inflation has occurred. We use the derivation of quantum fluctuations in the manner of E.Stewart an D.Lyth1993 []. The definition of the slow-roll parameters are shown in the way in A.Liddle, P.Parsons, and John D.Barrow 1994[]

B.3.1 Evolution of pertrubations

We derive the primordial power spectra based on E. Stewart and D. Lyth 1993 [] based on the time evolution of the background universe and the perturbative variables. At linear order of perturbation, the perturbative variables with the different spin components are independent with each other, allowing us to compute the scalar, vector, and tensor modes separately. Firstly, we derive the perturbation of scalar modes as

$$ds^2 = a(\eta)^2\left\{-(1+2A)d\eta^2 + 2\partial_i B dx^i d\eta dx^i + \Big[(1+2\mathcal{R})\delta_{ij} + 2\partial_i\partial_j H_T\Big]dx^i dx^j\right\}. \tag{B.3.1}$$

For convenience we define ζ as

$$\zeta = \mathcal{R} - \frac{H}{\dot{\phi}}\delta\phi\,, \tag{B.3.2}$$

The Fourier decomposition of ζ is given as

$$\zeta = \int \frac{d^3\mathbf{k}}{(2\pi)^3}\zeta_{\mathbf{k}}(\eta)e^{i\mathbf{k}\cdot\mathbf{x}}, \tag{B.3.3}$$

Since we consider that the isotropy of the background universe, the power spectrum of ζ is independent with the angular direction and thus the power spectrum of ζ is derived as

$$\langle\zeta_{\mathbf{k}}\zeta^*_{\mathbf{k}'}\rangle = \frac{2\pi^2}{k^3}P_\zeta\delta^3(\mathbf{k}-\mathbf{k}')\,. \tag{B.3.4}$$

Similar to the scalar perturbations, the power spectrum of the tensor mode is derived. The metric perturbation for the tensor mode is given as

$$ds^2 = a(\eta)^2[-d\eta^2 + (\delta_{ij}+2h_{ij})dx^i dx^j]\,, \tag{B.3.5}$$

The perturbative tensor mode h_{ij} satisfies transverse and traceless gauge condition, i.e., $\partial_i h^i_j = 0$ and $h^i_i = 0$. The Fourier decomposition of h_{ij} is

$$h_{ij} = \int \frac{d^3\mathbf{k}}{(2\pi)^3}\sum_{\lambda=+,\times} h_{\mathbf{k},\lambda}e_{ij}(\mathbf{k},\lambda)e^{i\mathbf{k}\cdot\mathbf{x}}\,. \tag{B.3.6}$$

Note that the tensor mode should be decomposed by the orthonormal polarisation basis

e_{ij} that are determined by the transverse and traceless gauge conditions,

$$\begin{aligned} &e_{ij} = e_{ji}, e_{ii}, k_i e_{ij} = 0, \\ &e_{ij}(\mathbf{k},\lambda)e^*_{ij}(\mathbf{k},\mu) = \delta_{\lambda\mu}, e_{ij}(-\mathbf{k},\lambda) = e^*_{ij}(\mathbf{k},\lambda)\,. \end{aligned} \tag{B.3.7}$$

Then the power spectrum of the tensor mode P_T is derived as

$$\langle h_{\mathbf{k},\lambda} h_{\mathbf{k}',\lambda}\rangle = \frac{2\pi^2}{k^3} P_T \delta^3(\mathbf{k}-\mathbf{k}')\,,. \tag{B.3.8}$$

We define the useful quantity called as the tensor to scalar ratio,

$$r = \frac{P_T}{P_R}. \tag{B.3.9}$$

B.3.2 Mukhanov-Sasaki equation

To describe the dynamics of the quantum fluctuation, it is convenient to use a peculiar gauge-invariant quantity called Mukhanov-Sasaki variable. Mukhanov-Sasaki variable is defined as

$$u = -z\zeta\,. \tag{B.3.10}$$

Here $z = a\dot{\phi}/H$ is given by the background. u satisfies the following action

$$S_{\rm MS} = \frac{1}{2}\int d\eta d^3\mathbf{x}\left[\left(\frac{du}{d\eta}\right)^2 - (\partial_i u)^2 + \frac{1}{z}\frac{d^2 z}{d\eta^2}u^2\right]. \tag{B.3.11}$$

and by variating u we obtain the Mukhanov-Sasaki equation

$$\frac{d^2 u(\eta,k)}{d\eta^2} + \left(k^2 - \frac{1}{z}\frac{d^2 z}{d\eta^2}\right) = 0\,, \tag{B.3.12}$$

Since the primordial perturbations during inflation behaves quantum-wise, the physical quantity becomes an operator. We explicitly denote u as an operator $\hat{u}$. $\hat{u}$ is quantised by the canonical quantisation. As the background universe is conformally flat, the quantisation procedure in the Minkowski space-time is applicable. By expanding with the creation and annihilation operators and the plane waves, we obtain

$$\hat{u}(\eta,\mathbf{x}) = \int \frac{d^3\mathbf{k}}{(2\pi)^3}\left\{u_k(\eta)\hat{a}_{\mathbf{k}}e^{i\mathbf{k}\cdot\mathbf{x}} + u^*_k(\eta)\hat{a}^\dagger_{\mathbf{k}}e^{-i\mathbf{k}\cdot\mathbf{x}}\right\}, \tag{B.3.13}$$

where the commutation relations of the creation and annihilation operators are

$$\begin{aligned}
&\left[\hat{a}_{\mathbf{k}}, \hat{a}^{\dagger}_{\mathbf{k}'}\right] = \delta^3(\mathbf{k} - \mathbf{k}'), \\
&\left[\hat{a}_{\mathbf{k}}, \hat{a}_{\mathbf{k}'}\right] = 0 = \left[\hat{a}^{\dagger}_{\mathbf{k}}, \hat{a}^{\dagger}_{\mathbf{k}'}\right], \\
&\hat{a}_{\mathbf{k}}|0\rangle = 0.
\end{aligned} \tag{B.3.14}$$

Note that $u_{\mathbf{k}}(\eta, \mathbf{x}) = u_k(\eta)$ thanks to the isotropy of the background. u_k is called mode function. From Mukhanov-Sasaki equation Eq. (B.3.12) is also satisfied with $u_(\eta, k)$ as

$$\frac{d^2 u_k}{d\eta^2} + \left(k^2 - \frac{1}{z}\frac{d^2 z}{d\eta^2}\right) u_k = 0\,, \tag{B.3.15}$$

Note that the Wronskian preserves. The value of the Wronskian is determined by the canonical quantisation as

$$u_k \frac{du_k^*}{d\eta} - \frac{du_k}{d\eta} u_k^* = i\,, \tag{B.3.16}$$

The explicit form of $z^{-1}d^2z/d\eta^2$ is derived as

$$\frac{1}{z}\frac{d^2 z}{d\eta^2} = 2a^2H^2\left(1 + \epsilon_H - \frac{3}{2}\eta_H + \frac{1}{2}{\eta_H}^2 - \frac{1}{2}\epsilon_H\eta_H + \frac{1}{2aH}\frac{d\epsilon}{d\eta} - \frac{1}{2aH}\frac{d\eta_H}{d\eta}\right), \tag{B.3.17}$$

η is related to

$$\eta = \int \frac{dt}{a} = \int \frac{da}{a^2 H} = -\frac{1}{aH} + \int da \frac{\epsilon_H}{a^2 H}, \tag{B.3.18}$$

Note that this relation is exact. Once ϵ_H and η_H satisfies the slow roll condition Eq. (B.2.4), it is good approximation that ϵ_{H*} and η_{H*} remains constant. By the constancy of the slow roll parameter, we obtain

$$\begin{aligned}
\eta &= -\frac{1}{aH}\left(\frac{1}{1 - \epsilon_{H*}}\right), \\
\frac{1}{z}\frac{d^2 z}{d\eta^2} &= \frac{1}{\eta^2}\left({\nu_*}^2 - \frac{1}{4}\right), \\
\nu_* &= \frac{1 + \epsilon_{H*} - \eta_{H*}}{1 - \epsilon_{H*}} + \frac{1}{2}.
\end{aligned} \tag{B.3.19}$$

By using the approximation in Eq. (B.3.19), the Mukhanov - Sasaki equation is

rewritten as

$$\frac{d^2u_k}{d\eta^2} + \Big[(k^2 - \frac{1}{\eta^2}\left({\nu_*}^2 - \frac{1}{4}\right)\Big]u_k = 0. \tag{B.3.20}$$

This equation is in the category of Bessel differential equation, and the analytic solutions are given by the first and the second Hankel functions, i.e., ${H_\nu}^{(1)}$ and ${H_\nu}^{(2)}$ as

$$u_k = \sqrt{\frac{\pi}{4k}}\sqrt{-k\eta}\Big[\alpha_k {H_\nu}^{(1)}(-k\eta) + \beta_k {H_\nu}^{(2)}(-k\eta)\Big], \tag{B.3.21}$$

The normalization condition in Eq. (B.3.16) then reads

$$|\alpha_k|^2 - |\beta_k|^2 = 1, \tag{B.3.22}$$

Note that there are certain arbitrariness to choose α_k and β_k. This is due to. In the literature, the Bunch-Davis vacuum is often taken at the sub-horizon limit $k/aH \to \infty$, i.e.,

$$\alpha_k = e^{i\frac{\pi}{2}(\nu_* + \frac{1}{2})}, \beta_k = 0, \tag{B.3.23}$$

then we obtain

$$\begin{aligned} &k/aH \to \infty \Longrightarrow u_k = \frac{1}{\sqrt{2k}}e^{-k\eta}, \\ &k/aH \to 0 \Longrightarrow e^{i(\nu_* - \frac{1}{2})\frac{\pi}{2}}2^{\nu_* - \frac{3}{2}}\frac{\Gamma(\nu_*)}{\Gamma(\frac{3}{2})}\frac{1}{\sqrt{2k}}(-k\eta)^{\frac{1}{2}-\nu_*}. \end{aligned} \tag{B.3.24}$$

From Eqs. (B.3.13) and (B.3.14), the two-point correlation function of ζ is given as

$$\langle 0|\hat{\zeta_{\mathbf{k}}}\hat{\zeta}^\dagger_{\mathbf{k}'}|0\rangle = \frac{|u_k|^2}{z^2}\delta^3(\mathbf{k} - \mathbf{k}'). \tag{B.3.25}$$

In the limit $k/aH \to 0$, the two-point correlation function Eq. (B.3.25) is specifically given and we obtain the power spectrum as

$$P_\zeta^{\frac{1}{2}}(k) = \sqrt{\frac{k^3}{2\pi^2}}\left|\frac{u_k}{z}\right| = 2^{\nu_* - \frac{3}{2}}\frac{\Gamma(\nu_*)}{\Gamma(\frac{3}{2})}\frac{1}{\sqrt{2k}}(1 - \epsilon_{H*})^{\frac{1}{2}-\nu_*}\frac{H^2}{2\pi|\dot{\phi}|}\Bigg|_{k=aH}. \tag{B.3.26}$$

The similar calculation is available for the tensor perturbation. The action is derived

as

$$S_h = \frac{1}{2}\int d\eta d^3\mathbf{x}\left[\left(\frac{dh_{ij}}{d\eta}\right)^2 - (\partial_l h_{ij})^2\right],$$
$$= \frac{1}{2}\int d^3\mathbf{k}\sum_{\lambda=+,\times}\int d\eta\left[\left|\frac{dv_{\mathbf{k},\lambda}}{d\eta}\right|^2 - \left(k^2 - \frac{1}{a}\frac{d^2a}{d\eta^2}\right)|v_{\mathbf{k},\lambda}|^2\right]. \quad \text{(B.3.27)}$$

where we use

$$v_{\mathbf{k},\lambda} = a h_{\mathbf{k},\lambda}\,, \quad \text{(B.3.28)}$$

The quantisation of v_k is

$$\hat{v}_{\mathbf{k},\lambda}(\eta) = v_k(\eta)\hat{a}_{\mathbf{k},\lambda} + v_k^*(\eta)\hat{a}^\dagger_{-\mathbf{k},\lambda}, \quad \text{(B.3.29)}$$

$$\left[\hat{a}_{\mathbf{k},\lambda}, \hat{a}^\dagger_{\mathbf{k}',\sigma}\right] = \delta_{\lambda\sigma}\delta^3(\mathbf{k}-\mathbf{k}'),$$
$$\left[\hat{a}_{\mathbf{k},\lambda}, \hat{a}_{\mathbf{k}',\sigma}\right] = 0 = \left[\hat{a}^\dagger_{\mathbf{k},\lambda}, \hat{a}^\dagger_{\mathbf{k}',\sigma}\right],$$
$$\hat{a}_{\mathbf{k},\lambda}|0\rangle = 0, \quad \text{(B.3.30)}$$

By variating Eqs (B.3.27) and we obtain the equation of motion for v_k as

$$\frac{d^2v_k}{d\eta^2} + \left(k^2 - \frac{1}{a}\frac{d^2a}{d\eta^2}\right)v_k = 0. \quad \text{(B.3.31)}$$

By taking the Bunch-Davis vacuum as same as the scalar mode,

$$k/aH \to \infty \Longrightarrow v_k = \frac{1}{\sqrt{2k}}e^{-k\eta},$$
$$k/aH \to 0 \Longrightarrow e^{i(\mu_*-\frac{1}{2})\frac{\pi}{2}}2^{\mu_*-\frac{3}{2}}\frac{\Gamma(\mu_*)}{\Gamma(\frac{3}{2})}\frac{1}{\sqrt{2k}}(-k\eta)^{\frac{1}{2}-\mu_*}\,, \quad \text{(B.3.32)}$$

where

$$\mu_* = \frac{1}{1-\epsilon_{H*}} + \frac{1}{2}, \quad \text{(B.3.33)}$$

and compute

$$\langle 0|\hat{h}_{\mathbf{k},\lambda}\hat{h}^\dagger{}_{\mathbf{k}',\sigma}|0\rangle = \frac{|v_k|^2}{a^2}\delta_{\lambda\sigma}\delta^3(\mathbf{k}-\mathbf{k}'), \quad \text{(B.3.34)}$$

and finally we obtain the power spectrum of the tensor mode, P_T, as

$$P^{\frac{1}{2}}{}_T(k_*) = 2^{\mu_*-\frac{3}{2}}\frac{\Gamma(\mu_*)}{\Gamma(\frac{3}{2})}(1-\epsilon_{H*})^{\mu_*-\frac{1}{2}}\left.\frac{H}{2\pi}\right|_{k=aH}. \tag{B.3.35}$$

B.3.3 Asymptotic values of power spectra

In Eqs. (B.3.29) and (B.3.35), we have obtained P_ζ and P_T with the constant slow-roll parameters. Since the constancy of the slow-roll parameters are guaranteed at the linear order, we further approximation P_ζ and P_T at the linear order of ϵ_{H*} and η_{H*}. μ_* and ν_* are given as

$$\begin{aligned}\nu_* &= \frac{3}{2} + 2\epsilon_{H*} - \eta_{H*},\\ \mu_* &= \frac{3}{2} + \epsilon_{H*},\end{aligned} \tag{B.3.36}$$

and thus the power spectra are approximately obtained as

$$\begin{aligned}P^{\frac{1}{2}}{}_\zeta(k) &= \left[1 + (2-\ln 2 - b)(2\epsilon_{H*} - \eta_{H*}) - \epsilon_{H*}\right]\left.\frac{H^2}{2\pi|\dot\phi|}\right|_{k=aH} + O(\mathrm{SRP}^2),\\ P^{\frac{1}{2}}{}_T(k) &= \left[1 - (\ln 2 + b - 1)\epsilon_{H*}\right]\left.\frac{H}{2\pi}\right|_{k=aH} + O(\mathrm{SRP}^2).\end{aligned} \tag{B.3.37}$$

where b denotes the Euler-Mascheroni constant $2-\ln 2-b \simeq 0.7296$, $\ln 2+b-1 \simeq 0.2704$. By using the relation at the horizon crossing for each scale k, i.e., $\ln k = d\ln Ha \simeq \frac{da}{a} = dN$, the spectral index of ζ, n_ζ reads

$$\begin{aligned}n_\zeta(k) &= 1 + \frac{d\ln P_\zeta}{d\ln k},\\ &\simeq 1 - 4\epsilon_{H*} + 2\eta_{H*} - 2(1+c){\epsilon_{H*}}^2,\\ &\quad - \frac{1}{2}(3-5c)\epsilon_{H*}\eta_{H*} - \frac{1}{2}(3-c){\xi_{H*}}^2 + O(\mathrm{SRP}^3),\\ &= -6\epsilon_{V*} + 2\eta_{V*} + \frac{1}{3}(44-18c){\epsilon_{V*}}^2)\\ &\quad + (4c-14)\epsilon_{V*}\eta_{V*} + \frac{2}{3}{\eta_{V*}}^2 + \frac{1}{6}(13-3c)\xi^2{}_{V*} + O(\mathrm{SRP}^3).\end{aligned} \tag{B.3.38}$$

where $c \equiv 4(\ln 2 + b) - 5 \simeq 0.08145$. The tensorial spectral index n_T is given by

$$\begin{aligned} n_T(k) &= \frac{d \ln P_T}{d \ln k}, \\ &\simeq -2\epsilon_{H*} - (3+c){\epsilon_{H*}}^2 + (1+c)\epsilon_{H*}\eta_{H*} + O(\mathrm{SRP}^3), \\ &= -2\epsilon_{V*} - \frac{1}{3}(8+6c){\epsilon_{V*}}^2 + \frac{1}{3}(1+3c)\epsilon_{V*}\eta_{V*} + O(\mathrm{SRP}^3). \end{aligned} \tag{B.3.39}$$

The tensor to scalar ration is obtained as

$$\begin{aligned} r &= \frac{25}{2}\epsilon_{H*}\left[1 + 2c(\epsilon_{H*} - \eta_{H*}) + O(\mathrm{SRP}^2)\right], \\ &= \frac{25}{2}\epsilon_{V*}\left[1 + 2(c - \frac{1}{3})(2\epsilon_{V*} - \eta_{V*}) + O(\mathrm{SRP}^2)\right]. \end{aligned} \tag{B.3.40}$$

B.3.4 Example 1: power law inflation

The power law inflation models, i.e., $a \propto t^p (p > 1)$ provide the constant ϵ_H and η_H, having the analytic solutions. Specifically, $1/p \equiv \epsilon_{H*} = \eta_{H*}$ and we obtain the power spectra shown in Eq. (B.3.37) as

$$P^{\frac{1}{2}}{}_{\zeta}(k_*) = \left[2^{\frac{1}{p-1}} \frac{\Gamma(\frac{3}{2} + \frac{1}{p-1})}{\Gamma(\frac{3}{2})} \left(1 - \frac{1}{p}\right)^{\frac{p}{p-1}}\right] \sqrt{\frac{p}{2}} \left(\frac{k}{k_*}\right)^{-\frac{1}{p-1}}, \tag{B.3.41}$$

and the tensor to scalar ration is

$$r = \sqrt{\frac{2}{p}}. \tag{B.3.42}$$

B.3.5 Example 2: natural inflation

The natural inflation models are provided $V(\phi)$ as

$$V(\phi) = \Lambda^4 \left[1 + \cos\left(\frac{\phi}{f}\right)\right], \tag{B.3.43}$$

By imposing $\phi/f \ll 1$, the equations of motion of the background are given as

$$\begin{aligned} H &= \sqrt{\frac{2}{3}}\Lambda^2, \\ V_\phi &= -\frac{\Lambda^4}{f^2}\phi, \\ \epsilon_{H*} &\simeq 0, \eta_{H*} \simeq \frac{3}{2}\left(\sqrt{1+\frac{2}{3f^2}}\right), \end{aligned} \tag{B.3.44}$$

Then the power spectra in Eq. (B.3.37) are

$$\begin{aligned} P^{\frac{1}{2}}{}_\zeta(k) &\simeq -\left[2^{\eta_{H*}}\frac{\Gamma\left(\frac{3}{2}-\eta_{H*}\right)}{\Gamma\left(\frac{3}{2}\right)}\right]\frac{\Lambda^2}{\sqrt{6}\pi\phi_*\eta_{H*}}\left(\frac{k}{k_*}\right)^{\eta_{H*}}, \\ P^{\frac{1}{2}}{}_\mathcal{T}(k) &= \frac{\Lambda^2}{\sqrt{6}\pi}. \end{aligned} \tag{B.3.45}$$

The spectral index for the scalar power spectrum n_ζ is derived as

$$n_\zeta = 1 + 2\eta_{H*}\,. \tag{B.3.46}$$

B.4 EFT of Inflation

This is a note how to compute the primordial power spectra in inflationary epoch in the Lifshitz regime of Horava gravity. The main purpose of this note is to summarize my previous computation in more formal way and also make it understood how a scalar graviton gets decoupled with the adiabatic mode before the adiabatic mode is preserved.

B.4.1 Construction of the action in unitary gauge

We consider an action that breaks time diffeomorphism invariance $t \to \tilde{t}(x)$ and preserve spatilally deffeomorphism invariance $x^i \to x^i + \xi^i(x)$. If we choose the unitary gauge, we can choose the time coordinate $t = \tilde{t}$. Then we can obtain a total Lagrangian as

$$\begin{aligned} S = \int d^4x\sqrt{-g}\Bigg[&\frac{1}{2}M_{\rm Pl}^2 R - c(t)g^{00} - \Lambda(t) + \frac{1}{2!}M_2^4(t)(g^{00}+1)^2 + \frac{1}{3!}M_3^4(t)(g^{00}+1)^3 \\ &- \frac{\bar{M}_1^3(t)}{2}(g^{00}+1)\delta K^\mu{}_\mu - \frac{\bar{M}_2^2(t)}{2}\delta K^\mu{}_\mu{}^2 - \frac{\bar{M}_3^2(t)}{2}\delta K^\mu{}_\nu \delta K^\nu{}_\mu\Bigg], \end{aligned} \tag{B.4.1}$$

where $\delta K_{\mu\nu} = K_{\mu\nu} - a^2 H h_{\mu\nu}$ and $h_{\mu\nu}$ is spatially induced metric. If we consider the FRW metric which is given by

$$ds^2 = -\mathrm{d}t^2 + a^2(t) g_{ij} \mathrm{d}x^i \mathrm{d}x^j \,. \tag{B.4.2}$$

The background solutions are given as usual

$$H^2 = \frac{1}{3M_{\rm Pl}^2} \left[c(t) + \Lambda(t) \right] , \tag{B.4.3}$$

$$\frac{\ddot{a}}{a} = \dot{H} + H^2 = \frac{1}{3M_{\rm Pl}^2} \left[2c(t) - \Lambda(t) \right] . \tag{B.4.4}$$

Solving for $c(t)$ and $\Lambda(t)$ Eq. (B.4.1) is rewritten as

$$\begin{aligned} S = \int d^4x \sqrt{-g} \Bigg[& \frac{1}{2} M_{\rm Pl}^2 R + M_{\rm Pl}^2 \dot{H} g^{00} - M_{\rm Pl}^2 (3H^2 + \dot{H}) + \frac{1}{2!} M_2^4(t) (g^{00}+1)^2 + \frac{1}{3!} M_3^4(t) (g^{00}+1)^3 \\ & - \frac{\bar{M}_1^3(t)}{2} (g^{00}+1) \delta K^\mu{}_\mu - \frac{\bar{M}_2^2(t)}{2} \delta K^\mu{}_\mu{}^2 - \frac{\bar{M}_3^2(t)}{2} \delta K^\mu{}_\nu \delta K^\nu{}_\mu \Bigg] , \end{aligned} \tag{B.4.5}$$

B.4.2 Action for the Goldstone Boson

Then we now observe that the breaking symmetry of time translation will produce a new degree of freedom, which originate from gauge symmetry due to the general covariance. Time translation is defined with some function $\pi(t, \mathbf{x})$ on space-time as

$$t \to \tilde{t}(t) = t + \pi(t, \mathbf{x}) \,, \tag{B.4.6}$$

In a usual case that time translation symmetry preserves, π never appears in the Lagrangian, which behaves just a gauge degree of freedom. On the other hand π becomes a physical variable. due to the breaking of time translation symmetry. Under the unitary gauge such that the background time is constant as $t = \tilde{t}(t)$, it is quite easy how π behaves as a Nambu-Goldstone mode. Here we consider a general case and then we treat π in the same way. First of al, we begin with

$$\int d^4x \sqrt{-g} \left[A(t) + B(t) g^{00}(x) \right] , \tag{B.4.7}$$

Under a broken time Diffs. $t \to +\xi^0(x)$, $\mathbf{x} \to \tilde{\mathbf{x}} = \mathbf{x}$, g^{00} transforms as :

$$g^{00}(x) \to \tilde{g}^{00}(\tilde{x}(x)) = \frac{\partial \tilde{x}^0(x)}{\partial x^\mu}\frac{\partial \tilde{x}^0(x)}{\partial x^\nu} g^{\mu\nu}(x)\,, \tag{B.4.8}$$

The action written in terms of the transformed fields is given by:

$$\int d^4x \sqrt{-\tilde{g}(\tilde{x}(x))}\left|\frac{\partial \tilde{x}}{\partial x}\right|\left[A(t) + B(t)\frac{\partial \tilde{x}^0}{\partial x^\mu}\frac{\partial \tilde{x}^0}{\partial x^\nu} g^{00}(x)\right], \tag{B.4.9}$$

$$\int d^4\tilde{x}\sqrt{-\tilde{g}(\tilde{x})}\left[A(\tilde{t}-\xi^0(x(\tilde{x}))) + B(\tilde{t}-\xi^0(x(\tilde{x})))\frac{\partial(\tilde{t}-\xi^0(x(\tilde{x})))}{\partial \tilde{x}^\mu}\tilde{g}^{\mu\nu}(\tilde{x})\frac{\partial(\tilde{t}-\xi^0(x(\tilde{x})))}{\partial \tilde{x}^\nu}\tilde{g}^{\mu\nu}(\tilde{x})\right], \tag{B.4.10}$$

$$\xi^0(x(\tilde{x})) \to -\tilde{\pi}(\tilde{x})\,, \tag{B.4.11}$$

$$\pi(x) \to \tilde{\pi}(\tilde{x}) = \pi(x) - \xi^0(x)\,, \tag{B.4.12}$$

Then we assume that all coupling terms such as

$$M_{\rm Pl}^2 \dot{H}\dot{\pi}\delta g^{00},\ M_2^4\dot{\pi}\delta g^{00}\,,$$

are negligible. In other words, this happens when we take the energy scale E satisfies $E \gg E_{\rm mix}$. Here $E_{\rm mix}$ is the energy scale at which the interaction terms become relevant. Under the assumption we obtain the action with the NG boson π as

$$S_\pi = \int d^4x\sqrt{-g}\left[\frac{1}{2}M_{\rm Pl}^2 R - M_{\rm Pl}^2\dot{H}\left(\dot{\pi}^2 - \frac{(\partial_i\pi)^2}{a^2}\right) + 2M_2^4\left(\dot{\pi}^2 + \dot{\pi}^3 - \dot{\pi}\frac{(\partial_i\pi)^2}{a^2}\right) - \frac{4}{3}M_3^4\dot{\pi}^3\right], \tag{B.4.13}$$

Then we pick up some examples. If we consider an inflationary model provided that it is well described under a slow-roll approximation, the interaction terms with $\dot{H}$ becomes sub-dominant.

$$g_{ij} = a^2(t)\left[1 + 2\zeta(t,\mathbf{x})\delta_{ij} + h_{ij}\right], \tag{B.4.14}$$

where h_{ij} is a tensor mode. We compute time translation $t \to t - \pi(x)$. This translation gives translation of the scale factor $a(t) \to a(t - \pi(x,t))$. Due to the Diffs invariance

of the metric g_{ij}, ζ is given by

$$\zeta(t, \mathbf{x}) \to -H\pi(t, \mathbf{x})\,. \tag{B.4.15}$$

Here, ζ corresponds to the curvature perturbation.

B.5 Preservation of adiabatic perturbation

B.5.1 Adiabatic perturbation

Spatial curvature perturbation $\mathcal{R}$

$$\gamma_{ij} = a^2 e^{2\mathcal{R}} \delta_{ij}\,, \tag{B.5.1}$$

We consider four dimentional de Sitter space. The spacial metric in a de Sitter space is

$$\gamma_{ij} = e^{2Ht+2\mathcal{R}} \delta_{ij}\,, \tag{B.5.2}$$

The metric γ_{ij} stays invariant with a certain coordinate transformation

$$t \to t - s, \mathbf{x} \to e^s \mathbf{x} \tag{B.5.3}$$

As a result, any perturbative fluctuation $\mathcal{R}$ is not physical on a de Sitter space. In the general space-time that is assymptotically de Sitter space, however,

$$\mathbf{x} \to e^s \mathbf{x},\ \mathcal{R} \to \mathcal{R} - s\,, \tag{B.5.4}$$

This instantly conclude that $\mathcal{R}$ does not have the mass term in its Lagrangian, preventing $\mathcal{R}$ from decay at lower energy scale, or equivalently at super-horizon scale. This is why the $\mathcal{R}$ is "frozen out" at the horizon crossing scale.

In the inflationary universe, the spacial curvature $\mathcal{R}$ and the inflaton fluctuation φ are both gauge-dependent. Thus we normally choose the gauge-invariant curvature perturbation, ζ,

$$\zeta \equiv \mathcal{R} - \frac{H}{\dot{\phi}}\varphi\,, \tag{B.5.5}$$

When the inflaton weakly couples with the curvature, namely, the slow-roll regime, interaction terms between ζ and φ eventually disappears at $k/aH \to 0$. Recall, the

power spectrum of ζ

$$\mathcal{R} \to \mathcal{R} - HT\,, \tag{B.5.6}$$

$$\varphi \to \varphi - \dot{\phi}T\,, \tag{B.5.7}$$

After horizon exit, the curvature fluctuaion ζ seeds the density fluctuation, $\delta\rho$, at sub-horizon scale through

$$\zeta = \mathcal{R} + \frac{\delta\rho}{\rho + P}\,, \tag{B.5.8}$$

By solving the equation of motions, it is shown that

$$\zeta' \simeq \mathcal{O}\left(\left(\frac{k}{aH}\right)^2\right)\,, \tag{B.5.9}$$

meaning the initial two-point correlation of ζ is still preserved outside the horizon. For this property ζ is sometimes called as the adiabatic fluctiation in the sense that ζ would not source additional fluctuation at super horizon. In general, if there are non-trivial interactions with other fields in the background spacetime with matter fields, the adiabatic fluctuations are sourced by these materials and are no longer in conservation mode. In general, entropy fluctuation occurs. For more information, [167] should be referred.

Appendix C

Formulae for angular auto and cross correlations

We briefly summarise the expansion with spherical harmonics of physical quantities. We argue how angular power spectra are given by representative physical variables by a representative physical variable A as,

$$A(t, \mathbf{x}, \mathbf{n}) = \sum_{\ell=0}^{\infty} \sum_{m=-\ell}^{m=\ell} a_{\ell m}(t, \mathbf{x}) Y_{\ell m}(\mathbf{n}) \,, \tag{C.0.1}$$

We specify a certain 2d surface in the spacetime with a coordinate $(t, \mathbf{x})$. $\mathbf{n}$ denotes a unit vector on unit 2d sphere. Once we determine a certain projection process, the coordinate variables on the surface are functions with respect to $\mathbf{n}$,i.e., $(t(\mathbf{n}), \mathbf{x}(\mathbf{n}))$. Hereafter we omit the arguments of the coordinates in $a_{\ell m}$ as $a_{\ell m}(\mathbf{n})$. The angular correlation between two physical variables A and B are given as

$$\left\langle A(\mathbf{n}) B(\mathbf{n}') \right\rangle = \sum_{\ell, m, \ell', m'} \langle a_{\ell m} b_{\ell' m'} \rangle \, Y_{\ell m}(\mathbf{n}) Y^*_{\ell' m'}(\mathbf{n}') \,, \tag{C.0.2}$$

The bracket on the both sides of Eq. (C.0.2) denotes a ensemble average of the quantities of what are in the bracket. To compute the ensemble average, we apply a hypothesis owing to process the average. In cosmology, most of the cases, we apply the hypothesis of homogeneity and isotropy of the Universe, namely the cosmological principle. Under the cosmological principle, the average in the angular direction should be independent in the direction, resulting the ensemble average of the coefficient in the right hand side

of Eq. (C.0.2) satisfies the following condition,

$$\langle a_{\ell m} b_{\ell' m'} \rangle = C_{AB,\ell} \delta_{\ell\ell'} \delta_{mm'} \,, \tag{C.0.3}$$

where $C_{AB,\ell}$ is the angular correlation coefficient between A and B, and $\delta_{\ell\ell'}$ and $\delta_{mm'}$ are the delta functions. In particular, the auto power $C_{AA,\ell}$ is given as

$$C_{AA,\ell} = \frac{1}{2\ell+1} \sum_{m=-\ell}^{m=\ell} \langle a_{\ell m} a^*_{\ell m} \rangle \,, \tag{C.0.4}$$

Inserting the coefficients in Eq. (C.0.3) into Eq. (C.0.2) and we obtain

$$\big\langle A(\mathbf{n}) B(\mathbf{n}') \big\rangle = \sum_{\ell=0}^{\infty} \frac{2\ell+1}{4\pi} C_{AB,\ell} P_\ell(\mathbf{n}\cdot\mathbf{n}') \,, \tag{C.0.5}$$

where we use the addition theorem of the spherical harmonics,

$$P_l(\mathbf{n}\cdot\mathbf{n}') = \frac{4\pi}{2\ell+1} \sum_{m=-\ell}^{m=\ell} Y_{\ell m}(\mathbf{n}) Y^*_{\ell m}(\mathbf{n}') \,, \tag{C.0.6}$$

Here $P_\ell(x)$ gives Legendre polynomial. The coefficients a_{lm} is inversely given by,

$$a_{\ell m} = \int d\Omega_{\mathbf{n}} A(\mathbf{n}) Y^*_{\ell m}(\mathbf{n}) \,, \tag{C.0.7}$$

by using the orthogonality of $Y_{\ell m}(\mathbf{n})$ as

$$\int d\Omega_{\mathbf{n}} Y_{lm}(\mathbf{n}) Y^*_{\ell' m'}(\mathbf{n}) = \delta_{\ell\ell'} \delta_{mm'} \,, \tag{C.0.8}$$

If $A(\mathbf{n})$ is constant in the whole sky, i.e., $A(\mathbf{n}) = \bar{A}$, the coefficient $a_{\ell m}$ is computed from Eq. (C.0.7) as

$$\begin{aligned} a_{\ell m} &= \int d\Omega_{\mathbf{n}} \bar{A} Y^*_{\ell m}(\mathbf{n}) \\ &= \sqrt{4\pi}\bar{A} \int d\Omega_{\mathbf{n}} Y_{00}(\mathbf{n}) Y^*_{\ell m}(\mathbf{n}) \\ &= \sqrt{4\pi}\bar{A} \delta_{0l} \delta_{0m} \,, \end{aligned} \tag{C.0.9}$$

This explicitly shows that the constant mode of a physical quantity is recasted by a_{00}.

C.1 angular correlations in imperfect sky

Ideally, the angular correlations of the CMB or galaxy distributions should be measured on the whole sky. Under the cosmological principle, the observables in the average of the angular direction is a good estimator corresponding to the ensemble of the physical conditions that presumably realise in the Universe. In reality, however, only the part of the sky is for the cosmological measurements, simply because we live in the galaxy with the bunch of stars and gases that act as a foreground, ending up with the incompletion of the cosmological ensemble. We treat such an imperfect information carefully to what we can practically apply for the cosmological purposes. Here, we examine properties of the angular correlation on the covered sky. We consider a certain physical variable $A(\mathbf{n})$ as

$$A(\mathbf{n}) = \sum_{\ell=0}^{\infty} \sum_{m=-\ell}^{\ell} a_{\ell m} Y_{\ell m}(\mathbf{n}) \,, \tag{C.1.1}$$

Then we consider the window function $W(\mathbf{n})$ that artificially covers depending on the area of the sky Ω,

$$W(\mathbf{n};\Omega) = \begin{cases} 1 \ (\mathbf{n} \in \Omega) \\ 0 \ (\mathbf{n} \notin \Omega) \end{cases} \tag{C.1.2}$$

The window function $W(\mathbf{n};\Omega)$ works on the variable $A(\mathbf{n})$ in the form of a multiplier as a consequence of the fair sample hypothesis. Then the observed value of $A(\mathbf{n})$ is given as

$$A(\Omega) \equiv W(\mathbf{n};\Omega) A(\mathbf{n}) \tag{C.1.3}$$

where we denote $A(\Omega)$ as the variable limited in the uncovered sky. Notice that $W(\mathbf{n})$ changes the normalization of any angular average by the factor $f_{\rm sky} \equiv \int d\Omega W(\mathbf{n})/4\pi$. Since the window function acts on the spherical orthogonal basis, we define

$$W(\mathbf{n};\Omega) Y_{\ell m}(\mathbf{n}) \equiv \sum_{\ell',m'} W_{\ell\ell'}{}^{mm'} Y_{\ell' m'}(\mathbf{n}) \,, \tag{C.1.4}$$

Then we define the observed angular coefficient as

$$A_{\ell m} \equiv \sum_{\ell',m'} W_{\ell\ell'}{}^{mm'} a_{\ell m} \,, \tag{C.1.5}$$

We define the window function $W(\mathbf{n};\Omega)$ in the form of the Fourier coefficient on the sphere,

$$I_{\ell m} = \int d\Omega_{\mathbf{n}} W(\mathbf{n};\Omega) Y^*_{\ell m}(\mathbf{n})\,, \tag{C.1.6}$$

For the later convenience, we introduce the coefficient $J_{\ell m}$

$$J_{\ell m} = \int d\Omega_{\mathbf{n}} W(\mathbf{n};\Omega) Y_{\ell m}(\mathbf{n}) Y^*_{\ell m}(\mathbf{n})\,, \tag{C.1.7}$$

Notice that $J_{\ell m}$ is the Fourier coefficient of the map $W(\mathbf{n};\Omega)$. Interestingly the angular average of $J_{\ell m}$ robustly coincide with the sky coverage,

$$\begin{aligned} J_\ell \equiv \frac{1}{2\ell+1}\sum_{m=-\ell}^{m=\ell} J_{\ell m} &= \int \frac{d\Omega_{\mathbf{n}} W(\mathbf{n};\Omega)}{4\pi}\left[\frac{4\pi}{2\ell+1}\sum_{m=-\ell}^{m=\ell} Y_{\ell m}(\mathbf{n}) Y^*_{\ell m}(\mathbf{n})\right], \\ &= \int \frac{d\Omega_{\mathbf{n}} W(\mathbf{n};\Omega)}{4\pi} P_\ell(1) = \int \frac{d\Omega_{\mathbf{n}} W(\mathbf{n};\Omega)}{4\pi} = f_{\rm sky} \end{aligned} \tag{C.1.8}$$

Here we use Eq. (C.0.6) to extract the Legendre polynomial and the boundary condition for the Legendre polynomial, $P_\ell(1) = 1$.

C.2 Statistical preliminaries for galaxy surveys

C.2.1 Variance of galaxies

We argue how we apply galaxy surveys for obtaining information of cosmology. What we should care when we use the data of galaxy distribution is the discreteness of galaxies in the sky. In a real survey, galaxies are observed as luminous points in the sky, leading a peculiar statistical error on measuring the density fluctuation in the Universe. The statistical characteristics of the galaxy distribution is Poisson statistics via its discreteness. Let us start with an array n_i $(i = 1, 2, ..., N_{\rm pix})$ s.t $\sum_i n_i = N_{\rm gal}$. We compute the mean value of the galaxies distributed in each pixel. Without no preference of the pixel, namely, equipartition in pixels, the mean value is fairly given by $\lambda = N_{\rm pix}/N_{\rm gal}$. Then the Poisson statistics provides a certain n_i that is likely to be the distribution of galaxies around the mean value λ. The statistical measures, i.e, the mean and the variance of n_i are computed as

$$\langle n\rangle = \lambda\,,\ \langle n^2\rangle - \langle n\rangle^2 = \lambda\,, \tag{C.2.1}$$

To reconstruct these statistical behaviours from observational data, we use standard arithmetic estimators as

$$\langle n \rangle_{\rm obs} \ , \ \sigma^2_{\rm obs} \equiv \left\langle n^2 \right\rangle_{\rm obs} - \langle n \rangle^2_{\rm obs} \ , \tag{C.2.2}$$

$$\langle A \rangle_{\rm obs} \equiv \frac{1}{N_{\rm pix}} \sum_{i=1}^{N_{\rm pix}} A_i \, , \tag{C.2.3}$$

According to the central limit theorem, at large $N_{\rm pix}$, the two statistics above makes a relation as $\langle A \rangle = \langle A \rangle_{\rm obs} + \mathcal{O}(1/N_{\rm pix})$, practically $\langle A \rangle \approx \langle A \rangle_{\rm obs}$. Hereafter '$\approx$' denotes the equality on the central limit theorem that is exactly identical to the true equal when $N_{\rm pix} \to \infty$. For convenience we define the contrast δ_i as

$$\delta_i \equiv \frac{n_i - \langle n \rangle}{\langle n \rangle} \, , \tag{C.2.4}$$

Hereafter we omit the difference between the two statistics. Notice that $\langle \delta \rangle = 0$. From the central limit theorem we obtain

$$\left\langle \delta^2 \right\rangle \approx \frac{\lambda}{\lambda^2} \approx \frac{N_{\rm pix}}{N_{\rm gal}} \, , \tag{C.2.5}$$

Notice that $\left\langle \delta^2 \right\rangle$ proportionally grows with $N_{\rm pix}$. This fundamentally captures the feature that the estimator cannot tell any difference of a observed statistics from the uniform distribution of pixels. However, the randomness of the pixels is able to removed by dividing by $N_{\rm pix}$, namely a meaningful estimator is $\sigma^2 \equiv \left\langle \delta^2 \right\rangle / N_{\rm pix}$. In fact, if δ_i is realised under the Gaussian statistics with the variance σ_0^2, the randomness of the pixels exactly increases by a factor $N_{\rm pix}$, leading us to estimate σ_0^2 via $\sigma_0^2 \approx \sigma^2 = 1/N_{\rm gal}$. In more detail, we compute $\left\langle \delta^2 \right\rangle$ by the following integration,

$$\left\langle \delta^2 \right\rangle \approx \int \Pi_i d\delta_i \times \sum_j \delta_j^2 \times \{ {\rm Norm}(0, \sigma_0^2) \}^{N_{\rm pix}} = N_{\rm pix} \sigma_0^2 \, , \tag{C.2.6}$$

where ${\rm Norm}(0, \sigma_0^2)$ denotes the normal Gaussian distribution with the variance σ_0^2. More optimal way to derive the same property of the distribution of the points is as follows. $n_i = 0$ or 1.

C.3 number density contrast

For preliminary, let me type out all the equations how the distribution of galaxies in redshifts is projected on an observed sky. Starting with the definition of the number

density contrast on an observed sky as

$$\delta_g(z_{\rm obs},\theta,\varphi) \equiv \frac{\Sigma(z_{\rm obs},\theta,\varphi)-\bar{\Sigma}(z_{\rm obs})}{\bar{\Sigma}(z_{\rm obs})}\,, \tag{C.3.1}$$

Here $\Sigma(z_{\rm obs},\theta,\varphi)$ is the surface number density of galaxies (more general any astronomical objects) at $z = z_{\rm obs}$. $\bar{\Sigma}(z_{\rm obs})$ is the background density computed by $\bar{\Sigma}(z_{\rm obs}) = \int d\Omega\Sigma(z_{\rm obs},\theta,\varphi)/4\pi$, where $d\Omega$ denote infinitesimal solid angle. For simplicity, we temporarily omit $z_{\rm obs}$ from the functions used for the computation. To derive $\Sigma(\theta,\varphi)$, we count the number of galaxies for each redshift. We define the number density of galaxies at a certain redshift z as $n(z,\theta,\varphi)$. The differential volume element at z is given with the comoving distance $\chi(z)$ via $d\Omega d\chi\chi^2$. By integrating along χ we obtain Σ as

$$\Sigma(z,\theta,\varphi) = \int_{\chi}^{\chi_*} d\chi\chi^2 n(z,\theta,\varphi) \tag{C.3.2}$$

where $\chi_* = \chi(z_*)$ and $\chi_{\rm obs} = \chi(z_{\rm obs})$ respectively. Under the assumption of isotropy of the Universe, $\bar{\Sigma}$ is given with the mean number density $\bar{n}(z)$ via

$$\bar{\Sigma} = \int_{\chi_{\rm obs}}^{\chi_*} d\chi\chi^2\bar{n}(z)\,, \tag{C.3.3}$$

Replacing Σ and $\bar{\Sigma}$ in Eq. (C.3.1) with the right hand side of Eqs. (C.3.2) and (C.3.3) we obtain the final expression of δ_g as

$$\delta_g(z_{\rm obs},\theta,\varphi) = \int_{z_{\rm obs}}^{z_*} dz f(z)\tilde{\delta}_g(z,\theta,\varphi)\,, \tag{C.3.4}$$

$$\tilde{\delta}_g(z,\theta,\varphi) \equiv \frac{n(z,\theta,\varphi)-\bar{n}(z)}{\bar{n}(z)} = b(z)\delta_m(z,\theta,\varphi)\,, \tag{C.3.5}$$

$$f(z) \equiv \frac{d\chi/dz\cdot\chi^2\bar{n}}{\int_{\chi_{\rm obs}}^{\chi_*} d\chi\chi^2\bar{n}} = \frac{d\Sigma/dz}{\bar{\Sigma}}\,, \tag{C.3.6}$$

where $\delta_m(z,\theta,\varphi)$, the density contrast. We notice that $f(z)$ describe the probability distribution of galaxies since $\int dz f(z) = 1$. Proportionality of $\tilde{\delta}_g$ to δ_m reasonably captures at linear level that the formation of galaxies takes place in a dense region. $b(z)$ is called **bias factor**.

Bibliography

[1] Shun Arai, Purnendu Karmakar, and Atsushi Nishizawa. Cosmological evolution of viable models in the generalized scalar-tensor theory. 2019.

[2] Atsushi Nishizawa and Shun Arai. Generalized framework for testing gravity with gravitational-wave propagation. III. Future prospect. *Phys. Rev.*, D99(10):104038, 2019.

[3] Shun Arai, Sergey Sibiryakov, and Yuko Urakawa. Inflationary perturbations with Lifshitz scaling. *JCAP*, 1903(03):034, 2019.

[4] Shun Arai and Atsushi Nishizawa. Generalized framework for testing gravity with gravitational-wave propagation. II. Constraints on Horndeski theory. *Phys. Rev.*, D97(10):104038, 2018.

[5] D. J. Fixsen, E. S. Cheng, J. M. Gales, John C. Mather, R. A. Shafer, and E. L. Wright. The Cosmic Microwave Background spectrum from the full COBE FIRAS data set. *Astrophys. J.*, 473:576, 1996.

[6] D. N. Spergel et al. First year Wilkinson Microwave Anisotropy Probe (WMAP) observations: Determination of cosmological parameters. *Astrophys. J. Suppl.*, 148:175–194, 2003.

[7] P. A. R. Ade et al. Planck 2013 results. I. Overview of products and scientific results. *Astron. Astrophys.*, 571:A1, 2014.

[8] S. Perlmutter et al. Measurements of Omega and Lambda from 42 high redshift supernovae. *Astrophys. J.*, 517:565–586, 1999.

[9] Adam G. Riess et al. Observational evidence from supernovae for an accelerating universe and a cosmological constant. *Astron. J.*, 116:1009–1038, 1998.

[10] Alan H. Guth. The Inflationary Universe: A Possible Solution to the Horizon and Flatness Problems. *Phys. Rev.*, D23:347–356, 1981. [Adv. Ser. Astrophys. Cosmol.3,139(1987)].

[11] Alexei A. Starobinsky. A New Type of Isotropic Cosmological Models Without Singularity. *Phys. Lett.*, 91B:99–102, 1980. [Adv. Ser. Astrophys. Cosmol.3,130(1987); ,771(1980)].

[12] K. Sato. Cosmological Baryon Number Domain Structure and the First Order Phase Transition of a Vacuum. *Phys. Lett.*, 99B:66–70, 1981. [Adv. Ser. Astrophys. Cosmol.3,134(1987)].

[13] P. de Bernardis et al. A Flat universe from high resolution maps of the cosmic microwave background radiation. *Nature*, 404:955–959, 2000.

[14] P.A.R. Ade et al. Planck 2013 results. XVI. Cosmological parameters. 2013.

[15] W. L. Freedman et al. Final results from the Hubble Space Telescope key project to measure the Hubble constant. *Astrophys. J.*, 553:47–72, 2001.

[16] P. A. R. Ade et al. Planck 2015 results. XIII. Cosmological parameters. *Astron. Astrophys.*, 594:A13, 2016.

[17] Dragan Huterer and Michael S. Turner. Prospects for probing the dark energy via supernova distance measurements. *Phys. Rev.*, D60:081301, 1999.

[18] Michael S. Turner and Martin J. White. CDM models with a smooth component. *Phys. Rev.*, D56(8):R4439, 1997.

[19] P. J. E. Peebles and Bharat Ratra. The Cosmological constant and dark energy. *Rev. Mod. Phys.*, 75:559–606, 2003. [,592(2002)].

[20] K. S. Stelle. Classical Gravity with Higher Derivatives. *Gen.Rel.Grav.*, 9:353–371, 1978.

[21] Gerard 't Hooft. Dimensional reduction in quantum gravity. *Conf. Proc.*, C930308:284–296, 1993.

[22] Luca Amendola and Shinji Tsujikawa. *Dark Energy: Theory and Observations.* 2010.

[23] Jurjen F. Koksma and Tomislav Prokopec. The Cosmological Constant and Lorentz Invariance of the Vacuum State. 2011.

[24] L. Verde, T. Treu, and A. G. Riess. Tensions between the Early and the Late Universe. In *Nature Astronomy 2019*, 2019.

[25] Gregory Walter Horndeski. Second-order scalar-tensor field equations in a four-dimensional space. *Int. J. Theor. Phys.*, 10:363–384, 1974.

[26] Tsutomu Kobayashi, Masahide Yamaguchi, and Jun'ichi Yokoyama. Generalized G-inflation: Inflation with the most general second-order field equations. *Prog. Theor. Phys.*, 126:511–529, 2011.

[27] Antonio De Felice and Shinji Tsujikawa. f(R) theories. *Living Rev.Rel.*, 13:3, 2010.

[28] C. Deffayet, Xian Gao, D. A. Steer, and G. Zahariade. From k-essence to generalised Galileons. *Phys. Rev.*, D84:064039, 2011.

[29] Cedric Deffayet, Oriol Pujolas, Ignacy Sawicki, and Alexander Vikman. Imperfect Dark Energy from Kinetic Gravity Braiding. *JCAP*, 1010:026, 2010.

[30] Giulia Gubitosi, Federico Piazza, and Filippo Vernizzi. The Effective Field Theory of Dark Energy. *JCAP*, 1302:032, 2013. [JCAP1302,032(2013)].

[31] Jérôme Gleyzes, David Langlois, Federico Piazza, and Filippo Vernizzi. Essential Building Blocks of Dark Energy. *JCAP*, 1308:025, 2013.

[32] Emilio Bellini and Ignacy Sawicki. Maximal freedom at minimum cost: linear large-scale structure in general modifications of gravity. *JCAP*, 1407:050, 2014.

[33] Clifford Cheung, Paolo Creminelli, A. Liam Fitzpatrick, Jared Kaplan, and Leonardo Senatore. The Effective Field Theory of Inflation. *JHEP*, 03:014, 2008.

[34] Jérôme Gleyzes, David Langlois, Michele Mancarella, and Filippo Vernizzi. Effective Theory of Dark Energy at Redshift Survey Scales. *JCAP*, 1602(02):056, 2016.

[35] Jacob D. Bekenstein. The Relation between physical and gravitational geometry. *Phys. Rev.*, D48:3641–3647, 1993.

[36] Guillem Domenech, Atsushi Naruko, and Misao Sasaki. Cosmological disformal invariance. *JCAP*, 1510(10):067, 2015.

[37] C. Deffayet, Gilles Esposito-Farese, and A. Vikman. Covariant Galileon. *Phys. Rev.*, D79:084003, 2009.

[38] Jérôme Gleyzes, David Langlois, Federico Piazza, and Filippo Vernizzi. Healthy theories beyond Horndeski. *Phys. Rev. Lett.*, 114(21):211101, 2015.

[39] David Langlois and Karim Noui. Degenerate higher derivative theories beyond Horndeski: evading the Ostrogradski instability. *JCAP*, 1602(02):034, 2016.

[40] David Langlois and Karim Noui. Hamiltonian analysis of higher derivative scalar-tensor theories. *JCAP*, 1607(07):016, 2016.

[41] G. W. Horndeski. Second-Order Scalar-Tensor Field Equations in a Four-Dimensional Space. *International Journal of Theoretical Physics*, 10:363–384, September 1974.

[42] Takeshi Chiba, Takahiro Okabe, and Masahide Yamaguchi. Kinetically driven quintessence. *Phys. Rev.*, D62:023511, 2000.

[43] C. Armendariz-Picon, Viatcheslav F. Mukhanov, and Paul J. Steinhardt. Essentials of k essence. *Phys. Rev.*, D63:103510, 2001.

[44] Alberto Nicolis, Riccardo Rattazzi, and Enrico Trincherini. The Galileon as a local modification of gravity. *Phys. Rev.*, D79:064036, 2009.

[45] Jibril Ben Achour, David Langlois, and Karim Noui. Degenerate higher order scalar-tensor theories beyond Horndeski and disformal transformations. *Phys. Rev.*, D93(12):124005, 2016.

[46] Hayato Motohashi, Karim Noui, Teruaki Suyama, Masahide Yamaguchi, and David Langlois. Healthy degenerate theories with higher derivatives. *JCAP*, 1607(07):033, 2016.

[47] David Langlois. Dark energy and modified gravity in degenerate higher-order scalar–tensor (DHOST) theories: A review. *Int. J. Mod. Phys.*, D28(05):1942006, 2019.

[48] B. P. Abbott et al. GW170817: Observation of Gravitational Waves from a Binary Neutron Star Inspiral. *Phys. Rev. Lett.*, 119(16):161101, 2017.

[49] B. P. Abbott et al. Gravitational Waves and Gamma-rays from a Binary Neutron Star Merger: GW170817 and GRB 170817A. *Astrophys. J.*, 848(2):L13, 2017.

[50] Ippocratis D. Saltas, Ignacy Sawicki, Luca Amendola, and Martin Kunz. Anisotropic Stress as a Signature of Nonstandard Propagation of Gravitational Waves. *Phys. Rev. Lett.*, 113(19):191101, 2014.

[51] Atsushi Nishizawa. Generalized framework for testing gravity with gravitational-wave propagation. I. Formulation. *Phys. Rev.*, D97(10):104037, 2018.

[52] Kurt Hinterbichler. Theoretical Aspects of Massive Gravity. *Rev. Mod. Phys.*, 84:671–710, 2012.

[53] Claudia de Rham. Massive Gravity. *Living Rev. Rel.*, 17:7, 2014.

[54] B. P. Abbott et al. Multi-messenger Observations of a Binary Neutron Star Merger. *Astrophys. J.*, 848(2):L12, 2017.

[55] Atsushi Nishizawa and Takashi Nakamura. Measuring Speed of Gravitational Waves by Observations of Photons and Neutrinos from Compact Binary Mergers and Supernovae. *Phys. Rev.*, D90(4):044048, 2014.

[56] P. A. R. Ade et al. Planck 2015 results. XIII. Cosmological parameters. *Astron. Astrophys.*, 594:A13, 2016.

[57] Noemi Frusciante, Ryotaro Kase, Kazuya Koyama, Shinji Tsujikawa, and Daniele Vernieri. Tracker and scaling solutions in DHOST theories. *Phys. Lett.*, B790:167–175, 2019.

[58] Omer Farooq, Foram Ranjeet Madiyar, Sara Crandall, and Bharat Ratra. Hubble Parameter Measurement Constraints on the Redshift of the Deceleration?acceleration Transition, Dynamical Dark Energy, and Space Curvature. *Astrophys. J.*, 835(1):26, 2017.

[59] Antonio De Felice and Shinji Tsujikawa. Conditions for the cosmological viability of the most general scalar-tensor theories and their applications to extended Galileon dark energy models. *JCAP*, 1202:007, 2012.

[60] Jérôme Gleyzes. Parametrizing modified gravity for cosmological surveys. *Phys. Rev.*, D96(6):063516, 2017.

[61] J. Gleyzes, D. Langlois, and F. Vernizzi. A unifying description of dark energy. *International Journal of Modern Physics D*, 23:1443010, January 2014.

[62] Lucas Lombriser and Andy Taylor. Breaking a Dark Degeneracy with Gravitational Waves. *JCAP*, 1603(03):031, 2016.

[63] Ivan de Martino, Mariafelicia De Laurentis, and Salvatore Capozziello. Constraining $f(R)$ Gravity by the Large-Scale Structure. *Universe*, 1(2):123–157, 2015.

[64] Emilio Bellini and Raul Jimenez. The parameter space of Cubic Galileon models for cosmic acceleration. *Phys. Dark Univ.*, 2:179–183, 2013.

[65] Alexandre Barreira, Baojiu Li, Wojciech A. Hellwing, Carlton M. Baugh, and Silvia Pascoli. Nonlinear structure formation in the Cubic Galileon gravity model. *JCAP*, 1310:027, 2013.

[66] Janina Renk, Miguel Zumalacarregui, and Francesco Montanari. Gravity at the horizon: on relativistic effects, CMB-LSS correlations and ultra-large scales in Horndeski's theory. *JCAP*, 1607(07):040, 2016.

[67] Eric V. Linder. Challenges in connecting modified gravity theory and observations. *Phys. Rev.*, D95(2):023518, 2017.

[68] Antonio De Felice, Tsutomu Kobayashi, and Shinji Tsujikawa. Effective gravitational couplings for cosmological perturbations in the most general scalar-tensor theories with second-order field equations. *Phys. Lett.*, B706:123–133, 2011.

[69] Yong-Seon Song, Gong-Bo Zhao, David Bacon, Kazuya Koyama, Robert C. Nichol, and Levon Pogosian. Complementarity of Weak Lensing and Peculiar Velocity Measurements in Testing General Relativity. *Phys. Rev.*, D84:083523, 2011.

[70] Andrew Johnson, Chris Blake, Jason Dossett, Jun Koda, David Parkinson, and Shahab Joudaki. Searching for Modified Gravity: Scale and Redshift Dependent Constraints from Galaxy Peculiar Velocities. *Mon. Not. Roy. Astron. Soc.*, 458(3):2725–2744, 2016.

[71] Levon Pogosian and Alessandra Silvestri. What can cosmology tell us about gravity? Constraining Horndeski gravity with Σ and μ. *Phys. Rev.*, D94(10):104014, 2016.

[72] Wayne Hu and Ignacy Sawicki. A Parameterized Post-Friedmann Framework for Modified Gravity. *Phys. Rev.*, D76:104043, 2007.

[73] Bhuvnesh Jain and Pengjie Zhang. Observational Tests of Modified Gravity. *Phys. Rev.*, D78:063503, 2008.

[74] P. A. R. Ade et al. Planck 2015 results. XIV. Dark energy and modified gravity. *Astron. Astrophys.*, 594:A14, 2016.

[75] Luca Amendola, Martin Kunz, and Domenico Sapone. Measuring the dark side (with weak lensing). *JCAP*, 0804:013, 2008.

[76] Edmund Bertschinger and Phillip Zukin. Distinguishing Modified Gravity from Dark Energy. *Phys. Rev.*, D78:024015, 2008.

[77] Scott F. Daniel, Robert R. Caldwell, Asantha Cooray, and Alessandro Melchiorri. Large Scale Structure as a Probe of Gravitational Slip. *Phys. Rev.*, D77:103513, 2008.

[78] Eric V. Linder. No Slip Gravity. *JCAP*, 1803(03):005, 2018.

[79] Rampei Kimura, Tsutomu Kobayashi, and Kazuhiro Yamamoto. Vainshtein screening in a cosmological background in the most general second-order scalar-tensor theory. *Phys. Rev.*, D85:024023, 2012.

[80] W. W. Zhu et al. Tests of Gravitational Symmetries with Pulsar Binary J1713+0747. *Mon. Not. Roy. Astron. Soc.*, 482(3):3249–3260, 2019.

[81] James G. Williams, Slava G. Turyshev, and Dale H. Boggs. Progress in lunar laser ranging tests of relativistic gravity. *Phys. Rev. Lett.*, 93:261101, 2004.

[82] F. Hofmann and J. Muller. Relativistic tests with lunar laser ranging. *Class. Quant. Grav.*, 35(3):035015, 2018.

[83] A. Genova, E. Mazarico, S. Goossens, F. G. Lemoine, G. A. Neumann, D. E. Smith, and M. T. Zuber. Solar system expansion and strong equivalence principle as seen by the NASA MESSENGER mission. *Nature Communications*, 9:289, January 2018.

[84] Frank S. Accetta, Lawrence M. Krauss, and Paul Romanelli. New limits on the variability of G from big bang nucleosynthesis. *Phys. Lett.*, B248:146–150, 1990.

[85] Jean-Philippe Uzan. Varying Constants, Gravitation and Cosmology. *Living Rev. Rel.*, 14:2, 2011.

[86] Oliver Zahn and Matias Zaldarriaga. Probing the Friedmann equation during recombination with future CMB experiments. *Phys. Rev.*, D67:063002, 2003.

[87] Ken-ichi Umezu, Kiyotomo Ichiki, and Masanobu Yahiro. Cosmological constraints on Newton's constant. *Phys. Rev.*, D72:044010, 2005.

[88] Silvia Galli, Alessandro Melchiorri, George F. Smoot, and Oliver Zahn. From Cavendish to PLANCK: Constraining Newton's Gravitational Constant with CMB Temperature and Polarization Anisotropy. *Phys. Rev.*, D80:023508, 2009.

[89] Johannes Noller and Andrina Nicola. Cosmological parameter constraints for Horndeski scalar-tensor gravity. 2018.

[90] Alessio Spurio Mancini, Fabian Kohlinger, Benjamin Joachimi, Valeria Pettorino, Bjorn Malte Schafer, Robert Reischke, Samuel Brieden, Maria Archidiacono, and Julien Lesgourgues. KiDS+GAMA: Constraints on Horndeski gravity from combined large-scale structure probes. 2019.

[91] Ryo Nagata, Takeshi Chiba, and Naoshi Sugiyama. Observational consequences of evolution of primordial fluctuations in scalar - tensor cosmology. *Phys. Rev.*, D66:103510, 2002.

[92] Junpei Ooba, Kiyotomo Ichiki, Takeshi Chiba, and Naoshi Sugiyama. Planck constraints on scalar-tensor cosmology and the variation of the gravitational constant. *Phys. Rev.*, D93(12):122002, 2016.

[93] David Langlois, Michele Mancarella, Karim Noui, and Filippo Vernizzi. Effective Description of Higher-Order Scalar-Tensor Theories. *JCAP*, 1705(05):033, 2017.

[94] Jibril Ben Achour, Marco Crisostomi, Kazuya Koyama, David Langlois, Karim Noui, and Gianmassimo Tasinato. Degenerate higher order scalar-tensor theories beyond Horndeski up to cubic order. *JHEP*, 12:100, 2016.

[95] Marco Crisostomi, Kazuya Koyama, and Gianmassimo Tasinato. Extended Scalar-Tensor Theories of Gravity. *JCAP*, 1604(04):044, 2016.

[96] Paolo Creminelli, Matthew Lewandowski, Giovanni Tambalo, and Filippo Vernizzi. Gravitational Wave Decay into Dark Energy. *JCAP*, 1812(12):025, 2018.

[97] Jolyon K. Bloomfield, Éanna É. Flanagan, Minjoon Park, and Scott Watson. Dark energy or modified gravity? An effective field theory approach. *JCAP*, 1308:010, 2013.

[98] David Langlois, Ryo Saito, Daisuke Yamauchi, and Karim Noui. Scalar-tensor theories and modified gravity in the wake of GW170817. *Phys. Rev.*, D97(6):061501, 2018.

[99] M. Crisostomi, Kazuya Koyama, D. Langlois, K. Noui, and D. A. Steer. Cosmological evolution in DHOST theories. *JCAP*, 1901(01):030, 2019.

[100] Marco Crisostomi, Matthew Lewandowski, and Filippo Vernizzi. Vainshtein regime in Scalar-Tensor gravity: constraints on DHOST theories. 2019.

[101] Marco Crisostomi and Kazuya Koyama. Self-accelerating universe in scalar-tensor theories after GW170817. *Phys. Rev.*, D97(8):084004, 2018.

[102] Janina Renk, Miguel Zumalacarregui, Francesco Montanari, and Alexandre Barreira. Galileon gravity in light of ISW, CMB, BAO and H_0 data. *JCAP*, 1710(10):020, 2017.

[103] C. D. Kreisch and E. Komatsu. Cosmological Constraints on Horndeski Gravity in Light of GW170817. *JCAP*, 1812(12):030, 2018.

[104] Johannes Noller and Andrina Nicola. Radiative stability and observational constraints on dark energy and modified gravity. 2018.

[105] Shin'ichi Hirano, Tsutomu Kobayashi, and Daisuke Yamauchi. On the screening mechanism in DHOST theories evading gravitational wave constraints. *Phys. Rev.*, D99(10):104073, 2019.

[106] Paolo Creminelli, Giovanni Tambalo, Filippo Vernizzi, and Vicharit Yingcharoenrat. Dark-Energy Instabilities induced by Gravitational Waves. 2019.

[107] Shin'ichi Hirano, Tsutomu Kobayashi, Daisuke Yamauchi, and Shuichiro Yokoyama. Constraining degenerate higher-order scalar-tensor theories with linear growth of matter density fluctuations. *Phys. Rev.*, D99(10):104051, 2019.

[108] Paolo Creminelli and Filippo Vernizzi. Dark Energy after GW170817 and GRB170817A. *Phys. Rev. Lett.*, 119(25):251302, 2017.

[109] Jeremy Sakstein and Bhuvnesh Jain. Implications of the Neutron Star Merger GW170817 for Cosmological Scalar-Tensor Theories. *Phys. Rev. Lett.*, 119(25):251303, 2017.

[110] Jose Maria Ezquiaga and Miguel Zumalacarregui. Dark Energy After GW170817: Dead Ends and the Road Ahead. *Phys. Rev. Lett.*, 119(25):251304, 2017.

[111] T. Baker, E. Bellini, P. G. Ferreira, M. Lagos, J. Noller, and I. Sawicki. Strong constraints on cosmological gravity from GW170817 and GRB 170817A. *Phys. Rev. Lett.*, 119(25):251301, 2017.

[112] Bin Hu, Marco Raveri, Noemi Frusciante, and Alessandra Silvestri. Effective Field Theory of Cosmic Acceleration: an implementation in CAMB. *Phys. Rev.*, D89(10):103530, 2014.

[113] Miguel Zumalacárregui, Emilio Bellini, Ignacy Sawicki, Julien Lesgourgues, and Pedro G. Ferreira. hi-class: Horndeski in the Cosmic Linear Anisotropy Solving System. *JCAP*, 1708(08):019, 2017.

[114] E. Bellini et al. Comparison of Einstein-Boltzmann solvers for testing general relativity. *Phys. Rev.*, D97(2):023520, 2018.

[115] H. Hildebrandt et al. KiDS-450: Cosmological parameter constraints from tomographic weak gravitational lensing. *Mon. Not. Roy. Astron. Soc.*, 465:1454, 2017.

[116] M. A. Troxel et al. Dark Energy Survey Year 1 results: Cosmological constraints from cosmic shear. *Phys. Rev.*, D98(4):043528, 2018.

[117] Chiaki Hikage et al. Cosmology from cosmic shear power spectra with Subaru Hyper Suprime-Cam first-year data. *Publ. Astron. Soc. Jap.*, 71(2):Publications of the Astronomical Society of Japan, Volume 71, Issue 2, April 2019, 43, https://doi.org/10.1093/pasj/psz010, 2019.

[118] Luca Amendola et al. Cosmology and fundamental physics with the Euclid satellite. *Living Rev. Rel.*, 16:6, 2013.

[119] Alexandra Abate et al. Large Synoptic Survey Telescope: Dark Energy Science Collaboration. 2012.

[120] D. Spergel et al. Wide-Field InfraRed Survey Telescope-Astrophysics Focused Telescope Assets WFIRST-AFTA Final Report. 2013.

[121] Enis Belgacem et al. Testing modified gravity at cosmological distances with LISA standard sirens. 2019.

[122] David Mattingly. Modern tests of Lorentz invariance. *Living Rev. Rel.*, 8:5, 2005.

[123] V. Alan Kostelecky and Neil Russell. Data Tables for Lorentz and CPT Violation. *Rev. Mod. Phys.*, 83:11–31, 2011.

[124] Stefano Liberati. Tests of Lorentz invariance: a 2013 update. *Class. Quant. Grav.*, 30:133001, 2013.

[125] Clifford M. Will. The Confrontation between general relativity and experalvesment. *Living Rev. Rel.*, 9:3, 2006.

[126] Kent Yagi, Diego Blas, Nicolás Yunes, and Enrico Barausse. Strong Binary Pulsar Constraints on Lorentz Violation in Gravity. *Phys. Rev. Lett.*, 112(16):161101, 2014.

[127] Kent Yagi, Diego Blas, Enrico Barausse, and Nicolás Yunes. Constraints on Einstein-Aether theory and Hořava gravity from binary pulsar observations. *Phys. Rev.*, D89(8):084067, 2014. [Erratum: Phys. Rev.D90,no.6,069901(2014)].

[128] Lijing Shao, R. Nicolas Caballero, Michael Kramer, Norbert Wex, David J. Champion, and Axel Jessner. A new limit on local Lorentz invariance violation of gravity from solitary pulsars. *Class. Quant. Grav.*, 30:165019, 2013.

[129] Jose Beltran Jimenez, Federico Piazza, and Hermano Velten. Evading the Vainshtein Mechanism with Anomalous Gravitational Wave Speed: Constraints on Modified Gravity from Binary Pulsars. *Phys. Rev. Lett.*, 116(6):061101, 2016.

[130] Emmanuel N. Saridakis. Horava-Lifshitz Dark Energy. *Eur. Phys. J.*, C67:229–235, 2010.

[131] Sourish Dutta and Emmanuel N. Saridakis. Observational constraints on Horava-Lifshitz cosmology. *JCAP*, 1001:013, 2010.

[132] Tsutomu Kobayashi, Yuko Urakawa, and Masahide Yamaguchi. Cosmological perturbations in a healthy extension of Horava gravity. *JCAP*, 1004:025, 2010.

[133] Cristian Armendariz-Picon, Noela Farina Sierra, and Jaume Garriga. Primordial Perturbations in Einstein-Aether and BPSH Theories. *JCAP*, 1007:010, 2010.

[134] Diego Blas, Mikhail M. Ivanov, and Sergey Sibiryakov. Testing Lorentz invariance of dark matter. *JCAP*, 1210:057, 2012.

[135] B. Audren, D. Blas, J. Lesgourgues, and S. Sibiryakov. Cosmological constraints on Lorentz violating dark energy. *JCAP*, 1308:039, 2013.

[136] B. Audren, D. Blas, M. M. Ivanov, J. Lesgourgues, and S. Sibiryakov. Cosmological constraints on deviations from Lorentz invariance in gravity and dark matter. *JCAP*, 1503(03):016, 2015.

[137] Diego Blas, Mikhail M. Ivanov, Ignacy Sawicki, and Sergey Sibiryakov. On constraining the speed of gravitational waves following GW150914. *JETP Lett.*, 103(10):624–626, 2016. [Pisma Zh. Eksp. Teor. Fiz.103,no.10,708(2016)].

[138] Nicolas Yunes, Kent Yagi, and Frans Pretorius. Theoretical Physics Implications of the Binary Black-Hole Mergers GW150914 and GW151226. *Phys. Rev.*, D94(8):084002, 2016.

[139] A. Emir Gumrukcuoglu, Mehdi Saravani, and Thomas P. Sotiriou. Horava gravity after GW170817. *Phys. Rev.*, D97(2):024032, 2018.

[140] Petr Horava. Quantum Gravity at a Lifshitz Point. *Phys. Rev.*, D79:084008, 2009.

[141] Nima Arkani-Hamed, Paolo Creminelli, Shinji Mukohyama, and Matias Zaldarriaga. Ghost inflation. *JCAP*, 0404:001, 2004.

[142] Marc H. Goroff and Augusto Sagnotti. The Ultraviolet Behavior of Einstein Gravity. *Nucl. Phys.*, B266:709–736, 1986.

[143] K. S. Stelle. Renormalization of Higher Derivative Quantum Gravity. *Phys. Rev.*, D16:953–969, 1977.

[144] Andrei O. Barvinsky, Diego Blas, Mario Herrero-Valea, Sergey M. Sibiryakov, and Christian F. Steinwachs. Renormalization of Hořava gravity. *Phys. Rev.*, D93(6):064022, 2016.

[145] Andrei O. Barvinsky, Diego Blas, Mario Herrero-Valea, Sergey M. Sibiryakov, and Christian F. Steinwachs. Renormalization of gauge theories in the background-field approach. *JHEP*, 07:035, 2018.

[146] Andrei O. Barvinsky, Diego Blas, Mario Herrero-Valea, Sergey M. Sibiryakov, and Christian F. Steinwachs. Hořava Gravity is Asymptotically Free in 2 + 1 Dimensions. *Phys. Rev. Lett.*, 119(21):211301, 2017.

[147] Tomohiro Takahashi and Jiro Soda. Chiral Primordial Gravitational Waves from a Lifshitz Point. *Phys. Rev. Lett.*, 102:231301, 2009.

[148] Gianluca Calcagni. Cosmology of the Lifshitz universe. *JHEP*, 09:112, 2009.

[149] Elias Kiritsis and Georgios Kofinas. Horava-Lifshitz Cosmology. *Nucl. Phys.*, B821:467–480, 2009.

[150] Shinji Mukohyama. Scale-invariant cosmological perturbations from Horava-Lifshitz gravity without inflation. *JCAP*, 0906:001, 2009.

[151] Tsutomu Kobayashi, Yuko Urakawa, and Masahide Yamaguchi. Large scale evolution of the curvature perturbation in Horava-Lifshitz cosmology. *JCAP*, 0911:015, 2009.

[152] William Donnelly and Ted Jacobson. Coupling the inflaton to an expanding aether. *Phys. Rev.*, D82:064032, 2010.

[153] Paolo Creminelli, Jorge Norena, Manuel Pena, and Marko Simonovic. Khronon inflation. *JCAP*, 1211:032, 2012.

[154] Adam R. Solomon and John D. Barrow. Inflationary Instabilities of Einstein-Aether Cosmology. *Phys. Rev.*, D89(2):024001, 2014.

[155] Mikhail M. Ivanov and Sergey Sibiryakov. UV-extending Ghost Inflation. *JCAP*, 1405:045, 2014.

[156] Amjad Ashoorioon, Diego Chialva, and Ulf Danielsson. Effects of Nonlinear Dispersion Relations on Non-Gaussianities. *JCAP*, 1106:034, 2011.

[157] Amjad Ashoorioon, Roberto Casadio, Ghazal Geshnizjani, and Hyung J. Kim. Getting Super-Excited with Modified Dispersion Relations. *JCAP*, 1709(09):008, 2017.

[158] David Wands, Karim A. Malik, David H. Lyth, and Andrew R. Liddle. A New approach to the evolution of cosmological perturbations on large scales. *Phys. Rev.*, D62:043527, 2000.

[159] Steven Weinberg. Adiabatic modes in cosmology. *Phys. Rev.*, D67:123504, 2003.

[160] D. Blas, O. Pujolas, and S. Sibiryakov. On the Extra Mode and Inconsistency of Horava Gravity. *JHEP*, 10:029, 2009.

[161] Diego Blas, Oriol Pujolas, and Sergey Sibiryakov. Models of non-relativistic quantum gravity: The Good, the bad and the healthy. *JHEP*, 04:018, 2011.

[162] D. Blas, O. Pujolas, and S. Sibiryakov. Consistent Extension of Horava Gravity. *Phys. Rev. Lett.*, 104:181302, 2010.

[163] Guy D. Moore and Ann E. Nelson. Lower bound on the propagation speed of gravity from gravitational Cherenkov radiation. *JHEP*, 0109:023, 2001.

[164] Paolo Creminelli, Jérôme Gleyzes, Jorge Noreña, and Filippo Vernizzi. Resilience of the standard predictions for primordial tensor modes. *Phys. Rev. Lett.*, 113(23):231301, 2014.

[165] Shinji Tsujikawa. Disformal invariance of cosmological perturbations in a generalized class of Horndeski theories. *JCAP*, 1504(04):043, 2015.

[166] Shinji Mukohyama. Horava-Lifshitz Cosmology: A Review. *Class. Quant. Grav.*, 27:223101, 2010.

[167] Christopher Gordon, David Wands, Bruce A. Bassett, and Roy Maartens. Adiabatic and entropy perturbations from inflation. *Phys. Rev.*, D63:023506, 2001.

[168] Ted Jacobson. Extended Horava gravity and Einstein-aether theory. *Phys. Rev.*, D81:101502, 2010. [Erratum: Phys. Rev.D82,129901(2010)].

[169] Daniel Baumann, Daniel Green, and Rafael A. Porto. B-modes and the Nature of Inflation. *JCAP*, 1501(01):016, 2015.

[170] David Seery and James E. Lidsey. Primordial non-Gaussianities in single field inflation. *JCAP*, 0506:003, 2005.

[171] Daniel Baumann and Daniel Green. Equilateral Non-Gaussianity and New Physics on the Horizon. *JCAP*, 1109:014, 2011.

[172] P. A. R. Ade et al. Planck 2015 results. XVII. Constraints on primordial non-Gaussianity. *Astron. Astrophys.*, 594:A17, 2016.

[173] N. Kaiser. Clustering in real space and in redshift space. *Mon. Not. Roy. Astron. Soc.*, 227:1–27, 1987.

[174] A. J. S. Hamilton. Linear redshift distortions: A Review. In *Ringberg Workshop on Large Scale Structure Ringberg, Germany, September 23-28, 1996*, 1997.

[175] J. C. Jackson. A critique of Rees's theory of primordial gravitational radiation. *Mon. Not. Roy. Astron. Soc.*, 156:1P, Jan 1972.

[176] John A. Peacock et al. A Measurement of the cosmological mass density from clustering in the 2dF Galaxy Redshift Survey. *Nature*, 410:169–173, 2001.

[177] Lado Samushia et al. The clustering of galaxies in the SDSS-III Baryon Oscillation Spectroscopic Survey: measuring growth rate and geometry with anisotropic clustering. *Mon. Not. Roy. Astron. Soc.*, 439(4):3504–3519, 2014.

[178] Antony Lewis and Anthony Challinor. Weak gravitational lensing of the CMB. *Phys. Rept.*, 429:1–65, 2006.

[179] J. A. Peacock and M. Bilicki. Wide-area tomography of CMB lensing and the growth of cosmological density fluctuations. *Mon. Not. Roy. Astron. Soc.*, 481(1):1133–1148, 2018.

[180] T. M. C. Abbott et al. Dark Energy Survey year 1 results: Cosmological constraints from galaxy clustering and weak lensing. *Phys. Rev.*, D98(4):043526, 2018.

[181] Diego Blas, Julien Lesgourgues, and Thomas Tram. The Cosmic Linear Anisotropy Solving System (CLASS). Part II: Approximation schemes. *"JCAP"*, 2011(7):034, Jul 2011.

[182] Benjamin D. Wandelt, Eric Hivon, and Krzysztof M. Gorski. The pseudo-C_ℓ method: cosmic microwave background anisotropy power spectrum statistics for high precision cosmology. *Phys. Rev.*, D64:083003, 2001.

[183] E. Hivon, K. M. Gorski, C. B. Netterfield, B. P. Crill, S. Prunet, and F. Hansen. Master of the cosmic microwave background anisotropy power spectrum: a fast method for statistical analysis of large and complex cosmic microwave background data sets. *Astrophys. J.*, 567:2, 2002.

[184] K. M. Gorski, Eric Hivon, A. J. Banday, B. D. Wandelt, F. K. Hansen, M. Reinecke, and M. Bartelman. HEALPix - A Framework for high resolution discretization, and fast analysis of data distributed on the sphere. *Astrophys. J.*, 622:759–771, 2005.

[185] George Miley and Carlos De Breuck. Distant Radio Galaxies and their Environments. *Astron. Astrophys. Rev.*, 15:67, 2008.

[186] James J. Condon, W. D. Cotton, E. W. Greisen, Q. F. Yin, R. A. Perley, G. B. Taylor, and J. J. Broderick. The NRAO VLA Sky survey. *Astron. J.*, 115:1693–1716, 1998.

[187] Tom Mauch, T. Murphy, H. J. Buttery, J. Curran, R. W. Hunstead, B. Piestrzynski, J. G. Robertson, and E. M. Sadler. SUMSS: A wide-field radio imaging survey of the southern sky. 2. The Source catalogue. *Mon. Not. Roy. Astron. Soc.*, 342:1117, 2003.

[188] Robert H. Becker, Richard L. White, and David J. Helfand. The FIRST Survey: Faint Images of the Radio Sky at twenty centimeters. *Astrophys. J.*, 450:559, 1995.

[189] Philip N. Best, J. N. Arts, H. J. A. Rottgering, R. Rengelink, M. H. Brookes, and J. Wall. CENSORS: A Combined EIS - NVSS survey of radio sources. 1. Sample definition, radio data and optical identifications. *Mon. Not. Roy. Astron. Soc.*, 346:627, 2003.

[190] M. H. Brookes, P. N. Best, J. A. Peacock, H. J. A. Rottgering, and J. S. Dunlop. A Combined EIS-NVSS Survey Of Radio Sources (CENSORS) III: Spectroscopic observations. *Mon. Not. Roy. Astron. Soc.*, 385:1297, 2008.

[191] Chris Blake and Jasper Wall. Measurement of the angular correlation function of radio galaxies from the NRAO VLA Sky Survey. *Mon. Not. Roy. Astron. Soc.*, 329:L37–L41, 2002.

[192] Chris Blake, Pedro G. Ferreira, and Julian Borrill. The Angular power spectrum of NVSS radio galaxies. *Mon. Not. Roy. Astron. Soc.*, 351:923, 2004.

[193] Kendrick M. Smith, Oliver Zahn, and Olivier Dore. Detection of Gravitational Lensing in the Cosmic Microwave Background. *Phys. Rev.*, D76:043510, 2007.

[194] Rupert Allison et al. The Atacama Cosmology Telescope: measuring radio galaxy bias through cross-correlation with lensing. *Mon. Not. Roy. Astron. Soc.*, 451(1):849–858, 2015.

[195] M. Bilicki et al. Photometric redshifts for the Kilo-Degree Survey. Machine-learning analysis with artificial neural networks. *Astron. Astrophys.*, 616:A69, 2018. [Astron. Astrophys.616,A69(2018)].

[196] J. T. A. de Jong et al. The third data release of the Kilo-Degree Survey and associated data products. *Astron. Astrophys.*, 604:A134, 2017.

[197] Tristan L. Smith, Elena Pierpaoli, and Marc Kamionkowski. A new cosmic microwave background constraint to primordial gravitational waves. *Phys.Rev.Lett.*, 97:021301, 2006.

[198] Maciej Bilicki, Thomas H. Jarrett, John A. Peacock, Michelle E. Cluver, and Louise Steward. 2MASS Photometric Redshift catalog: a comprehensive three-dimensional census of the whole sky. 2013. [Astrophys. J. Suppl.210,9(2014)].

[199] M. Bilicki et al. WISE x SuperCOSMOS photometric redshift catalog: 20 million galaxies over 3pi steradians. 2016. [Astrophys. J. Suppl.225,5(2016)].

[200] Róbert Beck, László Dobos, Tamás Budavári, Alexander S. Szalay, and István Csabai. Photometric redshifts for the SDSS Data Release 12. *Mon.Not.Roy.Astron.Soc.*, 460(2):1371–1381, Aug 2016.

[201] Lotfi Boubekeur, Paolo Creminelli, Jorge Norena, and Filippo Vernizzi. Action approach to cosmological perturbations: the 2nd order metric in matter dominance. *JCAP*, 0808:028, 2008.

[202] Antonio De Felice, Jean-Marc Gerard, and Teruaki Suyama. Cosmological perturbations of a perfect fluid and noncommutative variables. *Phys. Rev.*, D81:063527, 2010.

[203] Jérôme Gleyzes, David Langlois, Federico Piazza, and Filippo Vernizzi. Exploring gravitational theories beyond Horndeski. *JCAP*, 1502:018, 2015.